Establishment of the South African baseline surface radiation network station at De Aar

by

Daniël Johannes Esterhuyse

Submitted in fulfilment of the requirements for the degree of

MASTER OF SCIENCE (METEOROLOGY)

in the Faculty of Natural and Agricultural Sciences of the

University of Pretoria

July 2004

Dedicated to my dearest mother, who never had the opportunity to realise her intense love for nature in formal scientific training. Mom, this one is for you, out of gratefulness for this opportunity granted to me.

Opgedra aan my dierbare moeder, wat nooit self die geleentheid gehad het om haar intense liefde vir die natuur te kon realiseer in formele wetenskaplike opleiding nie. Mamma, hierdie een is vir u, uit dankbaarheid vir die geleentheid wat aan my gebied is.

ABSTRACT

Establishment of the South African baseline surface radiation network station at De Aar

Daniël Johannes Esterhuyse

Promotor: Prof. C.J. de W. Rautenbach
Department: Department of Geography, Geoinformatics and Meteorology
Faculty: Faculty of Natural and Agricultural Sciences
University: University of Pretoria
Degree: *Magister Scientae* (Meteorology)

Summary

The South African Weather Service (SAWS) was offered a unique opportunity to become involved in the prestigious global Baseline Surface Radiation Network (BSRN) project in 1995. This study is an academical and technical document describing and elucidating aspects regarding the eventual establishment of the BSRN measurement facility at De Aar that embodies South Africa's involvement.

The dissertation opens with an introductory chapter offering background information and an explanation of circumstances leading to South Africa's involvement in this project, including reasons exactly why De Aar was chosen to be the South African BSRN site. This is followed by details on a scientific measurement plan including necessary information on radiation processes in the atmosphere, measurement techniques and associated instrumentation. The next chapter is devoted to the design of a radiometric measurement system answering to the scientific plan, with more details on instrumentation, peripherals, calibration and data management strategies.

Three years of real measured data since station establishment, is used as a basis to apply and evaluate the various quality assurance techniques of the central BSRN data-archive. Special reference is made in a separate chapter to the two partial solar eclipses that traversed Southern Africa in 2001 and 2002, in the form of case studies.

This dissertation is illustrated by several photos, and rounded off by details of the station-to-archive file format as laid down by the international BSRN data-archive, a useful table reflecting sunrise, sunset, solar transit, day length and Top Of Atmosphere (TOA) radiation, an explanation on climate zone classification, as well as a useful technical guide on setting up a pyrgeometer.

Apart from the academic content this document also intends to serve as a guideline for station operation and future development of whatever form, for both the station scientist and the station manager. Such developments can include the establishment of other BSRN stations, or in general the enhancement of the quality of solar radiation measurements over the entire Southern Africa Developing Community (SADC) region.

The author wishes to state that in presenting this document in English, he does not wish to promote English as scientific language at the expense of Afrikaans. The choice of language was taken purely on the basis of broader international involvement and a wider local usefulness of this document.

EKSERP

Totstandkoming van die Suid-Afrikaanse grondvlak-stralingsnetwerkstasie by De Aar

Daniël Johannes Esterhuyse

Studieleier: Prof. C.J. de W. Rautenbach
Departement: Departement van Geografie, Geoinformatika en Weerkunde
Fakulteit: Fakulteit Natuur- en Landbouwetenskappe
Universiteit: Universiteit van Pretoria
Graad : *Magister Scientae* (Weerkunde)

Samevatting

Die Suid-Afrikaanse Weerdiens het in 1995 ‘n unieke geleentheid ontvang om deel te wees van die hoogs aangeskrewe grondvlak-stralingsnetwerk “(BSRN)” projek. In hierdie studiestuk wat akademies sowel as tegnies van aard is, word ‘n uiteensetting gelewer en toeligting gegee van aspekte rakende die uiteindelike instrumentele opstelling by De Aar wat Suid-Afrika se betrokkenheid in hierdie projek beliggaam.

Die verhandeling open met ‘n inleidende hoofstuk wat agtergrondinligting lewer sowel as ‘n uiteensetting gee van die redes presies waarom juis op De Aar as die Suid-Afrikaanse BSRN stasie besluit is. Dit word opgevolg deur besonderhede van die wetenskaplike metingsplan, wat nodige inligting oor stralingsprosesse in die aarde se atmosfeer, metingstegnieke, sowel as bybehorende instrumentasie insluit. ‘n Volgende hoofstuk word gewy aan die ontwerp van ‘n stralingsmetingstelsel wat aan die wetenskaplike plan kan verantwoord, en dit sluit die volgende in: meer besonderhede rakende instrumentasie, bykomstighede, kalibrasie en data-versorging.

Drie jaar van werklike waargenome data sedert die totstandkoming van die stasie, word as vertrekpunt geneem om die verskeie kwaliteitskontroletegnieke wat die sentrale BSRN data-argief gebruik, te evalueer in ‘n volgende hoofstuk. In die vorm van gedetailleerde gevallestudies word in ‘n afsonderlike hoofstuk spesiale melding gemaak van die twee gedeeltelike sonsverduisterings wat beide oor Suidelike Afrika beweeg het in 2001 en 2002.

Die verhandeling word geïllustreer deur verskeie fotos, en word afgerond deur besonderhede van die stasie-tot-argief formaat vir ‘n datalêer soos vasgestel deur die internasionale BSRN-argief, ‘n nuttige tabel wat sonop-en sonondertye, sonmiddaguur-tyd en daglengte, sowel as Top Van Atmosfeer straling bevat, ‘n verduideliking rakende klimaatsone-klassifisering, en ‘n nuttige tegniese gids om ‘n pyrgeometer op te stel.

Benewens die akademiese inhoud, is die dokument ook bedoel om as riglyn te dien vir die stasie-bestuurder en -wetenskaplike rakende die werking van die stasie en toekomstige ontwikkeling in watter vorm ookal. Sodanige ontwikkelings kan uitbreidings wees aan die bestaande stasie of moontlike ontwikkeling van ‘n ander nabygeleë BSRN stasie in ‘n buur-land, tot voordeel van stralingsmeting in die Suider- Afrikaanse Ontwikkelingsgemeenskap.

Die outeur wil hiermee onomwonde verklaar dat hy nie poog om met hierdie verhandeling Engels as wetenskapstaal ten koste van Afrikaans te bevorder nie. Die besluit om dit in Engels aan te bied, was suiwer geneem op grond van wyer internasionale betrokkenheid sowel as wyer plaaslike bruikbaarheid van die dokument.

ACKNOWLEDGEMENTS

The author wishes to expresses his sincere thanks to the following persons and institutions for their assistance and contribution towards making this dissertation possible:

1. The South African Weather Service (SAWS)

for being continually committed to the Baseline Surface Radiation Network (BSRN) programme through the Global Atmosphere Watch (GAW) which forms part of the Climate Systems Directorate of the SAWS ;

for providing generous logistical support for the continuation of this project ;

for granting a part-time bursary that helped to make this study possible ;

2. The World Meteorological Organization (WMO)

for continued commitment towards the project ;

for generous financial support in providing a first consignment of instrumentation for establishment of the site, as well as a second consignment of spare parts ;

for providing continuous financial support enabling SAWS staff to attend overseas conferences and workshops in order to maintain valuable overseas contact and keep abreast with latest technology ;

3. The University of Pretoria

for providing the opportunity to submit this dissertation as fulfilment for an M.Sc.(Meteorology) degree ;

4. The late Cal Archer (1925 – 2000)

for his sheer inspiration and encouragement in a mentorship role to me as a young scientist in this field for the first five years of my employment at the SAWS ;

for his seemingly unlimited source of knowledge and often original, but always ingenious and surprisingly simple solutions for practical problems ;

for sustaining early correspondence vital in establishing the station even at a stage where it was not sure if South Africa was to be part of the programme or not ;

5. Dr Ellsworth Dutton (International project leader)

for generous and sustained encouragement during the course of this project, including two site visits to South Africa ;

6. The personnel of De Aar weather office

for their dedication in maintaining the day-to-day chores and operation of the station. Guys, without your sustained effort this would not have been possible.

TABLE OF CONTENTS

CHAPTER 3 SYSTEM DESIGN

LIST OF SYMBOLS

UPPER CASE LETTERS

A Area (m^2)

AU Astronomical unit (1.5×10^{11}m)

A_0 Radius vector of solar distance (dimensionless)

C_1 Thermopile long-wave sensitivity constant (ca. 4 $mV.kW^{-1}.m^{-2}$)

E Radiant energy flux density (from a non-specific source per unit area) ($W.m^{-2}$)

E_{LW} Long-wave energy flux density ($W.m^{-2}$)

E_{OLR} Energy flux of outgoing Long-wave Radiation density ($W.m^{-2}$)

E_{SW} Short-wave energy flux density ($W.m^{-2}$)

E_{TOA} Energy flux density at the top of the atmosphere ($W.m^{-2}$)

E_v Excitation voltage used in pyrgeometer operation (mV)

F Radiometer reading (nominal units)

H (solar) Hour Angle (radians)

I Electric current (Ampere)

P Electric power (Watt)

Q Radiation flux density leaving the surface of the sun ($W.m^{-2}$)

R_c (calculated) Resistance of the pyrgeometer case thermistor (Ohm)

R_d (calculated) Resistance of the pyrgeometer dome thermistor (Ohm)

R_E Mean radius of the Earth (6.37×10^6 m)

R_v Resistance of the pyrgeometer precision resistor (Ohm)

S_0 Total radiant energy flux of the sun (3.9×10^{26} W)

S (annual mean) Solar constant, (1371 $W.m^{-2}$)

T Absolute temperature (K)

T_b Instrument body (case) temperature (K)

T_d Instrument dome temperature (K)

V_c Pyrgeometer case thermistor potential difference (mV)

V_d Pyrgeometer dome thermistor potential difference (mV)

W Power, energy flux ($Joules.s^{-1}$; Watts)

Z Solar zenith angle (degrees)

$Z(t)$ Solar zenith angle at time instant t , or a short time interval

LOWER CASE LETTERS

c Speed of light in vacuum (3 x 10^{8} m.s^{-1})

e Surface vapour pressure (hPa)

g Gravity acceleration on the Earth's surface (9.8 m.s^{-2})

h Planck's constant (6.62 x 10^{-34} J.s^{-1})

k_1 Pyrgeometer calibration constant 1 (dimensionless)

k_2 Pyrgeometer calibration constant 2 (dimensionless)

k_3 Pyrgeometer calibration constant 3 (dimensionless)

m Kasten optical air mass (dimensionless)

p Thermopile voltage (mV)

t Time (seconds)

GREEK LETTERS

α Planetary albedo, estimated at 0.3

δ Solar declination (radians)

ε Atmospheric emmissivity (dimensionless)

φ Site latitude (radians)

λ Wavelength (m)

κ Stefan-Bolzmann's constant in specific corresponding units (1.38 x 10^{-23} J.m^{-2}.K^{-1})

σ Stefan-Bolzmann's constant in specific corresponding units (5.67 x 10^{-8} W.m^{-2}.K^{-4})

θ Solar azimuth angle (radians)

ξ Equation of time (radians)

DATE FORMAT

The author is aware of the standard ISO- 8601 format for writing dates, i.e. **CCYY-MM-DD**, for example, 1964-02-10 meaning "The 10th of February 1964 AD". However, to omit any ambiguousity and also make dates equally well presentable in text, headings, figures and captions, it was decided to use alternatively the formats **DD Mmm CCYY** (written as "10 Feb 1964" with regards to the said example) in tables and figures, as well as **DD Month CCYY** (written as "10 February 1964) where most appropriate.

LIST OF FIGURES

LIST OF TABLES

LIST OF ACRONYMS AND ABBREVIATIONS

AMS	American Meteorological Society
AOD	Aerosol Optical Depth
ARM	(American) Atmosphere Radiation Monitoring
AVG	(Mathematical) Average
AWS	Automatic Weather Station
BOM	(Australian) Bureau of Meteorology
BSRN	Baseline Surface Radiation Network
CD	Compact Disk
CMDL	(American) Climate Monitoring and Diagnostics Laboratory
COSPAR	Committee on Space Research
CSI	Campbell Scientific Incorporated
DJF	December-January-February (average of summer data) – see also MAM, JJA and SON
DL	One-minute average value of downwelling longwave radiation – see also LWD
DSDFS	One-minute average value of diffuse radiation.
DSDIR	One-minute average value of direct radiation.
DSGL1	One-minute average value of calculated global radiation using the relationship between direct, diffuse and the solar zenith angle.
DSGL2	One-minute average value of global radiation using an unshaded pyranometer.
DSTM	(A complex definition involving DSGL2 and TOA radiation, in section 4.3.2.1.)
ECMWF	European Centre for Medium-Term Weather Forecasts
EMPA	*"Eidgenössische Materialprüfungs- und Forschungsanstalt"* (Swiss Federal Laboratory for Materials Research and Testing)
EPLAB	Eppley Laboratories
ERBE	Earth Radiation Budget Experiment
ETHZ	*"Eidgenössische Technische Hochschule Zürich"* (Swiss Federal Institute of Technology)
FTP	File Transfer Protocol
GAW	Global Atmosphere Watch
GBSRN	Global Baseline Surface Radiation Network
GEWEX	Global Energy and Water Cycle Experiment
GPS	Global Positioning System (by satellites)
GSFC	Goddard Space Flight Centre (the combination NASA-GSFC is often used).

HTTP	Hyper-text Transfer Protocol
ICSU	International Council of Scientific Unions
INFM	"*L'Istituto Nazionale per la Fisica della Materia*" (The (Italian) National Institute for the Physics of Matter)
IPC	International Pyrheliometric Comparisons (such as IPC VIII, IPC IX, etc.)
IPCC	Intergovernmental Panel on Climate Change
IPS	International Pyrheliometric Scale
IR	Infrared (radiation)
ITCZ	Inter-tropical Convergence Zone
IUCC	Information Unit on Climate Change
JJA	June-July-August (average of winter data) – see also DJF, MAM and SON.
KNMI	"*Koninklijk Nederlands Meteorolgisch Instituut*" (Royal Dutch Meteorological Institute).
LAN	Local Area Network
LW	Longwave (Radiation)
LWD	Longwave Downwelling (Radiation)
MAM	March-April-May (average of autumn data) – see also DJF, JJA and SON
NASA	(American) National Aeronautic Space Agency. See also GSFC.
NEPAD	New Plan for African Development
NH	Northern Hemisphere
NIP	Normal Incidence Pyrheliometer
NOAA	National Oceanic Atmospheric Administration
NREL	(American) National Renewable Energy Laboratory. See also SERI.
OLR	Outgoing Longwave Radiation
OSD	One-minute standard deviations (of BSRN measurements)
PAR	Photosynthetically Active Radiation
PC	Personal Computer
PDF	Portable Document File (computer format)
PIR	Precision Infrared Radiometer
PMOD	*"Physikalisch-Meteorologisches Observatorium Davos"* (World Radiation Centre) – also see WRC
PSP	Precision Spectral Pyranometer
PWV	Precipitable Water Vapour
RTM	Radiative Transfer Model(s)
SADC	Southern African Development Community
SAST	South African Standard Time
SAWB	South African Weather Bureau
SAWS	South African Weather Service

SERI	Solar Energy Research Institute (now known as NREL).
SGP	(American) Southern Great Plains
SH	Southern Hemisphere
SON	September-October-November (average of spring data) – see also DJF, MAM and JJA
SRB	Surface (Solar) Radiation Budget
STD	Standard Deviation
SURFRAD	(American) Surface Radiation Project
SW	Shortwave (Radiation)
TOA	Top Of (the) Atmosphere
UL	One-minute average value of upwelling longwave (radiation)
UNEP	United Nation's Environmental Programme
UPS	Uninterruped Power Supply
USSR	Union of Socialistic Soviet Republics
UT	Universal Time
UV	Ultraviolet (Radiation)
WAN	Wide Area (computer) Network
WCRP	World Climate Research Programme
WRDC	World Radiation Data Centre (St. Petersburg, Russia)
WRMC	World Radiation Monitoring Centre (Zürich, Switzerland)
WMO	World Meteorological Organization
WRC	World Radiation Centre (also see PMOD: the combination PMOD-WRC is often used)
WRR	World Radiometric Reference

CHAPTER 1

BACKGROUND

1.1 INTRODUCTION

1.1.1 Global need for accurate radiation measurements

Solar radiation energy is the fundamental driving force behind the formation of all weather and climate systems on Earth (Van den Bos, 1997; Persson, 2000). It has a significant influence on both atmosphere and ocean circulation patterns (Di Pasquale and Whitlock, 1993; Whitlock, 1993). Complex interactions between the atmosphere and ocean involving turbulent fluxes of momentum, mass and heat (latent and sensible heat) in the marine atmosphere boundary layer, as well as the subsequent exchange of energy to the higher atmosphere where clouds may form, are not yet fully understood (Morel, 1990; IUCC, 1993). Terrestrial heat fluxes may lead to convection, turbulence, cloud formation and eventually rainfall, thereby shaping the continental climate. Although solar energy is obviously regarded as an important driving force, there are still many uncertainties about the particular role of solar energy in these processes.

With respect to future scenarios, there is also considerable disagreement amongst experts about the magnitude of climate change, or more specifically, global warming that might occur during the next decades (IPCC, 2001).

The determination of a global climatology, based upon the natural terrestrial radiation budget, is therefore fundamental (Mc Arthur, 1998) in order to facilitate research towards creating a better understanding of the already recognized role that radiation plays in climate processes (Gilgen *et al.*, 1993). A conventional network of surface solar radiometry, to a great extent operated independently in individual countries as part of a meteorological measurement programme. Thus it was admittedly unable to serve as an accurate source of information to understand and explain the global radiation budget (Ohmura *et al.,* 1998). As a matter of fact, it is described as “meagre at best” (Long and Ackerman, 1994).

Hence, the need arose for a denser international network of ground-based radiometers with

the necessary accuracy and data integrity. Such a network, if in existence, will have to set new global standards in surface radiometric measurement.

1.1.2 The establishment of a new radiometric network

During a meeting of the joint scientific committee for the World Climate Research Programme (WCRP) of the World Meteorological Organisation's International Council of Scientific Unions (WMO ICSU) in Geneva (19 to 21 October 1988) an urgent need was expressed for establishing a global baseline network of stations that are capable to accurately measure surface solar and terrestrial radiative fluxes. This network will contribute to meet requirements set for long-term data collection of global surface radiation balance components (Gilgen *et al.*, 1995).

The network was initially meant to serve as support for research projects of the WCRP and other scientific programs (Schiffer, 1990). According to Gilgen (1991) and Mc Arthur (1998) its main missions were identified as follows:

- Monitor the background (least influenced by human activities) shortwave (SW) and longwave (LW) radiative components and their changes with the best methods available (accurate enough to reveal any long-term trends).
- Provide verification data for the calibration of satellite-based estimates of the surface radiation budget.
- Produce high-quality observational data to be used for validating the theoretical calculation of radiative fluxes by various mathematical models.

The word "*surface*" was particularly important in the naming of such a network, since the Earth's surface transforms about 60% of the incident solar energy absorbed by the Earth (Ohmura *et al.*, 1998). Therefore, surface measurements are likely to contain the best information concerning global radiative fluxes. It was also important to locate individual network sites in contrasting climate zones (Morel, 1990) in order to extract as much information as possible from "climate change hotspots".

1.1.2.1 **Launching the project** *(Würzburg, Germany, 30 October to 3 November 1989)*

During a special workshop of WCRP and the Committee on Space Research (COSPAR) on

the global surface radiation budget for climate change, an announcement for the establishment of a new radiation network was officially made (DeLuisi, 1989). It was then called the Global Baseline Surface Radiation Network (GBSRN). However, the qualification "Global" (G) was soon omitted from the acronym GBSRN and was never used since. The most important outcome of the Würzburg meeting was the drafting of a scientific measurement plan for the newly established network (expanded in Chapter 2 of this dissertation).

1.1.2.2 South Africa's first involvement

The late Cal Archer (1925 -2000) from the South African Weather Service (SAWS) attended the Würzburg conference (Schiffer, 1990) but in an unofficial capacity, since sanctions against the domestic policy of the South African government of that time prevented formal participation. However, this contact later proved to be vital, because South Africa's willingness to establish a Baseline Surface Radiation Network (BSRN) station within the borders of the country, had already been shown clearly at this early stage. An interesting fact is, that Namibia, and not South Africa, had initially been mentioned as the candidate country to represent the southern African region (De Luisi, 1989).

1.1.3 How the project unfolded

1.1.3.1 First workshop *(Washington DC, USA, 3 to 5 December 1990)*

Following the Würzburg meeting, this workshop was the first of a tradition of regular steering meetings, and attended by various stakeholders in the BSRN programme, to discuss issues of mutual importance, to share ideas and expertise, and to resolve issues of importance. The following points were addressed (WCRP-54, 1991):

- Measurements based on the 1989 recommendations, must commence as soon as possible, utilizing a "pilot" group of stations. Notwithstanding the fact that BSRN operational procedures still needed to be formalized, practical avenues (instrument standardization, objective assessment of instrument characteristics and local operational procedures) were also in need to be established. The first "pilot" group consisted of the following six stations: (1) Payerne in Switzerland, (2) Cape Grim in Australia, (3) Boulder in the USA, (4) Schleswig in Germany, (5) a

"Canadian site" and (6) a "USSR site".

- Resolution needed to be sought on pyrheliometer errors, calibration uncertainties surrounding diffuse and reflected SW pyranometers, downwelling LW instrumentation and the influence of domes and observation height on long wave measurements.
- Analysis of the measurement uncertainty and estimation of the effect of random and systematic errors on the final results, also needed quantification.
- Furthermore, a scheme for instrument calibration (compliance to World Radiometric Reference (WRR) standards) needed to be established as well.

Individuals, as well as groups, that had been formed, were addressing these issues. Feedback and recommendations were expected at the following workshop.

At the first workshop it was also decided that:

- Personnel involved in instrument calibration should be encouraged to visit various other sites in order to exchange knowledge and expertise. This approach should widen technical expertise in radiation measurements in relation to the measurements of other land-based meteorological parameters.
- Special assistance should be given to developing countries to enable them to establish a local BSRN site where needed. (South Africa later benefited from this decision).
- Close collaboration between the BSRN and Global Atmosphere Watch (GAW) programmes of the WMO was regarded as beneficial in the light of mutual exchange of high-quality data, optimal usage of measurement sites, in order to attract more scientific expertise to the programme.
- A detailed BSRN operations manual (on instrumentation, installation, calibration and maintenance) needs to be compiled as a matter of urgency. This enormous task was assigned to Dr Bruce Mc Arthur (Canada), which he completed seven years later in the form of a 255-page document.
- A central BSRN data archive centre needs to be identified. It was initially decided to host this at the National Aeronautic Space Agency's (NASA) Langley Research Centre (designated as the Surface Radiation Budget (SRB) Satellite Data Analysis Centre).
- Atmospheric Radiation Measurement (ARM) sites in the USA, sharing BSRN ideals, can successfully complement the BSRN. Some of these sites were eventually amongst the first to deliver BSRN data.

A circular letter (Whitlock, 1990) containing draft plans for the data format and archiving plan was circulated immediately after the first workshop (before the end of 1990). Later reference to this draft indicated that is was indeed “excellent” (WCRP-64, 1991). As a matter of fact, it was adopted to be the official BSRN plan with only a few alterations (Gilgen *et al.*, 1991).

1.1.3.2 **Second workshop** *(Davos, Switzerland, 6 to 8 August 1991)*

The World Radiation Centre (WRC-PMOD) was host for the second workshop, which was characterized by the following highlights (WCRP-64,1991):

- The draft data format and management plan was finalized and adopted.
- The basic set of BSRN measurement parameters were finalized, being:
    1. Direct solar radiation
    2. Diffuse solar radiation
    3. Global solar radiation
    4. Downward LW radiation
    5. Upward LW and SW radiation (optional)
    6. Surface three-hourly SYNOP measurements, where possible
    7. Twice-daily radiosonde soundings at a nearby facility, where possible
    8. Measurement of screen temperature, atmospheric pressure and relative humidity, as co-located meteorological data, where possible
- No decision was yet made on the reporting and sampling frequency on the above parameters.
- A proposition for the World Radiation Monitoring Centre (WRMC) in Zürich, Switzerland as official international database, was made and accepted.
- The data must be collected and submitted to the database in one-month batches with a maximum delay of three months, to allow for local quality control, transfer to magnetic media, etc (no File Transfer Protocol (FTP) facility existed as yet).
- The target date for first BSRN data to enter the database was set at between September 1991 and March 1992. The final date was 1 January 1992.

Other outcomes of the second workshop were:

- The Scientific Evaluation Panel, who was to be an integral part of the BSRN management system, was established, and responsibilities were defined.

- Feedback from a workshop on pyrgeometer errors, that took place five months earlier in Toronto, Canada, were presented. Unlike the World Radiometric Reference (WRR) for SW measurements, no absolute reference existed for LW radiation. In fact, it was recognized that it is not yet well understood.

Investigations were made on the following technical issues:

- Quantification of uncertainties related to circumsolar radiation in measuring global/direct/diffuse radiation and other pyranometer errors.
- Calibration of a pyrheliometer taking turbidity into account.
- The characterization and calibration of LW radiometers.

Meanwhile, the first data received as BSRN data, were the January 1992 sets from the four USA stations of Barrow, Bermuda, Boulder and the South Pole. Of the 27 proposed sites at that time, five more became archiving (submitted data) during the same year. They were Ny Alesund-Spitzbergen (Norway), Payerne (Switzerland), Kwajalein (Marshall Islands, USA), Ilorin (Nigeria) and Georg von Neumayer (Germany / Antarctica) (Gilgen *et al.*, 1993). Figure 1.1 shows the geographical location of this "pioneer" group of BSRN stations in 1992/1993, together with provisional (planned) BSRN sites.

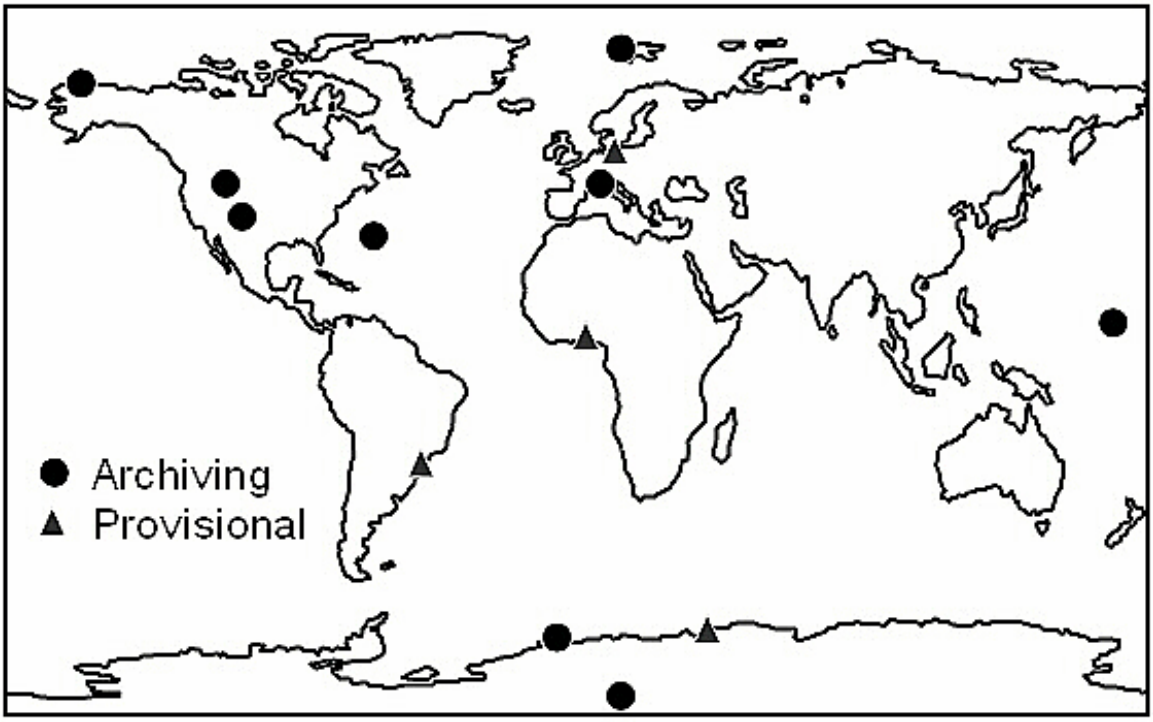

Figure 1.1 *The first group of archiving "pioneer" BSRN stations for 1992/1993, together with the provisional sites at that time*

1.1.3.3 **Third workshop** *(Zürich, Switzerland, 12 to 16 September 1994)*

The premises for the third workshop was the *Eidgenössische Technische Hochschule Zürich* (ETHZ), translated as the Swiss Federal Institute of Technology, which had previously been decided to be the central location of the BSRN database.

Key points addressed at this meeting (WCRP, 1995) were:

- Establishment of the database at ETHZ was completed with the purchasing of suitable computer equipment and the assignment of a full-time position for a data manager (Dr Hermann Hegner). The database was designed by Dr. Hans Gilgen, also from ETHZ, who based it upon the database of the Global Energy Balance Archive (GEBA) that was in existence since 1988 (Gilgen *et al.*, 1997). Data files were already received from the pioneer stations, and would be processed in due course.
- The ideal for BSRN data sampling and reporting frequency was set at one-minute average, standard deviation, minimum and maximum of one-second samples. It was appreciated that not all stations could comply immediately, hence records at longer intervals were also acceptable up to the end of 1997.
- The importance of co-located meteorological data (surface and upper-air) was again emphasized, but no final format of such observations was decided upon.
- Data to the database needed to be dispatched to the archive in one-month batches within a period of six months of the time of observation.
- Spectral optical depth measurements needed to be included as part of the extended BSRN observations programme, wherever possible.
- Co-operation with the ARM project was encouraged.

The BSRN Manual was in preparation, although not completed yet. The completion of this manual was set as a priority.

Working groups were formed to investigate:

- The need for continuously using an all-weather cavity radiometer (with a window) as reference for an operational pyrherliometer.
- The possibility of standardizing LW calibration procedures and measurements.

- Solutions for BSRN stations operated in extreme cold conditions.
- The communication between BSRN stations to exchange expertise (Email-list).

Following the annual BSRN report to the Working Group on Radiative Fluxes on 23 July 1996, Pierre Morel, former Director of the WCRP, described the BSRN as ***"a major success story of the WCRP".***

1.1.3.4 Fourth workshop *(Boulder, CO, USA, 12 to 16 August 1996)*

At this stage, 351 monthly files were generated by 11 BSRN stations and submitted to the database, but only 177 of them passed the stringent consistency checks (WCRP,1997). These sites were situated over a wide selection of oceanic, polar, subtropical, equatorial and high-altitude locations. There were also 17 other stations pending at that stage.

The fourth workshop was set to make decisions on the future of the network, and which additional sites, if any, were needed to complete the first phase of the network.

- Additional measurements at stations were to be in order of priority: (a) Aerosol Optical Depth (AOD), (b) Cloud base height, (c) Ultraviolet-B (UVB) and (d) Photosynthetically Active Radiation (PAR).
- A shaded, ventilated pyrgeometer was accepted to be suitable for LW measurements in BSRN.

The first draft of the operations manual was presented to the group and advice was given on a few unclear issues. Sub-groups were formed to report back to Dr Mc Arthur, and a final target date for completion of the first version of the manual (version 1.0) was set for December 1996.

An internet BSRN homepage (*http://bsrn.ethz.ch*) was introduced. This was envisaged to serve as a public platform from where detailed information about the WRMC, particulars of existing and planned stations, as well as general news could be displayed and obtained. An additional FTP site was also regarded as an important facility that could make data submission to clients much easier. Finally, an Internet-based retrieval interface for clients was also in the process of being established.

Some technical issues surfaced and as a consequence working groups were assigned to investigate the following:

- Outstanding pyrheliometric questions and the sensible use of a cavity radiometer.
- The thermal offset that occurs in pyranometers (how accurately can “nothing” be measured?)
- Establishment of a LW radiation measurement standard similar to the WRR in SW measurements. As a first attempt, pyrgeometer round-robin calibrating experiments were organized.

Amidst all this activity, the Southern Hemisphere (SH) was still poorly represented with only a few stations (Figure 1.2), compared to the populated Northern Hemisphere (NH). The large African continent was specifically poorly represented with only one station, namely Ilorin in Nigeria.

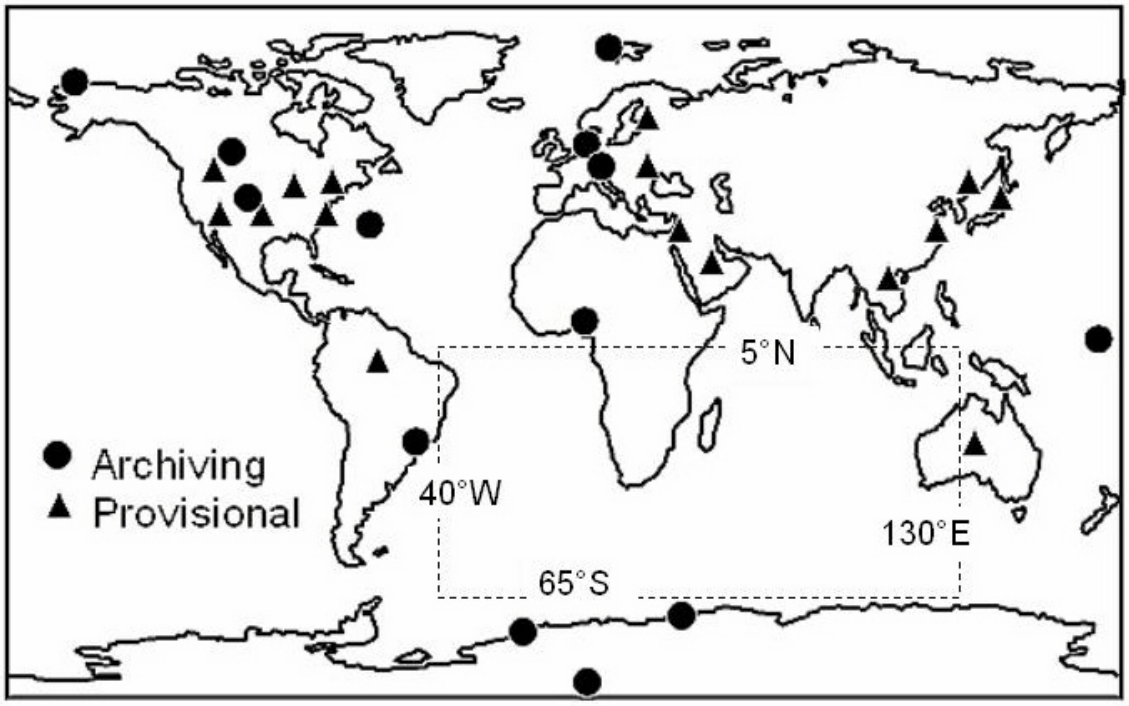

Figure 1.2 *BSRN locations (archiving and provisional) at the time South Africa was considered to join the network. The observational gap is shown in dashed lines.*

1.2 SOUTH AFRICA’S INVOLVEMENT

1.2.1 Strategic importance of South Africa in a global network

Figure 1.2 depicts the existing operational and proposed BSRN stations towards the end of 1995 (at the time South Africa re-considered its position since the 1989 proposal). An

observation gap in the SH (including the southern oceans) is indicated, spanning from approximately 5°N to 65°S (70° interval in latitude) and 40°W to 130°E (170° interval in longitude), which needed urgent representation. This observation gap accounts for about 18% of the Earth's total surface. From Figure 1.2 it is also evident that the SH was poorly represented with only 3 operational stations versus 20 of the NH. South Africa was strategically well placed to fulfil the need for representation at that time.

Another important factor is the much smaller ratio of land versus ocean in the SH versus the NH. This makes it difficult to deploy a sufficiently dense and reliable ground network for measuring meteorological parameters among which are surface fluxes of radiation. The use of remote sensing as a medium for weather observations is therefore much more popular in the SH than in the NH, where large surface areas are covered by continents. The presence of adequate satellite verification points for "ground truthing" in the form of reliable ground-based stations, which do not exist in the SH. This emphasises the fact that South Africa, as a result of its strategic location, could make a significant contribution.

1.2.2 South Africa's unique contribution

As mentioned before, South Africa was represented at the 1989 Würzburg conference and showed interest in offering a location to be developed as a BSRN site. At that time, the three most possible ground locations were the following (Archer 1989):

1. The Mossgas oil-drill platform just offshore the town of Mosselbaai as a possible marine ground truth site for satellite verification.
2. Since the ozone monitoring programme of the SAWS was re-instated at the Irene Weather Office, just south of Pretoria, possible co-location of land-based ozone measurements by the Dobson spectrophotometer and BSRN measurements were considered.
3. The weather office at Upington as a land-based, non-urban observation site, that is representative of a southern African semi-arid Savannah climate.

At that time the last option (option 3) emerged as more favourable, seen in the light that Namibia was the initial candidate country to represent southern Africa in the GBSRN and Upington was the closest location to Namibia. For various reasons (not outlined here) the development of a BSRN site was not followed up in the years thereafter, and thus, the initial offer to South Africa eventually lapsed (Archer,1997).

Six years later, during November 1995 at the Eighth International Pyrheliometric comparisons (IPC-VIII) in Davos, Switzerland, South Africa was again represented. The offer to South Africa was re-opened, and a new proposal was made.

This offer was provisionally accepted, by virtue of a better outlook towards the future which was the result of an open door to WMO and associated assistance since the first democratic elections of April 1994 and the associated stability in terms of a political future. Without international involvement and co-operation, a South African BSRN site would have had very little chance of success.

However, the previous suggestion to make the Weather Office of Upington a BSRN site was no longer supported (Archer, 1997), and a new suitable location had to be found.

1.2.3 Selection of the most suitable site

Since the 1989 inception, the BSRN management gathered a lot of new site location information and experience and subsequently, had a clearer picture of particular site requirements. Hence the new offer for South Africa's participation also included a new set of criteria for selecting a suitable site. These criteria were clearly outlined in a letter received from the BSRN Project Manager after South Africa's 1995 indication of intent to participate.

Automatic weather stations were not part of the equation, since the presence of staff for the best part of 24 hours a day is essential at all prospective BSRN sites. This meant in essence, that only Weather Offices would be considered, of which there were not a large number in operation in South Africa. A Weather Office with a stable future would obviously be strongly recommended. In 1995 the SAWS had Weather Offices at the following locations:

1. Pretoria : SAWS Headquarters
2. Johannesburg International Airport
3. Cape Town International Airport
4. Durban International Airport
5. Port Elizabeth Airport
6. Bloemfontein Airport
7. Kimberley Airport
8. Upington Airport

9. George Airport
10. Pietersburg (now Polokwane) Airport
11. Bethlehem
12. Springbok
13. Calvinia
14. Irene
15. De Aar

Specific requirements and implications for selecting a candidate site for South Africa are listed below:

(i) *The site must be well away from coastal locations. None of the BSRN marine applications were envisaged for the proposed South African site.*
This severely narrowed the possible candidate sites, since a number of Weather Offices (3, 4, 5 and 9) are coastal sites located at major airports.

(ii) *The site must be located in a non-urban environment, as far as possible from urban influences, although it must be accessible to at least one trained person once a day.*
This eliminated all of the larger Weather Offices located in or around major metropolitan areas, namely 1, 2, 6, 7, 10 and 14.

(iii) *At the proposed site a first-order climate station with top-quality equipment manned by dedicated staff is required.*
All of the weather offices are indeed staffed first-order stations and at the time most of them operated 24 hours per day. Remaining were Weather Offices 8, 11, 12, 13 and 15.

(iv) *The quantities of direct radiation, diffuse radiation, long wave down welling radiation and desirably global radiation, must be measured continuously, with backup and calibration facilities also being available.*
These criteria implied that n fact, none of the existing SAWS radiation instrumentation could be used, and therefore, an entirely new facility had to be built altogether. However, the WMO offered a complete set of basic instrumentation to initiate the programme. This option, therefore, did not favour or eliminate any existing Weather Offices.

(v) *It is desirable to have surrounding land of uniform character in surface and land-use for a radius of at least 50 km from the site to yield a representative satellite*

impression.

The following sites were disqualified: Weather Office 13 (situated alongside a major river (The Orange) and resulting lush surrounding vegetation not representative of the area) and Weather Offices 11 and 12 (mountainous area that is not regularly representative, more in the case of Bethlehem than Springbok)

(vi) *Upper-air measurement facilities and possibly weather radar must exist within 100 km from the site.*

Weather Office 13 does not have radar or upper-air measurement facilities available.

By means of elimination, Weather Office number 15 (De Aar) stood out as the best remaining site that met the necessary criteria and had all the required facilities on the premises. The Weather Office of De Aar in the Bo-Karoo region of the Northern Cape Province of South Africa (Figure 1.3), was therefore chosen to be the location for the South African BSRN station.

1.2.4 The best location : De Aar

Although the process described in section 1.2.3, that led to De Aar, looks like an elimination process, the following aspects counted strongly in its favour and re-affirmed that the best choice had indeed been made :

- The small town, having a mere 30 500 inhabitants[1] had very little metropolitan growth over the last five decades, and not significantly more is planned. Therefore, the existing population and activities are not envisaged to have any significant impact ("urban heat island") on the radiation regime.
- Development of the area around the proposed site was also not envisaged in the near future (Van den Berg, Town Clerk of De Aar, pers. comm), and as a result, the site has a pristine atmosphere that is amongst the cleanest in South Africa, and representative of the surroundings.
- It is located in a semi-arid region with relatively low rainfall, i.e. a relatively low occurrence of clouds.
- The aerial appearance of the land is uniform in the sense that no major deviations from the land appearance, such as large water bodies or associated green

1. United Nations Population Information: http://www.world-gazetteer.com/c/c_za.htm

vegetation, exist. In fact, the famous "Karoo-Koppies" of that region (Figure 1.4) are known to be "*if you've seen one, you have seen them all".*

- The likelihood of snow falling is 1 out of 450, or it can be expressed as 0.8 snow-days per year (SAWB, 1986). Monthly average maximum and minimum temperatures vary from 0°C during the austral winter to 33°C during the austral summer (Figure 1.5). The long-term minimum rainfall for every month is zero since there was always a calendar month in history where no rain fell (Figure 1.6).
- Rainfall can be regarded as sporadic, since the maximum values are several times the magnitude of the mean values. Maximum rain occurs in March, endemic of the summer rainfall region that comprises the entire eastern interior of the Southern African plateau.
- The site is also centrally located in the country (Figure 1.3).

Figure 1.3 *Provincial map of South Africa depicting the central position of De Aar*

As listed in Table 1.1, the De Aar Weather Office has the following references:

Table 1.1 *Essential references for De Aar Weather Office*

Latitude	*30.665°S*
Longitude	*23.993°E*
Altitude above mean sea level	*1287 m*
Local time zone	*GMT + 2 hours*
SYNOP number	*68538*
Civil aviation METAR code	FADY

Figure 1.4 *The instrument camp at De Aar Weather Office, where the BSRN site is located. Note the semi-arid landscape and uniform"Karoo-koppies" in the background*

In the following sections, climate statistics (SAWB, 1986) applicable to De Aar are discussed:

1.2.4.1 Temperature

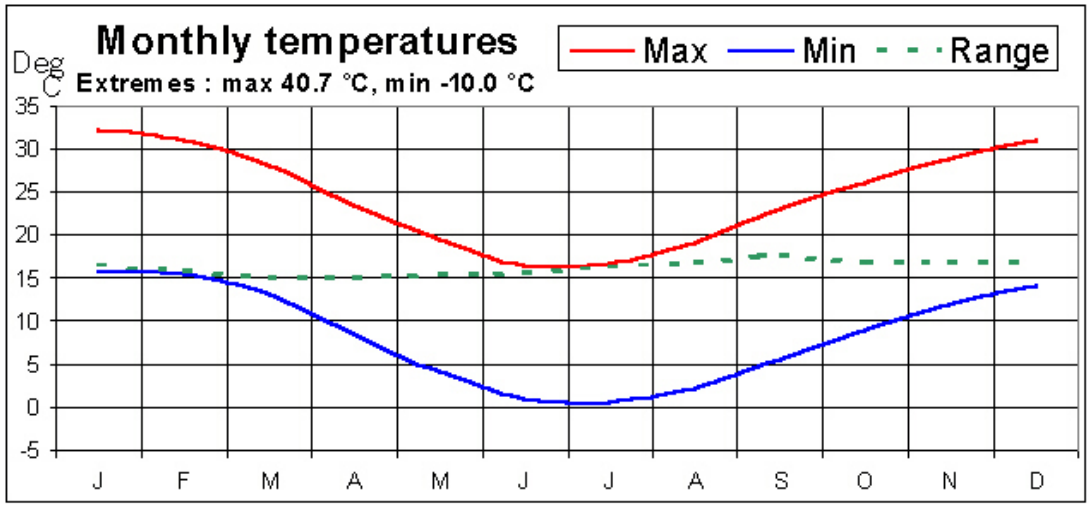

Figure 1.5 *Monthly average maximum and minimum temperature as well as temperature range, measured in ^{o}C at the De Aar Weather Office*

Monthly average temperatures at De Aar (Figure 1.5) have a very small range – even though there are significant fluctuations during the course of a year, the range (monthly maximum minus monthly minimum) is consistently 16 degrees with a deviation of only one degree. Extreme temperatures recorded in De Aar's history were -10.0°C and 40.7°C, respectively.

1.2.4.2 Precipitation

Monthly precipitation at De Aar (Figure 1.6) shows the following characteristics of episodic occurrence

- The long-term extreme per month is several times the mean (ca. 4 to 7 times).
- The annual mean (305 mm) is substantially (22%) lower than the means of the annual maxima and minima (391 mm).
- The corresponding monthly minumum is zero for all the months of the year. Hence, for this record, no rain fell at least once in each calendar month in history, even during the rain season. That is why "minimum" does not feature in Figure 1.6.

The annual average rainfall maximum occurs in March, typical of the summer rainfall region which dominates the central interior of the Southern African plateau. The peaks for extreme rainfall, however, occur in January and February.

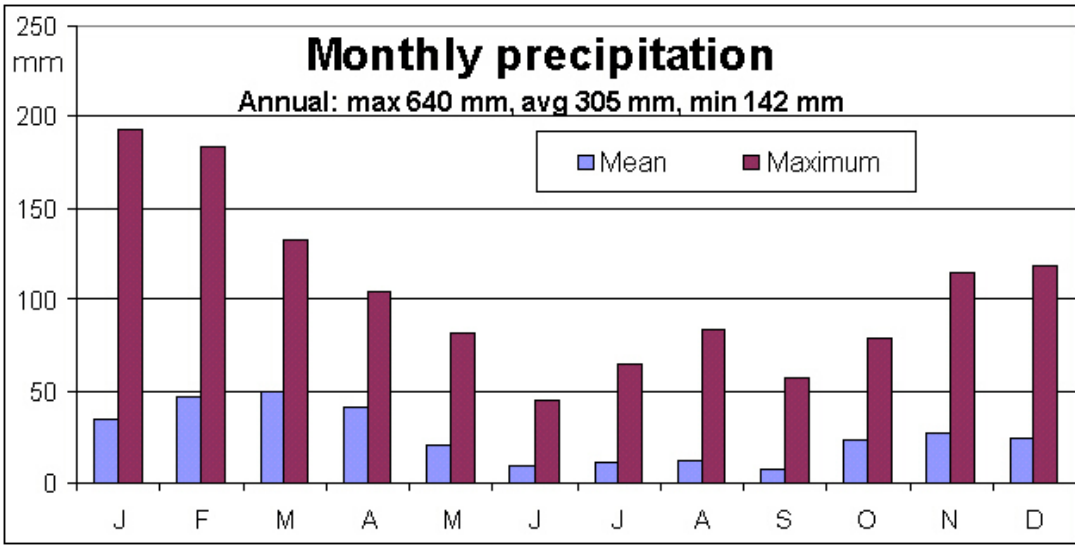

Figure 1.6 *Monthly mean precipitation (light shaded bars) and maximum precipitation (dark shaded bars) for De Aar Weather Office in mm. Note that the minimum precipitation per month is zero.*

1.3 SITE DEVELOPMENT AT DE AAR

During October 1996 a four-man delegation made the first contact with Mr George Wolfaardt (Officer in charge of the De Aar Weather Office), as well as with Mr Johan van den Berg (Town Clerk of De Aar). In turn for the publicity De Aar was to enjoy as a result of this unique development, the Town Council offered their support in principle by assisting with the establishment of infrastructure (Archer, 1997).

In February 1997, the BSRN international project leader has approved the site. Overseas training of local scientists on station management followed in October the same year in order to establish the South African BSRN station. The training included:

- A visit to the Kipp & Zonen factory in Delft, Netherlands, where the manufacturing process (largely by hand) of the various types of radiometers was observed. Having witnessed the rigorous process, the high prices of Kipp and Zonen radiometers are appreciated.
- A visit to the BSRN data centre in Zürich, Switzerland, where personal consultation took place between the visiting local scientists and the BSRN data manager, quality control specialist and other staff members. They are the very people to whom the station scientist is accountable to for data delivery and a personal contact was vital in the process of establishing a good working relationship.
- A visit to the BSRN site and station scientist in Payerne, Switzerland, regarded as a site with the best technological development and serves as an example of what can be achieved (Heimo, 1993). This station was originally selected as one of the "pilot" sites in 1991, and remained on the leading edge of development ever since.
- A visit to the World Radiation Centre (PMOD-WRC) in Davos, Switzerland, where regular calibration, such as the five-yearly International Pyrheliometric Comparisons (IPC), as well as world-leading development in instruments and measurement techniques in radiation and calibration are performed. The famous "group of seven" WRR pyrheliometers, discussed in Section 2.5.2. are housed and operated here.
- A visit to Boulder, Colorado, USA, where the BSRN project leader and associates are stationed. Useful discussions with station scientists, instrument engineers and

data technologists were held. The well-known 300 meter high monitoring tower at the BSRN Station in Boulder was visited.

The WMO-sponsored instruments for the South African station, as well as a cavity reference pyrheliometer with an automated control box, solar tracker, uninterrupted power supply, and main accessories for the initial installation, such as data loggers and field enclosures, were received in Pretoria between December 1997 and January 1998.

The complete set of hardware was erected on the rooftop of SAWS headquarters in Pretoria. The system was wired to function in full operation as it would on-site. This included uninterrupted operation of the solar tracker with all the radiometers, ventilators and data loggers for more than one year (WCRP,1998), whilst Wide Area Network (WAN) computer links between Pretoria and De Aar were developed and installed by the SAWB's Information Technology (IT) group.

This development also allowed for time to test numerous configurations in order to establish the best working system. Fine adjustments to the system were also undertaken and developed. Finally, the entire communication system between De Aar and Pretoria was simulated and tested several times. The advice, practical ideas and eventual unique solutions in this respect, provide by Cal Archer, must be emphasized.

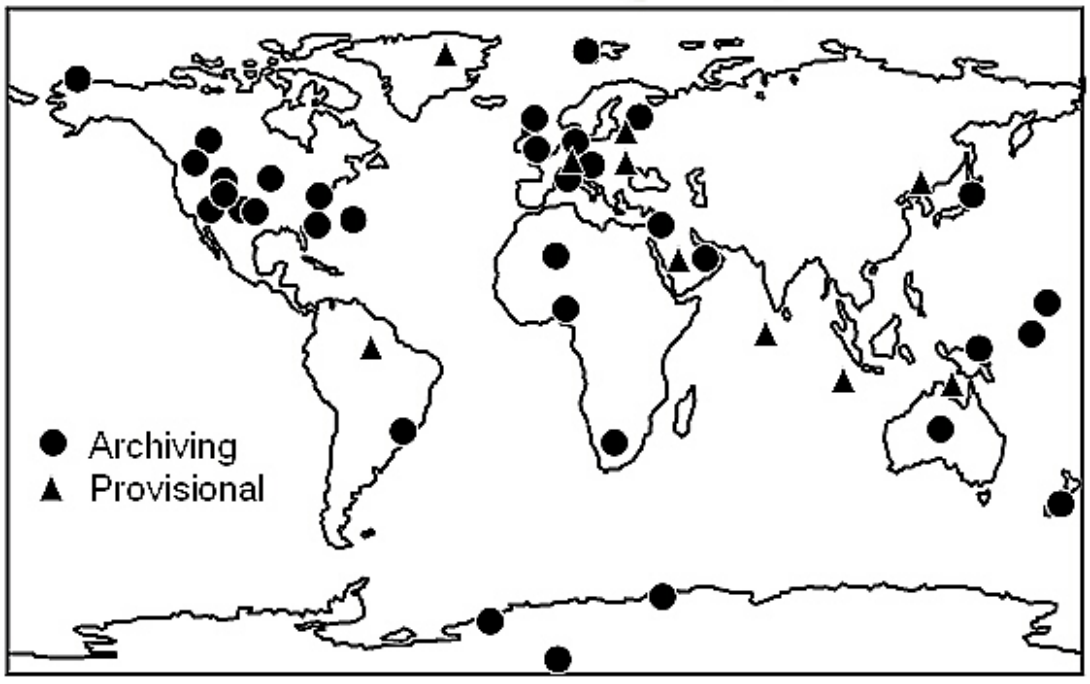

Figure 1.7 *BSRN sites, both archiving and provisional, in 2003*

At the same time, plans to prepare the site at De Aar for final installation were introduced. One trip to survey the site and surroundings, and to liase with the Town Council, was undertaken in February 1998. This was followed by the delivery and installation of the uninterrupted power supply, power cabling, communication facilities as well as foot-mounting brackets for the radiometers in December 1998.

The Town Council unfortunately had to withdraw their offer to erect a security fence, but instead installed a certified 220 Volt power point on the site. In June 1999, a barbed-wire security fence with a lockable pedestrian gate was erected by a local service provider around the perimeter of the site hillock, taking special precaution to make as little impact on the environment and projected measurement plan as possible. By 2000 the De Aar station was in full operation (WCRP, 2001; WCRP, 2002), and since then is making a significant contribution to the global BSRN as in 2003 (Figure 1.7).

1.4 OBJECTIVES OF THIS RESEARCH

The objectives of this research focus on the establishment of the De Aar BSRN station and the subsequent quality control of recorded data.

The primary objective of this research is to document the technical and other means by which the De Aar BSRN station, which embodies the application of international standards of radiation measurement to South Africa, was established.

This objective has been achieved by means of a thorough study of BSRN data requirements, as well as practical experience incurred by the author. The author was both instrumental towards and actively involved in the management and application of the many procedures that preceded the final installation. As official station scientist he visits the De Aar site on a regular basis, ideally twice annually, to perform major maintenance on the site, including radiometer calibration. To keep abreast with the latest developments in technology and maintain sound international relations, several workshops were attended and institutions in countries such as Switzerland, Holland, Hungary, Australia, Canada and the USA visited.

The secondary objective of this research is to develop, evaluate and introduce quality assurance procedures (according to BSRN requirements) in such a way that it can be applied on a routine basis to measured data before submission to the WRMC archive.

This has been achieved by detailed analysis of the available BSRN data spanning three years since inception of the site, as well as study of relevant literature. For this purpose, software (FORTRAN code and Microsoft Excel spreadsheets) has been developed by the author.

The methods applied in this research are:

- Thorough literature study of the background to the BSRN programme and how South Africa became involved
- An explanation of the scientific measurement plan, and how the design and testing of the South African system led towards realising the measurement plan in South Africa
- Detailed analysis of the available data of the BSRN station since inception, and application of the various quality assurance techniques.

Apart from the academic content, the author wishes to compile a useful document as reference tool with respect to South Africa's involvement in the BSRN programme and a guideline for future generations, embarking on future developments. This could include either upgrading of the existing facility, or the establishment, should the need arise, of new BSRN sites in the Southern African Development Community (SADC) region.

1.5 ORGANISATION OF THIS DISSERTATION

Following this Chapter (introduction to the BSRN programme and South Africa's involvement), the following topics per chapter were studied:

Chapter 2: Scientific plan

The logical next step after the introduction is the definition of a sound scientific measurement plan for the South African BSRN site and the elucidation of numerous aspects surrounding it. These aspects include basics of radiation measurement in the atmosphere, associated measurement techniques and instrumentation.

Chapter 3: System design

Forthcoming from the measurement plan, is the design of a useful measurement system to

materialize the plan. In this case, some site operational issues encountered during the initial phases of the project are investigated. This is brought in context with radiometer calibration and data management.

Chapter 4: Quality control

After a system has been designed and installed, the resultant data needs to be quality controlled. This Chapter explains the different terminology involved, elucidates the various WRMC quality control procedures and presents an analysis of three complete years of BSRN data to which the said procedures have been applied.

Chapter 5: Case studies

Special and very unique measurement opportunities presented themselves when two total solar eclipses traversed Southern Africa in 2001 and 2002. In both cases, a significant amount of the partial phases were visible over De Aar, in pristine measurement conditions, that delivered data lending itself to various forms of comparisons.

Chapter 6: Conclusions and recommendations

A summary on the position of the South African BSRN site in all its contexts is presented, along with the most important findings and subsequent conclusions forthcoming from this study.

References:

A standard and exhaustive listing of all sources that were consulted in this research.

Appendices:

Appendix A.	Photo pages
Appendix B.	Station-to-archive file format
Appendix C.	Specific data for a typical year at De Aar
Appendix D.	The Köppen climate zone classification
Appendix E.	Connection and operation of a pyrgeometer

CHAPTER 2

SCIENTIFIC PLAN

In any scientific endeavour, the existence and application of a sound scientific plan is an important link. Within the BSRN, it takes the form of a data measurement and data management plan. Many of the aspects of this plan were already directly or indirectly addressed in the previous Chapter, hence this Chapter does not endeavour to be a repetition, but a contextualization and in some ways, expansion. Having sketched the plan, this Chapter then moves forward to focus on processes leading to radiation fluxes in the Earth's atmosphere, as well as associated measurement techniques to best capture those radiation fluxes. This comprises relevant instrumentation, completing the larger picture of a radiation measurement plan.

2.1 SCIENTIFIC GOALS AND OBJECTIVES OF THE BSRN

Unlike networks that have evolved from a hypothesis through a design phase and then proceed to instrumentation implementation, the BSRN has developed in a "segmented" manner (Mc Arthur as quoted by Dutton, 1996). For BSRN to become a reality, much resources were drawn from existing infrastructure. In some cases, upgrades to meet BSRN standards were made as described by Heimo *et al.* (1993). Notwithstanding these facts, the mission and vision for the BSRN remained clearly defined as outlined in section 2.1:

2.1.1 Goals

The original goals for measurements in the BSRN, as defined at the 1990 Washington workshop and associated correspondence, are as follows (Gilgen *et al.*, 1991; Mc Arthur, 1998):

Goal 1: To monitor surface radiation fluxes to the best possible accuracy using the best possible methods.

Goal 2: To provide data for calibrating satellite-based estimates of surface radiative fluxes.

Goal 3: To provide data suitable for boundary values in atmospheric modelling and application in atmospheric model verification.

2.1.2 Objectives

These goals are now further expressed in terms of specified objectives, as sketched by authors such as Mc Arthur (1998):

Within goal 1:

Objective 1.1: To measure both the surface SW and LW radiation components at specific locations with sufficient accuracy in order to reveal long-term trends.

Objective 1.2: To standardize and maintain the best possible site operation procedures throughout the global network.

Objective 1.3: To obtain simultaneous (parallel) measurements of meteorological parameters such as clouds, ozone and upper air profiles, that may contribute to research related to the measurement of solar radiation fluxes.

Objective 1.4: To establish a cost-effective central data processing, archiving and data management centre.

Within goal 2:

Objective 2.1: To determine specific parameters to characterize a site for satellite applications (albedo, clouds, aerosols) in a quantitative manner.

Objective 2.2: To validate a site for remote sensing measurements by performing in-situ measurements of surface reflectance over a large area comparable to one pixel of satellite imagery.

Objective 2.3: To develop cost-effective equipment and methods for spectral ultraviolet (UV) and infrared (IR) solar radiation budget measurements that will contribute to the improvement of satellite algorithm design and validation of satellite SRB determinations.

Objective 2.4: To perform investigations to improve the design and performance of "standardized" instrumentation, such as sunphotometers and pyranometers, and incorporate, improve and develop more sophisticated remote sensing instrumentation to enhance the cloud-observation abilities of the global BSRN.

Within goal 3:

Objective 3.1: To meet SRB measurement standards by improving the quality of measurement, especially downwelling irradiance, being quantities included in the basic BSRN measurement programme.

Objective 3.2: To study the radiative properties of broken and inhomogeneous clouds, in order to improve the current understanding thereof.

2.1.3 Practical significance

These objectives find practical significance in the following way:

Objective 1.1

The measurement of surface fluxes is the very basic and most feasible form of radiation measurement, since ground-based equipment can best utilize manageability and uniform global deployment in a terrestrial network. It can also best exploit existing radiometric infrastructure. Although the emphasis in basic measurements is placed on downwelling

parameters, upwelling parameters from various tall structures of varying height should not be neglected, when measurable. Upwelling quantities add significant value when combined with the basic (downwelling) quantities, as described in Section 6.3.2.8. It also provides a firmer ground for quality control techniques as discussed in various sections of Chapter 4, and summarized in Section 6.3.2.8.

It is desirable to measure both SW and LW radiation fluxes to foster a sound understanding of solar-earth-radiation fluxes and processes. The specificness of locations is aimed at reaching a fair amount of representativity of sites with comparable radiation accuracy transcending global climate zones, as elucidated in Section 2.2.7.2. The objective of revealing long-term trends reflects on the need for superior accuracy, since a trend is only visible once a "signal" is significantly discernible from "noise".

Objective 1.2

Any form of measurement is only as good as the procedures followed to attain it, like "a chain is only as strong as its weakest link". The establishment of standard operating procedures and their deployment, as far as practically possible in terms of procedures, cleaning, maintenance and calibration at all sites in the network, is a necessary condition towards producing data of comparable quality on a global scale.

One proven way to effectively ensure data and procedural uniformity in a truly global project, is the implementation of site audits. Site audits are successfully in operation in other WMO measurement endeavours such as GAW, where the Swiss Federal Laboratory for Materials Research and Testing (EMPA) is conducting regular site audits. This takes the form of data audits, as well as system performance audits, as described by Hofer *et al.* (1998) and WMO (2003).

In the BSRN context, however, the added value versus cost factor remains to be justified. Large amounts of travel and subsistence fees will have to be spent over a long period to drive this process, and a suitably qualified candidate is most likely involved in a number of research projects at his/her institution. The author suggests, that partnerships with other GAW institutions, sharing resources and expertise, can be formed to partially address this issue.

Objective 1.3

Simultaneous measurement of meteorological parameters at sites within a reasonable distance of the radiation measuring site, preferable on the same site, greatly improves the understanding of behaviour in radiation parameters.

The surface measurement of temperature and humidity aids in understanding the clear-sky LWD flux, whilst knowledge on aerosol loading improves the understanding of diffuse radiation. Knowledge on surface vegetation aids in quantifying surface albedo and associated radiation processes. Knowledge on surface and upper-air winds aids in trajectory modelling that can explain the transport to and existence of aerosol loading in a particular area. Ozone measurements complements measurement of UV readings, whilst knowledge on Precipitable Water Vapour (PWV) also enhances understanding of pressure, temperature and humidity of the upper-air profile as measured directly using balloon-tethered rawinsondes. The upper-air profile creates a three-dimensional picture of the atmosphere, which leads to the foundation of a Radiative Transfer Model (RTM) input. The said measurements are also input parameters to aid the modelling of global climate change.

Objective 1.4

The effective management of any dataset is vital towards the success of the associated measurement endeavour. Therefore, central responsibility with respect to data management must be assumed by a well-established institution and the data must be uniformly quality controlled, using the same procedures for all captured data. In the case of BSRN, this role is well assumed by the WRMC in ETHZ. This centre serves as the focal point from which queries with respect to the data can be answered, and effectively addresses the question of where data-ownership and the associated intellectual property resides.

Objective 2.1

One of the original aims of the BSRN programme at its inception was to serve as a measure for satellite ground truthing (WCRP-64, 1991). Remote sensing is the most effective and area-efficient way of surface-data collection in the SH since it has less land available for the deployment of terrestrial stations compared to the NH. However, remote sensors such as satellites, need a reliable ground measuring site which can serve as a reference. Another

factor that must be taken into consideration, is that the characteristics of remote sensors change with time (WCRP-64, 1991), therefore, the satellite involvement with ground sites also has a dynamic and sustained character. The BSRN can determine, in a quantitative manner, specific parameters to characterize a site for satellite applications (albedo, clouds, aerosols), and in this way establish a sound partnership with the satellite community.

Objective 2.2

Representativeness of the measurements, in terms of usefulness to the satellite community, is also an important link in any measurement plan. In the case of De Aar, it was ascertained before assuming the site, that the surrounding geography ("Karoo-koppies") exhibits the most practically uniform land in the vicinity of a suitable site in South Africa (as discussed in Section 1.2.3) It can also be mentioned that, in order to validate the site for remote sensing measurements, in-situ measurements of surface reflectance over a large area should be comparable to one pixel of satellite imagery. Therefore the usefulness of De Aar as a satellite site is probably the best South Africa can offer.

Objective 2.3

The specific measurement of radiation in bands of the electromagnetic spectrum outside visible wavelengths is justified, since it is known that a small variability in solar output translates to significant changes in, for example, UV irradiance (Fröhlich, 1989). The involvement of special measurements is therefore another branch of BSRN having potential to serve additional needs. In the Southern African context, BSRN measurements of UV radiation can also link to the public UV irradiance awareness campaign of the SAWS since South Africa is one of the countries in the world that has exceptionally high UV irradiance exposure during the Austral summer.

Furthermore, cost-effective equipment and methods for the measurement of the spectral UV and IR radiation budget will contribute to the improvement of satellite algorithm design and validation of satellite SRB determinations.

Objective 2.4

Special emphasis is placed upon the deployment of sunphotometry and cloud-imaging by means of automatic video capturing and analysis. The influence of the erring human hand are increasingly excluded in routine observations in order to obtain the quality of observation required for measurements of high accuracy. Despite the automation of almost all weather measurements, the quantification and identification of cloud types in SYNOP and other observations were one of the parameters that was still measured manually. Recent developments now facilitate the recording of clouds automatically and in greater detail, using software analysis of video-captured images.

Objective 3.1

The specific referral to SRB standards is aimed towards being representative of rendering data for verification of remotely sensed quantities. Other institutions and projects involved in this effort are the Global Energy and Water Cycle Experiment (GEWEX), the European Centre for Medium Term Weather Forecast (ECMWF), the National Oceanic and Atmospheric Administration (NOAA), as well as a variety of local and regional radiation climatologies with the potential of many applications (Dutton, 2002). Modern remote sensing is capable of accurately sensing downwelling quantities.

Objective 3.2

As mentioned in Objective 2.4, cloud studies can now be automated. Therefore digital ways of comparing cloud properties and radiation numbers can lead to the better understanding of how especially broken and inhomogeneous clouds influence the micro-climate.

2.2 ASPECTS OF THE SCIENTIFIC PLAN

2.2.1 Data sampling rate

The uniform standard format of BSRN measurements, is one-second samples of each quantity, summarized and archived every minute as the average, standard deviation, minimum and maximum of all the samples for that particular minute (WCRP-54, 1991;

WCRP-64, 1991). The decision for 1 Hz sampling was based upon the 1/e response time for first-class instruments. The ratio 1/e constant for a given radiometer is the time necessary for the radiometer output to become equal to 1/e = 1/2.718 = 0.368 of the initial input value. In first-class radiometers it is close to one second, therefore, 1 Hz- samples are an attempt not to misrepresent any feature in radiation fluxes (Ohmura *et al.*, 1998).

The logical unit of data submission to the central data centre in Zürich is one month. In that monthly report, the radiation data are reported in the said quantities per minute. The time-frame (being an international network) is Universal Time (UT) for all measurements (no daylight savings are incorporated).

2.2.2 Accuracy

Since the Würzburg meeting, certain radiometric accuracy targets were set. It was hoped that with improved observational techniques and deeper research, those targets would be met. Table 2.1 reflects the evolution of these BSRN targets through the years.

Table 2.1 *Evolution of target radiometric accuracy in BSRN. Values in W.m^{-2}*

Quantity	1	2	3	4
Direct radiation	2	-	2	2
Diffuse radiation	5	10	5	5
Global radiation	5	15	5	5
Reflected SW radiation	-	15	-	-
Downwelling LW radiation	20	30	10	10
Upwelling LW radiation	-	30	-	-

Key to columns of Table 2.1:

1. Initial excpected accuracy as deemed necessary by satellite and model communities (Morel,1990).

2. First refinement (WCRP-54) in March 1991.

3. Second refinement (WCRP-64) in November 1991.

4. Achieved in 1995 (Ohmura *et al.*, 1998, Mc Arthur, 1998) and based upon uncertainty estimates for best-known practices in calibration and quality control at existing BSRN sites. The numbers are expected acceptable maximum deviations from the "true" measured values in Watts per square metre ($W.m^{-2}$). The deviations are expressed as the uncertainty from the true value for a 1-minute average over an ensemble of 1Hz measurements (Ohmura *et al.*, 1998).

Discussion of Table 2.1 in terms of each measurement quantity:

2.2.2.1 Direct radiation

The target accuracy for direct radiation is 2 $W.m^{-2}$ – therefore the most accurate radiometer, a cavity, (Figure 2.4), needs to feature in the measurements. However, this poses a challenge to BSRN for two reasons:

- A cavity radiometer samples once roughly every 1 to 3 minutes when in full operation (WRC, 2001), while the BSRN requires one-second samples on a continuous basis.

- For operation in all weather conditions, protection is needed. The delicate inner parts need to be protected from rain. Wind protection is also needed to preserve the thermal properties of the radiometer. However, this protection (typically a window) is known to absorb significant portions of the solar spectrum (discussed in Section 3.1.1.2). The presence of a window therefore limits the radiometer in terms of desired accuracy.

To resolve these issues, simultaneous operation of a thermopile pyrheliometer (Figure 2.5), together with the cavity radiometer was recommended by Mc Arthur (1998). This is expected to take the form of parallel measurements. While the thermopile samples at 1 Hz, the cavity takes measurements as often as practically possible (1 to 3 minutes).

A further recommendation is, that the pyrheliometer has a body temperature sensor in order to compensate for thermal offsets that may be experienced by the thermopile. The pyrheliometer and cavity radiometer ideally forms part of a tracker system, which makes use of a quadrant sensor to actively point the radiometers towards the sun.

2.2.2.2 Global radiation

Global radiation is measured with an unshaded pyranometer (Figure 2.6), preferably on a fixed stand, to allow for minimum distortion of azimuthal errors induced if mounted on a horizontally rotating tracker platform. Target accuracy is also 2 $W.m^{-2}$ - though a number of factors lead to uncertainties in the measurement. These factors include non-linear output of the sensor, uneven response of the thermopile, the cosine error, as described in Section 3.1.2.2, and thermopile thermal offsets, as discussed in Section 3.1.2.3. The standard BSRN one-minute statistics reported are derived from 1 Hz samples taken on a continuous basis. The pyranometer is recommended to be perpetually ventilated and to have a body temperature sensor to compensate for thermal offsets not covered by the ventilation.

2.2.2.3 Diffuse radiation

The target accuracy of diffuse radiation is 4 $W.m^{-2}$. This is less strict than the direct and global components since additional factors impact on the measurement accuracy. These factors are: unevenness of the solar occultation (shading), uneven balance of the radiometer resulting from unsteadiness of the solar tracker table and uneven azimuthal responses of the radiometer due to a horizontally revolving tracker table. Diffuse radiation is measured by means of a shaded pyranometer, preferably identical to the global irradiance pyranometer. The pyranometer should also be ventilated to minimize thermal offsets, and a body temperature sensor should be present in order to attempt to correct recorded data for thermal offsets.

2.2.2.4 Reflected SW radiation

A pyranometer, mounted on a tall structure and facing downwards, is recommended. This pyranometer should be treated in any other respect like a global pyranometer, except for a shielding plate to block direct radiation at very low solar elevation angles. A minimum height of 30 metres is recommended to yield a representative view of the surroundings.

2.2.2.5 Downwelling LW radiation

Target accuracy for downwelling LW radiation is the lowest for basic quantities: 10 $W.m^{-2}$.

This accuracy is believed to be improved (Philipona *et al.*, 2001) by Swiss modification of the pyrgeometer instrument, where the dome temperature is measured on more than one spot. (Philipona, 1995). The quantities associated with long-wave radiation, are (a) output from the thermopile, (b) body temperature, and (c) dome temperature. The one-minute statistics of LW irradiance are compiled from 1 Hz samples. However, a few practical challenges lead to the calculation of the LW irradiance using the logger's internal programming. Such a programme requires extensive coding and can only be executed in the course of two to three seconds, rendering the frequency of sampling less than 1 Hz. The pyrgeometer must also be ventilated (Van Lammeren and Hulshof, 1994) and shaded continuously (Section 3.1.3). The reported parameters towards WRMC are one-minute statistics of LW irradiance only.

2.2.2.6 Upwelling LW radiation

The instrument and operational procedure to measure upwelling LW radiation is identical to the one for downwelling LW radiation, except that it is facing downward and supported by a similar structure to the description in Section 2.2.2.4.

2.2.2.7 Ancillary measurements

Surface meteorological parameters are needed to add value to the understanding of surface fluxes of especially the LW portion of the electromagnetic spectrum. They are (a) Stevenson screen temperature, (b) relative humidity and (c) pressure. These quantities are measured, at the same height from ground level as the LW instrument. The standard WMO meteorological instrument height is 1.2 metres (Meteorological Office, 1982).

2.2.3 Data acquisition

Time accuracy should be of highest quality. Mc Arthur (1998) recommended that it to be less than 1% of the averaging period (in the BSRN case less than 1 second). Data needs to be acquired in the most economical format possible, as far as space restrictions on the logging devices and the required number of significant figures for accuracy are concerned (discussed in Section 3.1.6).

2.2.4 Calibration

Accurate calibration is a critical component of any radiometric system (Asmus and Grant, 1999). In wide terms, calibration of an instrument is performed when a reliable reference instrument is operated side by side with the site's operational instrument. The reference instrument has traceability to a world standard, and the resultant deviations from the site operational instrument output, with respect to the standard, are used to rectify the field instrument sensitivity (Reda, 1996) and possibly retrospectively recalculate recorded data from the field instrument (discussed in Section 3.2.2).

2.2.5 Data management

Effective data management is a vital link between data acquisition and submission to the international database. This process is ideally performed by the site scientist, since this person is involved in the entire station operation and is therefore in the best position to judge the validity of any given set or subset of data. The De Aar data management is described in more detail in Section 3.3.

2.2.6 International database

Communication to the international database is established using fixed formats and established protocols, detailed in Appendix B. For data submission, FTP channels to WRMC at ETHZ in Zürich were established. Upon completion of a dataset and subsequent submission to WRMC, the datafile is handled in a way prescribed by the database, details of which are referred to in Section 3.4.2.

2.2.7 Site selection criteria

Selection of suitable sites, addressing the necessary criteria, is also critical for the functioning of a global network, such as the BSRN. Criteria for site selection, as formulated after the Würzburg meeting (De Luisi, 1989) are outlined in the following two sections, viz. Section 2.2.7.1 and Section 2.2.7.2.

2.2.7.1 Satellite measurements

Geographical locations most suitable for satellite validation algorithms were proposed by Schiffer (1990) and Mc Arthur (1998), and are listed in Table 2.2.

Table 2.2 *Site evaluation criteria based upon a selection of desirable surface/atmospheric characteristics and satellite algorithm comparisons*

Characteristic	Locations representing	Example location
Radiation field values	Large variability in synoptic and seasonal time scales	Siberia
Satellite Algorithm Performance	A range of difficulty for set retrievals	Equatorial Indian Ocean, Temperate Oceania
Cloud properties	A range of cloud types	Tropical Pacific
Climate change	The potentially higher sensitivity of a region to changes in global climate	Antarctic Coast, Northern Canada
Satellite coverage	A range dependance on orbit, viewing angle, overlap regions	Spitzbergen, Norway
Unusual atmospheric phenomenon	A range of unusual atmospheric phenomenon (aerosol, clear skies, etc.)	Sahel, Tropical Pacific
Surface cover	A range of surface cover (e.g. snow, sea, ice, ocean, vegetated, desert, etc.)	South Ocean, Ice Island, Equatorial Africa
Climatic regions	A range of climatic regions (polar, tropical, etc.)	Ice Island, Central Australia, Antarctic Coast
Upwelling flux studies	Area where upwelling flux studies would be of particular value to validation, because of the site qualities and in some cases the existence of SRB measurement facilities.	Boulder Tower at Boulder, Colorado, USA
Calibration	Locations possessing relatively uniform and high surface reflectance properties for satellite calibrations	Prairie, Amazon basin

Surface radiation flux information, disseminated at a spatial resolution suitable for climate research, especially over oceans, is presently obtained from satellites. However, there is evidence in the literature, that satellite measurements are in “acute” need for ground-truthing (Whitlock *et al.*, 1995; Pinker *et al.*, 1995; also quoted by Ohmura *et al.*, 1998). The analysis

under discussion by these authors was specifically performed over the African continent where little snow is expected. Yet there were systematic differences in albedo measurements, despite the fact that it was expected that the improved algorithm should at least make a distinction between snow and clouds. These inconclusive results indicated that more reliable remotely sensed information is needed, in which BSRN data may be of significant value.

2.2.7.2 Climate zones

Application of the Köppen climate zone criteria (described in Appendix D) shows how the evolution of the network continued to cover climate zones in a fair and representative way.

Table 2.3 *Evolution of the BSRN climate zone representation*

Group of stations	Climate zone (A to E)					Total
	A	B	C	D	E	
Pioneer group of 1992	Bermuda (Af) Kwajalein (Aw)	Boulder (BS)	Payerne (Cfb)		Ny Alesund (ET) Barrow (ET) Neumayer (EF) South Pole (EF)	**8**
Group up to 1996			Carpentras (Cs) Billings (Cfa) Tateno (Cfa)	Regina (Dfb)		**4**
Group up to 1998	Ilorin (Aw)	Sede Boqer (BW) Alice Springs (BW) De Aar (BS)	Florianopolis (Cwa) Lindenberg (Cfb)	Toravere (Dfc)	Syowa (EF)	**8**
Additions up to 2003	SGP1 (Am) Manus (Aw) Nauru (Am)	Tamanrasset (BW) Boulder SURFRAD (BS) Desert Rock (BW)	Lauder (Cfa) Penn State (Cfa) Goodwin Creek (Cfb)	Fort Peck (Dfb) Bondville (Dfb)		**11**
Total	**6**	**7**	**9**	**4**	**5**	**31**

In Table 2.3, the active BSRN sites up to 2003 are classified into the five main climate zones, and it is also shown how this classification came about by considering the network evolution since 1992. It shows that the total number of stations per climate zone represents a fair distribution. Keep in mind that *not* all provisional sites as described in Chapter 1 eventually became active.

This Section concludes elucidation of aspects of the scientific plan. The measurement plan can best be described, if specific information regarding radiation processes in the atmosphere are first exposed. Hence, in the next Section, a basic introduction to radiation in the atmosphere leads to a discussion of measurement techniques and associated instrumentation.

2.3 RADIATION

Planck's Equation expresses electromagnetic radiation emitted by a black body (irradiance) as a function of temperature and wavelength (Iqbal, 1983):

$$E = \frac{2hc^2}{\lambda^5} * \frac{1}{e^{hc/\lambda\kappa T} - 1} \qquad (2.1)$$

where

E = Radiant energy flux density from a radiation source (W.m^{-2})

T = Absolute temperature of the source (K)

h = Planck's constant (6.62 x 10^{-34} J.s^{-1})

c = Speed of light in vacuum (3 x 10^{8} m.s^{-1})

κ = Stefan-Bolzmann's constant in specific corresponding units (1.38 x 10^{-23} J.m^{-2}.K^{-1})

λ = Wavelength (m)

In a meteorological context, Equation 2.1 may be applied to two sources of significance. They are the Sun as the primary source of radiation (solar radiation) and the Earth as a secondary source (terrestrial radiation). Figure 2.1 features graphs of E versus λ using the assumed mean temperatures of the two sources, (Sun: 5800K and Earth: 288K, respectively).

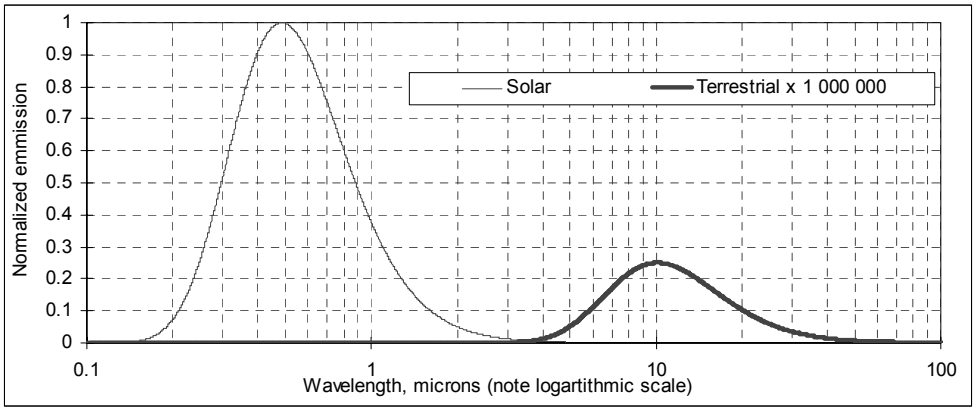

Figure 2.1 *Normalized emission (E) versus wavelength (λ) plots of Planck's Equation (2.1) for both solar and terrestrial radiation. Thin black line: Solar radiation, thick black line: Terrestrial radiation*

Discussion of Figure 2.1:

- For all practical terms, solar (SW) and terrestrial (LW) radiation occupy discrete portions of the electromagnetic spectrum. The overlap between the two spectra is small - about 1 part in 4 x 10^4 of the area under the SW portion of Figure 2.1. Therefore, no ambiguity should exist between reference to SW or LW radiation. According to Kondratyev (1972), wavelengths larger than 3.5 μm occupy about 0.9 % of the radiant energy in the extraterrestrial solar spectrum.

- SW radiation peaks at 0.5 μm while LW peaks at 10 μm. These numbers (λ_{max}) are confirmed by Wien's displacement law, denoting radiation peaks as a function of absolute temperature only (λ_{max} = 2897 / T), with λ in μm and T in Kelvin.

- The relative magnitude of LW radiation is several orders of magnitude less than that of SW radiation. In real terms, the two radiation peaks in Figure 2.1 have a ratio of 1 to 4 million (4 x 10^6).

2.3.1 Radiation in the atmosphere

A beam of incident solar radiation entering the atmosphere, is scattered in all directions (vertically and horizontally) by clouds and other particles, as it traverses the atmosphere. A part of the beam is reflected by clouds and absorbed by atmospheric constituents, such as water vapour (H_2O), oxygen (O_2) and ozone (O_3). The respite (remainder) of this beam reaches the surface of the Earth, where it is either reflected or absorbed (Figure 2.2).

The reflected beam traverses the atmosphere a second time and hence experience the same absorption and scattering for a second time. Since atmospheric pressure (and therefore absorbing gases) has a maximum closest to the Earth's surface, the lower part of the atmosphere absorbs the largest portion of incident, as well as reflected SW radiation. This absorbed energy is re-radiated as LW radiation in all directions, partially contributing to the Earth's greenhouse effect.

The solar radiation not taken up by sensible heating of the Earth's surface, adjacent atmosphere and latent heat of evaporation, is absorbed by the surface of the Earth and re-radiated as LW radiation, where the Earth serves as a secondary source. The emitted LW

radiation is absorbed (more efficiently than SW radiation) by the atmosphere as it leaves the surface of the Earth. However, not all outgoing LW radiation is absorbed, only the portion within the "atmospheric window" (8 μm to 11 μm) – (Bunskoek *et al.*, 1998).

The re-absorbed LW radiation is subsequently re-radiated again in all directions, including back towards the surface of the Earth, causing a counter-effect. This counter-radiation is also responsible for the Earth's greenhouse effect, maintaining the surface and lower atmosphere of the Earth at a much higher temperature than would be the case for an Earth without an atmosphere.

2.3.2 The greenhouse effect

Consider the sun as an isotropic (omni-directional) source of radiation that has an energy flux of S_0 = 3.877 x 10^{26} W. Next, consider the Earth as an object at an annual mean distance of one astronomical unit AU = 1.5 x 10^{11} m intercepting a fraction of the solar radiation equal to the projected fraction area of the Earth in its orbit around the sun, when seen as a sphere of radius A. The radiation reaching the Earth at the Top Of Atmosphere (TOA), as an annual mean value, is now equal to

$$
\begin{aligned}
E &= S_0 / 4\pi.(AU)^2 \\
&= 3.877 \times 10^{26}\ \text{W} / (4\pi * (1.5 \times 10^{11}\ \text{m})^2) \\
&= 1371\ \text{W.m}^{-2}
\end{aligned}
$$

The calculated value (1371 W.m^{-2}) for E equals the widely used annual average value of extra-terrestrial solar radiation, known as the *solar constant*, exhibiting a $\pm$ 3 % variation through the course of one year under the influence of varying Sun-Earth distance.

Note that S_0, the radiant energy flux of the sun, has internal variations due to solar sunspot cycles. Although there is a discernible cycle of 11 years in sunspot activity on the solar surface, its influence on the actual value of the solar constant is negligible - about 0.07 % between the minimum and maximum irradiance measured as a result of sunspot activity (Fröhlich, 1989).

Consider now that the Earth absorbs a portion of this radiation (incoming flux) and re-radiates it (outgoing flux), and that the Earth is in radiative equilibrium. This is not an exact

assumption, but to disregard imbalances over time periods shorter than one year due to seasonality, assume this happens over the time-span of several years.

The incoming flux depends upon the absorbed fraction intercepted on the projected area of a sphere with the size of the Earth. The projected area is a disk of radius R_E, while the absorbed portion equals the remainder not reflected as a result of the planetary albedo. Hence

$$\textit{Incoming flux} = S\,.\,(1-\alpha).\,\pi R_E^2 \qquad (2.2\text{ a})$$

where

α = Planetary albedo, estimated at 0.3

S = Solar constant, 1379 W.m^{-2}

The outgoing flux consists of all the absorbed radiation re-radiated from the entire surface of a sphere (Earth) of radius R_E. Hence

$$\textit{Outgoing flux} = E_{OLR}\,.\,4\pi R_E^2 \qquad (2.2.b)$$

where

E_{OLR} = Outgoing Longwave Radiation (OLR) flux per unit area.

If $\quad \textit{Incoming flux} = \textit{Outgoing flux}$

$$S.(1-\alpha).\pi R_E^2 = E.4\pi R_E^2$$

which re-arranges to

$$E_{OLR} = (1-\alpha) * (S / 4)$$
$$= (1-0.3) * (1379 / 4)$$
$$= \underline{241\ \text{W.m}^{-2}}$$

Applying Stefan-Bolzmann's law to equate this energy per unit area flux to a temperature T, assuming the Earth is a blackbody, leads to

$$E_{OLR} = \sigma T^4$$

and therefore

$$T = (241 / \sigma)^{1/4}$$
$$= 255\ \text{K} = \underline{-18\ °\text{C}}$$

This means, that the Earth, when viewed in pure theoretical terms, should have an *average* annual temperature of -18°C. This is the *average* Earth blackbody temperature as seen from space.

However, the mean surface temperature, as measured on the Earth, is 288 K, or +15°C. The 33°C difference is directly attributed to the greenhouse effect, whereby atmospheric constituents render the atmosphere opaque to long-wave radiation leaving the Earth's surface. The opaqueness of the atmosphere is mostly due to the presence of gases, such as water vapour (H_2O), oxygen (O_2) and carbon dioxide (CO_2).

2.3.3 Radiation fluxes on Earth

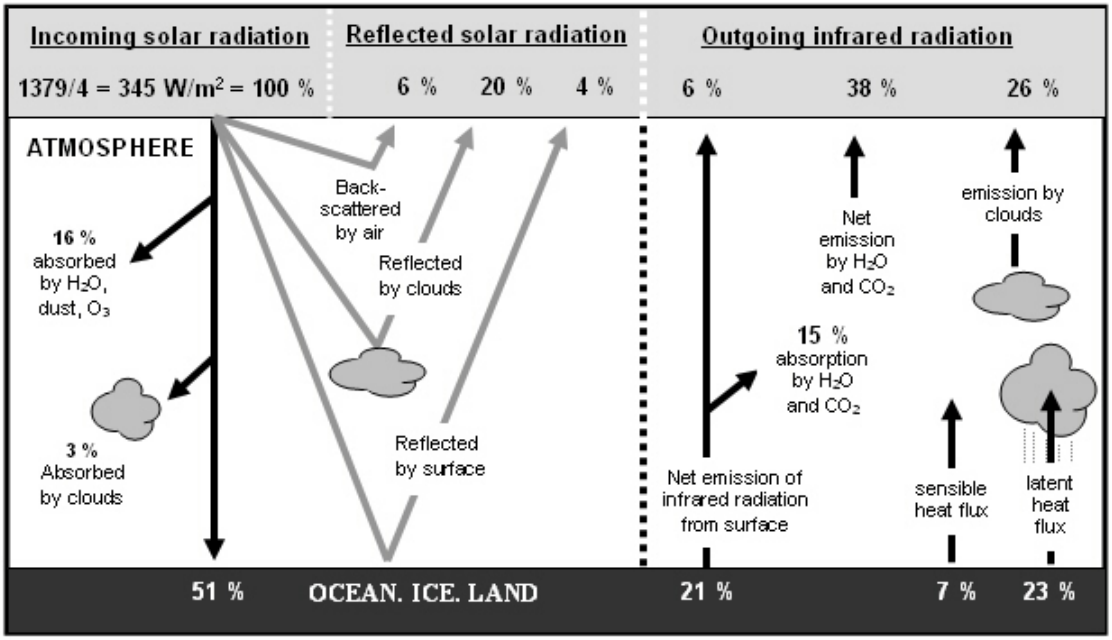

Figure 2.2 *Schematic representation of radiative fluxes in the atmosphere (after Wallace and Hobbs, 1977). The primary short-wave radiation component is direct solar radiation (left panel), while diffuse radiation is composed of scattered radiation by clouds and aerosol particles in the air (right panel). For an observer on the ground, global radiation is the sum of the diffuse and direct components. The reflected short-wave radiation is the portion not absorbed by Earth-atmosphere system (30% or albedo = 0.3). Long-wave radiation emitted by the Earth is partially absorbed by the atmosphere and re-radiated to the Earth-atmosphere system.*

Any observer on the surface of the Earth facing the sky, will experience a variety of energy fluxes, summarized and quantified in Figure 2.2 (Wallace and Hobbs, 1977), and described in the following short paragraphs.

- Downwelling SW radiation is a combination of direct (beam) and diffuse (scattered in all directions, therefore indirect), collectively known as global radiation.

- Upwelling SW radiation represents reflected radiation, dependent upon the reflectivity (surface albedo) of the Earth's surface. Surface albedo is a function of surface characteristics (soil and vegetation type, water, ice, etc.) and is defined as the ratio of reflected radiation to incoming radiation.

- Downwelling LW radiation is counter-radiation in the atmosphere, as LW radiation leaving the Earth's surface is absorbed and re-radiated in all directions, including downwards. It also includes a small portion of extraterrestrial solar radiation within the LW spectrum.

- Upwelling LW radiation is terrestrial radiation not absorbed by the atmosphere, plus the portion radiated upwards by the lower atmosphere.

Clear skies (free from scattering clouds and with few aerosols) is known to transmit a large percentage of the solar beam and therefore exhibits a relatively small amount of diffuse radiation at the surface, while a partly cloudy sky and / or more turbid sky has progressively more diffuse radiation as the cloudiness and / or turbidity increases (Long and Ackerman, 2000). An overcast sky transmits little or no direct radiation and almost all radiation reaching the surface is then diffuse.

2.4 MEASURING RADIATIVE FLUXES

Radiant energy dE arriving from the solar surface at the Earth, may be expressed (Seckmeyer *et al.*, 2001) as follows:

$$E_{SW} = \frac{dQ}{dtdAd\lambda} \tag{2.3}$$

where

E_{SW} = SW radiative flux density for an observer on Earth

Q = Radiative flux from the surface of the sun, arriving at the TOA

t = Time interval

A = Unit area

λ = Wavelength

The individual components such as global, direct or diffuse components are redefined from the definition of Q in Equation 2.3 using appropriate restrictions such as

- Direct radiation: limit the field of view as to include only the solar disk
- Diffuse radiation: including all except the solar disk
- Global radiation: the entire field of view

As far as LW radiation is concerned, it may be regarded as emanating from a grey body (i.e., not an entirely "black" body) at temperature T with emmissivity ε:

$$E_{LW} = \varepsilon \sigma T^4 \qquad (2.4)$$

where

E_{LW} = LW radiative flux density for an observer on Earth

ε = Atmospheric emmissivity (the "greyness" of the radiating object)

σ = Stefan-Bolzmann constant

T = Absolute effective temperature of radiating atmosphere

In order to measure radiation flux densities as described in Section 2.3.3, instrumentation needs to respond positively, exclusively, predictably and unambiguously to radiation input signals. The measurement of radiative flux density requires that flux density be measured from a certain solid angle, within a certain spectral range and with a certain spectral response (Kipp and Zonen, 1997a). The entire celestial dome (sky) irradiates towards the Earth from a solid angle of 2π sterradians. A physical instrument having a field of view facing the celestial dome, therefore receives radiation represented by the integral of radiation elements across its entire field of view. Therefore it has to be perfectly aligned with the horizon (i.e., radiometrically levelled) so that the instrument's field of view co-incides with the radiation source.

Quantifying the energy incident on a plane surface is a difficult field exercise, since it involves a series of conversion processes. Incident solar energy is converted into thermal energy, which is converted to electrical energy (NREL, 1993) that can be measured by a

millivoltmeter. One such device is the thermopile - the heart of the most types of modern radiation instruments (described in Section 2.5.1).

From Section 2.3.3, the following surface radiative fluxes are measurable quantities:

- Downwelling SW: Direct solar beam radiation
- Downwelling SW: Global solar radiation
- Downwelling SW: Diffuse solar (sky) radiation
- Upwelling SW: Reflected solar radiation
- Downwelling LW: Terrestrial sky radiation
- Upwelling LW: Terrestrial earth radiation

In order to qualify as a BSRN site, it was decided that the measurement of all downwelling quantities must be undertaken, in a specific frequency as listed in Table 2.4(a).

Table 2.4 (a) *Basic radiation measurement parameters at BSRN stations*

Quantity	Unit	Reporting resolution	Sampling interval	Reporting interval
Global radiation	$W.m^{-2}$	1	1 sec	1 min
Direct radiation	$W.m^{-2}$	1	1 sec	1 min
Diffuse radiation	$W.m^{-2}$	1	1 sec	1 min
Downward LW radiation	$W.m^{-2}$	1	1 sec	1 min

Another set, listed in Table 2.4(b), of non-radiation quantities to increase understanding of the measured radiation quantities is also a pre-requisite for a site to qualify as a BSRN station (Hegner *et al.*, 1998).

Table 2.4 (b) *Basic non-radiation measurement parameters at BSRN stations*

Quantity	Unit	Reporting resolution	Sampling interval	Reporting interval
Air temp at long-wave instrument height	°C	0.1	-	1 min
Relative humidity at long-wave instrument height	%	0.1	-	1 min
Pressure at long-wave instrument height	hPa	1	-	1 min
Meteorological SYNOP observations	various	-	-	hourly
Upper-air rawinsonde meteorological balloon observations	various	-	-	daily

These basic measurements are not the only measurement efforts that sites should embark upon. The *expanded* programme of BSRN allows sites to measure one or more of the parameters listed in Table 2.5, to both serve as checks and balances for related basic BSRN quantities, but also to aid as en enrichment of existing data in future research.

Table 2.5 *Extended measurement parameters at BSRN stations*

Quantity
Direct SW radiation at WMO wavelengths (368nm, 500nm, 778 nm) and specified bandwidths
Cloud amount and type – if possible by video camera imaging
Vertical distribution of temperature and water vapour (lidar), cloud-base height and aerosol
Precepitable water measured with microwave radiometer, or newly developed GPS techniques
Ozone (total column amount using Dobson spectrophotometer and/or vertical distribution using ozone-sounding or Dobson Umkehr technique)
Reflected (upwelling) SW radiation from a tall tower
Upwelling LW radiation from a tall tower
Thermal spectral infrared radiation
Hemispherical total solar spectral irradiance
Spectral albedo measurements

2.5 INSTRUMENTATION

2.5.1 A vital component: Thermopile

The basic radiation-sensing element of a modern non-photovoltaic radiometer, as used at BSRN stations, is a thermopile. All four sensors that measure basic quantities at BSRN stations have thermopile sensing elements.

A thermopile (Figure 2.3) is an array of several thermocouples and makes use of the Seebeck effect, discovered in 1821 by Thomas Seebeck. When thin strips of two dissimilar metals, such as bismuth and copper, are connected on one end, but not the other, a small electric potential is detected when the temperature is raised at one open end (“hot” end) with respect to ambient temperature.

While one open end ("cold" end) is maintained at ambient temperature by embedding it in a metallic body with large thermal inertia, the other, "hot" end, is exposed to solar radiation and allowed to rise in temperature[1]. In a thermopile, a larger effective area is created by joining the "hot" junctions thermally. The effect is further enhanced by covering it with black, allowing for the absorption of as much incident radiation as possible.

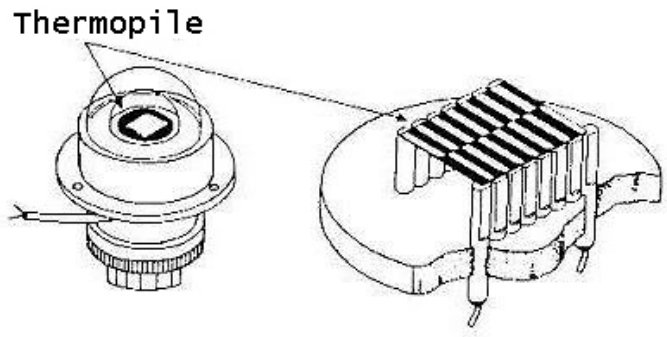

Figure 2.3 *A typical thermopile's position in a radiometer (left) and from closer up (right). The "hot" junctions are situated in the middle line between the two rows of spindles, housing the "cold" junctions firmly anchored in the radiometer body.*

Credit for the idea of combining several thermocouples into one thermopile goes to the Italian physicist Macedonio Melloni (1798-1854), who first constructed a thermopile for use in thermal radiation research. Later, his idea was developed by the Dutch professor Dr W.J.H. Moll (1876-1947) who introduced a more sensitive thermopile, which he used in his studies on infrared radiation based on W.C. Röntgen's research (the discoverer of X-rays). In 1924, the Polish meteorologist L. Gorczynski adapted the method even further to make the first pyranometer (Van Cittert-Eymers, 1979). In 1927, the first Moll-Gorczynsky pyranometers were in full production at the Kipp & Zonen factory in Delft, Netherlands.

Incident solar or terrestrial radiation raises the temperature of the "hot" end of the thermopile to produce an electric potential with respect to the "cold" junctions. This potential is directly proportional to the incident irradiance, and the proportionality, known as the calibration constant, a direct indication of the radiometer's sensitivity. These numbers range typically from about 5 $mV.K^{-1}.W.m^{-2}$ to 15 $mV.K^{-1}.W.m^{-2}$ in SW radiometers and about 4 $mV.K^{-1}.W.m^{-2}$ in LW radiometers.

[1] http://physics.kenyon.edu/EarlyApparatus/Thermodynamics/Differential_Thermopile/Differential_Thermopile.html

A thermopile has the following positive characteristics:

- Low impedance, thereby making the associated circuitry (such as data acquisition systems, e.g., data loggers) less susceptible to extraneous radiation and electrical noise[2].

- Spectral response in general is "flat", i.e., its response is very close to uniform throughout the spectral range in which it is sensitive and outside – 0.1 μm to 50 μm. (Kipp & Zonen, 1997b). This means that the relative intensity of an amount of measured SW radiation with respect to an amount of LW radiation would be the same for practical purposes between two different instruments. The latter is particularly important when calibrations are done.

- Sensitive to a wide range of electromagnetic radiation in general (typically including both SW and LW), making it versatile. If only sensitivity for a specific wavelength band is required, selectively transmitting domes are usually utilized.

2.5.2 Measuring direct radiation

Direct radiation forms the basis for SW radiation measurements since it has the least uncertainty of the basic BSRN irradiance quantities (Ohmura *et al.*, 1998). The instrument used for direct radiation measurements is known as a pyrheliometer. In this discussion two types are highlighted:

- Absolute cavity radiometer

- Thermopile pyrheliometer

Both instruments need to be pointed continually towards the sun in order to operate correctly, in other words, a method of continuous solar tracking needs to be applied.

The word *pyheliometer* comes from the Greek words $\pi\upsilon\rho$ (fire), $\eta\varepsilon\lambda\iota\sigma\sigma$ (sun) and $\mu\varepsilon\tau\rho\sigma\nu$ (measure) – signifying "that which measures fire coming from the sun" (Dominguez, 2001). Therefore, the pyrheliometer measures radiation emanating from the sun.

[2] http://www.fuji-piezo.com/Thermopile.htm

The International Pyrheliometric Comparison (IPC) events, which are regularly held (normally every 5 years) at the World Radiation Centre (WRC) in Davos, Switzerland, attract various standard pyrheliometers from participating countries. Instruments like the Eppley self-calibrating AHF, that is deployed at the BSRN site at De Aar (Figure 2.4), participated directly in three of the recent IPC events, i.e., 1980, 1985 and 1990 (Eplab, 1997). Furthermore, one such unit is a member of the World Standard Group (WSG).

The WSG is a group of seven carefully characterized reference cavity pyrheliometers held at WRC and used to define the WRR. These instruments are calibrated once a year to ensure stability (WMO, 1983) and must have a long-term stability of less than 0.2 %, as well as a precision better than the WRR, which is 0.3%. During IPC events, invited radiometers are compared to the WRR, using the sun as source and those radiometers then have direct traceability to the WSG (WRC, 2001).

Since the invention of pyrheliometers, the WRR underwent slight changes, as the scientific understanding and analysis techniques have improved. The current reference is just known as WRR, valid since 1 July 1980. The names, dates and relative magnitude (SAWB, 1959 and WMO, 1983) of the previous radiometric references are:-

- Angström scale (1905) = WRR / 1.026
- Smithsonian scale (1913) = WRR / 0.977
- International Pyrheliometric Scale (1956) = WRR / 1.022

2.5.2.1 The cavity radiometer

The cavity radiometer is considered to be a standard pyrheliometer – i.e. an instrument used by national solar radiation networks to standardize instruments deployed in routine measurements.

It works on the principle that electrical substitution in a specific cavity equals incident solar energy. Incident solar energy heats up a specially prepared cavity in a black tube known to have almost perfect emmissivity, through an aperture. When temperature equilibrium (which is accurately noted) is reached, the aperture is closed and heaters in the cavity are switched on, until the original noted temperature is reached. Power (P) of the heater can be

accurately measured and noted by using the relationship $P = V.I$, where V and I are the potential difference and current through the heating element, respectively. The aperture is then opened again and the process repeated. All of these functions can be done by manual controls on the control box, or automatically, and logged to a PC. (Hickey and Nelson, 1993).

Figure 2.4 *An Eppley AHF absolute cavity radiometer with control box*

Absolute cavity instruments are developed from first principles (Foukal, 1985), and are therefore the basis of radiometric measurements at a specific station or group of stations in a region. The drive in earlier BSRN years was therefore, to use cavity radiometers as primary routine sampling instruments, but it has shifted over the years more towards the cavity radiometers fulfilling the role of supportive instruments for operational pyrheliometers, operating in parallel at the most (Mc Arthur, 1998).

Arguments for and against using this instrument routinely, were discussed in Section 2.2.2.1.

2.5.2.2 The thermopile pyrheliometer

This aluminium tubular instrument (Figure 2.5) only has a very accurately levelled thermopile sensor at the back of the tube. It is characterized in such a way that its mV output is proportional to solar input (Kipp & Zonen, 1997a)

It has two sights in the form of small holes perfectly aligned with the field of view enabling accurate alignment with the solar beam. An Infrasil-1 quartz window in front protects the delicate interior from rain and dust and compensation is made for the “lost” radiation due to the presence of the window during calibration. The window is transmissible for wavelengths

within the solar spectrum excluding IR. Desiccant at the back keeps the interior free from moisture condensation and subsequent corrosion (Kipp & Zonen, 1997a).

Figure 2.5 *A Kipp & Zonen CH1 pyrheliometer. 1,2= beam sights, 3= quartz window, 4= (behind) desiccant gel*

The instrument's field of view is set at 5°. The apparent solar disk size is 0.5°, varying slightly inter-annually as the Sun-Earth distance changes. The remaining 4.5° allows for small solar tracker errors plus a certain amount of circumsolar radiation. In effect, a small area of the atmosphere around the Sun (solar aureole) is also in the field of view, sometimes causing errors in situations of low solar angle.

The field of view of such a pyrheliometer is also expected to be equal or at least closely comparable to the viewing area of the diffuse pyranometer occulted out by the disk, so that direct comparisons between direct, global and diffuse components can be made, for example, in the quality control tests described in Section 4.3.3.3 and 4.3.3.4.

2.5.3 Measuring diffuse radiation

A diffusometer is a conventional pyranometer with a shading device, usually connected to a tracker that continually blocks the direct solar beam from the pyranometer's field of view. A diffusometer is thus continually exposed to all of the diffuse radiation of the celestial dome.

The word *pyranometer* comes from the Greek words $\pi\upsilon\rho$ (fire), $\alpha\nu\alpha$ (up) and $\mu\varepsilon\tau\rho\sigma\nu$ (measure) – signifying "that which measures fire coming from above" (Dominguez, 2001). Therefore, the pyranometer measures radiation emanating from the sky.

A pyranometer (Figure 2.6), has a thermopile, covered by a double dome made of the same infrasil-1quartz, as the window of the CH1, and includes transmissibility for meteorological wavelengths, i.e., 0.3 μm to 28 μm (Van Lammeren and Hulshof, 1994). The reason for a double dome is for protection of the delicate thermopile, for insulation against environmental temperature shocks, and it serves as a shield that prevents radiation losses to the environment in cloudless conditions - a 'cold' sky (Campbell, 2001). The housing (body) is covered by a white cap, in order to shield the instrument metal body from excessive direct SW solar heating and subsequent false signals such as thermal offsets, described in more detail in Section 3.1.2.3. A desiccant plug keeps the instrument interior free from moisture and prevents rusting.

Figure 2.6 *A Kipp & Zonen CM21 pyranometer. 1= inner quartz dome, 2= outer quartz dome, 3= bevelled protective shield, 4= dessicant, 5= leveling bubble, 6= levelling screws*

The diffuse quantity is second in line with respect to the relative uncertainty for BSRN measurements (Ohmura *et al.*, 1998). There are specific reasons for this:

- The diffuse radiation quantity is small compared to direct, especially under clear-sky conditions. A low relative error results in a small absolute error.
- The diffusometer signal is the result of a 2π-steradian response - therefore the possible effect of "weak" or "strong" spots on the thermopile element are masked.
- The masking effect also reduces the impact of less-than-perfect levelling of the diffuse pyranometer.

The diffusometer shading is established either by means of a shading sphere, or a shading ring. Ideally a shading sphere, having the same field of view than the associated

pyrheliometer on site, is used. If a shading sphere is chosen, some form of solar tracking is needed to cover the diffuse pyranometer dome continuously as the sun is "moving".

A shading ring is employed at sites where a tracking device is not available. The ring is set up with its centre line tangent to the earth, parallel to the celestial equator and facing away from the nearest pole, inclined at an angle equal to the site's latitude. The ring casts a shadow on the diffuse pyranometer dome for an entire day without the need for solar tracking. The only adjustment needed from time to time is compensations for the solar declination, which cycles between extremes at the solar solstices. However, this ring also blocks a significant portion of the diffuse radiation, and a correction factor involving solar declination and estimated cloud cover needs to be applied (Batlles, 1995).

2.5.4 Measuring global radiation

Global radiation is measured by the same pyranometer used for measuring diffuse radiation, the only difference being that it is unshaded. The poor uncertainty of measurements taken by a single pyranometer is due to its poor directional response. The pyranometer is also more sensitive towards tilting errors, as opposed to the diffusometer. In the BSRN, the more accurate quantity of global irradiance (Dominquez, 2001) is derived from combining the diffuse and normal direct radiation components using Equation 2.5:

$$global(t) = diffuse(t) + direct(t).\ cosZ \qquad (2.5)$$

To clearly distinguish between calculated and directly measured global radiation, the BSRN literature refers to calculated global radiation using Equation 2.5 as DSGL1 (also referred to as "global1"), while the directly measured quantity using an unshaded pyranometer is DSGL2 (also known as "global2") (Gilgen *et al.*, 1995).

Despite the poor relative performance of global pyranometry, DSGL2 is still included in the basic BSRN measurement programme for the following reasons:

- It provides closure of the solar measurement program (NREL, 1993).
- It provides a means of continuously validating direct and diffuse measurements by direct comparison of DSGL1 and DSGL2.

- It provides a good quality control procedure (described in Sections 4.2.3.2 and 4.3.3.4) to identify questionable data, which have escaped other quality control procedures.

- It provides a means of calibrating the pyranometers, when the global/diffuse swopping method as proposed by Forgan (1996), is used in connection with the global/diffuse/direct relationship.

Global pyranometers are ventilated in the BSRN context, apart from uniformity, in an attempt to reduce thermal offsets to a minimum.

2.5.5 Measuring LW radiation

The pyrgeometer (Figure 2.7) as developed since 1970 by Eppley Laboratories at Newport, Rhode Island, is available in its present form since 1982.

The word *pyrgeometer* comes from the Greek words $\pi\upsilon\rho$ (fire), $\gamma\alpha\iota\alpha$ (Earth) and $\mu\varepsilon\tau\rho\upsilon\nu$ (measure) – signifying "that which measures fire coming from the Earth" (Dominguez, 2001). Therefore, the pyrgeometer measures radiation emanating, or similar to those emanating, from the Earth.

Figure 2.7 *An Eppley Precision Infrared Radiometer*

A pyrgeometer contains the same thermopile as a pyranometer and pyrheliometer. The only significant difference is, that the dome is coated on the inside by silicon, which is selectively transmissible to only longer wavelengths (4 µm to 50 µm). In this way, SW radiation is

prevented from reaching the thermopile. In operation, the pyrgeometer is also shaded in the same way as the diffusometer, and ventilated. This is discussed in Section 3.1.3.

At the first BSRN meeting in Washington (WCRP-54,1991), the target uncertainty for LWD measurements was set at 30 $W.m^{-2}$, as opposed to 5 $W.m^{-2}$ to 10 $W.m^{-2}$ for SW measurements at the time. That figure was anticipated to drop to 10 $W.m^{-2}$ with the implementation of improved measurement techniques, which was realized in 1995 (Ohmura *et al.*, 1998), thanks to an improved way of measuring the dome temperature by means of two thermistors instead of one. This is known as the Swiss modification and is expected to improve instrument performance considerably (Philipona *et al.*, 1998). With correct calibration (using Equation 3.3, (the PMOD Equation) and absolute calibration coefficients), an uncertainty of 5 $W.m^{-2}$ to 20 $W.m^{-2}$ is attainable and as little as 2 $W.m^{-2}$ with the Swiss modification.

2.6 CONCLUSION

To summarize, the BSRN is a small global network of quasi-homogeneous radiation stations striving to deliver the best quality radiation data aimed at specific applications, viz., climate research and satellite ground-truthing. Unique radiation processes in the atmosphere require specialized instrumentation, in order to detect and quantify them correctly and meet the high ideals set forth in BSRN.

CHAPTER 3

SYSTEM DESIGN

A complete solar and terrestrial radiation measuring system ideally consists of the following seamlessly integrated components:

- *Instruments: SW / LW and peripherals*
- *Maintenance (inspection and calibration routines)*
- *Data management strategy*
- *Communication with (international) database.*

In an ideal system design, integration strategies between components are sought, driven by the strict implementation of a design plan. However, this was not the case with BSRN - as discussed in Section 2.1 and pointed out by Mc Arthur (1995). This unique process was driven by utilization and upgrading of existing installations in continuous feed-back and learning. This also explains the frequent referrals to real situations incurred in this Chapter.

3.1 INSTRUMENTS

In the design of a measurement system, knowledge of pre-measurement processes have to be incorporated. These processes are combined with identification and the best possible quantification of sources of known error to be applied in the final step. The remedies for the sources finally need to be characterized and quantified to the extent that their application will add value to the eventual measurements.

Knowledge of the different radiation components is necessary, as well as their possible sources of error. These sources of error can be either eliminated or meaningful corrections can be applied, in order to minimize the impact of those errors in the final quality of archived or presented data. It is a known fact, that all measurements inhibit a certain degree of uncertainty, in fact, without expressing the uncertainty of a measurement, it lacks worth and credibility (Cook, 1999).

The art of making measurements is therefore to strive towards entertaining the minimum amount of uncertainty.

Figure 3.1 features the basic components of a typical radiation site layout (as found at the De Aar BSRN site).

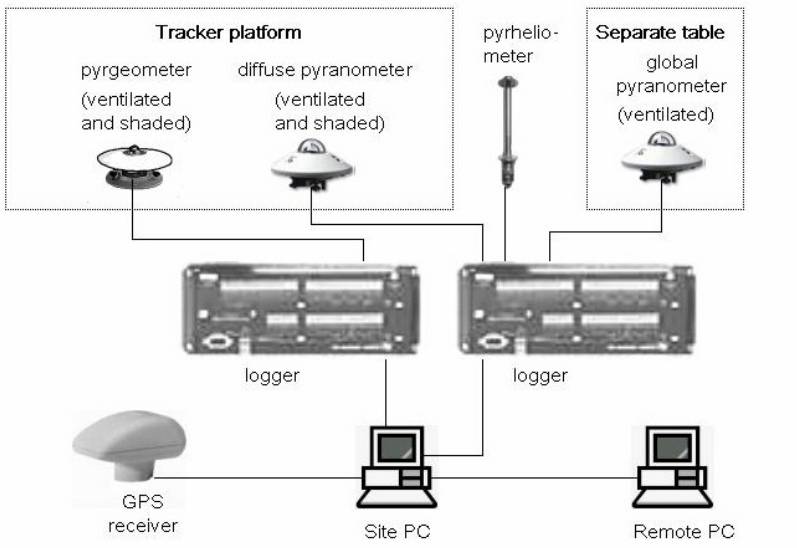

Figure 3.1 *Schematic layout of basic instrumentation at a BSRN site*

Each component, as well as the system as a whole, have its own unique sources and ways of inducing uncertainties in the eventual measurements. A system is indeed only as strong as its weakest link, so all of these factors, and in particular the sources of error, need to be taken into account when realizing a measurement programme and maintenance schedule.

3.1.1 Aspects of pyrheliometers

Pyrheliometers form the basis of SW measurements at a radiation site in general and a BSRN site in particular, as discussed in Section 2.5.2.

3.1.1.1 Operational errors

A pyrheliometer needs to be pointed towards the sun continuously, requiring a secure mounting on a solar tracker device, which, in turn, executes a reliable programme following the daily solar track in the sky. Any initial misalignment in either the tracker setup, mounting

of the pyrheliometer or any other form of error in the execution of the solar tracking may cause the pyrheliometer not to point exactly towards the sun, and subsequently yield erroneous readings.

This point is illustrated in Figure 3.2. A misalignment between the twin De Aar pyrheliometers (A and B) occurred during the morning of 26 January 2003 prior to about 10:00 UT. The sunspot of pyrheliometer A became misaligned by a discernible amount, similar to a routine tracker drift experienced, because the tracking system is passive. At the same time, and on the same tracker, pyrheliometer B remained in the correct position during this period. The outputs of pyrheliometers A and B are plotted against the left-hand Y-axis, in W.m^{-2}. The difference B minus A is plotted against the right-hand Y-axis, also in W.m^{-2}. Pyrheliometer B was restored to its correct position at about 10:00 UT.

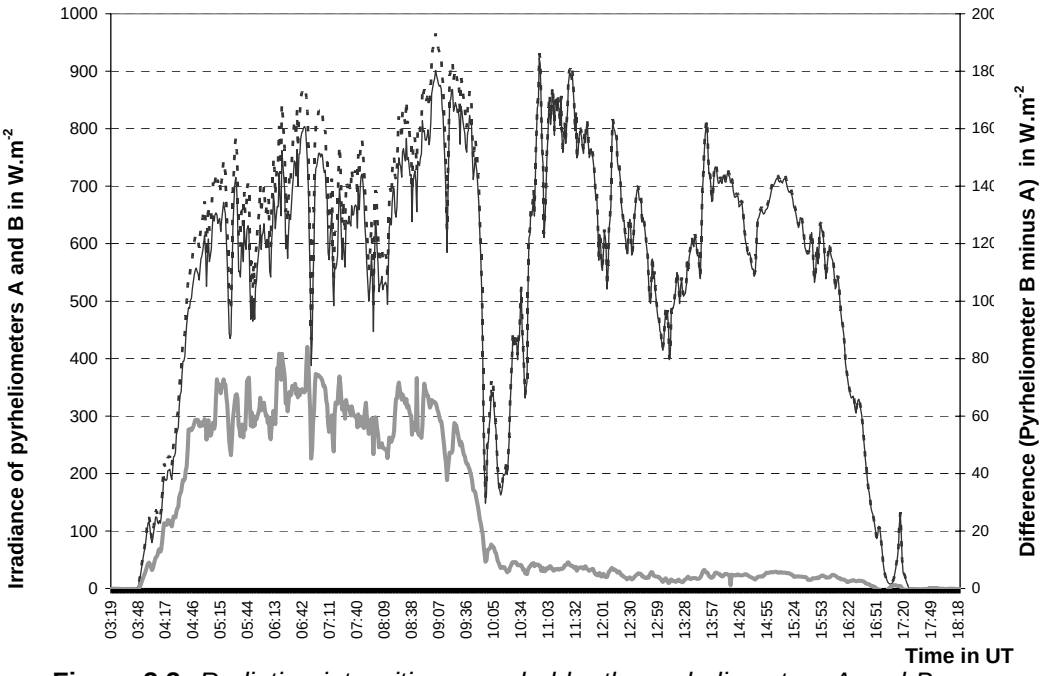

Figure 3.2 *Radiation intensities recorded by the pyrheliometers A and B, as well as their difference (B minus A) on 26 January 2003.*

During the period prior to the recovery, a difference of about 60 W.m^{-2} was observed, whilst after the recovery, it diminished to less than 10 W.m^{-2}. The 60 W.m^{-2} error exceeds the accuracy standards discussed in Section 2.2.2 by a substantial margin, emphasizing that correct tracking alignment is of paramount importance.

Tracker drifts are also addressed in Section 3.1.4 where the concept of double pyrheliometers is used in an attempt to address this issue. Double pyrheliometric measurement also aids in identifying cleaning times, as discussed in Section 3.1.5.

Another source of error is an unclean window, either from the outside (dirt collecting) or inside (moisture condensation). This can be rectified and should ideally be prevented by sound operational techniques and a regular inspection routine, leading to early identification and employing rapid remedial procedures.

Due to prolonged exposure to the solar radiation it is measuring, the instrument thermopile deteriorates with time. Typically, the black absorbent surface of the thermopile develops a shining surface leading to the thermopile becoming slightly more reflective, hence absorbs less radiation and subsequently seems to lose its sensitivity (Van der Molen and Koshiek, 1995). The true instrument sensitivity will therefore deviate from the number quoted in the original calibration certificate, hence regular comparison against a reliable standard instrument (calibration) is necessary in order to use the instrument output as a true irradiance measurement.

Observed changes in pyrheliometer sensitivity at the De Aar site during the first three years of operation are listed in Table 3.1. The term "CH1" and the cited serial numbers refer to the pyrheliometer in use. Values are quoted in $mV.kW^{-1}.m^{-2}$. Note that the 1997 and 1999 values are the same, since factory calibration constants were initially used after installation.

Table 3.1 *Observed pyrheliometer sensitivities since the De Aar BSRN installation*

Calibration Date	Instrument CH1 serial number 970156	Instrument CH1 serial number 970157
14 July 1997	12.95	13.74
28 July 1999	12.95	13.74
25 January 2000	12.75	13.58
28 July 2000	12.70	13.55
24 March 2001	12.77	13.55
26 September 2001	12.79	13.55
28 March 2002	12.65	13.57
27 January 2003	12.62	13.44
Total Calibration Drift	2.55 %	2.18 %
Calibration drift per year	0.460%	0.394%

If no calibrations were done after the initial De Aar installation, the total calibration drift would translate to an error of 20 $W.m^{-2}$ in a typical reading of 800 $W.m^{-2}$. This also exceeds the required accuracy described in Section 2.2.2 by a significant margin, therefore, sustained and regular calibration is the most important aspect in BSRN site operation.

The sources of error mentioned so far are operational in nature, and by using proper observational techniques can, should and must be kept to a minimum for most of the time.

There are, however, other intrinsic errors and sources of uncertainties in pyrheliometric measurements that in principle cannot be avoided entirely. The approach towards these uncertainties and errors is not attempted elimination, but rather a management strategy to keep uncertainty to a minimum. Each of the following sub-sections highlights one of these errors.

3.1.1.2 Window errors

A window is usually mounted in front of a pyrheliometer to enable all-weather operation. Ohmura *et al.* (1998) refers to an investigation by a BSRN task team using cavity radiometers and several kinds of protective filters. It was found that the best protective filter is already blocking 23 $W.m^{-2}$ of radiation located in the LW region. In the 6.3 µm band (known for the absorption by water vapour), as much as 7 $W.m^{-2}$ is blocked. This implies, that uncertainties in water vapour absorption alone account for more than the 2 $W.m^{-2}$ uncertainty goal cited in Section 2.2.2, which thus becomes unattainable.

However, practical implications in operational circumstances call for the presence of a window. For continuous operation of normal incidence pyrheliometers, a window has to be fitted. This window protects the delicate thermopile from accumulation of dust, which would render it ineffective with time. It also prevents water from collecting in the tube when it is pointed skyward during a rainstorm, and the detrimental effects that the presence of moisture would have on the delicate interior parts.

Automatically closing, rain-triggered and motor-driven sheltering devices, as proposed and built by Heimo *et al*. (1993), were not an option at De Aar, due to the fact that they would not be effective and not warrant the high costs involved. Rainstorms in the Karoo are mostly of convective nature, and with low surface moisture. They are often driven by rapid and strong convective development, resulting in a large amount of rain falling, even before an automatic device would be able to close and shelter the radiometers.

The Infrasil I-301 window in front of the CH1 in operation at De Aar, has a theoretical cut off wavelength of 0.14 µm to 5.2 µm (9 eV to 0.24 eV) - (Cannas *et al.*, 2001, 2002). This is

well outside the bulk of the solar spectrum or the “meteorological radiation” interval of 0.3 µm to 3 µm. Therefore the manufacturer’s window was retained for the De Aar instruments.

3.1.1.3 Circumsolar radiation

The Sun - Earth distance varies by 3.4 % between the point of aphelion (152.6 million km) and perihelion (147.5 million km). This constitutes a theoretical solar disk size of between 0.52° and 0.54°, as seen by an observer on Earth.

The solar disk as observed from the Earth’s surface, however, appears to be larger, since atmospheric particulates, such as aerosols and water vapour, have a strong scattering ability. An annular area around the solar disk (solar aureole), is created by the atmospheric turbidity, radiating a certain amount of circumsolar radiation of which the inconsistency at any given moment is responsible for errors in the direct and diffuse radiation (Oliviéri, 1992).

The Kipp & Zonen CH1 (Figure 2.6.) deployed at the De Aar site has a full field of view, which is roughly ten times the diameter of the solar disk (5° ± 0.2°) to allow for interception of the entire apparent solar disk. A deviation of 0.75° from this ideal number is still within the tolerance limits (Kipp & Zonen, 1997a). A tenfold diameter means, that the area is hundredfold, therefore a 3% variation in a disk occupying 1% of the field of view, is not expected to have any significant impact on the measurements.

Research of circumsolar radiation by Major (1994 and 1995) describes the cavity radiometer’s penumbra and sky functions, dimension differences, as well as the exchange of LW radiation. This is necessary for the characterization of small differences for exact calibrations, such as those conducted by the WRR.

The De Aar pyrheliometers are kept within the 0.75° limit, as recommended by the manufacturer, as far as possible. When calibrating, the cavity radiometer is attached to the solar tracker and aligned for the calibration period using the manual sunspot-sights.

Variations in the solar output (e.g., due to the 11-year sunspot cycle) are in the order of a few parts per thousand (Frölich, 1989 and Willson *et al.*, 2003) and are expected not to play any significant role.

3.1.1.4 Thermal offsets

Thermal offsets influence all types of thermopile radiometers, including pyrheliometers. However, unlike pyanometers, the manufacturers have not attempted ventilation to try and equate sensor and instrument body temperatures. The CH1 instruction manual (Kipp & Zonen, 1997a) quotes an offset of 3 $W.m^{-2}$ in response to a change of 5 $K.h^{-1}$ in environmental temperature. The experience at De Aar is, that the pyrheliometer zero offset (presenting itself visibly during night-hours) is definitely smaller for pyrheliometers than pyranometers. In Section 3.1.2.3, thermal offsets in pyranometers are discussed.

3.1.2 Aspects of pyranometers

Pyranometer thermopiles are also exposed to prolonged exposure to solar irradiance leading to a loss of sensitivity rendering a need for frequent calibration.

A number of different methods to perform pyranometer calibrations were discussed by Forgan (1995), of which the simple method detailed in Mc Arthur (1998), involving global/diffuse swopping, is used at De Aar. The observed calibration drift in the operational BSRN pyranometers in $mV.kW^{-1}.m^{-2}$, since their installation at De Aar, is listed in Table 3.2. Note that the 1997 and 1999 values are the same, since factory calibration constants were used since the first installation.

Table 3.2 *Observed pyranometer sensitivities since the De Aar BSRN installation*

Calibration date	Pyranometer CM21 serial number 970442	Pyranometer CM21 serial number 970443
31 October 1997	19.68	23.36
28 July 1999	19.68	23.36
25 January 2000	19.60	23.00
28 July 2000	19.55	22.84
24 March 2001	19.50	22.84
26 September 2001	19.41	22.70
28 March 2002	19.29	22.68
27 January 2003	19.27	22.49
Total Calibration Drift	2.08 %	3.72 %
Calibration drift per year	0.397%	0.710%

Since installation, the same two pyranometers were in operation, regularly swopped after every calibration episode. Between calibration periods they are used alternatively as global and diffuse instruments, following the recommendation by Forgan (1996). This way of calibrating and operation was in fact the only option for De Aar, since the initial instrumental consignment only included two CM21 pyranometers, and there were no other similar pyranometers in possession of the SAWS at that stage.

3.1.2.1 Operational errors

The impact of operational errors should be kept as small as possible for BSRN measurements. These errors include the following:

- The pyranometer has a built-in sprit level that is preset at the factory to be precisely aligned in all directions to the thermopile (radiometric levelling). A correctly set bubble level on site is assumed to render a perfectly level thermopile.

- The diffuse pyranometer needs to be mounted on the rotating solar tracker platform in order to make use of the solar shading device for diffuse measurements. However, the platform is subject to being slightly off-balance at a given moment due to a certain amount of play induced in the tracker. The impact of off-balance pyranometers is less pronounced in diffuse pyranometers, because of the smaller overall signal (Ohmura *et al.*,1998).

- The accumulation of dirt and other deposits on the outer dome over time leads to erroneous readings. As with pyrheliometers, this is effectively neutralized by regular inspection (at least once per day) and subsequent dome cleaning, also after rainstorms, by site staff.

- If water enter the pyranometer either by moisture condensation or precipitation, the interior metal parts can corrode. This problem is addressed by the presence of dessicant granules in a small cavity in the body, extracting moisture. Granules are self-indicating, being typically pink in the presence of a certain amount of moisture and blue if dry.

- Shading errors, as a result of tracker errors or independently thereof, as a result of changing shading device geometry, lead to incorrect exposure of the diffuse pyranometer and erroneous readings. The disk should correspond to the field of view of the pyrheliometer to allow for correct application of the relationship global/diffuse/direct, but on the other hand, should also be adequately oversized (Heimo, 1993), so that small drifts encountered during unattended operation do not lead to large errors. Infrequent inspection due to rainy weather lasting for several days, can lead to a large shading error not being timeously identified. At De Aar it is highly unlikely since bad weather does not occur in long successions, and frequent inspection visits by site personnel are possible.

3.1.2.2 Cosine error

Ideally, a horizontally mounted pyranometer would measure radiation I, incident at a zenith angle Z, as a fraction of $I.cosZ$, for all angles between 0° and 90.83° (when the sun rises or sets). All radiometers, however, deviate from this ideal and its quantity is defined as the cosine error (Schreder *et al.*, 1998), expressed in Equation 3.1:

$$f_1(Z,\theta) = 100\{\frac{F(Z,\theta)}{F(Z=0°,\theta).\cos Z} - 1\} \qquad (3.1)$$

where Z = Incident (zenith) angle, measured between the level of incidence and a line normal to the horizontal level

θ = Azimuth angle

F = Radiometer's reading in nominal units at angles Z and θ, respectively

According to the manufacturer, CM21 pyranometers deployed at the De Aar site have a maximum cosine error of 1.3% at solar elevation of 10°. This translates to an error of less than 13 W.m^{-2} for global radiation at 1000 W.m^{-2} or an error of less than 4 W.m^{-2} for diffuse radiation of 300 W.m^{-2}. This compares positively with earlier Kipp & Zonen pyranometers, for which an error of -4% to +8% in the CM3 and 0.4% to 2.0% in the CM11 was the norm (Kipp & Zonen, 1992, 1995).

At low solar angles, the accuracy of global radiation is degraded by cosine errors (Augustine *et al.*, 2000). This is one of the motivations in the BSRN context for defining global radiation

(DSGL1) as the sum of diffuse (DSDFS) and normal direct (DSDIR * cos Z, where Z = solar zenith angle) radiation, as discussed in Section 2.5.4.

3.1.2.3 Thermal offsets

One weakness of pyranometers, is its susceptibility towards environmental temperature fluctuations and an induced phenomenon known as thermal offsets. This was the topic of thorough investigation and extensive documentation by authors, such as Smith (1999) and Dominguez (2001), who devoted entire dissertations to this topic. This offset quantity draws attention in the measured night-time quantities as a negative pyranometer signal in the absence of a solar signal. Hence the alternative term “night-time offset” or “zero offset”.

When the pyranometer dome is exposed to a “cool sky” (clear), mostly, but not necessarily at night, the pyranometer dome cools rapidly. This happens, because the radiometer dome has a large area exposed to the sky and only a small thermal mass with which to resist cooling. The cooling is transferred to the inner dome and thermopile, while the instrument body, unlike the dome, has large thermal inertia and does not cool off as quickly. This results in a reversed signal between the relatively warm body and the relatively cool thermopile, which is interpreted by the data acquisition system as a negative radiation quantity.

The negative quantity is not restricted to night-time measurements, as shown by the above authors. The impact of this error therefore has implications for present, as well as past pyranometer-generated daytime records, since a worldwide under-estimation of global, as well as diffuse quantities in climate records exists (Philipona, 2002). This was only discovered by combining measured and calculated quantities, using radiative transfer models. A responsible approach to the counteraction of thermal offsets should therefore be followed.

One such approach is proposed by Haeffelin *et al*. (2001). When thermistors are placed in the “cooling path”, thermal characteristics of the cooling components can be determined and accurate models to calculate the expected offset can be developed empirically. However, this approach requires, that the radiometers are dismantled and re-assembled again, which was not an option for SAWS.

A more common practice, also adopted at De Aar, is artificial ventilation (in terms of dedicated ventilators by the manufacturers) in a constant air stream over the instrument dome. This is an attempt to keep the dome temperature in synchronization with the ambient temperature, and ventilators ideally provide sufficient airflow to counteract the thermal offset.

However, there were times when the ventilators did not function. One such incident of notable proportion was the interruption in ventilation between 10 and 26 January 2003, as a result of lightning damage to the power supply unit on 8 December 2002.

The unventilated pyranometer output for this period is plotted against the global pyranometer (Figure 3.3) and the diffuse pyranometer (Figure 3.4) in two separate scatter-diagrams, as suggested by Dutton *et al.*, (2001).

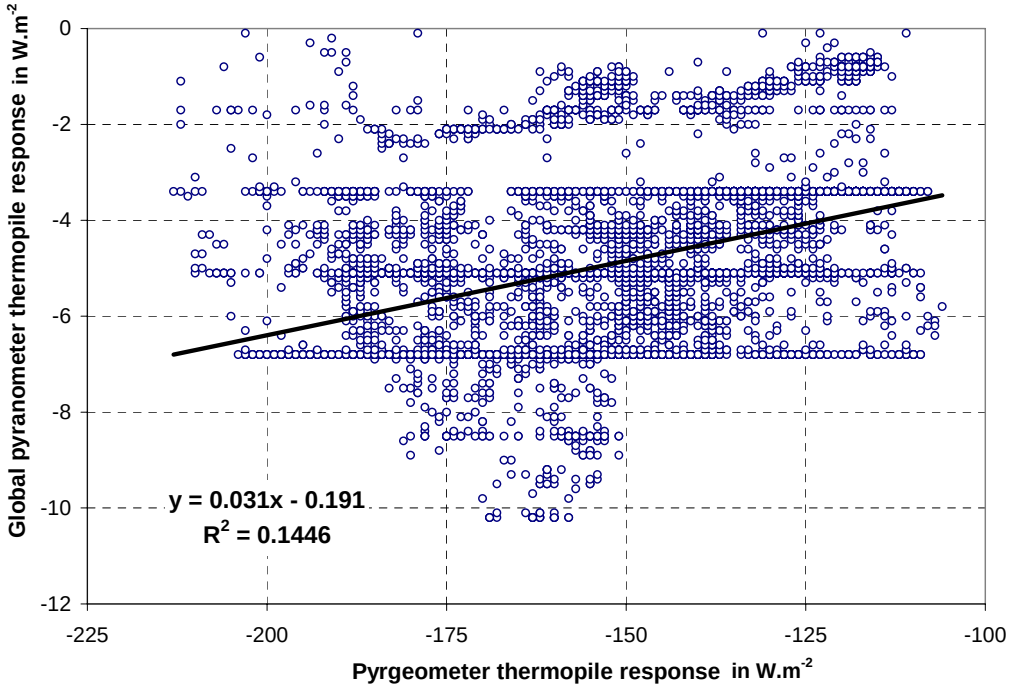

Figure 3.3 *Scatter plot for global pyranometer thermopile response versus pyrgeometer thermopile response for 10 to 26 January 2003*

Regression lines were drawn in both cases, but the R^2 correlation values are low and only a faint linear relationship between thermopile reactions of the pyrgeometer versus either the global or diffuse pyranometers exixts. The relatively large thermal offset errors during this period are well outside the pyranometer uncertainty goal, as discussed in Section 2.2.2.

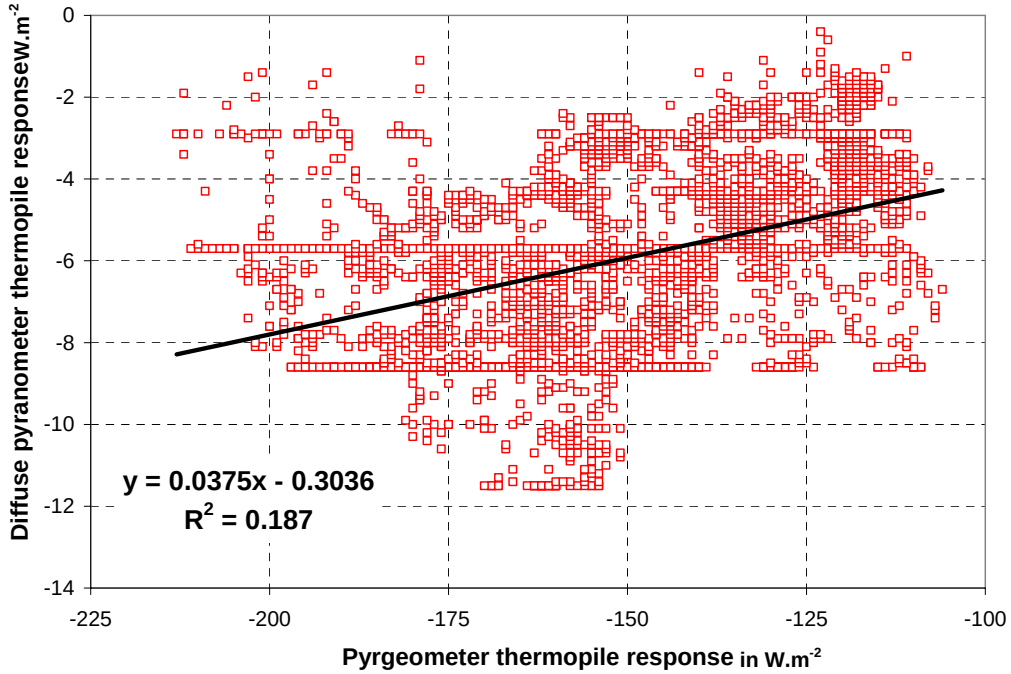

Figure 3.4 *Scatter plot for diffuse pyranometer thermopile response versus pyrgeometer thermopile response for 10 to 26 January 2003*

Another method to counteract thermal offsets is implemented by the Australian Bureau Of Meteorology (BOM). No artificial ventilation is applied and compensation for the measured quantities is calculated retrospectively, as described by Forgan (2001). This method has the following advantages:

- The system does not depend upon the proper functioning of ventilators, which have an uncertain reliability and efficiency.
- The compensation method, as detailed by Dutton *et al*. (2001), may be applied using only the thermopile outputs of the pyranometer and the pyrgeometer.
- This method also compensates for day-time thermal offset errors, which are difficult to determine otherwise.
- With no ventilators running, less power is consumed by the system.

3.1.2.4 Artificial ventilation and/or heating.

If snow or ice forms on the pyranometer dome, the option exists to heat the ventilating air with 5 W or 10 W, but not raising the ventilated air temperature by more than 0.1°C per W (Kipp & Zonen, 1994). However, for De Aar, having only 0.8 snow days per year (SAWB, 1986), the introduction of artificial heat is not justified. Winter is associated with dry air in an anticyclonic circulation over the interior of the country, including the De Aar region. The surface dewpoint is therefore in general so low that frost hardly forms.

Artificial ventilation has the advantage that the formation of dew and frost on the sensor dome is reduced, since there is a constant airflow and subsequent evaporation of any moisture droplets forming on the dome. However, care should be taken, that ventilation is not too strong, since significant measurement errors can be induced if the air flow is more than 3 $m.s^{-1}$ (Koshiek, 1996). Cleaning should also be done often because the added ventilation causes forced evaporation of moisture. If this moisture attracts atmospheric dust, it leads to a build-up of a thin layer of dirt (Kuik, 1997).

3.1.3 Aspects of pyrgeometers

The instrument used at De Aar for measuring surface LW radiation fluxes (wavelength more than 3.5 µm) at De Aar is the PIR, as discussed in Section 2.5.5 and featured in Figure 2.7.

The thermopile output of an upfacing PIR pyrgeometer was in first principal assumed to be proportional to Longwave Downwelling radiation (LWD), in a ratio equal to the thermopile's sensitivity to LW radiation. This approach led to erroneous measurements as described by authors such as Enz *et al.* (1975). The main cause of error was excessive solar heating of the (dark) instrument dome, re-radiating a significant amount of LW radiation from the dome towards the thermopile, resulting in measurements larger than true atmospheric LWD.

In an attempt to counteract radiative effects of the dome, a "compensation" circuit, as described by Fairall *et al.* (1998), was introduced to Eppley pyrgeometers. This circuit was meant to have an output equal to the dome radiative effect, so that when the circuit's output is superimposed upon the thermopile output, only true LWD is measured. Unfortunately this circuit is powered by a separate conventional dry cell battery, which is drained by the circuit relatively fast, leaving uncertainty as to the true amount of "compensation" it provides.

The big disadvantage is that no rectification of "data under suspicion" can be done afterwards, since the thermopile output is not recorded separately from the compensation circuit.

The BSRN community hence rejected the usage of the compensation circuit (WCRP-54,1991) and recommended that the effects are compensated for in an equation (3.3). The thermopile of a shaded ventilated pyrgeometer plus accurate individual temperatures of the metal body (case) and silicon-coated dome are used for this calculation. This Equation was introduced by Philipona *et al.* (1995):

$$E_{LW} = \frac{p}{C_1}(1 + k_1\sigma T_b^{\,3}) + k_2\sigma T_b^{\,4} + k_3\sigma(T_b^{\,4} - T_d^{\,4}) \qquad (3.3)$$

where

- p = thermopile millivoltage directly measured (expected to be -0.8 mV to 0.1 mV)
- C_1 = thermopile long-wave sensitivity constant (around 4 mV.W.m^{-2})
- σ = Stefan - Bolzmann constant
- T_b = instrument body (case) temperature
- T_d = instrument dome temperature
- k_1, k_2, k_3, = empirical constants

The exact values for k_1, k_2 and k_3 are unique for every instrument and can only be determined during an absolute controlled calibration (characterization) of a pyrgeometer - something that few BSRN sites have access to, or can even afford. However, if one assumes k_1 = 0, k_2 = 1 and k_3 = 3.5 , Equation 3.3 simplifies to

$$E_{LW} = \frac{p}{C_1} + \sigma T_b^{\,4} + 3.5\sigma(T_b^{\,4} - T_d^{\,4}) \qquad (3.4)$$

Equation 3.4. is in fact an earlier pyrgeometer equation described by Albrecht and Cox (1977), which was in common use for 18 years before Equation 3.3. was derived. Since SAWS do not have access to an absolute pyrgeometer calibration, Equation 3.4. was the more likely choice for LWD at De Aar. It was however, decided to perform an error analysis between Equations 3.3 and 3.4, using typical De Aar values for the variables, to quantify the expected error using Equation 3.4. instead of Equation 3.3.

3.1.3.1 Error analysis between two equations

Both equations consist of three terms, each characterized as follows:-

- Term 1: ($\frac{p}{C_1}(1+k_1\sigma T_b^{\,3})$ in Equation 3.3 or $\frac{p}{C_1}$ in Equation 3.4) equals net LW irradiance (upwelling LW minus downwelling LW).

- Term 2: ($k_2\sigma T_b^{\,4}$ in Equation 3.3 or $\sigma T_b^{\,4}$ in Equation 3.4) is the physical pyrgeometer body heat Term. This is just the application of the Stefan-Bolzmann equation to the pyrgeometer exposed to the sky as a blackbody radiator.

- Term 3: ($k_3\sigma(T_b^{\,4} - T_d^{\,4})$ in Equation 3.3 or $3.5\sigma(T_b^{\,4} - T_d^{\,4})$ in Equation 3.4) is the dome compensation Term. When the instrument is in operation, this Term is relatively small as a result of continuous shading of the instrument dome, leading to a small difference between T_b and T_d. Therefore, uncertainties in Term 3 as a result of 3.5 not being the exact number, are kept to a minimum.

Each of the terms is individually and exclusively influenced by the k-values: The error in k_1 will only influence Term 1, likewise k_2 only Term 2 and k_3 only Term 3. This means that the overall error can be assumed to be the sum of the errors for the respective terms.

The following long-term means applicable to Equation 3.4, were measured at De Aar:

- p = 0.713 mV
- C_1 = 0.000427 mV.W^{-1}.m^2
- T_b = 297.9 K
- T_d = 296.3 K
- E_{LW} = 312.9 W.m^{-2}

These numbers were used to evaluate the three terms of Equation 3.4 as -167.0 W.m^{-2}, 446.6 W.m^{-2} and 33.3 W.m^{-2} respectively. Note that the sum of these terms equals the long-term average of 312.9 W.m^{-2}.

The same long-term average values, as quoted above, were used to evaluate Equation 3.3, together with typical values for k_1, k_2 and k_3 found in absolute characterizations for the same PIR instruments used by Hirose (1998) and Philipona (1995). The errors in E_{LW}, using Equation 3.4 instead of Equation 3.3, was calculated for both the minimum and maximum of the Hirose and Philipona numbers, to set borders in the errors and show the range of these errors. These maximum and minimum errors were calculated term by term as the absolute (percentage) errors. In a further step, they were multiplied by the relative term size in the total LWD, to be normalized as relative (weighted) term errors, shown in Table 3.3.

Table 3.3. *Error estimation using Equation 3.4 for typical De Aar values instead of Equation 3.3*

Term	Equation 3.4		Equation 3.3				Absolute term error		Relative term error	
	Value for k	Term size in W.m^{-2}	Value for k		Term size in W.m^{-2}					
			Min	Max	Min	Max	Min	Max	Min	Max
Term1	0	-167.0	0.053	0.138	-180.2	-191.3	-7.94 %	-14.5 %	-4.72 %	-8.63 %
Term2	1	446.6	1.0024	1.0198	447.6	447.6	0.24 %	1.98 %	0.35 %	2.86 %
Term3	3.5	33.3	2.5	4.3	23.8	40.9	-28.6 %	22.9 %	-2.95 %	2.36 %

The sum of the extreme relative errors, irrespective of whether such an extreme is the result of the maximum or minimum value for k, now yields a "worst case scenario" percentage for both extremes, -11.24 % and 0.50 % respectively. The overall mean error using Equation 3.4 instead of Equation 3.3. is therefore the mean between these extremes. i.e. -5.37 %. This translates to 16.8 W.m^{-2}, using the long-term LWD average. It should be noted that it exceeds the range discussed in Section 2.2.2.

From Table 3.3 it became obvious that the main contributor to this error is Term 1, or more specifically, the fact that k_1 = 0 is used instead of a more realistic number between the typical values of k_1 = 0.053 and k_1 = 0.138.

3.1.3.2 Relative contribution of terms in LW equation

The significance of each of the three terms in Equation 3.4 is now illustrated by choosing representative days in different seasons and sky conditions. Continuous midnight-to-midnight plots of one-minute values of Term 1, Term 2 and Term 3, as well as LWD (sum of terms) are presented in Figures 3.5, 3.6, 3.7 and 3.8. All times are quoted in Universal Time

(UT). Note that South African Standard Time (SAST) = UT + 2 hours throughout the year. Figure 3.5 depicts a clear sky winter day (2 June 2000).

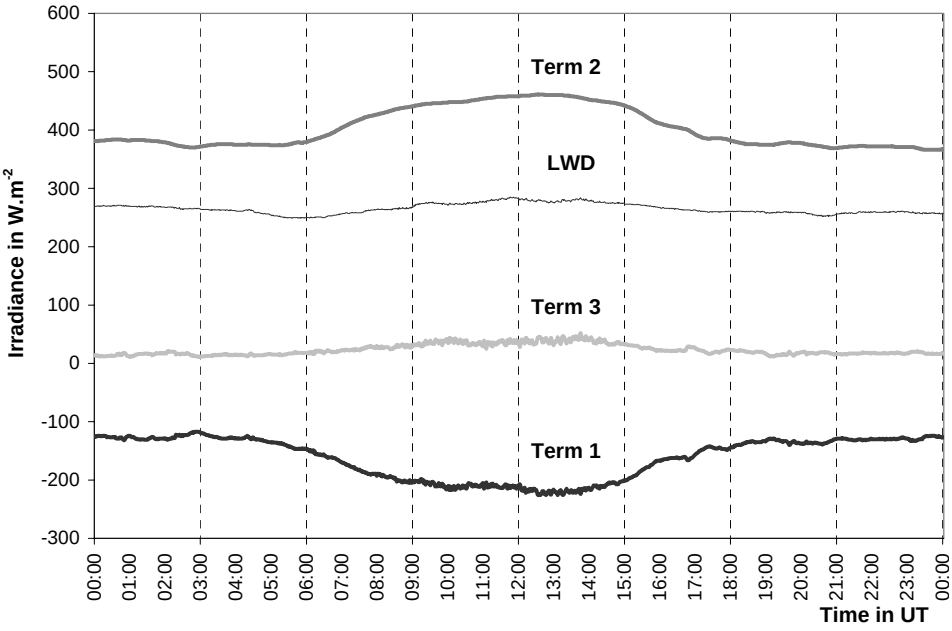

Figure 3.5 *Individual LWD term contribution on 2 June 2000*

The weather experienced on this day is typical for the country's interior during the winter. The diurnal pattern of atmospheric heating, starting at sunrise (05:14 UT) and ending at sunset (15:30 UT) is reflected in Term 2, while Term 1 is almost an exact mirror-image of Term 1, i.e., a classic example of "what goes in also goes out". The steadiness of Term 3 in proportion to the other terms, also results in the flat line for LWD. For this day, the minimum LWD = 249 $W.m^{-2}$, while the maximum LWD = 285 $W.m^{-2}$, hence the range of LWD for that day (maximum minus minimum) is only 36 $W.m^{-2}$.

Figure 3.6 (A partly cloudy winter day, 22 June 2000), shows the profound effect that clouds have on the measurement of LWD. Compared to 2 June 2000, sunrise is now 7 minutes later (05:21 UT), and sunset virtually at the same time (15:31 UT). Term 2 shows the same diurnal pattern than in Figure 3.5, but with a downward slope towards the late afternoon, which can be attributed to the presence of clouds.

For all three terms, as well as LWD, the values are similar to those of Figure 3.5. An exception is Term 3, which shows more features embedded in a relatively straight line. By far the biggest contributor to the differences between Figures 3.6 and 3.5 is Term 1. Notice how the characteristics of Term 1 are almost mirrored in LWD for that specific day. The presence of clouds prevents the emmission of LW radiation and leads to an overall higher

LWD level, although gaps in the clouds allow for emmissions, such as the “dip” between 12:50 UT and 13:50 UT.

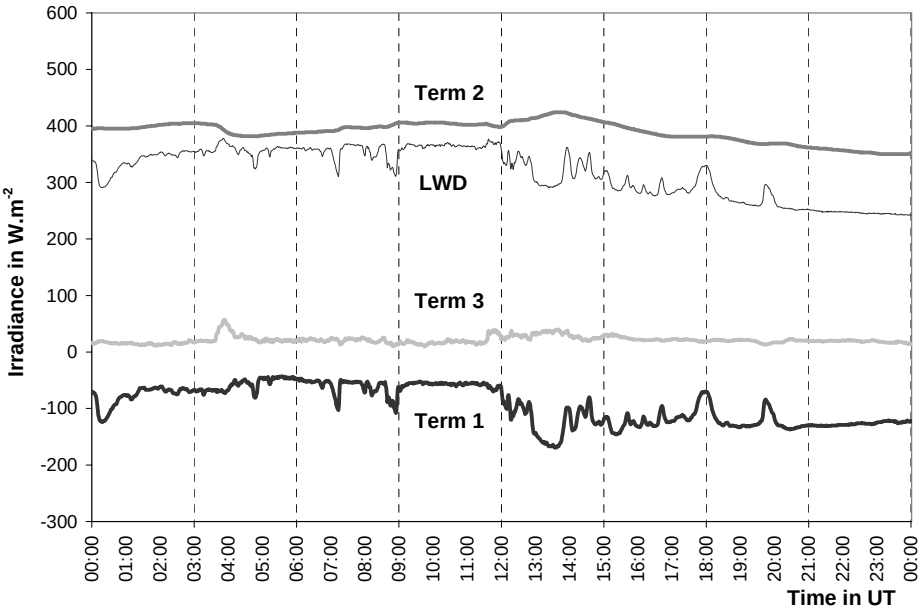

Figure 3.6 *Individual LWD term contribution on 22 June 2000*

Perfect clear-sky days in summer are rare and Figure 3.7 (30 December 2000) depicts a summer day with only thin clouds present - for all intents and purposes, a clear sky day.

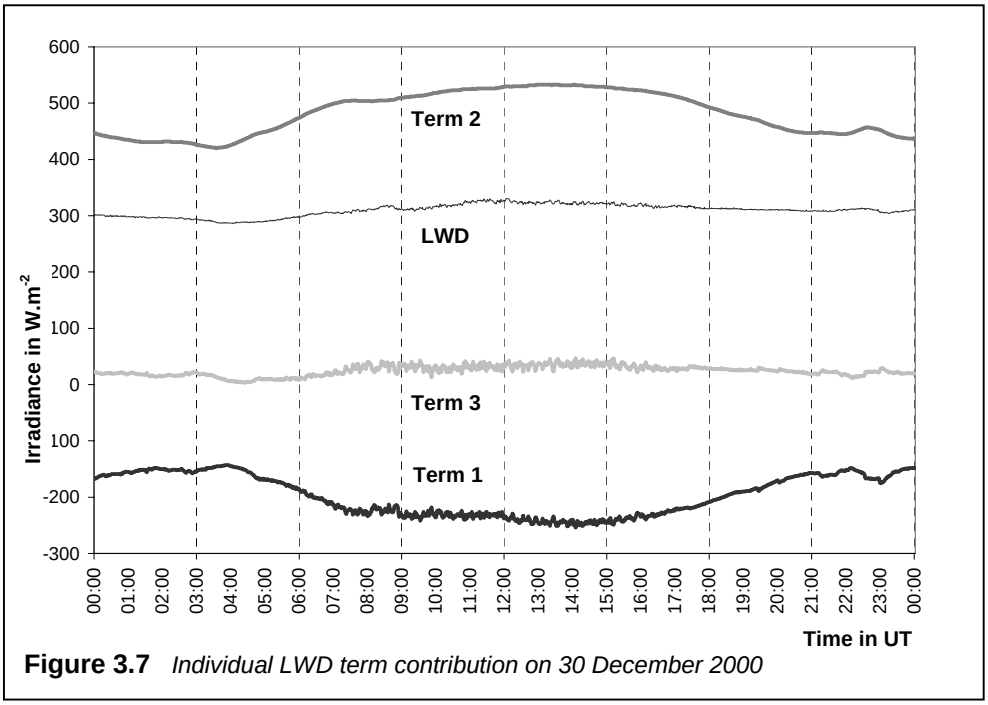

Figure 3.7 *Individual LWD term contribution on 30 December 2000*

The same pattern as in Figure 3.5 is present here, although sunrise occurs already at 03:23 UT and the sun sets at 17:30 UT. A longer day and more perpendicular incident SW

radiation is reflected in overall higher values for Term 2. This is mirrored in the same way as in Figure 3.5 through lower values in Term 1, since the incident SW radiation is re-radiated again almost in its entirety as LW radiation. Minimum LWD = 292 W.m^{-2}, Maximum LWD = 375 W.m^{-2}. The range of LWD is 83 W.m^{-2} for this clear summer day, compared to 36 W.m^{-2} for the clear winter day.

Figure 3.8 (11 December 2000) is the classic example of a summer day where clouds developed during the course of the day and either precipitated at the site, or drifted away, clearing towards the late afternoon.

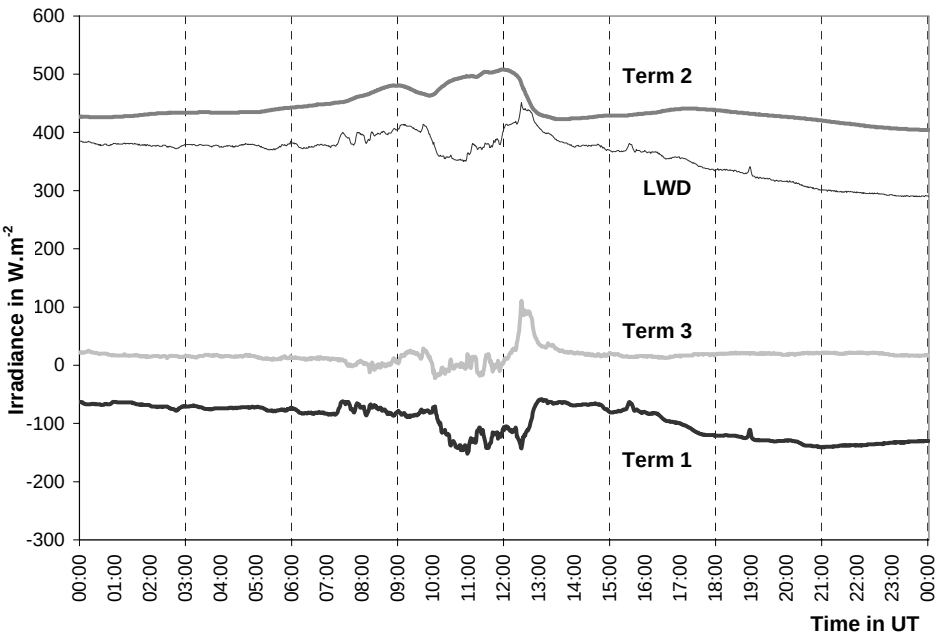

Figure 3.8 *Individual LWD term contribution on 11 December 2000*

From sunrise at 03:14 UT up to 08:00 UT, the SW radiation input increases and Term 2 shows a smooth and steady rise. Between 08:00 UT and 10:00 UT, cloudiness introduces features to Term 1 similar to those of a cloudy winter day (Figure 3.5), while Term 2 shows a marked decrease between 08:00 and 09:00. Between 10:00 UT and 13:00 UT, cloud cover increases and there was mild precipitation between 13:00 and 13:20. The prominent peak in Term 3 during this time, can be attributed to thermal shock as a result of the precipitation (cool water on the hot dome).

With the sky now clear after the mid-afternoon storm, Term 1 steadily decreases after 13:20 UT along with a more or less similar smooth line that can be seen prior to 08:00 UT, as the earth cools down and radiates long-wave radiation. Term 2 does not respond likewise, since the sun is already low at this stage and about to set. After sunset, (17:20 UT) a change in

the steady slope of Term 1's decline can be seen, leading to LWD values lower than during the corresponding summer clear sky day in Figure 3.7.

3.1.3.3 Artificial ventilation and/or shading

Modern operation of the pyrgeometer requires continuous shading of the dome, since SW radiation is easily absorbed by the dark dome, leading to heating, false secondary radiation towards the thermopile (Ji *et al*., 2000), and subsequent false signals.

The reason for ventilation of the pyrgeometer is the same as for a pyranometer, viz., equating the dome and "naked" thermopile temperatures as much as possible. In the case of the pyrgeometer, the ventilation also attempts to prevent a temperature gradient developing on the dome leading to false signals (Richardson, 2000). Philiopona (1995) showed, that pyrgeometer errors may largely be reduced by applying the Swiss modification, as discussed in Section 2.5.5.

Standard pyrgeometer and pyranometer ventilating devices were continuously operational at De Aar. The one exception is during power failures, which also resulted in tracker stoppages (Section 3.1.4.2). For the operational history of the De Aar BSRN station, tracker stoppages and ventilator failures are closely related.

3.1.4 Aspects of the solar tracking system

The presence of a shading ring to enable diffuse pyranometric measurements in the absence of solar tracking, was discussed in Section 2.5.3. However, the resultant data will have uncertainties due to the empirical and often inadequate correction factors that such a ring requires (Battles, 1995).

A ring and correction factors are not necessary for De Aar since the Sci-Tek two-axis solar tracking system comprises a shading device providing sufficient and continuous shading for the diffusometer (diffuse pyranometer) and pyrgeometer. However, the accuracy of all measurements except global radiation, therefore relies heavily on the accuracy of the tracker, and special care should be taken that the tracking device is accurate at all times.

Tracking failures have occurred for the following reasons since inception of the De Aar site:-

- Stopping of the solar tracking system due to power failures as a result of a combination of lightning strikes and/or routine maintenance on the municipal electricity supply leading to exhaustion of the Uninterrupted Power Supply (UPS).

- Power switched off during preparations for calibration and other site maintenance.

- Temporary misalignment of either the pyrheliometer or shading device.

3.1.4.1 Tracker misalignments

An active solar tracking system constantly observes the sun through a special series of sensors, which are aligned perfectly with the instruments. The sensor outputs constantly adjust the tracker drive motors and alignment in a feedback process for perfect solar tracking. A passive solar tracking system makes use of calculations of the solar position, and subsequent movement of the tracker motors to follow the sun "blindly".

An ideal solar tracking system is a passive system by default, able to switch to "active" mode when the sun is visible, and able to switch to passive mode when there is no visible sun.

The De Aar tracker is entirely passive, therefore regular inspections (three times a day, i.e., once near solar noon, once in the morning and once in the afternoon during about 45° solar elevation), are necessary to identify and rectify solar tracking errors.

One way of proactively addressing the effects of tracker errors, is to use redundant pyrheliometers. In Section 3.1.1.1 and Figure 3.2, the effect of a misalignment was illustrated and discussed. Taking readings from *both* pyrheliometers instead of one and picking the higher reading per recording interval, calls for a better aligned instrument every time. The philosophy of rather taking the best measurement of a given signal than the best measurement per individual instrument, (even if that signal arises from two different instruments; Ohmura *et al.,* 1998), is applied here.

In Figure 3.9, the readings for two (slightly) misaligned pyrheliometers are featured. By taking the higher of the readings, a better reading for direct radiation is obtained.

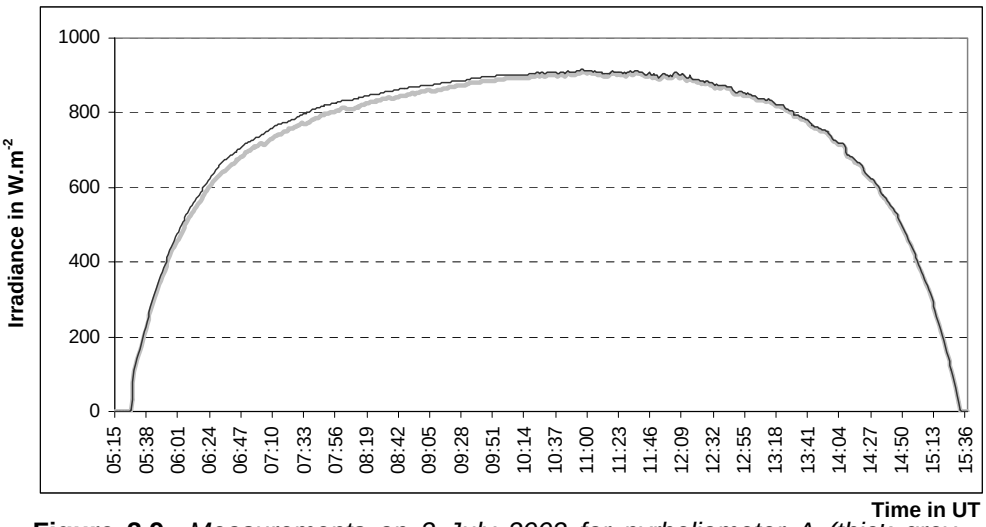

Figure 3.9 *Measurements on 2 July 2002 for pyrheliometer A (thick grey line), misaligned with pyrheliometer B (thin black line).*

3.1.4.2 Tracker stoppages

The best and only way to identify such occurrences is prompt and accurate reporting, backed up by skilled attendance to the problem. Using recorded data alone in an attempt to identify erroneous data is not the best way to correctly identify such events. An example of dealing with data from a prolonged tracker failure resulting from a power failure is shown in Figures 3.10 to 3.13.

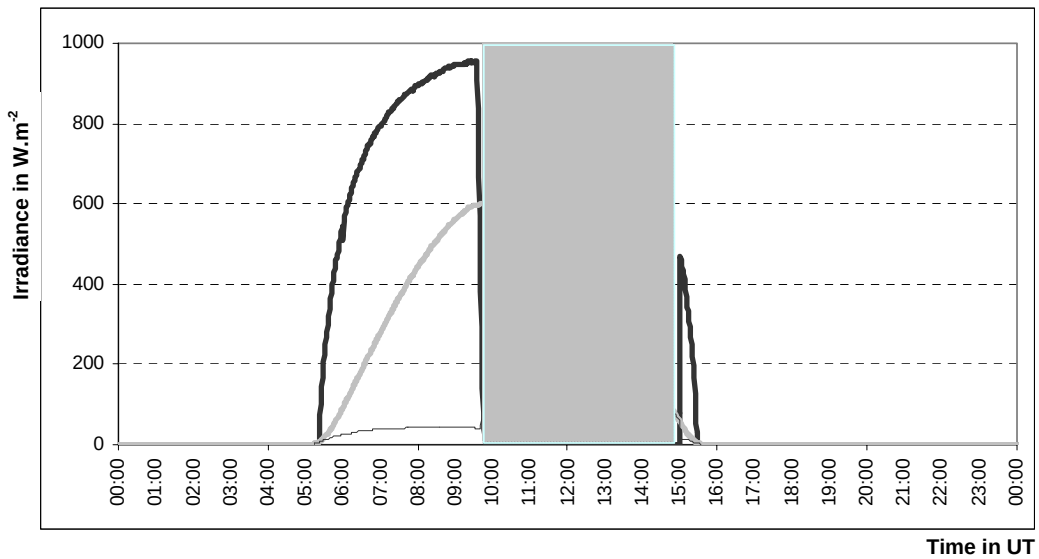

Figure 3.10 *Time-series for direct (thick black line), global (thick grey line) and diffuse (thin black line) radiation for 9 June 2002. The period of tracker failure is shaded.*

On 9 June 2002, maintenance on the commercial power lines commenced at 06:00 UT and the UPS was exhausted by about 10:00 UT. The power was restored at 15:00 UT.

In Figure 3.10, the impact of tracker failure is best illustrated in plots of SW radiation. The day was almost entirely cloud-free, except for a small incident of what appears to be scattered clouds, between 13:20 UT and 13:50 UT. This, however, did not interfere with what is intended to be illustrated here. The shaded area represents the period when the tracker stood still. Note that, immediately after the UPS power failed, output from the diffuse sensor increased sharply to co-incide with the global, while the direct radiation dropped to zero.

Now consider the equation

$$global(t) = diffuse(t) + direct(t)\cos Z \qquad (3.5)$$

where Z = solar zenith angle

in the context of

- DSGL2 = global radiation measured by the unshaded pyranometer
- DSGL1 = global radiation calculated using diffuse and direct radiation

Equation 3.5 then translates to

$$DSGL2 = DSGL1 \qquad (3.6)$$

Equation 3.6 should be valid before, after and during the tracker failure, as pointed out by Mc Arthur (1998), except for a small glitch on the moments of transition, due to different instrument reaction times. The "glitches" can be used to highlight the times of tracker failure. Consider a time-series graph of DSGL2 / DSGL1 for the same day shown in Figure 3.10.

For the entire day, including the period of tracker failure, DSGL2 / DSGL1 is close to 1 (Fig 3.11), with only a slight offset prior to tracker failure. The sharp "spikes" appear at sunrise (05:17 UT), sunset (15:29 UT) and to a comparable extent at the edges of the tracker failure times, indicated by the shaded area in Figure 3.11.

Since diffuse and direct instruments incur a "shock" signal during events such as tracker failures (diffuse exposed to higher than normal irradiance and the direct to less than normal), the different response times to adjust to normal leads to spikes similar to the sunrise/sunset spikes along the shaded areas represented in Figure 3.11. If "shocks" are used to identify tracker failure times, it would have limited use, since the "shock" effect would be masked in

partly cloudy to cloudy conditions where natural "shocks" of the same magnitude, can overrule the "shock" effect results from tracker failure.

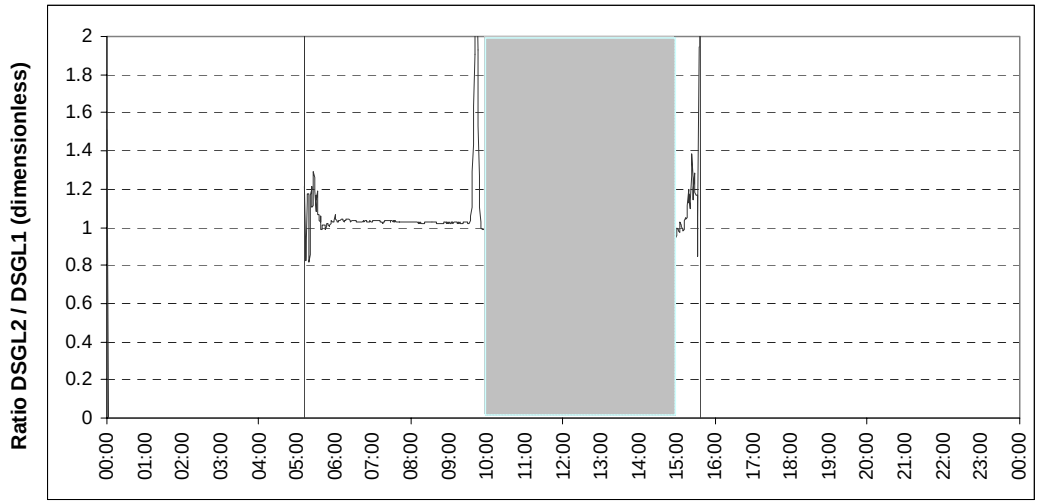

Figure 3.11 *Time-series of the ratio DSGL2/ DSGL1 for 9 June 2002. Tracker failure time is shaded.*

The tracker failure not only impacted on SW measurements, but also on the LW. The absence of shade on the pyrgeometer dome, leads to absorption of SW radiation, abnormally high temperature and re-radiation towards the thermopile, which receives a biased signal. In Figure 3.12, the values of the three terms of Equation 3.4, as well as LWD, are plotted for 9 June 2002. The shaded area represents the period of tracker failure.

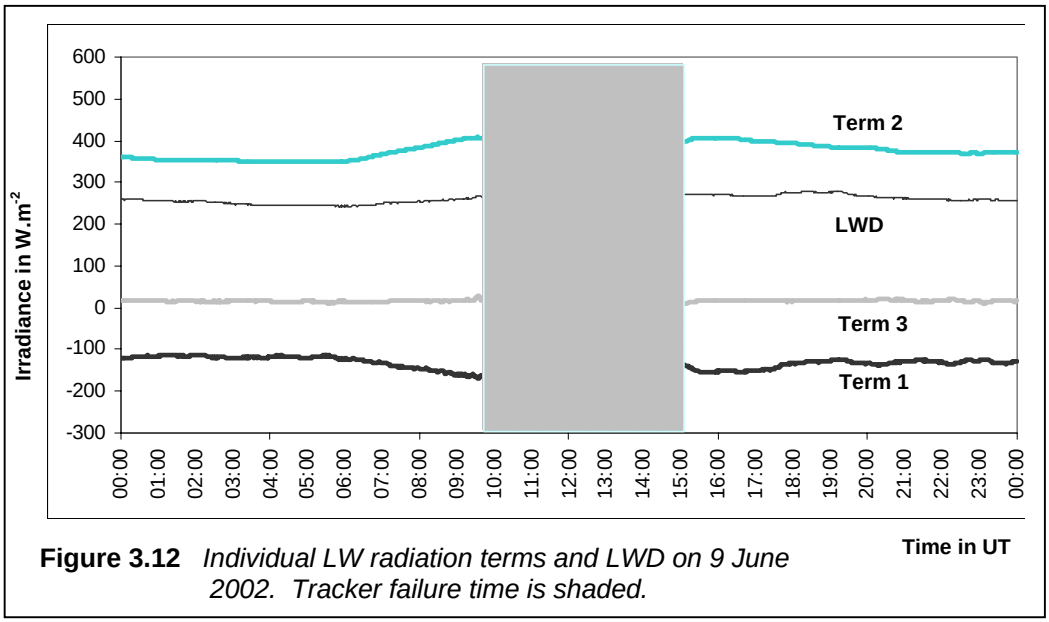

Figure 3.12 *Individual LW radiation terms and LWD on 9 June 2002. Tracker failure time is shaded.*

In Figure 3.12, Term 1 (the thermopile) shows a strong positive influence as a result of the solar heating. Term 2 (usually a smooth curve on a clear day, compared to Figure 3.5.)

shows signs of an impact from something else than LWD. Term 3 shows signs of an initial shock, recovering slowly. After shading is restored, it takes about half an hour to return to normal. Surprisingly little impact is shown on LWD using the scale of Figure 3.12.

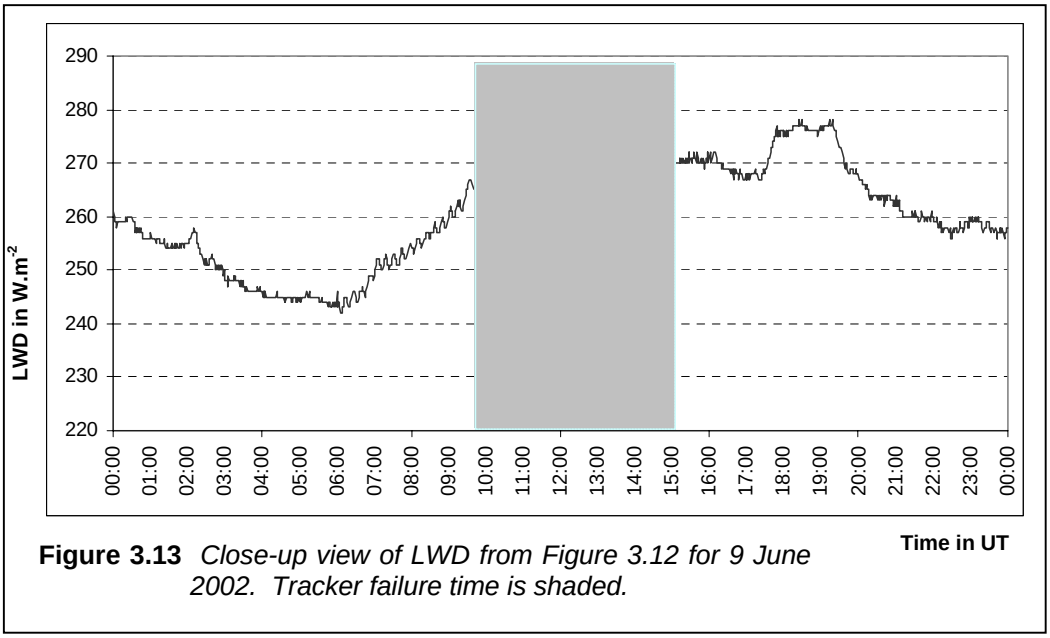

Figure 3.13 *Close-up view of LWD from Figure 3.12 for 9 June 2002. Tracker failure time is shaded.*

Figure 3.13 shows a closer view of LWD alone with an enhanced scale. A distinctive drop of about 10 $W.m^{-2}$ in LWD immediately after the tracker failure and a spike of about the same amount shortly before recovery, is observed.

3.1.5 Identifying instrument cleaning times

Normal station routine requires, that the time of daily dome and window cleaning is documented and reported. However, reporting instrument camp visit times and the subsequent deletion of data contaminated by human presence in the camp while cleaning the instruments often encompasses periods in the order of several minutes, for example ten. Normally one or two at the most of those ten minutes are truly unusable data. Here is a way of using the recorded data, to more accurately identify instrument cleaning times and serve to preserve more data.

As a result of the high 1 Hz sampling rate, the passage of a cleaning cloth over any of the sensors (even for a period of only one second) will guarantee that at least one sample less than the “true” irradiance is recorded. This false sample will reflect in the one-minute

statistics to different extents, depending on the sensor and the atmospheric conditions. Pyrheliometers reflect this effect maximally, given the narrow field of view. Thus, the cloth is expected to completely cover the aperture at a given moment and in principle a zero sample amidst a high irradiance level, is possible.

Redundant measurements for maintaining the record in case of occasional instrument failures for the many reasons instruments fail, are recommended (Mc Arthur, 1998). In the case of pyrheliometers, it can also be a means of identifying instrument cleaning times. The assumption is made that the human hand cleaning the two pyrheliometer windows, cannot do it simultaneously, and also is unlikely to spend exact time (up to the nearest millisecond) on each. Therefore those anomalies should be reflected in the data, and in particular, the standard deviation of the 1 Hz samples.

Table 3.4 lists a few succeeding one-minute averages (AVG) and corresponding one-minute standard deviations (OSD) for the two De Aar pyrheliometers, as well as for the diffuse and global pyranometers. The data was recorded between minutes 354 (05:54 UT) and 369 (06:09 UT) of day 186 of 2002 (4 July 2002). The OSD for the pyrheliometers, as well as the difference between the OSD for the two pyrheliometers, are shaded columns. The actual instrument cleaning time, is highlighted as a black row.

Table 3.4 *One-minute De Aar data for 4 July 2002 between minutes 354 and 369*

Year	Day of year	Minute of day	Pyrheliometer A		Pyrheliometer B		Diffuse pyranometer		Global pyranometer		Difference (N – M)
			AVG	OSD(M)	AVG	OSD(N)	AVG	OSD	AVG	OSD	
2002	186	354	276	0.5	284	0.5	24	0.0	50	0.8	0.0
2002	186	355	285	6.4	293	6.7	25	0.5	53	1.2	0.3
2002	186	356	300	2.0	308	2.0	26	0.6	56	0.3	0.0
2002	186	357	306	2.3	315	2.3	27	0.1	59	0.8	0.0
2002	186	358	314	2.4	323	2.5	27	0.0	61	1.5	0.1
2002	186	359	322	1.8	332	2.4	27	0.0	64	1.0	0.6
2002	186	360	327	1.4	340	2.1	29	1.0	66	0.2	0.7
2002	**186**	**361**	**330**	**17.6**	**345**	**11.2**	**30**	**0.3**	**69**	**0.6**	**-6.4**
2002	186	362	342	2.0	356	2.1	30	0.0	72	1.4	0.1
2002	186	363	348	1.9	362	1.9	30	0.0	74	1.0	0.0
2002	186	364	355	1.8	369	1.9	31	0.5	77	0.6	0.1
2002	186	365	360	1.5	374	1.5	32	0.6	79	0.8	0.0
2002	186	366	366	1.7	380	1.6	33	0.0	82	1.4	-0.1
2002	186	367	373	2.1	386	2.1	33	0.0	85	1.3	0.0
2002	186	368	381	2.2	394	2.2	33	0.0	87	1.0	0.0
2002	186	369	388	2.1	401	2.1	34	0.8	90	0.4	0.0

Relatively low OSD for both pyrheliometers are observed immediately before and after the minute (minute 361 = 06:01 UT) including the actual cleaning. This is indicative of a clear sky. The diffuse and global OSD are also low. At minute 361, the OSD for both pyrheliometers are abnormally high. This abnormality is also reflected in -6.4 (their difference, right column, shaded). The OSD for global and diffuse does not show any difference at that particular minute with respect to others.

The high OSD difference for pyrheliometers is put into perspective with Figure 3.14.

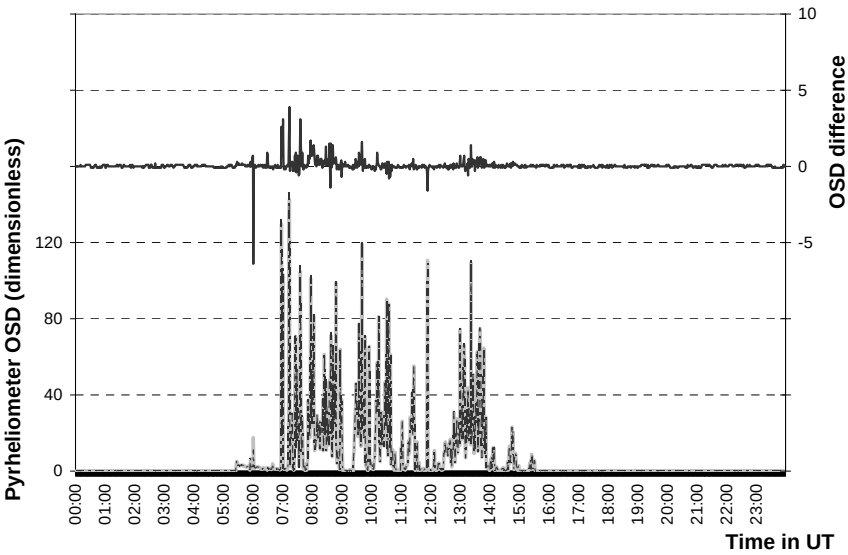

Figure 3.14 *Midnight-to-midnight time-series for 4 July 2002 of the shaded columns in table 3.4:* **(***Pyrheliometer A OSD (thick grey line) and pyrheliometer B OSD (dashed line) and difference (thin black line).*

Notice in Figure 3.14 that the outstanding number of -6.4 (at 06:01 UT) is by far the largest absolute difference between the pyrheliometers' OSD. This value, either positive or negative, never features elsewhere on that day, even though the OSD themselves reach high proportions as the day becomes partly cloudy from 07:00 UT onwards. Note that some differences in OSD are exhibited after 07:00 UT, but not to the extent of the -6.4 value.

To illustrate the conservativeness of pyrheliometer OSD difference with respect to individual pyrheliometer OSD fluctuations, consider Table 3.5. which depicts the same variables for the same day, 4 July 2002, but between minute 562 (09:22 UT) and minute 590 (09:50 UT).

Table 3.5 *One-minute De Aar data for 4 July 2002 between minutes 562 and 590.*

Year	Day of year	Minute of day	Pyrheliometer A		Pyrheliometer B		Diffuse pyranometer		Global pyranometer		Difference (N – M)
			AVG	OSD(M)	AVG	OSD(N)	AVG	OSD	AVG	OSD	
2002	186	562	782	0.5	793	0.3	132	2.2	584	2.6	-0.2
2002	186	563	782	0.1	794	0.2	140	2.6	593	2.7	0.1
2002	186	564	774	7.6	786	7.4	149	2.9	599	3.7	-0.2
2002	186	565	758	11.1	770	11.1	159	2.7	601	5.0	0.0
2002	186	566	663	22.4	675	22.5	168	3.2	557	14.4	0.1
2002	186	567	643	30.0	655	29.9	178	2.9	558	15.5	-0.1
2002	186	568	437	34.7	447	35.2	185	2.9	450	19.7	0.5
2002	186	569	554	45.9	566	46.3	195	2.1	529	27.8	0.4
2002	186	570	407	31.3	419	31.6	200	1.3	448	19.0	0.3
2002	186	571	506	36.6	518	36.5	206	2.0	512	22.5	-0.1
2002	186	572	575	22.9	587	23.1	212	1.5	556	14.2	0.2
2002	186	573	550	18.2	561	18.3	213	0.4	543	10.7	0.1
2002	186	574	571	32.1	581	32.1	212	1.8	554	19.5	0.0
2002	186	575	241	77.2	249	78.1	204	1.9	356	46.0	0.9
2002	186	576	185	19.8	192	20.4	202	0.7	322	12.4	0.6
2002	186	577	159	22.0	165	22.5	198	1.4	301	14.6	0.5
2002	186	578	146	14.4	152	14.7	192	1.7	288	8.0	0.3
2002	186	579	153	12.9	160	13.0	186	1.9	287	7.3	0.1
2002	186	580	237	55.4	245	55.9	180	2.0	331	32.9	0.5
2002	186	581	452	119.3	462	120.9	176	0.0	455	70.0	1.6
2002	186	582	545	21.6	557	21.8	170	3.3	502	15.1	0.2
2002	186	583	578	29.7	590	29.4	162	1.9	513	15.5	-0.3
2002	186	584	710	23.5	721	23.9	156	2.1	583	12.6	0.4
2002	186	585	691	17.6	703	17.5	148	2.1	566	10.7	-0.1
2002	186	586	629	42.5	641	42.9	141	2.5	523	27.3	0.4
2002	186	587	705	70.6	716	71.1	136	0.0	563	41.3	0.5
2002	186	588	765	4.8	776	4.7	134	1.3	594	1.9	-0.1
2002	186	589	777	2.4	788	2.4	129	1.3	598	1.5	0.0
2002	186	590	773	9.2	783	9.1	126	1.4	591	5.2	-0.1

Notice that high OSD for the individual pyrheliometers are not reflected in OSD difference close to the value of -6.4 featured in Table 3.4.

3.1.6 Aspects of the data acquisition system

Interaction between sensors and a data acquisition system may lead to a variety of errors experienced at De Aar, such as: runtime errors in the logger programme; wrong input signal measurement by logger due to ageing; overwriting of a data section in memory by program or vice versa; infrequent downloading leading to new data overwriting older data in logger and not enough room for error in case of power or computer failure, resulting in non-downloading of the logged data.

A good reliable and accurate datalogger forms the heart of any modern data acquisition system. It both measures and records sensor outputs as a basic function, while added value is the possibility of routine statistical calculations, such as the average, standard deviation, minimum and maximum of a number of samples on the data as they are collected. The latter proves to be a vital space saving mechanism when collecting data for the purpose of reporting the one-minute BSRN statistics. However, one disadvantage is, that the original samples are not available for re-evaulation should the need arise.

The ideal situation would be recording and storage of all measured samples, and applying calculations to produce the one-minute statistics only later on from the archived samples. An enormous logging and downloading capacity is a prerequisite, as well as a very reliable (ideally: dedicated) and short connection between the datalogger and site PC. This proved to be unfeasible for De Aar, given the large distance between the site at De Aar and SAWS Head Quarters in Pretoria, being 840 km apart. The best ecomonical logger byte-budget had to be compiled, to store as much information in the smallest space.

For typical data storage, note that one radiation parameter typically has 4 significant figures, therefore it needs a minimum of 5 digits to round the measured value off with confidence. One parameter therefore occupies 8 bytes of data (a space both sides, plus one for the decimal point). If every logged sample is date-and-time-stamped in the format *yyyy ddd hh mm ss* for future reference and/or recalculation it adds to a record containing 24 bytes, storing one sample per quantity. This is actually the area where a lot of space is still wasted, and, if resolved one way or the other, storing all the samples could be reconsidered.

In one minute, 60 samples are stored, 1440 bytes occupied per minute. For the basic quantities: global, direct and diffuse, the bytes amount to three times that amount. If LW measurements are also added to the same logger, three additional samples (thermopile, case and dome thermistors) are needed. This amounts to six times the said amount, 8640 per minute, or 12 441 600 bytes (11.86 MB) per day. This exceeds the logging capacity of a standard 1024 kb logger by almost 11½ times, neglecting room for a logging programme.

The raw data of 12 MB alone per day would fill the 10 GB hard drive, which was standard in a Personal Computer (PC) at that time, in less than 2 years leaving only little room for movement (backups or programs). Drastic economization steps had to be applied for De Aar, in order to create room for movement, whilst maintaining the highest possible resolution of data storage.

A very serious practical factor that had to be taken into consideration, was the distance of about 840 km between the site and headquarters. In the case of lightning strikes damaging the systems (three times between August 1999 and July 2003), enough room must exist on any given logger for data storage before a fresh PC can be dispatched to download the logger. This time lag is typically between 4 and 10 days.

The logging efforts were separated in a SW and a LW logger, each having unique characteristics and logging styles. This also doubled the logging capacity. In the case of a SW-logger, the samples can all can be processed in means, standard deviations, minima and maxima within the logger, without having to store 1 Hz samples. In the LW logger, recalculations warrant storage of original samples, whilst one-minute statistics of the measured components (thermopile, case and dome temperatures) cannot be applied to calculate the one-minute statistics of LWD. To store and date-time stamp all samples was not a feasible option, so a hybrid approach was followed. On the one hand, the logger program calculates LWD and reports one-minute statistics, but on the other hand, stores every n^{th} sample to have a number of samples per minute available for recalculations.

One sample in the new compact format looks like this :- *yyyy ddd hhmm dir1 dir2 dir3 dir4 dif1 dif2 dif3 dif4 glo1 glo2 glo3 glo4 lwd1 lwd2 lwd3 lwd4 temp hum pres* where yyyy = year, ddd = day of year (1 to 365 or 366), hhmm = time in hour and minute ; dir, dif, glo, lwd are the basic parameters direct, diffuse, global and downwelling longwave radiation, the number 1-4 behind these parameters are average, standard deviation, minimum and maximum, respectively; temperature, humidity, atmospheric pressure = meteorological quantities measured in a Stevenson screen. One record per minute in this new format, is 107 bytes long. This translates to 1.03 MB per week.

3.1.7 The usage of an on-site PC

A site PC is the “heart” of a data acquisition system, through its communication with a data logger. The PC compiles and sends a program to the logger and downloads data from the logger at preset intervals, it also stores and manages the downloaded data and communicates the data to the outside world, either by storage of data on removable media or transmission by means of network connections.

For De Aar BSRN, the multiple loggers demanded quasi-simultaneous processing in fast downloading of the relatively large volumes of data. This was achieved by a special serial port splitter, offering a unique serial port per device (logger). At the time of establishing the BSRN site at De Aar, modems and telephone connections were in the process of being phased out (Esterhuyse, 2000), and systems based upon a Wide Area Network (WAN) with PC terminals were the best outlook towards the future, and thus adopted.

3.1.8 Time keeping: Global Positioning System (GPS)

The high BSRN sampling frequency (1Hz) demands, that a high premium is placed on the correctness of time-stamping in sampled and derivated data products (one-minute statistics).

Time correctness is of further essence, since future research on data will involve the integration of datasets captured independently and under different circumstances and/or calculation of numbers, such as solar position, that involves accurate definitions of time. The biggest need for accuracy is when the sky is not clear, since small radiation features, which are the benefit of such high-resolution sampling, have to be correctly date- and time-stamped when captured.

At De Aar, the on-site PC is time-controlled by a Garmin GPS-36 polling a serial port once a second. The accurate PC time is transferred once every four hours to all system loggers and connected peripheral equipment.

3.2 MAINTENANCE SYSTEM

Due to the prolonged exposure of radiation instrumentation to solar radiation, regular maintenance is needed. This maintenance may consist of the following elements:

- Regular inspection (daily) of the general condition of the radiometers, including ventilation, levelling, pyrheliometer sun spots and shade spots. This also includes cleaning of all optical parts.

- Monthly inspection of the drying cartridges and electrical connections.

- Bi-annual (twice a year) calibration of the operational pyrheliometer, as well as swopping the global and diffuse pyranometers and turn-calibrate the pyranometers using the pyrheliometer calibration and the global/diffuse/direct relationship in Equation 3.5.

3.2.1 Regular inspection

A list of daily tasks comprises: Cleaning of instrument windows and domes, especially after precipitation events; Verification of tracker functions - reporting downtime. Verify, that all ventilators are functioning - and report downtimes. Inspection of solar spots on pyrheliometer and report misalignments.

3.2.2 Calibration

Regular calibration of SW radiation instruments, at least once a year, is recommended - six months being the normal proceedings (Mc Arthur, 1998). During a calibration event, the cavity radiometer is compared against the operational pyrheliometers. Conditions that have to be met, are the following:

- A cloudless day for periods when the global irradiance exceeds 700 $W.m^{-2}$
- No noticeable wind, as not to distort temperature stability in the cavity radiometer (WMO,1983).

The advantage of this *modus operandum* is that the pyrheliometers are not withdrawn from duty whilst in calibration mode. Their outputs are recorded with the cavity pyrheliometer's outputs, the ratios of (operational radiometer / cavity radiometer) are calculated for every period of integration (a "run") and new sensitivity constants are subsequently calculated for the pyrheliometers.

After the pyrheliometer constants are calculated, the global and diffuse pyranometers are swopped. The data of the periods before and after the swopping is used to determine new calibration constants for the pyranometers. In this way, the pyranometers are also out of operation for a short period of time, and if the swoppings are performed by night, no data at all need to be lost as a result of the calibration.

So far, only radiation measurement aspects have been discussed. A complete system comprises also management and communication of the recorded data.

3.3 DATA MANAGEMENT STRATEGY

A detailed plan on how data management is to be performed at sites, is featured in the work of Gligen *et al*. (1991). Some specific aspects, as realized at the De Aar site, are discussed in the following paragraphs.

3.3.1 On-site management

The outputs from the loggers should be visually displayed for easy inspection, identification and rapid rectification of typical operational bugs that might occur. Using a display system, frequent downloading from loggers leads to a minimum time lag and the displayed data is kept close to "real time". It also creates room for error, if systems are struck by lightning, they can be replaced with minimal data loss.

Another key element of the process is to keep individual file sizes manageable for easy handling afterwards, if only a small section of data (for example, a specific day) is required for any reason. One month of data of the SW and LW loggers combined, occupies 5 MB, which is difficult to handle (roughly 44000 records) if only one section of the data needed closer inspection. It was also difficult to handle by means of removable media of that time (a portable 3.5 inch disk holds about 1.44 MB). Bearing in mind that one day's data occupies the manageable size of about 160 kb per logger, daily files each assigned the date as a filename, was a logical choice. Memory-resident software truncates datafiles in midnight-to-midnight formats and assigns generic filenames to both LW and SW files. When preparing monthly submissions, the files for one particular month can be easily merged.

3.3.2 Management by station scientist

The main task of the station/site scientist is the supervision of BSRN data acquisition in terms of completeness and consistency (Hegner *et al*., 1998). In the process of doing so,

quality controls, assembly of files and preparation of data in the prescribed station-to-archive file format, are performed, using the dataflowstructure in Figure 3.15.

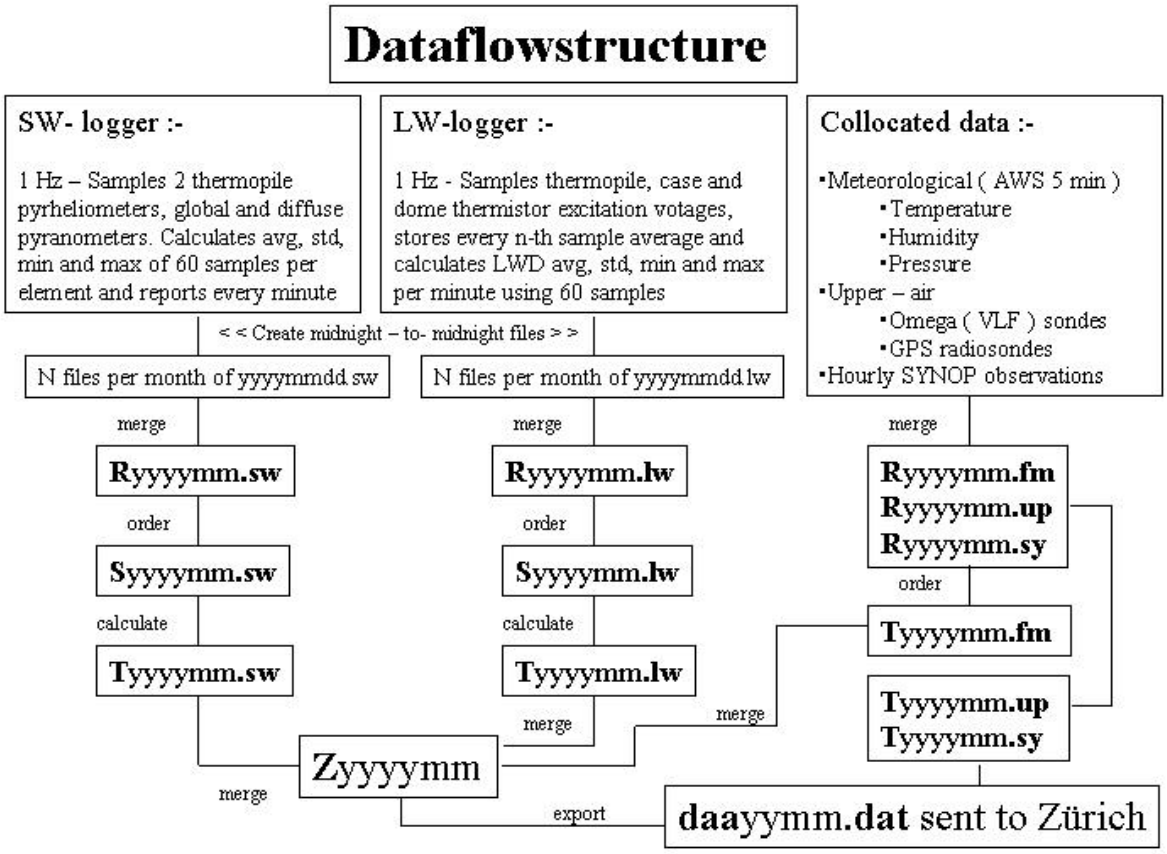

Figure 3.15 *Data management scheme for De Aar's data using generic filenames.*

The generic prefixes "R" (Raw), "S" (Sorted) and "T" (Final) each indicate different levels of refinement. A higher level of refinement is reached by running a tailor-made application developed in Fortan and run on the SAWS main-frame computers.

3.4 LIAISING WITH INTERNATIONAL DATABASE

During the Davos 1991 meeting (WCRP-64) it was decided to have all the BSRN data located at and managed by a central database, located at WRMC, ETHZ in Zürich, Switzerland. At the same institution (ETHZ), the database of GEBA is also maintained, and it follows naturally that the BSRN database was developed in the GEBA style.

3.4.1 The GEBA database

A short description of the GEBA database and relevant overlaps with the current BSRN database, to put them into perspective, is presented.

The GEBA was implemented in 1988 as a project of the Global Climate Program: Water and is a database of conventional surface radiation fluxes measured at approximately 1500 sites globally, in monthly mean values only, starting with data collected in the late 1940's up to present. A redesign of the database took place in 1994, which enabled removal of contradictions, updating of data and improving the quality control procedures for global radiation (Gilgen *et al*., 1998) but the basic format remained.

Although upward and downward flux densities of both solar and terrestrial radiation measurements appear in the database, the best represented parameter by far (87%) is global radiation, as measured with an upwardly facing horizontally mounted pyranometer according to the latest update (Gilgen and Ohmura, 1999). Extra value is added to the data by means of an extensive accompanying metadata file containing accurate descriptions of instrument types, units and varying degrees of compliance to the different pyrheliometric scales (Angstrom, IPS, WRR) that were phased in as these datasets were being recorded.

For quality control procedures, compliance of all data using the following procedures, each defined by physical properties founded in theoretical, as well as empirical quantities, are applied to the GEBA data (Gilgen *et al.*, 1997)

- The testing of "Physically possible" boundaries – i.e., the compliance of the data to numbers determined by physical constraints;
- The testing for "Physically probable" boundaries – i.e., a more strict test, identifying questionable data that passed the previous test;
- The compliance of global radiation data to a parameterized value, using total cloud amount;
- The compliance of standard deviations of a time series of yearly means for a data set, to predetermined boundaries;

- The compliance of a difference time series of yearly means, to predetermined values;

- Quantifying the conforming to a norm of differences that might exist in monthly climatologies, using long-term datasets.

The procedures were designed in order of increasing intricacy – i.e., a data value not passing procedure n, is very unlikely to pass procedure n+1, etc. Addition of quality control flags to all the data as a data point passes or fails a specific procedure is done the same way as for the BSRN database. The BSRN have different methodologies to test data boundaries, described and investigated in Chapter 4.

The synchronization of data collected in different time zones is not necessary, since the integration time for data is larger than one day (only monthly averages are used in GEBA). In the BSRN case, all data is recorded in UT to allow direct intercomparison, for any reason, of quantities taken in different time zones of the world.

3.4.2 The BSRN database

The WRMC, responsible for managing the BSRN database, is run by the Division of Climate Sciences at the Institute of Geography, ETHZ, Switzerland. Its main tasks towards the BSRN community are defined (WCRP-54, 1991) as: Receive data from the BSRN sites and, if the data fulfill the consistency requirements, insert them into the BSRN database; Check the quality of the radiation data and add quality control information to each radiation value in the BSRN database (quality check flags); Report doubtful values to BSRN stations and respond to queries; Update, maintain and safeguard the BSRN database; Combine the data from different sites, calculate and store statistics; Redistribute the data; Submit an annual report to the BSRN Science Review Panel; and distribute annual data approved by the review panel to the BSRN stations and external persons.

The database is therefore designed to play a very important supportive role in the ongoing functioning of the network, and in this respect, the maintaining of sound relationships with all the member sites, is vital.

A typical communication episode between the site scientist and database manager concerning a data file would be as follows:

- Archiving and compilation of one logical unit (month) of data under supervision of site scientist.

- Submitting of the monthly file, following the exact station-to-archive file format (details in Appendix B).

- Database manager runs basic programmes to check for data line lengths, the possibility of unacceptable characters and ambiguousities, and file consistency.

- If inconsistencies are found, the station scientist is notified and corrections are made. A corrected version of the data is submitted. The site scientist is the only person allowed to change data.

- The data quality is controlled, and feedback in the form of a monthly report is given to the site scientist.

- This process is repeated until the two parties agree to settle.

Data quality flags are added in the data stored at the BSRN database, but the flags are not included in data provided to outside parties. The station scientist is the only person in a correct position to change data, since he/she has access to the original data and observational procedures, and can hence be in the best position to identify erroneous values (Gilgen *et al.*, 1997).

3.5 CONCLUSION

In a radiation measuring system, the integration and management of components is vital in smooth functioning of the system. Staying abreast with new technology is an important step in maintaining its relevance. In the same way that frequent physical inspection of the instruments reveals operational errors that must be kept to a minimum, frequent reflection on the relevance of the entire measurements reveals shortcomings that can be rectified so that the system justifies its existence and serves its original purpose.

CHAPTER 4

QUALITY CONTROL

"Quality control must take place during the preparations towards data collection, during the measurement process and during transmission of the numerical values. Once data are recorded, only quality assessment (quality assurance) can be performed". (NREL, 1993)

"If we think of taking measurements as a test of our quality control process, quality assurance is the marking of the test. Unfortunately, as markers, we do not know the correct answers and we only know a fraction of the (obviously) incorrect ones. This means that even after all our efforts, we can never be 100% certain that the data is correct. Quality assurance procedures provide us with guides to flag data we believe to be suspect. In some cases, aided by operator notes, we can assure data is bad. In other cases, the best we can do is educated guesses." (Mc Arthur, 1995)

Since data accuracy and therefore data quality is the cornerstone of all BSRN measurements, this Chapter is devoted to quality control in the following manners :

- Different terminology and how quality control is applied in the BRSN by the WRMC.
- Elucidation of quality assurance procedures as applied by the WRMC database.
- Application and analysis of the WRMC procedures using real De Aar data.

To balance the high ideals sketched for a prefect measurement environment with practical reality, the two quotes at the beginning of this Chapter describe in essence what the process of quality control with data is all about in general, and BSRN in particular – it can never be 100% correct. Although the ideal of any measurement endeavour is to deliver the best and most accurate data at all times, practical experience shows, that there is always a quantity of data that is questionable to some degree. The true site scientist will develop ways in which to handle this data in a scientifically responsible way and keep the uncertainty, regarding the quality of such data, to a minimum.

Although scrutinizing data in itself is not pure science, it leads to improved data procedures, and a database with high integrity, which forms the basis from which good science can follow. This is actually the context in which the discussion of this Chapter is conducted.

4.1 CONTROL OVER THE QUALITY OF MEASUREMENTS

In the realm of concepts concerning control over the quality of measured data, quality control typically involves the following elements (NREL, 1993):

- Control in preparations for data collection (selection, calibration and installation of instruments);
- Control during the measurement process (inspection, calibration and maintenance of instruments);
- Control during the transmission and recording of numerical values (data acquisition systems, data archival and subsequent management);
- Controlling quality improvements by limited retrospective enhancement of measurements in cases of obvious and rectifiable mistakes.

If quality assessment is performed in real time or soon after the measurement process is completed, it can also provide valuable input to control the quality of future measurements, such as a real time data display on site (Long, 1996). A few good measurements widely spaced apart during the course of a day, have less value than a systematic set of measurements of comparable accuracy for the same day. Therefore, in essence, quality assurance has a definite dynamic character, something that site scientists must be aware of.

4.1.1 Terminology

The following definitions contextualize terms as they are used in this Chapter:

- Quality control: It is the larger holistic (Marion, 1993) and dynamic process involving the entire measurement effort starting with selection of instruments, continuing through the entire data acquisition process and maintenance routines, ending when the last backup of the data is being made. This encompasses all other processes striving to enhance data quality, whether it be past, present or future data.

- Quality assessment: It is the process of determining the value or rating the measurement by means of insertion of quality flags. This can be done using external ways of gauging, such as models, or internal ways ("comparing the data with itself"). The WRMC applies the latter in evaluating BSRN data.

- Quality assurance: After the measurement process, this is the "rubber stamp" of approval, which in itself has no control whatsoever over the measurement process itself. After assessment is made, only the assurance (or lack thereof) can be endorsed upon the recorded data.

- Quality enhancement: Retrospective or other means of attempting to enhance the quality of already recorded data. This is the only process whereby actual data is being changed. The utmost care and precision must be taken, so that the effort actually materializes in data quality *enhancement* and not *deterioration*. The BSRN site scientist of a particular site is the only person authorized to do quality enhancement on BSRN data for that specific site. This is because the site scientist is the person with access to all the relevant information leading to a questionable measurement, but he/she also has the best sense of judgement to offer solutions for data quality enhancement.

4.1.2 Measurement redundancy

Redundancy of measurements by means of a pair of operating instruments on as many parameters as possible, is a sound consideration for improvement of the quality of radiation measurements, as suggested by Mc Arthur (1998). Whilst two identical instruments in operation at a site can serve as "watchdogs" for one another, interruption of the measurement programme is less likely as a result of instrument failure if a backup is operating. The cost-factor of an instrument pair per measurement, makes this *modus operandum* impractical at De Aar and with exception of the double pyrheliometer as described in Sections 3.1.4 and 3.1.5, all the other measurements are carried out using only one instrument of each type.

The ideal way of exercising quality control, not only on the data, but actually on measurement processes, is by doing it on a continuous basis while the data is still as "fresh" as possible, as proposed by Long and Ackerman (1994). In this way, instrument or other hardware errors causing erroneous data, are identified and fixed as soon as possible. This

also ensures to drastically limit the generation of erroneous data as a result of any specific error.

4.1.3 Keeping data fresh

The application of fresh instrument calibration constants when calculating irradiance values is one way of adding quality to data by applying retrospective methods.

The black surface of a radiometer thermopile becomes more reflective with prolonged solar exposure, hence less radiation is absorbed by the sensing element, and the instrument's calibration factor gradually becomes smaller. Regular calibration (the recommended frequency is once every six months) and subsequent updating of the radiometer's calibration constant is therefore imperative if the recorded irradiance values are expected to be a true reflection of the irradiance values.

If the irradiance values are calculated while thermopile measurements are sampled, care must be exercised that the latest (freshest) calibration constant is applied featured in the system for real–time quality control on values as close as possible to the actual values. If this is not done, necessary adjustments must be made on recorded data, so that archived irradiance values reflect the latest thermopile sensitivity. A simple interpolation of the calibration factors between calibration episodes helps keeping the values as close as possible to the actual sensitivity during a specific month, as applied at the De Aar BSRN station.

4.1.4 Handling seemingly erroneous data

It must be emphasized, that if data is flagged, it does not mean that it is invalid. It is merely an indication that data lies outside the expected ranges (NREL, 1992). The procedure of WRMC to flag data and to report it to the station scientist, is aimed towards enabling the station scientist to rectify or delete erroneous data.

However, care must be taken not to simply delete data without a good reason, since data inherently also contains a record of instrument performance, which can contain valuable information to aid in any form of future remedial processes. The key element is, that retrospective remedial actions on data must be based upon a good reasoning and a logical explanation as to why it is done.

The quote of Mc Arthur (1995) at the beginning of this Chapter emphasizes that quality assurance, amidst all the exact scientific endeavours, is not an exact science in itself . The judgement of data quality and enhancement has a subjective component, which is a function of pure experience.

4.2 WRMC VALIDATION CHECKS

The WRMC uniformly and indiscriminately applies specific quality assurance procedures on BSRN radiation data submitted to the archive. Although the WRMC is not allowed to change any radiation data (that privilege belongs to the site scientist only), all data are flagged using a specific set of quality control procedures, as described in Sections 4.2.1 to 4.2.3. The data flags are reported to the site scientist, who re-evaluates the data and in the event of identification of errors, rectifies and re-submits the newer version of the dataset. The re-submitted data is re-evaluated at the database, re-flagged and returned. This process is repeated until the data can be regarded as reliable (Gilgen *et al*., 1991).

In the early BSRN years, the following main quality control procedures, were agreed upon (Gilgen *et al*., 1993):

- Procedure 1: Physically possible
- Procedure 2: Extremely rare
- Procedure 3: Across quantities
- Procedure 4: Comparison with a model
- Procedure 5: Eye check of time series plots

Each of these procedures consists of sub-procedures, each with specifications involving certain boundaries of various radiation quantities. In a later revision of the data quality control techniques (Hegner *et al*., 1998), it was mentioned that Procedures 4 and 5 were still under development at that time and were therefore not implemented. For the remaining three procedures, boundary values and descriptions were revised. These three main quality assurance procedures, as applied to BSRN data, are now detailed in the next three Sections (4.2.1 to 4.2.3). An evaluation with real De Aar data collected in the three years between June 2000 and May 2003, in Section 4.3.

4.2.1 Procedure 1 ("Physically possible")

This is the first, most basic, and roughest of the procedures. The intention is only to identify large and random errors that might be introduced in the initial data processing (Hegner *et al.*, 1998, Ohmura *et al.*, 1998). Data which are reasonably well controlled, should (at least in principle) be able to pass this test. Procedure 1 is applied to each radiation quantity individually, independent from other radiation fluxes or non-radiation data.

The sub-procedures for procedure 1 are listed in Table 4.1, together with the latest WRMC definition of lower and upper bounds per specified radiation quantity (Hegner *et al.,* 1998). All these quantities are based upon absolute maximum or minimum radiation quantities conceivable under general present climatic conditions of the Earth (Ohmura *et al.*, 1998).

Table 4.1 *Sub-procedures of WRMC procedure 1: Physically possible quantities*

Sub-procedure	Lower bound	Radiative quantity	Upper bound
1.1	0 W.m^{-2}	Direct solar irradiance (DSDIR)	1368 W.m^{-2} (annual mean solar constant)
1.2	0 W.m^{-2}	Diffuse sky irradiance (DSDFS)	TOA irradiance + 10 W.m^{-2}
1.3	0 W.m^{-2}	Global irradiance 2: measured with pyranometer (DSGL2)	1368 W.m^{-2} (annual mean solar constant)
1.4	0 W.m^{-2}	SW reflected irradiance (USR)	TOA irradiance + 10 W.m^{-2}
1.5	50 W.m^{-2}	LW Downwelling radiation (DL)	700 W.m^{-2}
1.6	50 W.m^{-2}	LW Upwelling radiation (UL)	700 W.m^{-2}

The following are relevant to Table 4.1:

- In this procedure, as well as other procedures, where applicable, TOA radiation (in W.m^{-2}) over a one-minute is evaluated by using the following equation (Iqbal, 1983):

$$TOA = \frac{S}{A_0}(\sin\delta\sin\varphi + \cos\delta\cos\varphi\cos(2\pi\xi + \varphi - \pi)) \qquad (4.1)$$

where

S = annual average of solar constant (1368 W.m^{-2})

A_0 = radius vector of solar distance

δ = solar declination in radians

φ = site latitude in radians

ξ = equation of time in radians

- The maximum theoretically possible TOA for De Aar is 1402 W.m^{-2}, using Equation 4.1 at the annual solar solstice during 22-23 December, when the solar zenith angle is just 7.2° (De Aar latitude (-30.7°) minus solar latitude (-23.5°) on that day).

- Using an atmopsheric transmission coefficient of 0.95 (highest ever measured at De Aar) and the absolute maximum TOA of 1402 W.m^{-2}, the associated global radiation at the summer solstice is expected to be 1332 W.m^{-2}, This is significantly less than the boundary of 1368 W.m^{-2} set in Sub-procedure 1.3, therefore all values of DSGL2 are expected to be less than 1368 W.m^{-2}.

- In Sub-procedures 1.5 and 1.6, the extremes of 50 W.m^{-2} and 700 W.m^{-2} for DL is based on the highly unlikely blackbody effective sky temperatures of -100°C and 60°C, respectively.

4.2.2 Procedure 2 ("Extremely rare")

This procedure is applied to data immediately after having passed Procedure 1. The specifications for interval limits are narrower than Procedure 1, in order to identify erroneous data that have escaped Procedure 1. The sub-procedures depicted in Table 4.2, are defined only in terms of the upper bound of radiative quantities which are physically possible. Under certain conditions, quantities can momentarily overshoot the limits, as detailed in Section 1.3. It was suggested (Dutton, 2002), that the sub-procedure limits are characterized per station to best fit extremely rare results specifically applicable to a certain location. However, the elucidation and evaluation of Procedure 2 is applied to stations in general, not on a one by one basis.

Kasten optical air mass value m (Kasten *et al*., 1989) is defined by

$$m = (\cos Z + 0.50572(96.07995 - Z)^{-1.6364})^{-1} \qquad (4.2)$$

where

Z = Solar zenith angle measured in degrees, not radians.

Table 4.2 *Sub-procedures of WRMC procedure 2: Extremely rare quantities*

Sub-procedure	Radiative quantity	Upper bound
2.1	Global irradiance 2 : measured with pyranometer (DSGL2)	TOA irradiance for Z < 80° TOA + 0.56(Z-93.9)² for Z ≥ 80°
2.2	Upward reflected SW irradiance (USR)	0.95 * DSGL2
2.3	Diffuse sky irradiance (DSDFS)	700 $W.m^{-2}$
2.4	Direct solar irradiance (DSDIR)	TOA irradiance * 0.9^{m} (where 'm' is optical air mass defined in Equation 4.2)
2.5	Downwelling LW irradiance (DL)	Upwelling LW irradiance + 30 $W.m^{-2}$
2.6	Upwelling LW irradiance (UL)	Downwelling LW irradiance - 30 $W.m^{-2}$

The following is applicable to table 4.2:

- Solar zenith angle Z (as applicable to sub-procedures 2.1 and 2.4) is measured in degrees, not radians.

- Very high diffuse radiation is likely to be achieved in overcast conditions, with highly transmitting cloud and high ground albedo. The current globally measured, audited and controlled record is 700 $W.m^{-2}$ for DSDFS[1].

- Global radiation values larger than TOA irradiance can be measured in areas of low latitude when scattered clouds pass in front of the sun and add reflected radiation from the cloud bottom to the already high level of global radiation.

- Since the Rayleigh extinction of normal beam radiation is about 9% at mean sea level[2], direct normal transmission coefficients are rarely more than 0.9 – although the altitude (1287m above sea level) of De Aar is expected to play a prominent role by increasing the effective transmission coefficient. The behaviour of transmission coefficients evaluating real De Aar data, are discussed in detail in Section 1.3.2.4.

[1] http://bsrn.ethz.ch/quality/procedure2
[2] http:// bsrn.ethz.ch/quality/procedure2

4.2.3 Procedure 3 ("Across quantities")

This procedure is applied immediately after Procedure 2, and the interval limits per sub-procedure are again narrower than those in Procedure 2, in order to identify errors that could have escaped Procedures 1 or 2. This procedure is unique in the sense, that it involves more than one quantity in any specific comparison process, hence the name "Across quantities".

The sub-procedures are based upon general, globally obtained, empirical relations of the different quantities measured (Hegner *et al.,* 1998) and therefore the best application for customization with respect to specific sites using local conditions, exists here. Details of the sub-procedures of Procedure 3 are listed in Table 4.3.

Table 4.3 *Sub-procedures of WRMC procedure 3: Across quantities*

Sub-procedure	Lower bound	Radiative quantity	Upper bound
3.1	$0.7 * \sigma T^4$	Downwelling LW irradiance (DL)	$1.0 * \sigma T^4$
3.2	$\Sigma(T - 10)^4$	Upwelling LW irradiance (UL)	$\sigma(T + 10)^4$
3.3	Global 2 (DSGL2) – Diffuse sky (DSDFS) - 50 $W.m^{-2}$	Direct solar irradiance horizontal component (DSDIR*cosZ)	Global 2 (DSGL2) – Diffuse sky (DSDFS) + 50 $W.m^{-2}$
3.4	Direct solar irradiance horizontal component (DSDIR*cosZ)-50 $W.m^{-2}$	Global 2 (DSGL2) – Diffuse sky (DSDFS)	Direct solar irradiance horizontal component (DSDIR*cosZ) + 50 $W.m^{-2}$

<u>The following are applicable to Table 4.3:</u>

- LWD is the equivalent of DL, the latter being used in the table for consistency towards the terms used in Hegner *et al.* (1998).

- T = (Stevenson) screen temperature in Kelvin measured at LW instrument height.

4.2.3.1 LW radiation

Sub-procedure 3.1 is based upon Stefan–Bolzmann's Equation, assuming the atmosphere as a blackbody radiation emitter:

$$E_{LW} = \varepsilon\sigma T^4 \tag{4.3}$$

where E_{LW} = Downwelling longwave irradiance in W.m^{-2}

T = (Stevenson) screen temperature in Kelvin

ε = Atmopsheric emmissivity

σ = Stefan-Bolzmann constant

Rearranging Equation 4.3 yields

$$\varepsilon = \frac{E_{LW}}{\sigma T^4} \tag{4.4}$$

Therefore, all values of E_{LW} passing sub-procedure 3.1 are those E_{LW} for which $0.7 < \varepsilon < 1.0$.

There are a number of parameterization schemes in the literature, that were used through the years to calculate ε in terms of other surface parameters, such as surface (screen) temperature and in some cases, surface humidity expressed as surface vapour pressure (e).

Bearing in mind that E_{LW} is the result of LWD radiation in an air column above a measuring point, including the entire atmosphere up to the TOA, the only sure way of determining LWD is to evaluate the radiative properties of the entire column in small increments using upper-air soundings. On the other hand, one point measurement on the surface cannot truly represent an entire air column.

However, one point measurement on the surface is sufficient under clear skies and the associated stable atmosphere as the result of settled weather. A stable upper-air profile follows the Standard Atmosphere to such an extent, that only the surface temperature is needed to describe it accurately enough for accurate LWD parameterizations.

The first attempts to estimate LWD, using surface parameters, were done by Angström in 1918, followed by Brunt in 1932 (Jiménes *et al*., 1987, Iziomon *et al*., 2003). The majority of

these attempts were empirical in nature. One exception is the pure theoretical approach as performed by Brutsaert (1975), using a clear-sky equation and making use of the standard atmosphere.

An intercomparison of selected parameterization schemes is now being offered. For the three-year data period at De Aar (June 2000 to May 2003), LWD data and simultaneous five-minute measurements of temperature and humidity (converted to vapour pressure) were used, together with SYNOP identification of clear skies (all in one observed dataset), to calculate percentage differences between measured LWD and calculated LWD from a set of parameterization schemes collected by Pirazzini (1998) and Olivieri (pers comms, 2003).

In total, there were 101 074 data points in the three-year period. The percentage differences (calculated LWD minus measured LWD), are listed in Table 4.4 as Mean (averages of the errors) and Root Mean Square (RMS) error (standard deviation of errors). The parameterization schemes are ordered in ascending RMS error order in Table 4.4.

Table 4.4 *Intercomparison of a number of LWD parameterization schemes using De Aar measured LWD and surface meteorological data*

Author(s)	Year	Equation	Mean error	RMS error
Centeno *	1982	$E_{LW} = [(5.77+0.996*0.601^{H})T^{1.1893}(U^{0.0665}/10^{4})] \sigma T^{4}$	-8.85	3.49
Satterlund	1979	$E_{LW} = 1.08 [1- \exp(-e^{T/2016})] \sigma T^{4}$	7.13	4.16
Konzelmann *et al.*	1994	$E_{LW} = [0.23 + 0.484 (e/T)^{1/8}] \sigma T^{4}$	-35.04	4.77
Andreas & Ackley	1982	$E_{LW} = [0.601 + 5.95 \times 10^{-5} e \exp(1500/T)] \sigma T^{4}$	-7.98	4.85
Marshunova	1966	$E_{LW} = (0.67+0.05e^{0.5}) \sigma T^{4}$	8.69	4.88
Efimova	1961	$E_{LW} = (0.746+0.0066^{e}) \sigma T^{4}$	3.82	4.95
Prata	1996	$E_{LW} = \{1-(1+46.5(e/T)\exp[-(1.2+3(46.5(e/T))^{1/2}]\} \sigma T^{4}$	29.61	5.05
K- Langlo *et al.*	1994	$E_{LW} = 0.765 \sigma T^{4}$	4.00	5.19
Brutsaert	1975	$E_{LW} = 1.24 (e/T)^{1/7} \sigma T^{4}$	-1.66	5.27
Brunt	1932	$E_{LW} = (0.51+0.066e^{0.5}) \sigma T^{4}$	-7.54	5.53
Ohmura	1981	$E_{LW} = (8.733 \times 10^{-3}T^{0.788}) \sigma T^{4}$	3.74	6.00
Guest	1998	$E_{LW} = -85.6 + \sigma T^{4}$	6.82	6.43
Idso and Jackson	1969	$E_{LW} = [1-0.26\exp(-7.77\times10^{-4}(273-T)^{2})] \sigma T^{4}$	8.59	7.86
Swinbank	1963	$E_{LW} = (9.365 \times 10^{-6}T^{2}) \sigma T^{4}$	7.40	8.23

* *NOTE:- The Centeno Equation was obtained from personal communication with Olivieri (2003) quoting* International Energy Agency *Task 17: Measuring and Modelling Spectral Radiation Affecting Solar Systems and Buildings: Review and Test of Parameterizations of Atmospheric Radiation* Report No. IEA-SHCP-17F-2 (December 1994). In this Equation, H represents the station height in km, and U the surface relative humidity in %.

The following is concluded from Table 4.4:

- All the listed parameterization schemes have RMS errors of between 3% and 10%.

- With the exception of the parameterization schemes of Konzelmann *et al*. (-35.04%) and Prata (29.61%), all featured parameterizations have mean errors of between -9% and 9%.

- The widely used equation of Swinbank (1963) has the highest RMS error of the quoted parameterization schemes for the De Aar data.

- By virtue of the lowest RMS error and a modest mean error, the equation of Centeno is found to be the best. It is fine-tuned for usage at De Aar by reverse-applying the systematic error of -8.852 %:

$$E_{LW} = [(6.28 + 1.084 * 0.601^{H}) T^{1.1893} \frac{U^{0.0665}}{10^{4}}] \sigma T^{4} \qquad (4.5)$$

Equation 4.5 can be used for estimating LWD when the operational pyrgeometer is not measuring LWD for any one of many reasons.

The usefulness of parameterization schemes is that, apart from controlling the quality of E_{LW} data, it can also be used to retrospectively estimate E_{LW} for periods where T and U were available, in order to fill data gaps, such as the completion of hourly, daily and monthly averages, in a long-term time series of those quantities.

For a stable, cloud-free atmosphere, 0.7 is regarded as a generally accepted value for emmissivity[3]. Any increase in this number is brought about by the presence of LW radiators, such as water vapour and clouds. A water film on the silicon pyrgeometer dome can also artificially register a higher value for LWD and therefore of the emmissivity, due to the higher hygroscopic properties of silicon. Other reasons for registering a higher value for the emmissivity may be mis-shading of the dome under sunny conditions, or wrong compensation for dome temperature in cases of no shading.

[3] http://bsrn.ethz.ch/quality/procedure3

4.2.3.2 Shortwave radiation

The last two sub-procedures in Table 4.3 are comparisons between global, diffuse and direct irradiances using solar zenith angle. The relationship

$$global(t) = diffuse(t) + direct(t)\cos Z \qquad (4.6)$$

should be satisfied in principle for all values of time (t) when Z < 90.83° (i.e., when the sun is visible). However, often this is not the case due to:

- Misalignment of the tracker device leading to erroneous measurement of either one of the quantities or a combination thereof.

- Incorrect calibration of one or a combination of the involved thermopile instruments.

- Differences in 1/e reaction times between the sensors in rapidly changing circumstances, resulting in Equation 4.6. not being satisfied at specific points in time.

- Skewness of the pyranometers brought about by incorrect levelling, resulting in an over-registering when titled slightly more towards the sun, or an under-registration when tilted away from the sun. The diffuse pyranometer (on the tracker) is particularly prone to such errors due to the rotating tracker table being not exactly level at all times.

In Table 4.3, the two sub-procedures in Points 3.3 and 3.4 are exactly the same, i.e., the defining inequalities are describing the same conditions. This statement can be substantiated as follows:

If $X = DSDIR * \cos Z$ and $Y = DSGL2 - DSDFS$

Then sub-procedure 3.3 can be rewritten: The test is passed if $(Y - 50\ \text{W.m}^{-2}) < X < (Y + 50\ \text{W.m}^{-2})$

(subtract Y consistently) $\mathbf{-50\ W.m^{-2} < X - Y < 50\ W.m^{-2}}$ (4.7)

Sub-procedure 3.4. can be rewritten as: The test is passed if $(X - 50\ \text{W.m}^{-2}) < Y < (X + 50\ \text{W.m}^{-2})$

(subtract X consistently) $-50\ \text{W.m}^{-2} < Y - X < 50\ \text{W.m}^{-2}$

(multiply by -1) $50\ \text{W.m}^{-2} > X - Y > -50\ \text{W.m}^{-2}$

(read from the right) $\mathbf{-50\ W.m^{-2} < X - Y < 50\ W.m^{-2}}$ (4.8.)

Equation 4.8 and therefore the latter of the two sub-procedures, is hence exactly the same sub-procedure as the first in Equation 4.7. Although 50 W.m^{-2} is considered to be a large error in any one of the individual LW quantities, the margin of 50 W.m^{-2} is allowed to give room to the addition of uncertainties in all three of the individual sensors (direct, global and diffuse). This is justified by the typical occurrence of ($DSGL2 - DSDFS - DSDIR$*cos$Z$) outside a boundary of 50 W.m^{-2}.

4.3 APPLICATION OF THE WRMC PROCEDURES

In this Section, each of the WRMC procedures discussed in Section 1.2 are applied to real De Aar data consisting of 36 monthly files for three complete years, viz., June 2000 until May 2003 inclusive. The data is presented here with the minimum procedures applied, but taking thermopile deterioration into account, as discussed in Section 4.1.3. The term "datapoint" refers to the one-minute average value, as recorded in the BSRN one-minute statistics.

For every sub-procedure in Section 4.2, the data is analyzed using a table, listing on a monthly basis how the one-minute data is distributed with respect to the upper and/or lower bounds of the sub-procedure. All the Tables (Tables 4.5 to 4.13) are presented as frequency tables. In two cases (Table 4.6 and Table 4.9) the table is only one column containing the frequency of boundary violations of the sub-procedure, plus the number of missing datapoints and/or the possible datapoints (the number of minutes per specific month). In all the other cases, a frequency distribution using bins related to fractions of the distance between the boundaries, is employed. In this way, the relative seriousness of boundary violations can be assessed. Where applicable, columns containing data, which violate boundaries of a specific sub-procedure are shaded.

4.3.1 Procedure 1 – "Physically possible"

4.3.1.1 Sub-procedure 1.1 *(The test for 0 W.m^{-2} < DSDIR < 1368 W.m^{-2})*

The lower and upper boundaries for this sub-procedure are 0 W.m^{-2} and 1368 W.m^{-2}, respectively. The range (between lower and upper boundary) is therefore 1368 W.m^{-2}, which equals 12 x 114 W.m^{-2}. Therefore the data in Table 4.5 was placed in 12 equally spaced frequency bins, each sized 114 W.m^{-2}. This is intended to show how the data is

distributed in the range between lower and upper boundary, as well as the relative seriousness of boundary violations.

Added columns, are: the number of points equal to 0 $W.m^{-2}$, the number of missing points and the possible number of points. For each frequency bin, the total number expressed as a percentage, is listed. This is also expressed as the total of seasonal averages, i.e. December-January-February (DJF) for summer, March-April-May (MAM) for autumn, June-July-August (JJA) for winter and September-October-November (SON) for spring.

Table 4.5 *Frequency distribution of DSDIR: June 2000 to May 2003, ref.to sub-procedure 1.1*

Month	Data bins in $W.m^{-2}$														
	= 0	1 to 114	115 to 228	229 to 342	343 to 456	457 to 570	571 to 684	685 to 798	799 to 912	913 to 1026	1027 to 1140	1141 to 1254	1265 to 1368	Mis-sing	Possible
Jun 2000	26120	1322	621	672	772	936	1416	2748	5570	2978	0	0	0	45	43200
Jul 2000	26808	1297	605	685	819	1074	1580	3100	6158	2245	0	0	0	269	44640
Aug 2000	24757	1356	848	875	1022	1252	1777	3193	5165	4367	0	0	0	28	44640
Sep 2000	25298	2242	569	643	675	870	1104	1943	3693	5255	880	0	0	28	43200
Oct 2000	22033	2926	1058	1006	1035	1080	1446	2277	3414	4710	2011	0	0	1644	44640
Nov 2000	19852	2435	784	826	1144	1181	1416	1553	2217	6018	2880	0	0	2894	43200
Dec 2000	19653	3381	1251	1727	3761	4201	3058	767	1306	3744	1759	0	0	32	44640
Jan 2001	20340	2821	745	700	810	898	1169	1772	2806	6822	5725	0	0	32	44640
Feb 2001	19747	3023	633	612	639	765	1042	1556	2802	6601	2867	0	0	33	40320
Mar 2001	23121	3885	746	674	736	840	1189	1640	3226	6436	692	0	0	1455	44640
Apr 2001	25965	4954	829	763	713	805	945	1431	2785	3951	0	0	0	59	43200
May 2001	26005	2694	749	732	836	1055	1445	2310	4962	3702	0	0	0	150	44640
Jun 2001	25255	2278	583	665	790	1018	1619	2900	5120	1889	0	0	0	1083	43200
Jul 2001	27401	2950	749	718	811	1110	1623	2579	3902	2766	0	0	0	31	44640
Aug 2001	24728	1639	735	798	848	1038	1310	2003	4675	6843	0	0	0	23	44640
Sep 2001	24701	2491	718	695	809	1096	1447	2287	3233	5158	10	0	0	555	43200
Oct 2001	23556	2183	716	774	938	1197	1640	2834	4590	5197	985	0	0	30	44640
Nov 2001	22950	3885	821	712	761	847	1115	1544	2547	5105	2881	0	0	32	43200
Dec 2001	20301	2153	686	697	804	969	1327	1941	3018	7546	5152	0	0	46	44640
Jan 2002	20949	2327	726	684	775	865	1178	1693	2786	6734	5884	0	0	39	44640
Feb 2002	19847	1904	601	615	728	905	1220	1628	2926	6488	3421	0	0	37	40320
Mar 2002	24042	2604	785	720	813	1007	1498	2587	5310	4776	197	0	0	301	44640
Apr 2002	25161	3661	934	861	781	809	1123	1571	3067	4719	480	0	0	33	43200
May 2002	27717	2184	739	796	946	1189	1555	2985	5924	565	0	0	0	40	44640
Jun 2002	26352	1635	607	713	843	1061	1606	3154	6790	115	0	0	0	324	43200
Jul 2002	26274	1801	785	853	1039	1405	2071	4399	5940	27	0	0	0	38	44640
Aug 2002	26795	2245	758	712	799	1019	1460	2406	4130	4285	0	0	0	31	44640
Sep 2002	23568	2627	829	829	1010	1132	1471	1874	3891	5801	141	0	0	27	43200
Oct 2002	22823	2498	953	928	1051	1120	1454	2196	3629	5985	1980	0	0	23	44640
Nov 2002	20032	2024	730	723	817	903	1266	1660	2751	6482	5787	0	0	25	43200
Dec 2002	21673	2557	685	724	841	991	1304	1892	3007	6824	4113	0	0	29	44640
Jan 2003	22026	3395	699	675	702	915	1225	1834	3042	7726	2357	0	0	44	44640
Feb 2003	22524	3190	729	829	670	755	948	1505	2638	6135	366	0	0	31	40320
Mar 2003	25579	2760	523	543	629	746	1026	1647	3099	7780	285	0	0	23	44640
Apr 2003	24950	2412	866	829	1026	1126	1694	2802	4100	3367	0	0	0	28	43200
May 2003	26599	2143	726	716	816	1036	1537	2796	5523	2725	0	0	0	25	44640
Total %	54.26	5.83	1.72	1.76	2.09	2.49	3.26	5.02	8.88	10.90	3.23	0.00	0.00	0.58	100
DJF %	48.13	6.37	1.74	1.87	2.50	2.90	3.22	3.76	6.28	15.09	8.14	0.00	0.00	0.03	100
MAM %	57.94	6.90	1.74	1.68	1.84	2.18	3.05	5.00	9.62	9.62	0.42	0.00	0.00	0.50	100
JJA %	59.27	4.18	1.59	1.69	1.96	2.51	3.66	6.70	12.01	6.45	0.00	0.00	0.00	0.45	100
SON %	52.79	6.01	1.85	1.84	2.12	2.44	3.19	4.69	7.73	12.81	4.53	0.00	0.00	1.33	100

From Table 4.5, the following inferences can be made:

- Missing DSDIR values are the result of window cleaning, calibration, tracker stoppages or other infrequent occurrences deeming deletion of data. For this dataset, missing values are only 0.58% of all possible values – a very low number, indicating an excellent performance of the twin pyrheliometers and solar tracker.

- The lower bound (0 $W.m^{-2}$) is satisfied for all values of DSDIR.

- The upper bound (1368 $W.m^{-2}$) is also satisfied – all DSDIR fall well within the required range. In fact, for 14 of the 36 months, DSDIR does not exceed 9/12 of the upper limit of 1368 $W.m^{-2}$.

4.3.1.2 Sub-procedure 1.2 *(The test for 0 $W.m^{-2}$ < DSDFS < TOA + 10 $W.m^{-2}$)*

Since TOA radiation is a varying parameter, exact division in frequency classes like in Table 4.5, was not practically possible. Instead, TOA radiation for every datapoint was calculated, and the frequency of DSDFS > TOA + 10 $W.m^{-2}$ listed in Table 4.6.

From Table 4.6, the following deductions are made:

- The majority of months have zero violations. Only 10 of the 36 months have more than 10 datapoint violations per month.

- The month with the most violations (202) is September 2001, followed by May 2001 (53 violations). This is illustrated in Figure 4.1.

- There is apparently no specific preferential season for the occurrence of violations – if the 202 violations of September 2001 are ignored, an even distribution between the seasons exists, DJF having slightly less violations than the other three seasons.

- One must bear in mind that the violations of procedure 1.2 only account for 0.033% of the entire dataset. Therefore, it involves a relatively small and in the most cases, insignificant number of values. Deleting all the datapoints violating this criterium will not add significantly to the amount of already missing data. However, the reason for this violation is investigated in Section 4.3.1.2.1.

Table 4.6 *Frequencies of DSDFS>TOA + 10 W.m^{-2}: June 2000 to May 2003, ref. to sub-procedure 1.2*

Month	Number of violations	Possible data points	Percentage violations
Jun 2000	0	43200	0.0000
Jul 2000	0	44640	0.0000
Aug 2000	0	44640	0.0000
Sep 2000	0	43200	0.0000
Oct 2000	4	44640	0.0090
Nov 2000	4	43200	0.0093
Dec 2000	17	44640	0.0381
Jan 2001	0	44640	0.0000
Feb 2001	2	40320	0.0050
Mar 2001	12	44640	0.0269
Apr 2001	9	43200	0.0208
May 2001	53	44640	0.1187
Jun 2001	2	43200	0.0046
Jul 2001	4	44640	0.0090
Aug 2001	26	44640	0.0582
Sep 2001	202	43200	0.4676
Oct 2001	0	44640	0.0000
Nov 2001	21	43200	0.0486
Dec 2001	8	44640	0.0179
Jan 2002	0	44640	0.0000
Feb 2002	2	40320	0.0050
Mar 2002	0	44640	0.0000
Apr 2002	9	43200	0.0208
May 2002	0	44640	0.0000
Jun 2002	8	43200	0.0185
Jul 2002	19	44640	0.0426
Aug 2002	33	44640	0.0739
Sep 2002	8	43200	0.0185
Oct 2002	35	44640	0.0784
Nov 2002	5	43200	0.0116
Dec 2002	0	44640	0.0000
Jan 2003	6	44640	0.0134
Feb 2003	28	40320	0.0694
Mar 2003	0	44640	0.0000
Apr 2003	0	43200	0.0000
May 2003	1	44640	0.0022
Average	14.39	43800	0.0329
DJF %	0.0162	MAM %	0.0211
JJA %	0.0231	SON %	0.0710

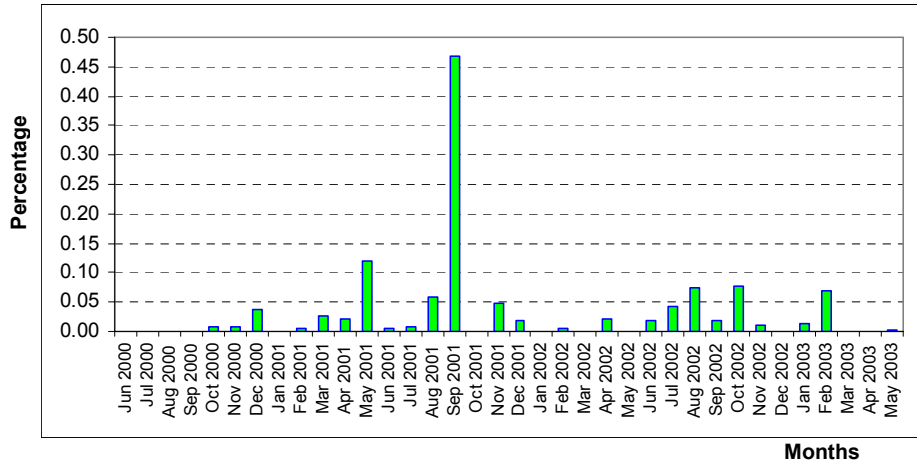

Figure 4.1 *From Table 4.6: Violations of sub-procedure 1.2, expressed as a percentage for all datapoints*

The last column of Table 4.6, viz., the violations of sub-procedure 1.2, are illustrated in Figure 4.1 as a percentage of all datapoints. The anomalous occurrence of violations of sub-procedure 1.2 during the month of September 2001 within a 36 month-period of observations, prompts the investigation in Section 4.3.1.2.1.

4.3.1.2.1 Closer inspection of violations of sub-procedure 1.2

As a result of diffuse radiation being present in the atmosphere a few minutes before sunrise and a few minutes after sunset, while TOA radiation equals zero, DSDFS and TOA radiation are bound to have a difference at the start and end of every day. This, however, is less than 10 $W.m^{-2}$ as a general rule, and does not explain the violations of sub-procedure 1.2.

Closer inspection reveals, that a difference of more than 10 $W.m^{-2}$ between DSDFS and TOA radiation does, however, appear near the end or the beginning of a specific day. The quantities DSDFS and TOA radiation are small at the beginning and end of a day, and a difference of 10 $W.m^{-2}$ between them is significant. If the time of observation is slightly offset between DSDFS and TOA, the difference can easily become larger than 10 $W.m^{-2}$.

A closer look at September 2001 reveals that there were small discrepancies between DSDFS and TOA radiation for only the first three days of the month, and the system recovered during the night of 3-4 September 2001. No anomalous system behaviour was reported or observed for these specific days. To illustrate this phenomenon, consider Figure 4.2 - a graph of TOA + 10 $W.m^{-2}$ and DSDFS for 2 September 2001.

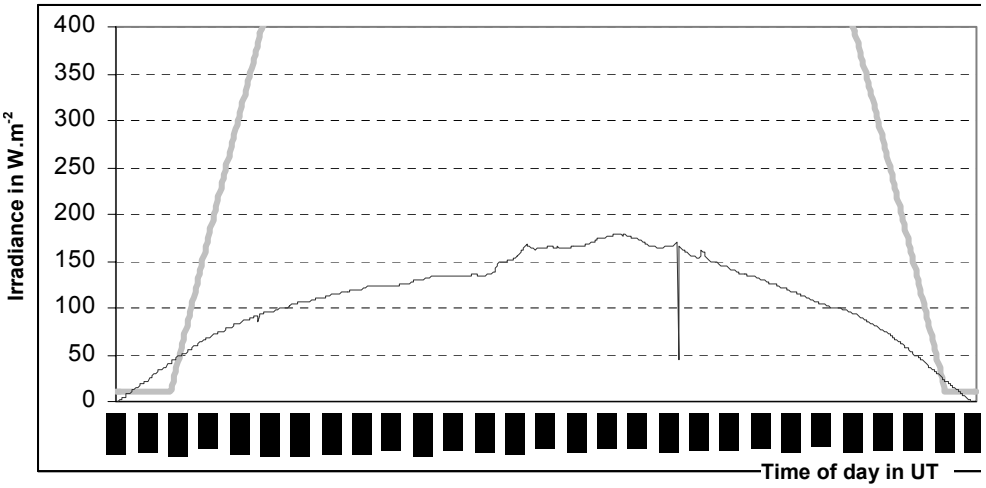

Figure 4.2 *TOA radiation + 10 $W.m^{-2}$ (thick grey line) and diffuse radiation (thin black line) for 2 September 2001*

A strange double offset w.r.t. the time at the beginning and the end of the day is observed, with DSDFS overshooting (TOA+10 $W.m^{-2}$) by a substantial amount between 04:04 UT and

04:39 UT at the beginning of the day, as well as 16:00 UT and 16:09 UT at the end of the day. (Sunsrise and sunset times at De Aar for 2 September 2001 are 04:39 UT and 16:09 UT, respectively). One last remark is, that this data possibly could have been incorrectly date-stamped by the logger (i.e. the DSDFS data attributed to 2 September 2001 actually belongs to a another, longer day). If the sunrise and sunset times were further spaced apart, more space would have allowed the DSDFS profile from sunrise to sunset, to fit in the space below TOA radiation + 10 $W.m^{-2}$. An accurate on-site GPS receiver updates the system time and transfers the time to the logger at least three times a day, so it is highly unlikely that this could have happened.

4.3.1.3 Sub-procedure 1.3 *(The test for 0 $W.m^{-2}$ < DSGL2 < 1368 $W.m^{-2}$)*

In Table 4.7, frequencies of DSGL2 datapoints with respect to twelfths of 1368 $W.m^{-2}$ – like in Table 4.5, are presented. The only exception is, that a column making provision for the number of datapoints larger than 1368 $W.m^{-2}$, is added. This column is shaded to indicate that it represents the number of datapoint violations of sub-procedure 1.3.

From Table 4.7 it is noted that:

- Out of all DSGL2 datapoints, the small percentage of 0.35 % are missing. The reason for missing values are generally the same for DSDIR (calibration, maintenance, cleaning), except tracker failures, since DSGL2 does not require solar pointing or tracking. This emphasizes that the global pyranometer was in excellent working condition.

- A number of one-minute global radiation values (89) are already violating this crude criterium. (Shaded column in table 4.7.) Even though this number only accounts for 0.0056 % of all the datapoints, it is still significant since violation of this crude criteria is not expected in BSRN. A closer investigation is performed in Section 4.3.1.3.1.

- The violations are restricted to summer months, which is logical since DSGL2 is expected to reach its highest value, approach and/or temporarily overtake the boundary of 1368 $W.m^{-2}$. The month of January 2001 (investigated in Section 4.3.1.3.1) has the most violations (26), followed by November 2001 (16).

Table 4.7 *Frequency distribution of DSGL2: June 2000 to May 2003 ref.to sub-procedure 1.3. Shaded area represents violations.*

Month	Data bins in W.m^{-2}															
	<= 0	0 to 114	115 to 228	229 to 342	343 to 456	457 to 570	571 to 684	685 to 798	799 to 912	913 to 1026	1027 to 1140	1141 to 1254	1255 to 1368	> 1368 W.m^{-2}	Missing	Possible
Jun 2000	24487	4187	2632	2391	2470	3785	3126	74	3	0	0	0	0	0	45	43200
Jul 2000	24989	4173	2713	2410	2562	3679	3560	160	44	1	0	0	0	0	349	44640
Aug 2000	23829	3925	2727	2603	2821	3679	4445	579	4	0	0	0	0	0	28	44640
Sep 2000	21625	5412	2687	2254	2055	2082	2686	3230	932	49	0	0	0	0	188	43200
Oct 2000	20490	3697	2427	2204	2220	1994	1888	1894	2390	3729	1031	0	0	0	676	44640
Nov 2000	18377	4407	2422	2088	1784	1614	1595	1645	1905	2155	3721	232	28	0	1227	43200
Dec 2000	18139	4352	2403	2130	1800	1758	1768	1849	2109	2600	4571	975	141	13	32	44640
Jan 2001	18720	3967	2388	2104	1949	1814	1717	1772	2060	2332	4143	1464	164	26	20	44640
Feb 2001	18114	3762	2267	2031	1658	1589	1549	1540	1864	2481	2938	441	61	2	23	40320
Mar 2001	21693	4354	2484	2378	1945	1848	1710	1819	2529	3014	654	61	11	0	140	44640
Apr 2001	22612	5525	3497	2426	1784	1718	1686	2312	1163	378	39	1	0	0	59	43200
May 2001	24515	4121	2940	2599	2494	2817	4105	865	90	7	1	0	0	0	86	44640
Jun 2001	24571	4406	2818	2531	2460	3700	2637	44	0	0	0	0	0	0	33	43200
Jul 2001	25293	5097	2885	2409	2373	2929	3288	250	78	6	0	0	0	0	32	44640
Aug 2001	23851	3622	2199	2088	2451	2680	3651	3614	427	32	2	0	0	0	23	44640
Sep 2001	21456	4880	2602	2122	1924	1758	2032	2826	2585	387	25	0	0	0	603	43200
Oct 2001	20905	4233	2771	2231	2054	1904	2209	2848	2200	2497	589	139	11	1	48	44640
Nov 2001	18379	5229	2705	2683	2239	1773	1545	1473	1660	1780	2911	552	223	16	32	43200
Dec 2001	18032	4522	2474	2261	1833	1708	1707	1760	2044	2459	4591	994	219	10	26	44640
Jan 2002	18630	4260	2441	2109	1903	1672	1709	1852	2036	2404	4404	1029	150	12	29	44640
Feb 2002	18023	3481	2085	1896	1863	1717	1633	1733	2037	2985	2678	147	14	1	27	40320
Mar 2002	21661	3989	2734	2228	2066	1954	1861	2164	3127	2013	680	80	10	0	73	44640
Apr 2002	22527	4404	2860	2400	2049	2078	2144	3105	1514	68	18	0	0	0	33	43200
May 2002	24836	4779	2963	2312	2312	2719	3837	813	38	1	0	0	0	0	30	44640
Jun 2002	24506	4030	2876	2436	2494	3555	3222	41	0	0	0	0	0	0	40	43200
Jul 2002	24941	4083	2583	2532	2665	3457	4093	210	41	7	0	0	0	0	28	44640
Aug 2002	23841	4834	2504	2552	2247	2147	2936	2953	524	68	8	1	0	0	25	44640
Sep 2002	21586	3829	2450	2297	2051	1916	1986	2591	3559	835	60	9	1	0	30	43200
Oct 2002	20516	4412	2115	1878	1854	2000	1954	2117	2471	4026	1145	105	17	0	30	44640
Nov 2002	18334	3821	2204	1986	1736	1856	1757	1919	2217	2593	4223	484	34	1	35	43200
Dec 2002	18571	4662	2835	2291	1952	1784	1634	1655	1991	2292	4060	772	110	7	24	44640
Jan 2003	19368	4581	2509	2305	1859	1693	1656	1712	2105	3062	2986	79	1	0	724	44640
Feb 2003	18113	5148	2566	2096	1602	1435	1413	1472	1621	2406	1587	0	0	0	861	40320
Mar 2003	21601	5530	2800	1972	1683	1557	1695	1975	3203	2339	100	0	0	0	185	44640
Apr 2003	22667	4007	2629	2403	2109	2044	2401	3881	935	74	18	0	0	0	28	43200
May 2003	24763	4397	2756	2446	2392	3073	4241	544	5	0	0	0	0	0	23	44640
Total %	49.1	10	5.9	5.2	4.79	5.16	5.5	3.8	3.3	3.1	3.1	0.6	0.1	0.0056	0.3499	100
DJF %	42.80	10.00	5.70	5.00	4.24	3.92	3.80	4.00	4.60	5.95	8.30	1.50	0.20	0.00	0.00	100
MAM %	52.10	10.40	6.50	5.30	4.75	4.99	6.00	4.40	3.20	1.99	0.40	0.00	0.00	0.00	0.00	100
JJA %	55.50	9.68	6.00	5.50	5.68	7.46	7.80	2.00	0.30	0.03	0.00	0.00	0.00	0.00	0.00	100
SON %	46.50	10.10	5.70	5.00	4.53	4.27	4.40	5.00	5.10	4.57	3.80	0.80	0.10	0.00	0.00	100

4.3.1.3.1 Inspection of January 2001

Figure 4.3 depicts DSGL2 datapoints for the month of January 2001, with all the night-time (zero) values removed for brevity. The Y-axis is divided in the same increments as Table 4.7.

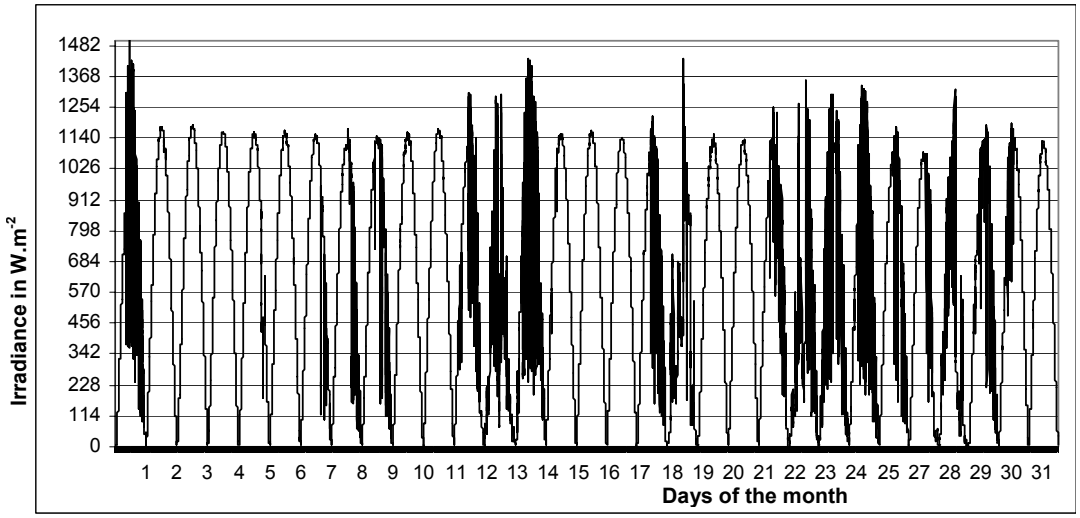

Figure 4.3 *DSGL2 datapoints for January 2001*

In Figure 4.3, note that clear-sky days or days with little or no clouds in the sky, are identified as days with smooth curves. Examples are: the 2nd to 10th as well as 15th to 17th, 20th and 21st and 31st. Days with clouds in the sky (partly cloudy to overcast) renders a distinctive unsmooth pattern, such as the 1st, 12th to 14th,18th, 19th and 22nd to 30th. It follows that the daily maximum value of DSGL2 for clear sky days, is remarkably consistent (ca. 1140 $W.m^{-2}$), whilst the 1368 $W.m^{-2}$ boundary is violated or almost violated on days with cloud interference. The best example is the 1st. (Daily maximum of DSGL2 > 1482 $W.m^{-2}$).

A closer inspection is now given to one individual day having the highest daily DSGL2 maximum for January 2001 (Figure 4.4). Note that the same increment of 114 $W.m^{-2}$ is also used in this graph, but the Y-axis extends two increments further than Figure 4.3.

From Figure 4.4, it can be deduced that cloudless skies, indicated by smooth profiles of DSGL2 (global), DSDIR (direct) and DSDFS (diffuse) existed since sunrise (03:25 UT) up to about 06:25 UT, after which global (thin black line) overshoots the boundary of 1368 $W.m^{-2}$ on a few occasions during the middle of the day. It reached a momentary peak of 1590 $W.m^{-2}$ roughly at 10:00 UT and occasionally also overshot the TOA value, mostly in the presence of low direct radiation (thick grey line). This pattern is maintained sunset at 17:30 UT. Thick and heavy clouds were reported during the afternoon, but no precipitation was recorded by the Automatic Weather Station (AWS).

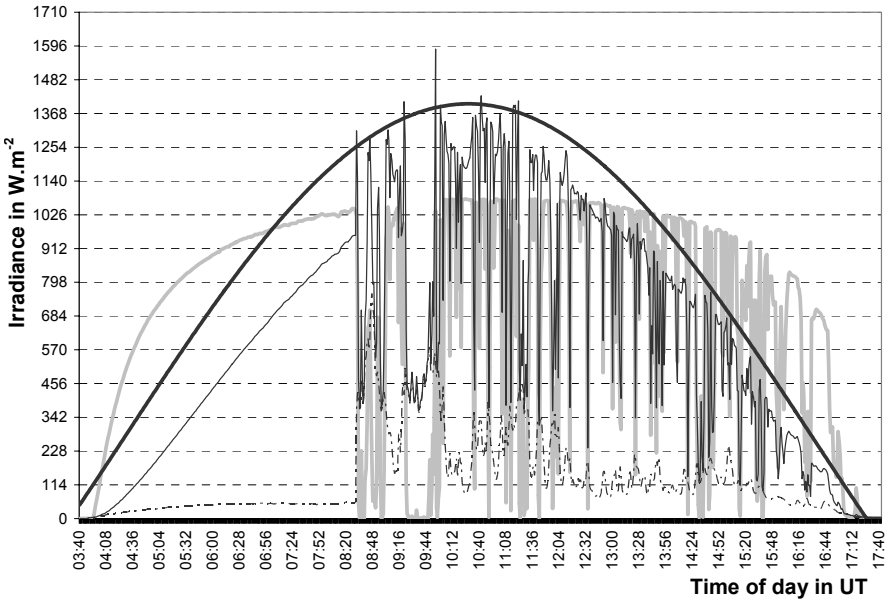

Figure 4.4 *Diurnal variation of TOA radiation (thick smooth black line), DSDIR (thick grey line), DSGL2 (thin black line) and DSDFS (dashed line) on 1 January 2001*

Consider another example on 20 November 2001 (Figure 4.5), The same scale and definitions as in Figure 4.4 are used.

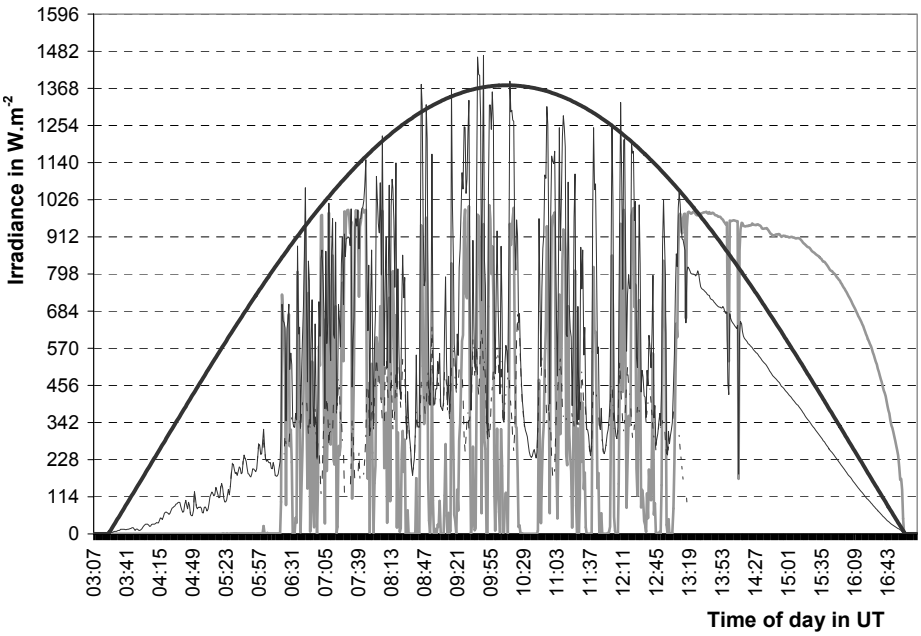

Figure 4.5 *Diurnal variation of TOA radiation (thick smooth black line), DSDIR (thick grey line), DSGL2 (thin black line) and DSDFS (dashed line) on 20 November 2001*

On this day, overcast conditions prevailed since sunrise (03:16 UT) until roughly 06:00 UT (global and diffuse graphs run concurrently with direct being equal to zero). Thereafter the same pattern, as shown in Figure 4.4 was followed: moderate diffuse values prevailed, TOA

radiation was overshot by global in numerous occasions. The situation restored at about 13:00 UT to smooth lines for global and direct, with diffuse having relatively low values (cloudless sky) until sunset at 17:03 UT.

The presence of clouds in hours around noon seems to be the responsible factor in these two cases. Clouds have both a diffusing and blocking effect on radiation. When broken cloud passes the pyranometer, the full direct beam is measured in intervals with diffuse radiation, plus reflected radiation from clouds, added in the same interval. The fact, that broken cloud creates streaks of intense sunlight and shadow on the pyranometer, forcing it to respond quickly to rapidly changing signals, seems to aggravate the situation. Note that the anomalously high peak-values are short bursts, i.e. seldom lasting for more than one minute at a time.

Since only 0.35 % of all global irradiance values are violating sub-procedure 1.3, simple deletion of these values is not deemed to make a significant impact on the dataset.

4.3.1.4 Sub-procedure 1.4 *(The test for 50 W.m^{-2} < LWD < 700 W.m^{-2})*

The quoted limits for LWD in this sub-procedure corresponds to sky blackbody temperatures of respectively -100°C and 60°C, respectively. In Table 4.8, the distribution per month is listed as frequencies as in Tables 4.5 and 4.7, but with 50 W.m^{-2} bins.

From Table 4.8 it is deduced that:

- Missing values (a minimum of 23 per month) are due to dome cleaning, maintenance, as well as tracker stoppages (the shading device is necessary to render good shading for correct application of the pyrgeometer Equation), and download failures as a result of lightning strikes. One such incident (the highest) occurred in December 2002.

- The total number of missing LWD datapoints is a relatively high percentage (1.132%), but this is biased by the high number of 3718 missing datapoints in December 2002. The average missing value percentage for the other 35 months is only 0.389 % - which is in line with DSGL2, DSDIR and DSDFS.

- No boundary violations - all the LWD datapoints fall within 50 W.m^{-2} to 700 W.m^{-2}.

- In line with expected seasonal trends, datapoints are clustered in a lower range, 201 W.m^{-2} to 400 W.m^{-2}, during the winter months. During the summer months, the highest concentration of datapoints is between 251 W.m^{-2} to 500 W.m^{-2}.

- The three-year LWD record minimum is 218 W.m^{-2} and the record maximum is 524 W.m^{-2} – which are respectively at cushion margins of 168 W.m^{-2} and 176 W.m^{-2}, respectively, within the boundaries of the rough Procedure 1.4.

Table 4.8 *Frequency distribution of LWD: June 2000 to May 2003 ref. to sub-procedure 1.4*

	Data bins in W.m^{-2}											
Month	101-150	151-200	201-250	251-300	301-350	351-400	401-450	451-500	501-550	551-600	Missing	Total
Jun 2000	0	0	4908	28435	8054	1769	0	0	0	0	34	43200
Jul 2000	0	0	7548	29246	4476	387	0	0	0	0	2983	44640
Aug 2000	0	0	3970	28177	11358	1109	1	0	0	0	25	44640
Sep 2000	0	0	3745	20025	15201	4202	0	0	0	0	29	43200
Oct 2000	0	0	1083	16193	18751	7919	670	0	0	0	24	44640
Nov 2000	0	0	8	8611	24413	9157	961	26	1	0	23	43200
Dec 2000	0	0	0	3285	25244	14082	1971	30	0	0	28	44640
Jan 2001	0	0	0	4946	21616	14927	3102	19	0	0	30	44640
Feb 2001	0	0	0	2230	18201	16930	2898	19	1	0	41	40320
Mar 2001	0	0	0	1729	18876	21400	2589	19	0	0	27	44640
Apr 2001	0	0	0	8955	20115	13244	860	0	0	0	26	43200
May 2001	0	0	0	2403	22588	16014	3607	6	0	0	28	44640
Jun 2001	0	0	2058	29838	10041	1239	0	0	0	0	24	43200
Jul 2001	0	0	10165	25412	8294	740	0	0	0	0	29	44640
Aug 2001	0	0	7321	28312	8427	550	0	0	0	0	30	44640
Sep 2001	0	0	2322	22616	12454	5773	7	0	0	0	28	43200
Oct 2001	0	0	272	11149	21450	10257	604	3	0	0	905	44640
Nov 2001	0	0	0	6101	19214	15757	2098	0	0	0	30	43200
Dec 2001	0	0	0	3679	26615	12115	2176	12	0	0	43	44640
Jan 2002	0	0	0	6345	21506	13114	3563	57	5	0	50	44640
Feb 2002	0	0	0	2787	20753	13645	3089	19	0	0	27	40320
Mar 2002	0	0	310	3883	19726	18787	1887	11	0	0	36	44640
Apr 2002	0	0	591	9348	19914	12618	701	5	0	0	23	43200
May 2002	0	0	4426	25689	10726	3759	10	0	0	0	30	44640
Jun 2002	0	0	9620	27080	5812	663	0	0	0	0	25	43200
Jul 2002	0	0	7992	30121	6253	246	0	0	0	0	28	44640
Aug 2002	0	0	7165	22689	10420	4340	0	0	0	0	26	44640
Sep 2002	0	0	889	21239	18454	2572	21	2	0	0	23	43200
Oct 2002	0	0	1475	15364	16822	8550	980	9	0	0	1440	44640
Nov 2002	0	0	1503	16177	19298	5316	860	19	1	0	26	43200
Dec 2002	0	0	1045	16906	12732	2233	6	0	0	0	3718	44640
Jan 2003	0	0	0	1440	21165	19079	2901	22	4	0	29	44640
Feb 2003	0	0	0	167	9797	22021	7468	97	5	0	765	40320
Mar 2003	0	0	0	2581	22872	16965	2198	0	0	0	24	44640
Apr 2003	0	0	0	9285	19544	13822	522	0	0	0	27	43200
May 2003	0	0	1123	24303	17509	1680	2	0	0	0	23	44640
Total %	0	0	5.048	32.78	37.364	20.75	2.907	0.02	0.001	0	1.132	100
DJF %	0.00	0.00	0.28	11.11	47.23	34.08	7.23	0.07	0.00	0.00	3.32	100
MAM %	0.00	0.00	1.63	22.19	43.28	29.77	3.13	0.01	0.00	0.00	0.01	100
JJA %	0.00	0.00	2.89	35.19	42.52	17.80	1.59	0.02	0.00	0.00	0.60	100
SON %	0.00	0.00	15.41	63.22	18.58	2.80	0.00	0.00	0.00	0.00	0.76	100

4.3.1.5 Sub-procedure 1.5 *(The test for 50 W.m^{-2} < UL < 700 W.m^{-2})*

At the time of preparation of this document, no UL data was measured, hence no data is available for verification. The focus is now turned to Procedure 2.

4.3.2 Procedure 2 – "Extremely rare"

The criteria is stricter under the "extremely rare" tests compared to Procedure 1, hence some datapoints that passed the test in Procedure 1, are bound to be identified as errors in Procedure 2.

4.3.2.1 Sub-procedure 2.1 *(The test for DSGL2 < TOA if Z < 80°, and DSGL2 < TOA + 0.56(Z-93.3°)² for Z ≥ 80°)*

This procedure involves calculating TOA radiation as well as Z for every DSGL2 datapoint. For brevity and simplicity, a new variable is defined: ***DSTM***. The definition is as follows:

If Z < 80° then DSTM = DSGL2 - TOA

if Z ≥ 80° then DSTM = DSGL2 – (TOA + 0.56 (Z - 93.3°)²)

Violations of the sub-procedure are therefore cases where DSTM < 0.

Consider Table 4.9, showing frequencies of violations in the same pattern as Table 4.6. Note, that the complex definition of DSTM, plus the absence of fixed borders, does not allow for a frequency distribution table like (for example) Table 4.8.

From Table 4.9, it is deduced that:

- During 33 out of 36 months, datapoints with DSTM < 0, occurred with monthly frequencies between 3% and 6%. They were evenly distributed between seasons.

- June 2002 has the highest number (5.77%) and June 2001 (0.07%) the lowest.

- Overall average violation of sub-procedure 2.1 is 4.10%, which is a significant figure. Therefore, these datapoints violating the criterium, cannot all be summarily deleted. Reasons for the violations are seeked in Sections 4.3.2.1.1 and 4.3.2.1.2.

Table 4.9 *Frequencies of DSTM < 0: June 2000 to May 2003, ref.to sub-procedure 2.1*

Month	Number of violations	Possible data points	Percentage violations
Jun 2000	2357	43200	5.46
Jul 2000	2311	44640	5.18
Aug 2000	2	44640	0.00
Sep 2000	1770	43200	4.10
Oct 2000	1881	44640	4.21
Nov 2000	2108	43200	4.88
Dec 2000	2007	44640	4.50
Jan 2001	2040	44640	4.57
Feb 2001	1700	40320	4.22
Mar 2001	1671	44640	3.74
Apr 2001	1560	43200	3.61
May 2001	251	44640	0.56
Jun 2001	31	43200	0.07
Jul 2001	1669	44640	3.74
Aug 2001	2268	44640	5.08
Sep 2001	1828	43200	4.23
Oct 2001	2153	44640	4.82
Nov 2001	1617	43200	3.74
Dec 2001	2417	44640	5.41
Jan 2002	2060	44640	4.61
Feb 2002	1833	40320	4.55
Mar 2002	1720	44640	3.85
Apr 2002	1549	43200	3.59
May 2002	1726	44640	3.87
Jun 2002	2494	43200	5.77
Jul 2002	2497	44640	5.59
Aug 2002	1978	44640	4.43
Sep 2002	1792	43200	4.15
Oct 2002	1852	44640	4.15
Nov 2002	2317	43200	5.36
Dec 2002	1796	44640	4.02
Jan 2003	1119	44640	2.51
Feb 2003	1200	40320	2.98
Mar 2003	1634	44640	3.66
Apr 2003	1604	43200	3.71
May 2003	2172	44640	4.87
Average	1750	43800	4.104
DJF %	4.159	JJA %	4.362
MAM %	3.494	SON %	4.405

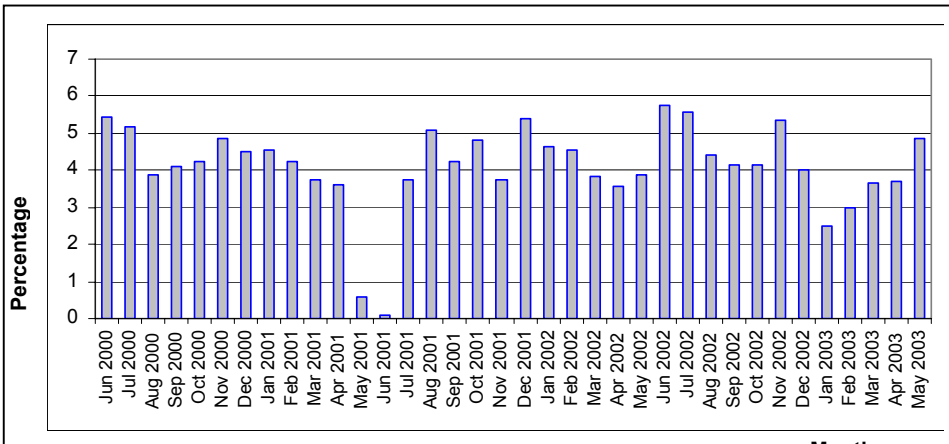

Figure 4.6 *From Table 4.9: violations of sub-procedure 2.1, expressed as a percentage for all datapoints*

The percentage violations per month of sub-procedure 2.1 is illustrated in Figure 4.6. Two extreme months, May 2001 (second-lowest) and June 2002 (highest), are now investigated.

4.3.2.1.1 May 2001 *(Second-lowest number of boundary violations: 0.56%).*

Although June 2001 had the absolute minimum number of violations, viz. 0.07%, it was decided to use the second-lowest month, May 2001, for illustrating violations of sub-procedure 2.1. because the very few violations occurring during June 2001 could not satisfactorily illustrate reasons for violations.

Figure 4.7 depicts DSTM in a time-series for the complete month of May 2001, but the night-time datapoints (zero), are removed for clarity. Note that smooth curves are associated with clear, cloud-free days, while the presence of clouds disturbs the pattern.

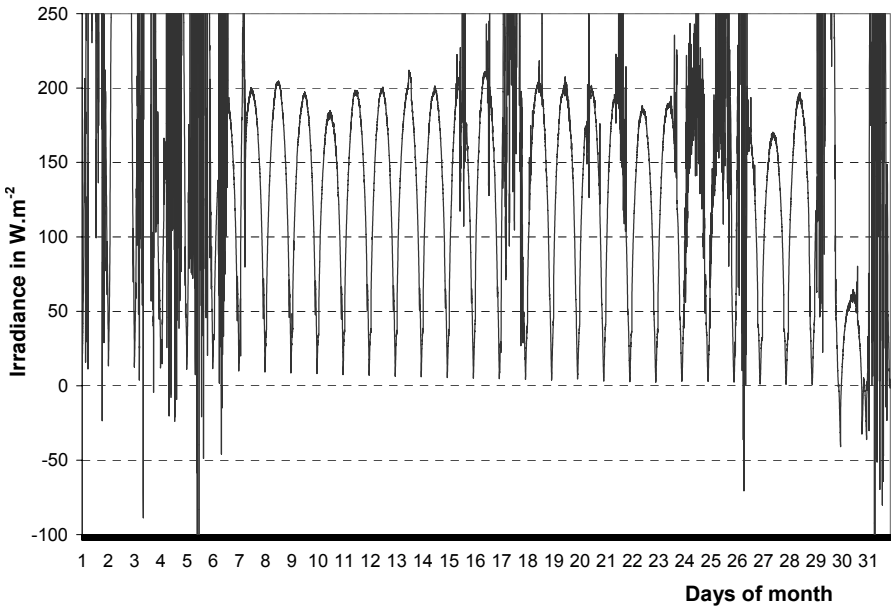

Figure 4.7 *Time-series for DSTM: May 2001*

From Figure 4.7 it can be deduced that datapoints for which DSTM<0 are restricted to certain days. The lower and upper boundaries for DSTM seem to follow 0 $W.m^{-2}$ and 200 $W.m^{-2}$, respectively, on clear days. On days with broken clouds, the lower and upper boundaries are both violated on the same day, like the 5th and 31st. A total of 251 datapoints do not satisfy the criterium DSTM<0, being 0.56% of all the values for that specific month.

Continuing with May 2001, the dependence of DSTM with respect to the solar angle is investigated in Figure 4.8, which is a scatter diagram of DSTM versus cos$Z$. The majority of night-time values were removed for simpilcity. The numbered notations on the graph are:

1. Point of sunrise: Z = 90.83°, therefore cos$Z$ = -0.014

2. Point of maximum solar elevation angle (Z and therefore, cos$Z$ is a minimum)

3. Inflection line, where the Z=80° (and cos$Z$ = 0.17) criterium separates DSTM values for low solar angles from DSTM values for high solar angles

4. For high solar elevation, there are also a few loose values of DSTM<0

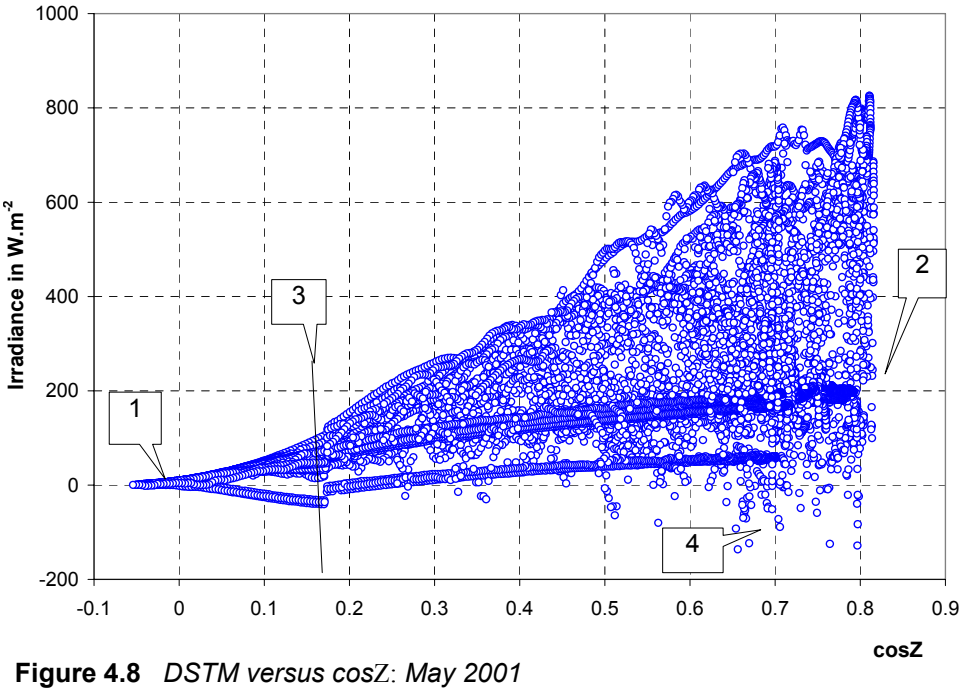

Figure 4.8 *DSTM versus cosZ: May 2001*

It follows from Figure 4.8, that the majority of DSTM datapoints < 0 are lying to the left of the inflection line (3), starting at zero for cos$Z$ = 0° and becoming significantly less than zero as cos$Z$ increases up to about 0.17. There are, however, also single values of DSTM less than zero for relatively high values of cos$Z$, in other words, high solar angles.

It should be kept in mind that this is the “second-best” month, hence the remaining 34 months in the 36 month- record have more violations of sub-procedure 2.1.

4.3.2.1.2 June 2002 *(Highest number of boundary violations: 5.77%)*

In Figure 4.9, similar to Figure 4.7, depicts a time-series of DSTM for June 2002.

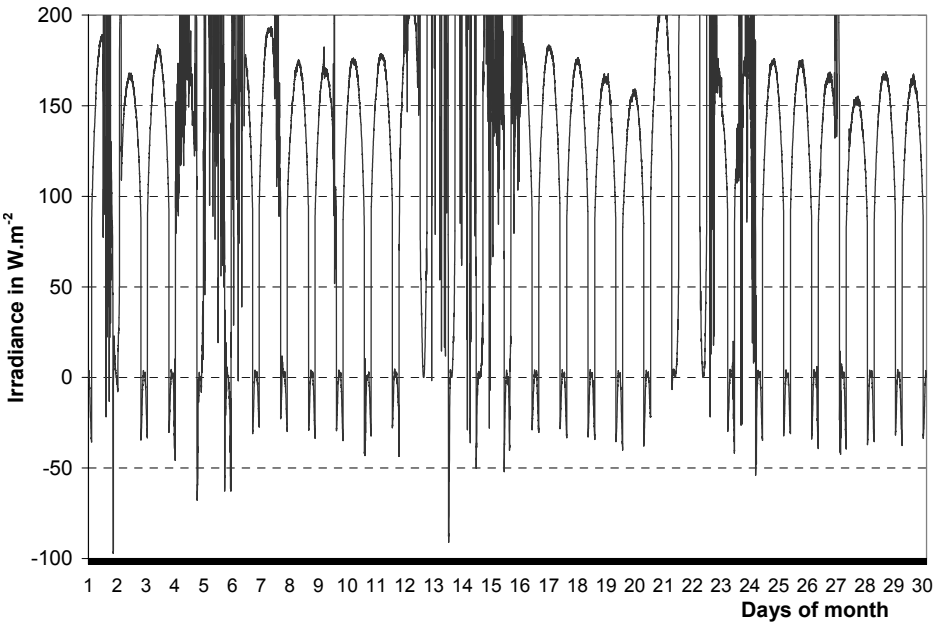

Figure 4.9 *Time-series for DSTM: June 2002*

For clear days in Figure 4.9, similar to Figure 4.7, a virtual maximum of 150 W.m^{-2} to 190 W.m^{-2} is maintainted, but with the exception that DSTM<0 violating days are now not only restricted to days where the virtual upper boundary is violated, but also portions of almost every day on June 2002.

In Figure 4.10, the scatter diagram of DSTM versus cos$Z$ is featured in a similar way as in Figure 4.8. The numbered notations for Figure 4.10 are:

1. Point of sunrise: Z = 90.83°, therefore cos$Z$ = -0.014

2. Point of maximum solar elevation angle (Z and therefore, cos$Z$, is a minimum)

3. Inflection line, where the Z=80° (and hence cos$Z$=0.17) criterium separates DSTM values for low solar angles from DSTM values for high solar angles

4. For high solar elevation, there are also a few loose values of DSTM<0

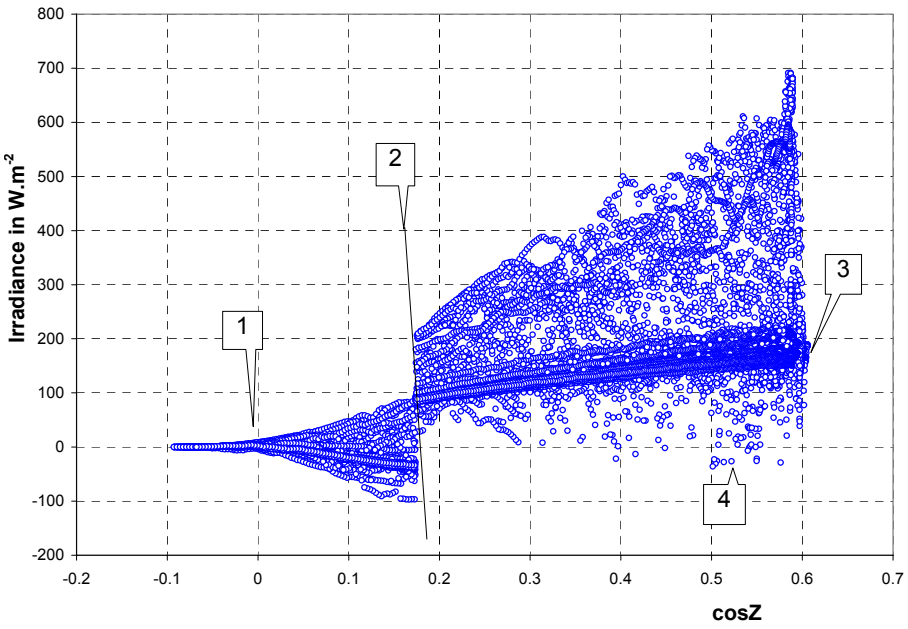

Figure 4.10 *DSTM versus cosZ: June 2002*

From Figure 4.10 it follows that DSTM datapoints less than zero are concentrated to the left of the inflection line (3), starting at zero for cos$Z$ =0, and becoming significantly lower than zero as cos$Z$ increases up to the inflection point, cos$Z$ =0.17. The relatively few values of DSTM less than zero for relatively high values of cos$Z$ are less in Figure 4.10, than Figure 4.8.

The values for DSTM < 0 for low values of cos$Z$ are attributed to a global pyranometer that reads values which are too high compared to an expected TOA value for these angles. This could either be the result of a skew pyranometer, tilted towards one end, or one that is incorrectly calibrated. The checking of pyranometer balance as part of the daily routine, should therefore be given a high priority in an effort to reduce these errors.

4.3.2.2 Sub-procedure 2.2 *(The test for USR < 0.95 * DSGL2)*

Since USR is not a basic BSRN measurement quantity that is measured at the De Aar BSRN station, no real data is available for the evaluation of this sub-procedure.

4.3.2.3 Sub-procedure 2.3 *(The test for DSDFS < 700W.m^{-2})*

Similar to Table 4.8, the DSDFS datapoints in Table 4.10 are placed in bins of 50 W.m^{-2} intervals. The violations of sub-procedure 2.3 are shaded.

Table 4.10 *Frequency distribution of DSDFS: June 2000 to May 2003, ref.to sub-procedure 2.3. Shaded area represents violations*

Months	Data bins in W.m^{-2}																	
	0	1-50	51-100	101-150	151-200	201-250	251-300	301-350	351-400	401-450	451-500	501-550	551-600	601-650	651-700	> 700	Missing	Possible
Jun 2000	24512	11084	5216	1108	635	304	210	70	13	3	0	0	0	0	0	0	45	43200
Jul 2000	25013	8618	7863	1336	595	391	307	134	33	3	0	0	0	0	0	0	347	44640
Aug 2000	23069	6111	8239	2837	888	651	468	457	289	127	40	4	2	0	0	0	1458	44640
Sep 2000	21635	5570	8455	2487	1360	983	754	603	465	313	249	155	105	28	9	1	28	43200
Oct 2000	20504	5991	7801	2318	1816	1225	960	705	752	530	261	84	38	9	2	0	1644	44640
Nov 2000	17579	7135	8298	1694	1400	1114	991	629	583	336	235	141	111	42	15	3	2894	43200
Dec 2000	18206	5480	10403	2995	2143	2248	1154	604	495	410	262	96	83	47	11	1	32	44640
Jan 2001	18853	10633	8459	1938	1301	923	619	583	417	341	222	117	74	80	15	3	32	44640
Feb 2001	18265	7750	7553	1967	1458	1208	770	422	316	250	192	111	35	0	0	0	23	40320
Mar 2001	21083	8035	6078	2213	1611	1235	946	650	522	315	210	170	59	18	0	1	1494	44640
Apr 2001	22564	7907	4357	2640	2109	1197	970	703	402	182	72	30	6	1	1	0	59	43200
May 2001	24449	11640	4017	1298	1156	784	472	328	210	86	33	16	1	0	0	0	150	44640
Jun 2001	24010	9780	5582	1204	739	420	294	48	32	7	0	0	0	0	0	0	1084	43200
Jul 2001	25232	9473	5102	1852	1308	834	474	225	75	28	6	0	0	0	0	0	31	44640
Aug 2001	23806	12302	4806	1158	877	596	442	243	170	161	49	7	0	0	0	0	23	44640
Sep 2001	21456	6940	6810	2530	1753	1189	759	466	327	189	74	51	36	10	2	1	607	43200
Oct 2001	20959	8027	7888	3441	1763	1148	656	345	136	117	68	21	3	0	0	0	68	44640
Nov 2001	18483	8366	6630	1862	1481	1565	1400	1164	837	551	398	238	125	53	15	0	32	43200
Dec 2001	18131	9828	10405	2014	1116	1064	831	562	332	203	89	25	11	2	1	0	26	44640
Jan 2002	18708	9426	9761	1957	1308	1062	834	536	409	252	185	98	57	17	2	0	28	44640
Feb 2002	18098	7955	8642	1473	1142	920	525	462	443	324	160	92	38	9	0	0	37	40320
Mar 2002	21717	8905	5957	2485	1950	1295	684	481	350	231	143	58	23	17	1	0	343	44640
Apr 2002	22581	8687	4787	2109	1338	1008	1101	672	395	220	185	84	0	0	0	0	33	43200
May 2002	24874	11204	3470	2124	1140	910	413	301	157	15	2	0	0	0	0	0	30	44640
Jun 2002	24546	12611	2820	1065	750	568	301	138	64	13	0	0	0	0	0	0	324	43200
Jul 2002	24983	9943	6101	1705	753	471	289	270	76	19	1	1	0	0	0	0	28	44640
Aug 2002	23883	10853	5619	1403	1251	784	471	245	93	14	0	0	0	0	0	0	24	44640
Sep 2002	21639	5978	9013	2043	1356	948	784	597	440	261	81	28	2	0	0	0	30	43200
Oct 2002	20574	7233	8717	2098	1677	1276	847	642	492	353	360	253	78	0	0	0	40	44640
Nov 2002	18398	8370	10854	1705	870	688	624	433	337	281	296	217	84	4	4	0	35	43200
Dec 2002	18700	10427	7904	2464	1619	1018	694	579	442	291	206	103	52	70	28	4	39	44640
Jan 2003	19449	7862	9275	2289	1610	1461	951	568	333	271	215	88	94	26	17	13	118	44640
Feb 2003	18164	4984	7943	2627	1946	1728	1063	675	397	358	240	72	74	9	0	0	40	40320
Mar 2003	21660	9247	7840	2020	1429	839	566	393	266	172	129	43	6	0	0	0	30	44640
Apr 2003	22724	7846	4711	2936	1601	1279	873	630	377	179	15	0	0	0	0	0	29	43200
May 2003	24815	9613	6327	1803	966	465	325	173	106	24	0	0	0	0	0	0	23	44640
%	39.5	16.605	12.53	3.71	2.5062	1.837	1.27	0.86	0.568	0.362	0.23	0.122	0.054	0.02	0.005	0.0014		
DJF %	42.87	19.13	20.68	5.09	3.54	3.00	1.91	1.28	0.92	0.69	0.46	0.21	0.13	0.07	0.02	0.01		
MAM %	52.22	21.01	12.03	4.97	3.37	2.28	1.61	1.10	0.70	0.36	0.20	0.10	0.02	0.01	0.00	0.00		
JJA %	55.58	23.03	13.04	3.47	1.98	1.27	0.83	0.46	0.21	0.10	0.02	0.00	0.00	0.00	0.00	0.00		
SON %	46.73	16.40	19.21	5.21	3.48	2.63	2.00	1.44	1.13	0.76	0.52	0.31	0.15	0.04	0.01	0.00		

From Table 4.10, it can be deduced that:

- The occurrence of DSDFS > 700 W.m^{-2} (violations of sub-procedure 2.3) is very rare. In total, there were only 27 datapoints (0.0014% of the entire record). January 2003 is the largest single contributor with 13 datapoints.

- Adjudicating susceptibility for violations, the summer months (DJF) have the most, whilst the winter months (JJA) have 4 bins clear to the left of the sub-procedure boundary.

Although the occurrence of violations of sub-procedure 2.3 is extremely low, January 2003 as the largest single contributor towards violations, (almost half of all), is now inspected.

4.3.2.3.1 January 2003 *(Largest contributor towards violations of sub-procedure 2.3.)*

Further inspection of DSDFS reveals that the 13 violating datapoints are all concentrated in one day, viz. 28 January 2003. This is illustrated in Figure 4.7.

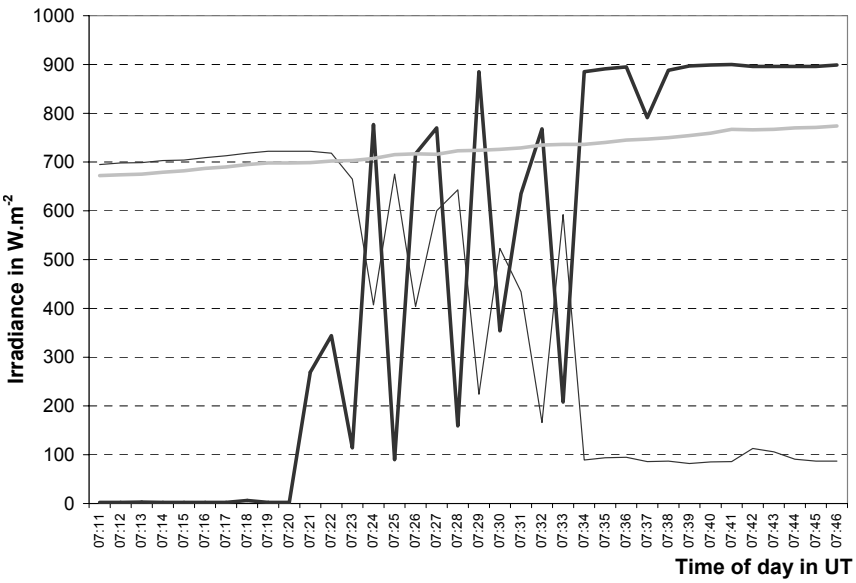

Figure 4.11 *A close-up view of 28 January 2003: (07:11UT-07:46UT): DSDIR (thick black line), DSDFS (thin black line) and DSGL2 (thick grey line)*

In Figure 4.11, the overcast morning (up to 07:20 UT) and a clear section (from 07:34 UT) sandwich an episode of intense bursts of sunshine, during which the boundary of 700 W.m^{-2} had not even been reached, alhough it can be expected due to the differential instrumental reaction times in situations such as this one, as mentioned in Section 3.1.4.2. The actual violations occur in the time period between 07:12 UT to 07:22 UT, where the diffuse (thin

black line) was overtaking the global by a systematic difference, which is just enough to push DSDFS over 700 W.m^{-2}. This could be the result of a slight misalignment in the balancing of either of the two pyranometers. However, this is a sporadic occurrence of temporary over-estimation of the diffuse irradiance and hence no cause for concern. The margin of over-estimation, (i.e., just over 700 W.m^{-2}) is also negligible.

4.3.2.4 Sub-procedure 2.4 *(DSDIR < TOA * 0.9^m)*

The definition of DSDIR in terms of the transmission coefficient τ and optical air mass m in sub-procedure 2.4, is as follows (Hegner *et al.*, 1998):

$$E_{dir} = E_{TOA}\tau^{m} \tag{4.9}$$

where

E_{dir} = Datapoint of DSDIR

E_{TOA} = Datapoint of TOA radiation

τ = transmission coefficient

m = Kasten optical air mass

Equation 4.9. may be re-arranged to:

$$\tau = (E_{dir} / E_{TOA})^{\frac{1}{m}} \tag{4.10}$$

Equation 4.10 means that violations of sub-procedure 2.4 equate to all datapoints for which τ > 0.9. This is illustrated in Figure 4.12 by means of the last column of Table 4.11.

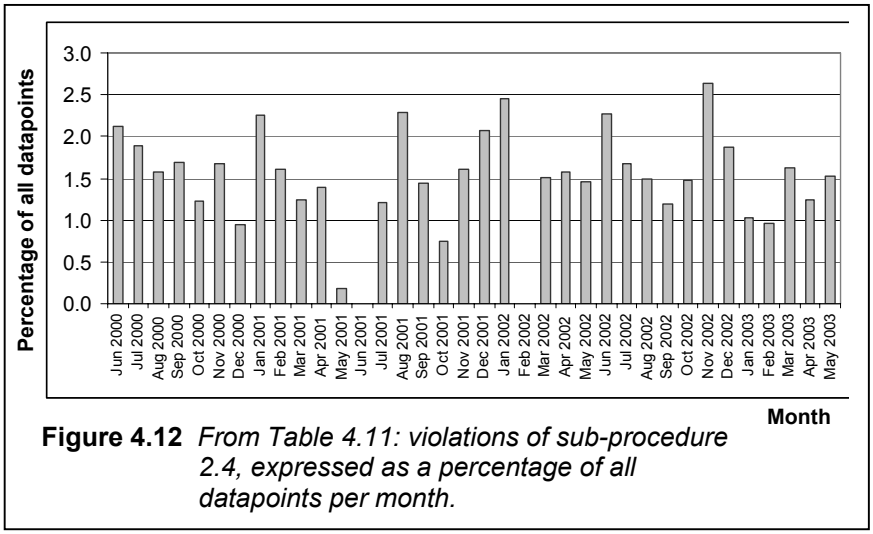

Figure 4.12 *From Table 4.11: violations of sub-procedure 2.4, expressed as a percentage of all datapoints per month.*

In Table 4.11, the frequency distribution of τ between 0.35 and 1.00, with increments of τ = 0.05, is presented for all datapoints per month of the data evaluation period. Violations of sub-procedure 2.4. are expected for 0.9 ≤ τ < 1.0, and the two columns containing the

number of datapoints for which this is true, are shaded. An extra column to allow for τ > 1.0 was created, although it is physically possible that τ > 1.0, due to DSDIR < TOA as a general rule (Equation 4.10). However, since DSDIR and TOA are independently acquired, allowance was made for τ > 1.0 so that these cases could be contextualized and added to the true number of violations of sub-procedure 2.4. This could also serve as a test for the soundness of the complex calculations concerning TOA, DSDIR and τ. Lastly, in Table 4.11, the "missing data"-column was not included, since the table does not reflect the expected presence total of measured datapoints. It evaluates properties of datapoints already present.

Table 4.11 *Frequency distribution of τ: June 2000 to May 2003, ref.to. sub-procedure 2.4. Shaded area represents violations*

	Data bins in fractions of m															
Month	Up to 0.35	0.35-0.40	0.40-0.45	0.45-0.50	0.50-0.55	0.55-0.60	0.60-0.65	0.65-0.70	0.70-0.75	0.75-0.80	0.80-0.85	0.85-0.90	0.90-0.95	0.95-1.00	> 1.00	% > 0.9
Jun 2000	27006	68	70	88	101	134	179	333	1461	5929	4585	2323	915	0	0	2.12
Jul 2000	27960	90	93	109	107	106	165	221	1280	5522	5603	2536	840	0	0	1.88
Aug 2000	25939	163	167	208	228	281	359	1646	3621	5264	3975	2078	676	27	0	1.57
Sep 2000	27400	140	165	191	217	289	553	1054	1953	5049	3671	1776	732	0	0	1.69
Oct 2000	26667	320	321	368	442	593	1366	1405	2879	5367	2777	1583	546	0	0	1.22
Nov 2000	25333	467	376	377	451	393	425	475	813	5692	5264	2405	721	0	0	1.67
Dec 2000	22908	1824	1455	2392	1567	1148	1052	1002	1099	3462	4529	1776	419	0	0	0.94
Jan 2001	23177	214	237	208	209	222	285	305	941	4169	9673	3984	1008	0	0	2.26
Feb 2001	22666	163	162	161	188	179	259	447	1104	5135	6524	2679	645	0	0	1.60
Mar 2001	28286	262	235	257	298	263	324	467	2184	5418	4298	1784	556	0	0	1.25
Apr 2001	30834	269	272	276	234	309	344	418	1123	4654	2540	1315	602	0	0	1.39
May 2001	28706	230	209	223	238	281	332	742	4459	6673	2306	154	79	0	0	0.18
Jun 2001	28322	117	143	170	274	458	664	2873	5831	3894	418	28	0	0	0	0.00
Jul 2001	29878	183	233	215	274	370	540	688	1726	4281	4021	1682	542	0	0	1.21
Aug 2001	26128	188	263	257	279	312	327	416	1319	7180	4603	2340	1005	15	0	2.28
Sep 2001	27706	177	205	234	322	353	760	1364	1961	5122	2925	1441	592	30	0	1.44
Oct 2001	25526	210	242	248	313	454	892	2166	4149	5553	3174	1371	333	1	0	0.75
Nov 2001	27120	249	289	326	339	345	361	414	989	4101	5703	2258	696	0	0	1.61
Dec 2001	22573	193	204	221	177	219	263	334	869	5226	9796	3634	912	12	0	2.07
Jan 2002	23323	200	184	220	234	253	289	356	606	4010	10084	3778	1094	0	0	2.45
Feb 2002	33924	1394	1253	804	554	472	446	395	357	328	319	64	0	0	0	0.00
Mar 2002	26887	211	194	233	273	315	399	1016	5080	4737	2949	1667	670	0	0	1.50
Apr 2002	28544	293	349	316	301	381	361	517	1436	4419	3869	1722	682	0	0	1.58
May 2002	29598	196	208	240	274	352	462	961	2537	5227	2545	1382	649	0	0	1.45
Jun 2002	27951	126	138	165	155	172	227	584	1479	6295	2996	1921	981	0	0	2.27
Jul 2002	27531	154	157	202	217	274	372	1179	4429	4981	2698	1691	745	0	0	1.67
Aug 2002	28739	159	188	197	239	235	463	610	2806	5052	3540	1738	638	26	0	1.49
Sep 2002	25928	294	278	296	332	381	563	884	3268	5898	3053	1504	513	0	0	1.19
Oct 2002	25581	341	327	349	400	492	691	1143	2869	4965	4859	1956	645	12	0	1.47
Nov 2002	22249	183	186	151	200	236	281	391	757	3945	9886	3586	1139	0	0	2.64
Dec 2002	24178	234	207	266	277	304	352	437	863	5058	8551	3069	836	0	0	1.87
Jan 2003	25281	243	238	274	255	314	390	499	2320	7026	5557	1773	460	0	0	1.03
Feb 2003	25881	284	271	271	324	295	354	443	1400	6291	2895	1215	386	0	0	0.96
Mar 2003	28269	170	165	124	169	158	269	506	1273	7011	3921	1867	728	0	0	1.63
Apr 2003	27091	291	303	339	300	506	824	1732	2621	4154	3047	1445	539	0	0	1.25
May 2003	28051	149	168	213	210	288	349	531	2762	5885	3434	1910	680	0	0	1.52
Total %	61.08	0.660	0.640	0.710	0.700	0.771	1.050	1.836	4.859	11.603	10.180	4.404	1.470	0.0078	0	1.4778
DJF %	57.59	1.22	1.08	1.24	0.97	0.87	0.95	1.08	2.46	10.47	14.90	5.65	1.48	0.00	0	1.46
MAM %	64.48	0.52	0.53	0.56	0.58	0.71	0.92	1.734	5.91	12.12	7.27	3.33	1.30	0.00	0	1.31
JJA %	59.40	0.61	0.61	0.65	0.77	0.89	1.50	2.36	4.99	11.62	10.51	4.55	1.51	0.01	0	1.52
SON %	66.79	0.37	0.41	0.43	0.48	0.58	0.80	1.79	5.17	10.91	7.21	3.60	1.43	0.01	0	1.44

The following conclusions can be drawn from Table 4.11 and Figure 4.12:

- Two months have no sub-procedure violations, i.e. June 2001 and February 2002.

- The month with the highest number of sub-procedure violations, is November 2002 (2.64%), and the lowest non-zero number occurs in May 2001 (0.18%).

- All months, except the four months mentioned, have an incidence of violations of between 1.0% and 2.5%.

- The total number of violations is 1.48% of all datapoints. If one puts this into context with the number of *missing* datapoints (0.58% from table 4.5.) for DSDIR from which τ is derived, then this is more than two and a half times the number of missing DSDIR datapoints, and therefore significant in its own right.

Inspection of τ within a number of randomly selected diurnal cycles, revealed, that highest τ -values consistently occurs when the sun is near the horizon, i.e., when solar zenith angle (Z) is about 90°. This suggests a possible correlation between τ and Z. April 2001 (1.39%) was chosen (1.39%) for a first investigation as a representative month with sub-procedure violations close to the 36-month average (1.48%), and a scatter diagram of τ versus Z was drawn (Figure 4.13)

4.3.2.4.1 April 2001 *(Sub-procedure violations representative of the 36-month average)*

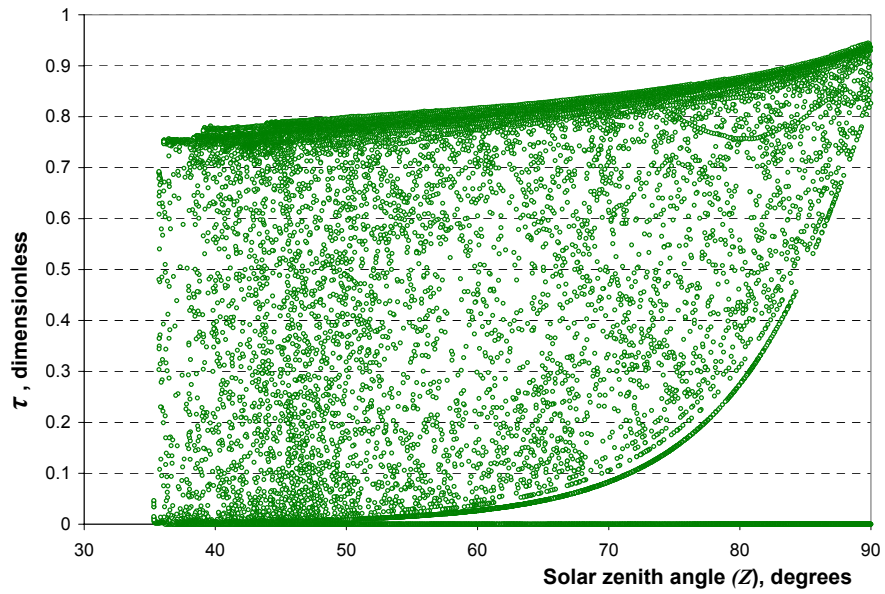

Figure 4.13 *Scatter diagram of τ versus Z: April 2001*

In Figure 4.13, all datapoints are encapsulated in an area defined by three distinct curves. The bottom curve represents the theoretical minimum TOA radiation value for any given Z. The quasi-vertical left boundary represents the highest solar elevation angle (lowest Z) possible for that month, and the curve on the top are datapoints representing cloudless sky. The domination of clear sky over the De Aar BSRN site in winter and even in April, as in this case, gravitates the majority of datapoints towards the top boundary. This is also the curve where the violating datapoints cluster. (τ > 0.9 for Z ca. 90°). In this specific case, the lowest Z for which τ > 0.9, is Z = 83.71°. This is still more than (a disturbing!) 7° separation from Z at sunset /sunrise (90.83°).

Looking at Equation 4.7 and realizing, that m, τ and TOA are all theoretically established values, the only explanation for an unusually high τ in this sub-procedure is that the actual value of DSDIR is too high. This leads to the conclusion that τ = 0.9 for the violation boundary possibly needs some empirical justification to allow more flexibility, taking take local conditions into account. At the moment, τ = 0.9 is applied by the WRMC as a universal measure for all BSRN stations, which clearly does not work for De Aar.

4.3.2.4.2 June 2001 *(Representative month with no sub-procedure violations)*

A month (June 2001) where no violations occurred, is represented in Figure 4.14.

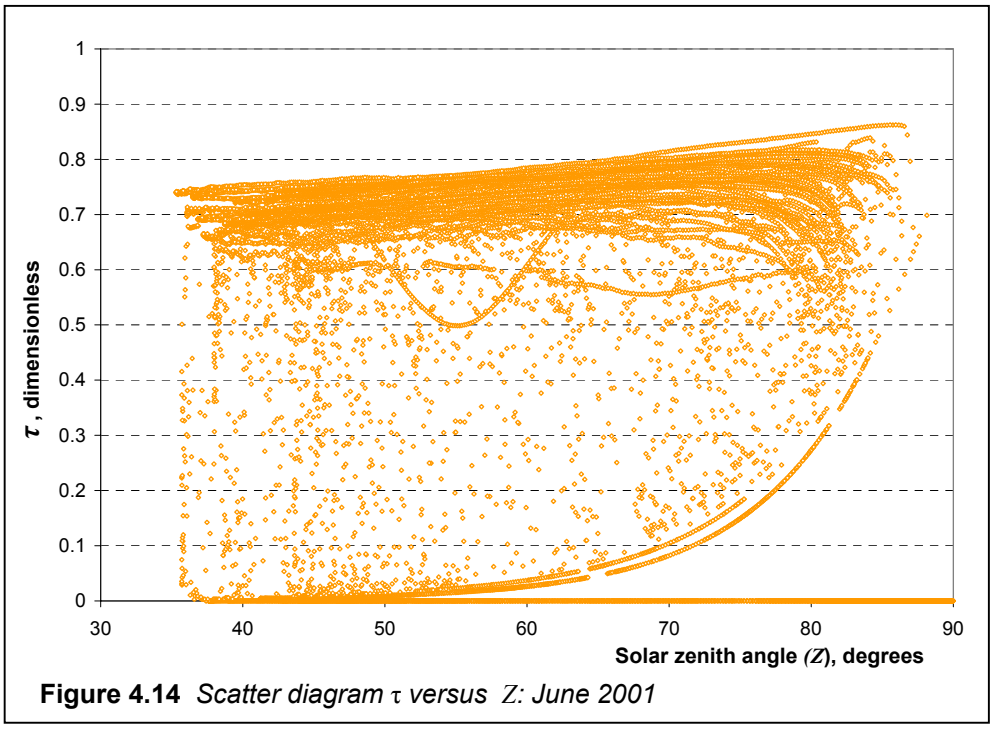

Figure 4.14 *Scatter diagram τ versus Z: June 2001*

The description of Figure 4.13 is also applicable to Figure 4.14. One exception is the area for 85° < Z < 90°, where significantly fewer points are found in Figure 4.13, possibly due to a

larger number of datapoints having gravitated towards the clear-sky (top) boundary in Figure 4.14. This confirms, that in winter, the majority of datapoints over the De Aar BSRN station represents clear (cloudless) sky.

To summarize, violations of sub-procedure 2.4 occurs when the sun is near the horizon. Deeper investigation into the applicability of station - specific boundaries for τ instead of the globally applied number of 0.9, is a suggested way of addressing this problem.

4.3.2.5 Sub-procedure 2.5 *(LWD < UL + 30 W m^{-2})* and

4.3.2.6 Sub-procedure 2.6 *(UL > LWD - 30 W m^{-2})*

These two sub-procedures involve UL, which is not a basic quantity measured at De Aar during this period. In fact, the defining inequalities are describing exactly the same conditions and it is therefore the same sub-procedure, in the same fashion that the two sub-procedures in Section 4.2.3.2 are the same.

4.3.3 Procedure 3 – "Across quantities"

This procedure, the third group of sub-procedures, now implements a finer sifting process than Procedure 2, therefore values that have escaped the previous procedures, are expected to be identified by this procedure to be suspect or erroneous.

Bear in mind that up to now, the radiation data were only compared against themselves or similar parameters, such as TOA radiation. No completely independent outside source was involved. A real test of data quality happens, when a comparison with independently measured quantities is done. In procedure 3, exactly this is implemented, but also involving more than just one measurement quantity. This in itself weakens the comparison accuracy, by introducing the inherent (and by the nature of the procedure) independent uncertainties in both quantities, creating a combined relatively larger uncertainty.

4.3.3.1 Sub–procedure 3.1 *(The test for DL between 0.7*σT^4 and σT^4)*

The first of the finer sub-procedures involves the comparison of surface (Stevenson screen) air temperature T from the 5-minute meteorological datasets, to LWD radiation. In Section 4.2.3.1, Equation 4.4 reflects the conditions describing this sub-procedure, i.e., 0.7 < ε < 1.0. Violations are therefore those datapoints for which ε < 0.7 or ε > 1.0. The distribution of ε in

bins versus months for the 36-month period, shown in Table 4.12, hence directly indicates LWD with respect to T. The chosen bin ranges for ε are 0.60 to 1.0, with increments of 0.05. Note that the number of possible datapoints for this sub-procedure are one fifth of the corresponding number for BSRN data since five-minute meteorological data was reconciled with the one-minute BSRN data. Shaded columns again represent sub-procedure violations: Lighter shading represents the number of violating one-minute values per specific month, darker shading the corresponding percentages.

Table 4.12 *Frequency distribution of ε: June 2000 to May 2003, ref.to sub-procedure 3.1. Shaded areas represent violations*

Month	% less than 0.70	Less than 0.60	0.60 to 0.65	0.65 to 0.70	0.70 to 0.75	0.75 to 0.80	0.80 to 0.85	0.85 to 0.90	0.90 to 0.95	0.95 to 1.00	More than 1.00	% more than 1.00	Possible data points
Jun 2000	3.88	0	0	335	3709	2900	563	356	267	162	58	0.67	8640
Jul 2000	13.43	144	49	1006	4260	2095	336	376	330	105	24	0.27	8928
Aug 2000	18.44	0	319	1327	3387	2630	572	230	152	24	1	0.01	8928
Sep 2000	15.60	0	151	1194	2812	1949	576	423	504	742	134	1.58	8640
Oct 2000	14.35	0	2	1238	3438	2329	990	374	168	32	157	1.80	8928
Nov 2000	3.95	0	4	339	2765	2965	780	504	540	392	60	0.72	8640
Dec 2000	6.78	0	9	596	3389	2870	936	396	253	135	23	0.27	8928
Jan 2001	8.08	0	9	712	3245	2215	1374	664	275	81	13	0.15	8928
Feb 2001	1.48	0	0	119	2013	2922	1491	693	354	112	3	0.04	8064
Mar 2001	0.37	0	0	33	1656	3229	1651	982	828	175	18	0.21	8928
Apr 2001	0.00	0	0	0	993	2895	1772	938	850	823	116	1.38	8640
May 2001	3.52	0	18	296	3333	3154	741	354	399	279	30	0.35	8928
Jun 2001	7.12	0	0	615	3530	2895	543	274	212	228	79	0.94	8640
Jul 2001	16.90	0	215	1294	3947	1534	525	368	363	332	201	2.29	8928
Aug 2001	22.47	0	25	1981	4085	1731	433	167	124	40	0	0.00	8928
Sep 2001	16.48	2	0	1422	3498	1263	616	259	460	772	81	0.97	8640
Oct 2001	6.81	0	50	558	3200	2396	930	754	619	69	7	0.08	8928
Nov 2001	3.04	0	0	263	2377	1964	1339	808	989	554	102	1.22	8640
Dec 2001	2.93	0	0	262	3221	3142	1038	393	282	241	25	0.29	8928
Jan 2002	11.55	0	32	999	2969	2170	1226	579	445	168	15	0.17	8928
Feb 2002	4.99	0	0	402	2994	2792	696	429	219	44	0	0.00	8064
Mar 2002	7.28	0	0	650	1818	2601	2102	807	536	72	11	0.13	8928
Apr 2002	8.95	0	39	734	2300	2404	1321	937	428	135	3	0.04	8640
May 2002	24.25	173	394	1598	2906	1735	451	419	509	558	101	1.14	8928
Jun 2002	15.49	0	2	1336	3925	1819	289	253	350	316	41	0.49	8640
Jul 2002	8.60	0	56	712	4517	1959	570	395	179	194	24	0.28	8928
Aug 2002	19.21	0	128	1587	3006	1782	630	390	509	552	80	0.92	8928
Sep 2002	10.66	0	0	921	3769	1962	632	553	254	206	25	0.30	8640
Oct 2002	26.61	0	138	2238	2959	1764	837	372	159	119	10	0.12	8928
Nov 2002	23.58	0	133	1904	3748	1557	522	274	214	60	16	0.19	8640
Dec 2002	5.49	0	0	490	2711	2870	1278	582	322	214	29	0.34	8928
Jan 2003	6.21	0	0	554	2386	3471	1644	551	285	31	6	0.07	8928
Feb 2003	0.35	0	0	28	781	2242	2318	1197	973	474	51	0.63	8064
Mar 2003	1.28	0	0	114	2006	3653	1045	679	656	567	208	2.33	8928
Apr 2003	2.60	0	0	225	1645	3629	1411	713	629	369	19	0.22	8640
May 2003	2.92	0	0	261	2444	3994	1251	468	263	206	41	0.46	8928
PERCENT	9.08	0.1	0.58	4.57	17.9	18.4	8.95	5.24	4.36	2.93	0.59	0.59	
DJF %	5.41	0.00	0.06	5.35	30.49	31.76	15.43	7.05	4.38	1.93	0.22	0.22	
MAM %	5.71	0.22	0.57	4.92	24.03	34.34	14.78	7.92	6.41	4.01	0.70	0.70	
JJA %	14.00	0.18	1.00	12.82	43.24	24.34	5.61	3.53	3.13	2.46	0.66	0.66	
SON %	13.43	0.00	0.61	12.82	36.33	23.08	9.19	5.49	4.97	3.75	0.77	0.77	

From Table 4.12, the following conclusions are drawn:

- Lower boundary violations (datapoints for which ε < 0.7) are on average substantially more (9.08%) than upper boundary (ε > 1.0) violations (0.59%). Bearing in mind that the lower boundary is tested under clear-sky conditions and the upper boundary under overcast conditions, the abundance of clear sky at BSRN De Aar for most of the year, explains the reasons for this phenomenon.

- Lower boundary violations are biased towards a maximum in the latter half of the year (JJA and SON), while upper boundary violations shows a minimum in summer (DJF).

- Only one month (April 2001) has no lower boundary violations, while two months (August 2001 and February 2002) have no upper boundary violations.

- Lower boundary violations occur at more than 20% of the time in the months of October 2002 (26.61%), May 2002 (24.25%), November 2002 (23.58%) and August 2001 (22.47%), while upper boundary violations exceed 2% of the time in the months of March 2003 (2.33%) and July 2001 (2.29%).

To illustrate the boundary violations towards both sides, Figure 4.15 represents a typical month, July 2001, having a 16.9% lower-boundary violation and a 2.29% upper-boundary violation rate. For clarity, individual time-series of LWD, σT^4 (T = surface temperature) as well as ε (σT^4/LWD) are presented.

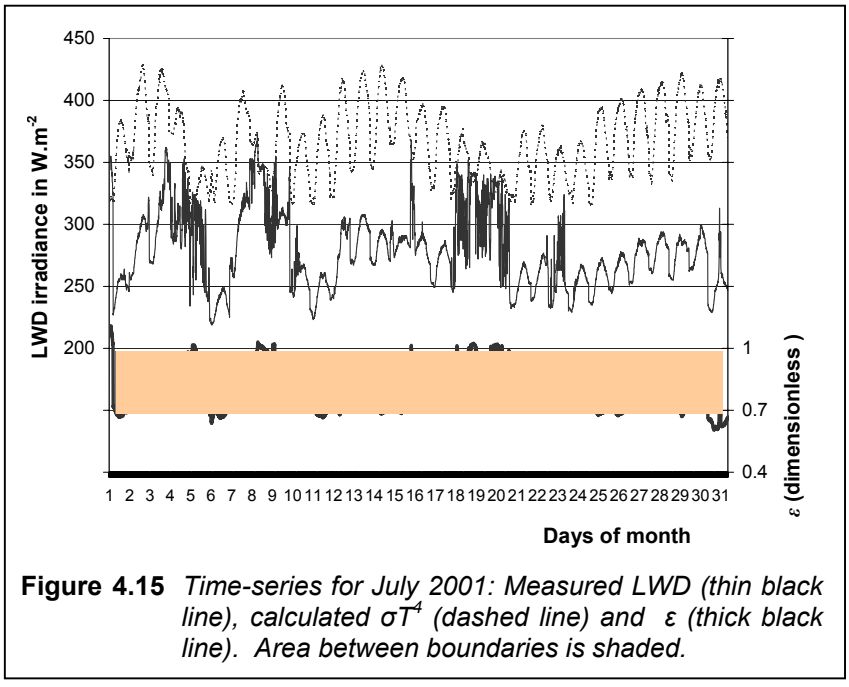

Figure 4.15 *Time-series for July 2001: Measured LWD (thin black line), calculated σT⁴ (dashed line) and ε (thick black line). Area between boundaries is shaded.*

In general, LWD and σT^4 show opposing, as well as concurrent trends to a large degree. Boundary violations (ε outside the shaded area in Figure 4.15) occur randomly and scattered throughout the month – there is no preferred time, although the lower boundary in general, is more frequently and severely tested.

For July 2001, the highest ε occurs on the 1st, 4th, 5th, 8th, 9th, 16th and 18th to 20th, representing relatively frequent but only slight passing through the 1.0 boundary. The violations of the lower boundary (cf Figure 4.15) only appear significant on the 31st. Lowest values of ε appear on the 10th to 17th and 23rd to 31st, suggesting that the sky was indeed clear during those times. If the threshold value for ε was only slightly lower than 0.7, a lot less violations would have occurred. This is again an example of how an indiscriminate application of one sub-procedure parameter to all stations in the world leads to a large number of violations. More research into acquiring site-specific parameters, would be a step towards addressing this problem.

One last comparison to elucidate the behaviour of ε, is an overall look at the relationship between ε and U. (U = relative humidity, expressed as a percentage). Figure 4.16 is a scatter diagram of ε versus U expressed in 18915 hourly values for June 2000 to May 2003.

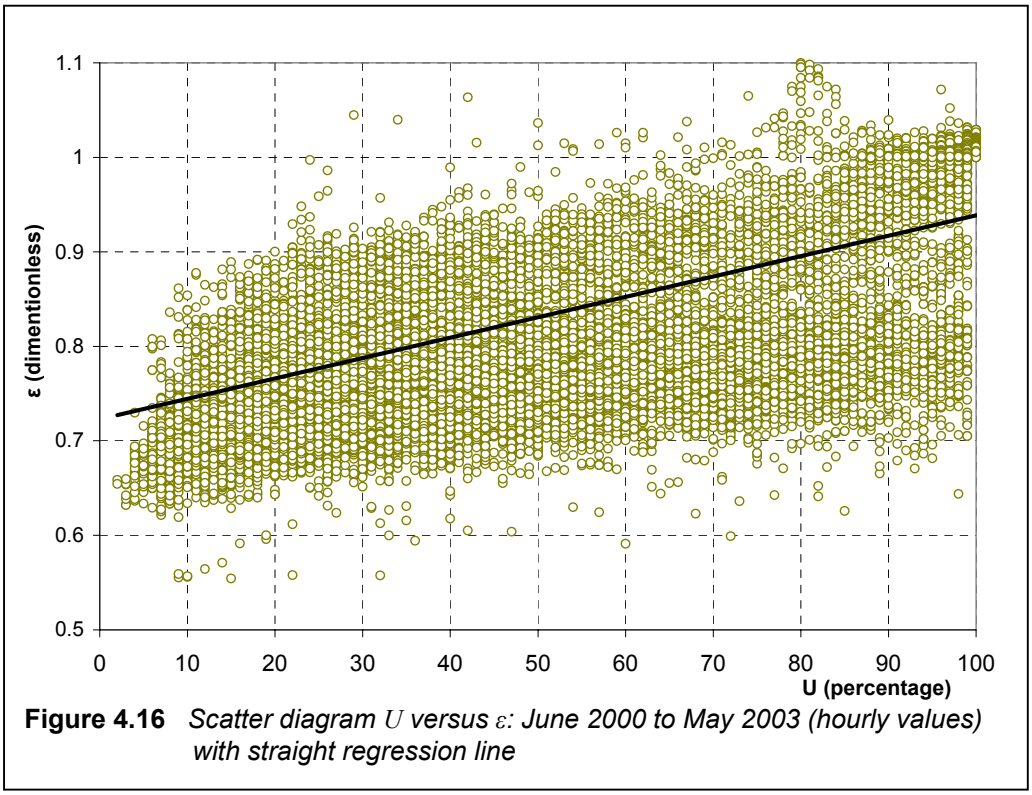

Figure 4.16 *Scatter diagram U versus ε: June 2000 to May 2003 (hourly values) with straight regression line*

From Figure 4.16, the impression (also indicated by the regression line) is that there is a trend for lower ε to be gravitated towards lower U and vice versa, although there is a large

tolerance both sides of the regression line, which is calculated as ***ε = 0.725 + 0.0013U.*** Correlance coefficient of R^2 is calculated as 0.2704, which is relatively low, but still has significance given the long record. Generally, upper boundary violations (ε > 1.0) occur towards higher U and lower boundary violations (ε < 0.7) towards lower U, although there are a number of outliers in both cases.

4.3.3.2 Sub–procedure 3.2 *(The test for UL between $\sigma(T-10)^4$ and $\sigma(T+10)^4$)*

Since UL is not a basic parameter measured at De Aar, there is no data and no analysis.

4.3.3.3 Sub–procedure 3.3 *(The test for DSDIR*cosZ between DSGL2 – DSDFS – 50 W.m^{-2} and DSGL2 – DSDFS + 50 W.m^{-2})*

and

4.3.3.4 Sub–procedure 3.4 *(The test for DSGL2 – DSDFS between DSDIR*cosZ - 50 W.m^{-2} and DSDIR*cosZ + 50 W.m^{-2})*

In Section 4.2.3.2 it was shown that procedures 3.3 and 3.4 refer to the same conditions, therefore these two procedures are treated as one in this Section. Equation 4.8 implies that evaluation involves calculating MM = DSGL2–DSDFS–DSDIR*cos$Z$ for all datapoints. Violations of sub-procedure therefore are cases where MM < -50 W.m^{-2} or MM > 50 W.m^{-2}.
It follows from Table 4.13, that:

- In general, datapoints are gravitated towards the upper boundary, i.e., DSGL2 > DSDFS + DSDIR * cos$Z$ to a larger extent than DSGL2 < DSDFS + DSDIR * cos$Z$.

- For every month, the majority of all datapoints lies between the borders, but there are certain months where substantial, and possibly serious, boundary violations occur.

- Most serious lower boundary violations (DSGL2–DSDFS–DSDIR*cos$Z$ < -50 W.m^{-2}) occurred in December 2000 (19.40%) and October 2001 (13.09%). The worst upper boundary violations (DSGL2–DSDFS–DSDIR*cos$Z$ > 50 W.m^{-2}) happened in December 2000 (17.86%), May 2001 (15.86%) and March 2002 (14.18%).

Although violations are numerous in specific months during which they occur, overall they only amount to 0.0038% for the lower boundary and 0.0044% for the upper boundary. The higher number for the latter confirms the datapoint gravitation towards the upper boundary.

Table 4.13 *Frequency distribution of DSGL2-DSDFS-DSDIR*cosZ: June 2000 to May 2003, ref.to sub-procedures 3.3 and 3.4. Shaded areas represent violations*

Month	%	Data bins in W.m^{-2}																%
	<-50	< -70	-70 to -60	-60 to -50	-50 to -40	-40 to -30	-30 to -20	-20 to -10	-10 to 0	0 to 10	10 to 20	20 to 30	30 to 40	40 to 50	50 to 60	60 to 70	> 70	>+50
Jun 2000	0.00	0	0	0	0	0	0	3	26479	16106	556	24	22	2	0	0	0	0.00
Jul 2000	2.93	1072	117	114	111	106	94	110	26987	15125	647	8	16	4	5	1	116	0.27
Aug 2000	0.00	0	0	0	0	1	3	19	37574	7018	15	0	0	2	0	0	0	0.00
Sep 2000	0.00	0	0	0	0	0	0	1	20586	8865	4105	5874	3290	456	11	0	0	0.03
Oct 2000	0.00	0	0	0	0	2	2	2	24364	10520	8384	1353	5	1	1	0	0	0.00
Nov 2000	0.02	9	0	0	0	0	1	1	20990	7230	3956	4043	3283	1468	290	164	1757	5.34
Dec 2000	19.40	7171	231	234	226	255	293	361	17561	7612	891	904	876	990	880	869	5279	17.86
Jan 2001	0.29	0	47	82	48	49	38	5	15236	11639	4332	6058	4058	1869	495	365	311	2.64
Feb 2001	0.00	1	0	0	0	0	0	1	12176	14206	4518	7211	1897	273	26	0	3	0.07
Mar 2001	0.00	0	0	0	0	0	1	0	16774	15223	5023	6058	740	371	155	155	132	0.99
Apr 2001	0.03	0	9	4	6	6	3	7	21110	14791	5342	1203	581	42	20	24	42	0.20
May 2001	0.00	0	0	1	221	519	940	1821	11661	2640	1724	1892	2669	1682	761	646	2902	15.86
Jun 2001	9.72	1514	716	1899	2232	2325	1644	1113	22695	4823	1077	779	596	440	335	279	733	3.17
Jul 2001	0.58	0	0	261	737	709	830	535	24001	14872	2534	109	20	21	4	0	0	0.01
Aug 2001	0.00	0	0	0	0	0	0	0	26434	17873	120	7	6	6	11	10	165	0.42
Sep 2001	7.06	2468	253	328	311	476	362	338	15332	16219	5347	1429	107	102	44	76	0	0.28
Oct 2001	13.09	5282	275	278	251	246	218	192	9493	19943	5790	2043	258	85	75	149	54	0.62
Nov 2001	0.00	0	0	0	0	1	0	2	14870	15666	5754	5749	961	152	30	2	3	0.08
Dec 2001	0.04	0	7	9	11	14	0	71	16465	12028	4487	5869	3938	1162	221	249	102	1.28
Jan 2002	0.34	0	94	59	46	49	38	48	9290	20056	7672	5713	1427	133	5	0	1	0.01
Feb 2002	0.01	3	0	0	1	0	0	1	9520	25236	4648	720	147	33	1	0	0	0.00
Mar 2002	1.38	314	129	142	80	27	227	90	13269	15621	3232	2567	1520	1418	1568	2069	2358	14.18
Apr 2002	0.00	0	0	0	0	0	0	0	10511	27200	4467	896	80	25	11	0	0	0.03
May 2002	0.00	0	0	0	134	1109	783	295	11107	20893	2089	1991	2447	3397	382	4	0	0.86
Jun 2002	0.00	0	0	0	0	0	0	5	10590	20440	2549	2655	3982	2911	46	1	11	0.13
Jul 2002	0.00	0	0	0	0	0	1	8	11518	19398	2852	2954	4242	3223	85	61	288	0.98
Aug 2002	0.00	0	0	0	0	0	0	4	11290	30973	1479	132	44	38	48	42	580	1.52
Sep 2002	0.00	0	0	0	1	1	1	1	7694	29694	5543	250	7	0	0	0	0	0.00
Oct 2002	0.00	0	0	0	0	0	0	0	9829	23256	9623	1407	149	52	78	44	192	0.71
Nov 2002	0.00	0	0	0	0	0	1	0	9977	20708	10016	2307	149	11	4	4	13	0.05
Dec 2002	0.00	1	0	0	1	2	15	16	9354	22700	8557	3462	428	76	13	0	7	0.04
Jan 2003	3.86	60	467	1192	849	903	1730	1060	17312	17700	3039	255	18	1	1	1	42	0.10
Feb 2003	0.40	0	0	159	27	18	18	10	18943	11802	8296	641	36	12	8	5	335	0.87
Mar 2003	0.02	0	5	5	7	11	17	17	25940	18143	445	25	5	1	3	1	5	0.02
Apr 2003	0.17	31	23	20	13	9	10	7	23906	18588	555	23	7	0	0	0	0	0.00
May 2003	0.75	167	73	93	37	24	37	50	25919	17547	623	27	18	15	0	0	0	0.00
%	0.004	1.147	0.155	0.309	0.339	0.435	0.463	0.393	39.11	37.57	8.897	4.860	2.412	1.298	0.356	0.331	0.979	0.004
DJF %	0.01	1.86	0.22	0.45	0.31	0.33	0.55	0.40	32.37	36.77	11.94	7.93	3.30	1.17	0.42	0.38	1.56	0.01
MAM %	0.00	0.13	0.06	0.07	0.13	0.43	0.51	0.58	40.31	37.90	5.91	3.69	2.03	1.75	0.73	0.73	1.37	0.01
JJA %	0.01	1.97	0.13	0.15	0.14	0.18	0.15	0.14	33.87	38.69	14.89	6.22	2.09	0.59	0.14	0.11	0.51	0.00
SON %	0.00	0.65	0.21	0.57	0.77	0.79	0.65	0.45	49.71	36.89	2.98	1.68	2.25	1.67	0.13	0.10	0.48	0.00

- Since three radiometers (global and diffuse pyranometers) and a pyrheliometer are involved in the evaluation of sub-procedues 3.3 and 3.4, using Equation 4.8, the margin of error is set to the relatively large value of 50 W.m^{-2}, as mentioned in Section 4.2.3.2. The distribution of MM = DSGL2–DSDFS–DSDIR*cos$Z$ have been tabulated using bin sizes of 10 W.m^{-2}, distributed between -70 W.m^{-2} and 70 W.m^{-2} (Table 4.13). Columns either side of the boundaries are shaded as in Table 4.12: datapoint numbers in a light shade, and percentages in a darker shade.

4.3.3.4.1 May 2001 *(Typical boundary violations of sub-procedure 3.3 and 3.4)*

A typical month exhibiting boundary violations (15.86% of the upper boundary), is now investigated. Figure 4.17 depicts a time-series of (DSGL2–DSDFS–DSDIR*cos$Z$) for May 2001.

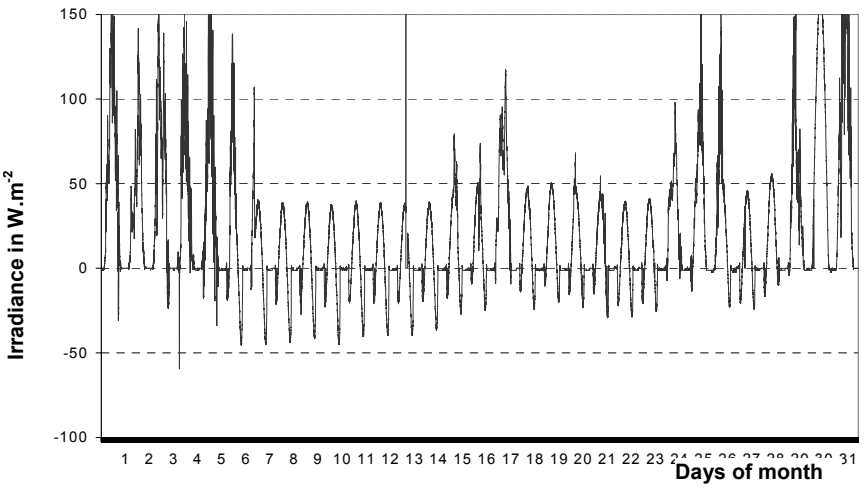

Figure 4.17 *Time-series of (DSGL2–DSDFS–DSDIR*cos$Z$): May 2001*

Violations of the 50 W.m^{-2} upper boundary are apparently distributed at random days throughout the month (Figure 4.17). A single spike violation of the upper boundary also exists.

Note that the first 6 days of the month all have large occasional overshootings of the upper boundary, as well as the 17th, 25th, 26th, and from the 19th to the 31st. Two specific days, typical of this behaviour, are now investigated. They are the 17th and 31st.

Firstly, consider 17 May 2001. It was a sunny day with frequent broken cloud passing the sun. Time-series of datapoints for the respective radiometers are depicted in Figure 4.18.

It follows from Figure 4.18 that the boundary violations (open circles above the 50 W.m^{-2} line against the right-hand axis) are restricted to the middle of the day, whilst DSGL2 does not overshoot TOA radiation. In fact, it maintains a healthy cushion throughout the day. Note that the time-series of DSDFS (dashed line) followed a similar trend as that of DSGL2-DSDFS-DSDIR*cos$Z$ (open circles) and DSDFS (dashed line) (Figure 4.18). This indicates that the features of DSDFS are echoed during violations. Thus, the violations are most likely the cause of DSDFS (dashed line) being too high.

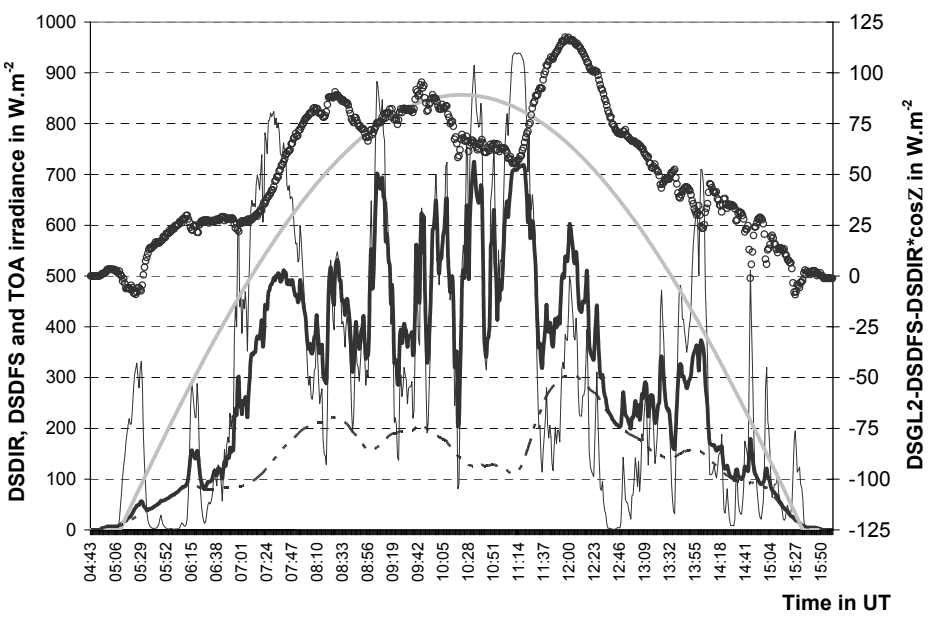

Figure 4.18 *Time-series on 17 May 2001 for DSDIR (thin black line), DSDFS (dashed line),DSGL2 (thick black line), TOA radiation (thick smooth grey line) and DSGL2-DSDFS-DSDIR*cosZ (open circles).*

An anomalously high DSDFS can be attributed to pyranometer skewness, or more likely, since the tracking is not active, a case of the shading device drifting off track and not fully shading the diffuse pyranometer, resulting in anomalously high values.

One of the most important recommendations is therefore, that the shading must be controlled regularly on site at different times of the day, and as soon as possible, the tracker be upgraded to an active tracker, which will be a major step towards eliminating this error.

Secondly, consider 31 May 2001, which was also a sunny day with the occasional passage of broken clouds. However, the clouds were thinner than those observed on the 17th. In Figure 4.19, a graph similar to Figure 4.18 is depicted.

From Figure 4.19, behaviour of DSGL2-DSDFS-DSDIR*cos$Z$ similar to Figure 4.18 is observed: a large number of upper-boundary violations (open circles above 50 W.m^{-2}). One exception is, that the relationship between DSGL2-DSDFS-DSDIR*cos$Z$ (open circles) and DSDFS (dashed line) is not as clearly exhibited as in Figure 4.18. The violations are mainly the result of DSGL2 (thick black line) overshooting TOA radiation (thick smooth grey line), leading to anomalously high values for DSGL2-DSDFS-DSDIR*cos$Z$.

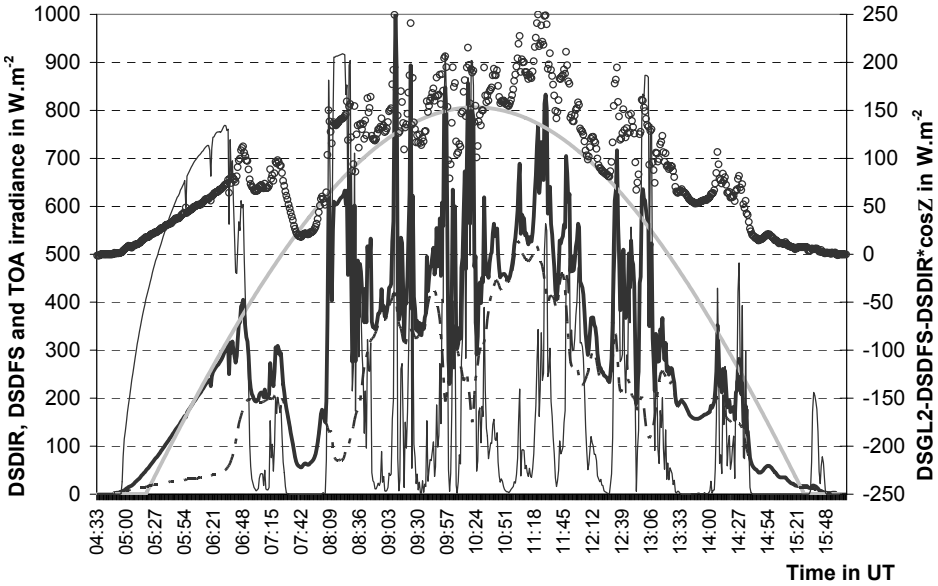

Figure 4.19 *Time-series on 31 May 2001 for DSDIR (thin black line), DSDFS (dashed line), DSGL2 (thick black line), TOA radiation (thick smooth grey line) and DSGL2-DSDFS-DSDIR*cosZ (open circles).*

Abnormally high DSGL2 can also be the result of temporary pyranometer skewness, since the other possible causes (misapplication of calibration or a mistake in the logger program) are highly unlikely.

This sub-procedure, the last of the finer sub-procedures, also exhibits by far the largest number of boundary violations in comparison to all the preceding sub-procedures.

4.3.4 Procedures 4 and 5

The originally proposed procedures 4 and 5 were not yet implemented at WRMC at the time of writing this document, therefore no further discussion is included here.

4.4 CONCLUSIONS

Quality assurance, as defined at the beginning of this Chapter, is in essence a dynamic process. In the BSRN context, it takes the form of continuous evaluation and effective feedback, in order to sustain the best possible measurements, as well as a retrospective character to apply corrections truly believed to enhance the quality of collected data. The WRMC employs a rigorous set of quality control procedures, which had all been investigated in detail throughout this Chapter. They identify a wide variety of errors in the standard BSRN one-minute data for a wide variety of diverse reasons.

When the WRMC procedures are applied to the experimental three-year De Aar dataset between June 2000 and May 2003, errors are identified. Some of these sub-procedure violations identify erroneous data which make up a small percentage of the overall dataset, and can thus be safely deleted. There are, however, single cases of substantial differences which would require deeper investigation, but such details are beyond the scope of this research.

Like all procedures of this kind, the WRMC quality control measures are not perfect, and the author acknowledges the fact, that WRMC is also in the process of undergoing stages of development. Two pairs of sub-procedures (2.5. and 2.6 as well as 3.3 and 3.4), listed in the database design notes as separate sub-procedures, had been demonstrated to refer to the same circumstances and are therefore identical. Another flaw in the procedures, which the author wishes to point out, is the inflexible definition of certain sub-procedure boundaries globally applied to all BSRN stations in the network.

This inflexible situation, leading to a large number of possibly falsely identified sub-procedure violations, could be improved with some refinement measures to the procedures, making allowance for local and site-specific circumstances, which can be determined by a combination of empirical and analytical methods. However, in the opinion of the author, this falls beyond the scope of this document.

CHAPTER 5

CASE STUDIES

In this Chapter, two recent solar eclipses that traversed Southern Africa in relatively short succession, are studied. They occurred on 21 June 2001 and 4 December 2002 and in both cases, a significant portion of the partial phases were visible at De Aar. Both days were clear sky days at De Aar for the entire day, and complete radiation measurements of all basic components without any missing data were possible. The Chapter comprises a short discussion on solar eclipses, followed by (for both eclipses individually), discussions of the path of totality, meteorological background leading to eclipse day, and time-series analysis of the basic radiation components for both eclipses, complemented by comparative tables.

5.1 SOLAR ECLIPSES: BACKGROUND

A solar eclipse is the relatively rare event when the moon in its orbit around the Earth, intercepts the direct line of sight between the Sun and Earth. The resulting shadow (projection of the Moon's umbra) cast on Earth, is called the path of totality. An observer in this narrow strip of land (usually about 200 km wide), will then experience a total solar eclipse. This event lasts theoretically a maximum of 7 minutes and 31 seconds[1], typically only about 1 to 3 minutes, depending on the moon-earth-sun distance ratio. An observer in the adjacent area (a few thousand km wide on both sides), experiences the projection of the Moon's penumbral shadow, i.e., a partial solar eclipse, the magnitude of which is dependant upon the distance from the observation point normal to the path of totality.

Not all solar eclipses have paths of totality. When the moon-earth distance is orientated relative to the sun-earth distance in such a way that an eclipse occurs, but the Earth in space misses the Moon's umbra, the result for an observer on Earth is either a penumbral (partial) eclipse or an annular eclipse. A specific eclipse event can also be hybrid, i.e., a combination of a partial and total eclipse.

[1] http://www.donastro.freeserve.co.uk/tycho.htm

The governing factor of solar eclipses on a temporal scale, the Saros cycle, is in fact an interwoven multitude of simultaneous moon-earth orbit interception cycles waxing and waning over centuries.[2] The period of a Saros cycle is 6585.3215 days (slightly more than 18 years). This is not an exact number of Earth revolutions (days), therefore solar eclipses do not follow exact occurrence in a cycle of days or multiples thereof, but rather seem to be randomly distributed on both a temporal and geographical scale.

For the period 2000 BC to 4000 AD, it has been determined that a total of 14263 eclipses have occurred or are yet to occur[3]. This translates to an average frequency of 2.38 eclipses per year, distributed per eclipse type as listed in Table 5.1:

Table 5.1 *Relative frequency of eclipse types (after NASA's Solar Eclipse Catalogue)*

All eclipses	Total	Partial	Annular	Hybrid
14263 (100 %)	3797 (26.6 %)	5029 (35.3 %)	4699 (32.9 %)	738 (5.2 %)

The last total solar eclipse that traversed South African soil in the 20th century, was on 1 October 1940, followed by the total eclipse of 4 December 2002, while the next total solar eclipse is expected only at 25 November 2030. In the 28 years between the eclipses of 2002 and 2030, there are 61 eclipses expected over the world, of which only 16 will have an impact through its partial phases on South Africa. Therefore, solar eclipses, total or otherwise, over a specific area, such as South Africa, are a relatively rare occurrence that deserve a closer look.

5.2 SOLAR ECLIPSES OVER SOUTHERN AFRICA

Shortly after the establishment of the BSRN site, two total solar eclipses traversed Southern Africa in relatively short succession: one in the winter afternoon of 21 June 2001, and another in the summer morning of 4 December 2002. The path of totality covered Southern Africa in both cases (the latter occurrence slightly further south), with the BSRN site in South Africa being well situated to receive a significant portion of both partial phases.

Comparative figures ref. to events regarding the two eclipses at the De Aar BSRN station, are listed in Table 5.2. All times are quoted in South African Standard Time (SAST), unless stated otherwise. The data was calculated using astronomical software (*www.calsky.com*).

[2] http://sunearth.gsfc.nasa.gov/eclipse/SEsaros/SEsaros.html
[3] http://sunearth.gsfc.nasa.gov/eclipse/SEcat/SEcatalog.html

Table 5.2 *Comparative data at De Aar BSRN station for the 2001 and 2002 eclipses over Southern Africa. Times are in SAST. Note that SAST = UT + 2 hours.*

Event	Eclipse of 21 June 2001	Eclipse of 4 December 2002
Time of sunrise	07:21:00	05:13:42
Time of sunset	17:30:36	19:14:48
Length of day	10:09:36	14:01:06
Time of solar noon	12:25:48	12:14:06
Start of partial phase (first contact)	13:30:34	07:25:09
Time instant of maximum eclipse	14:52:17	08:27:40
Solar elevation angle at maximum eclipse	25.9°	39.5°
Maximum fraction of solar disk obscured	60.7%	73.1%
End of partial phase (fourth contact)	16:04:56	09:37:33

5.3 ECLIPSE OF 21 JUNE 2001

5.3.1 General description

The path of totality for this total solar eclipse is illustrated in a global context in Figure 5.1 and in more detail in Figure 5.2, using a close-up view.

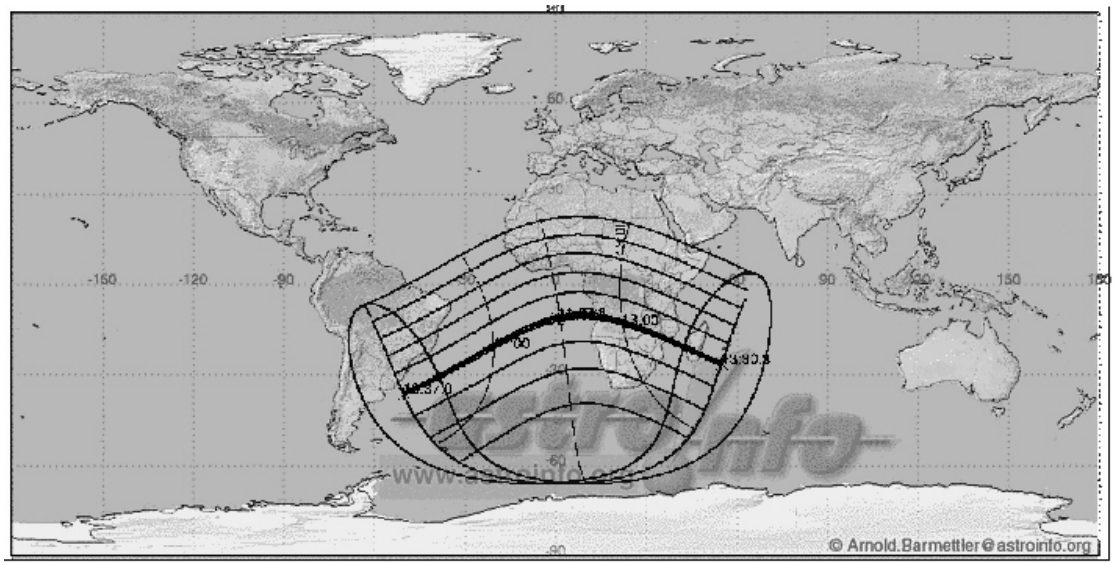

Figure 5.1 *Global orthographic projection of solar eclipse on 21 June 2001. Map by Arnold Barmettler at Astro-Info (www.astro-info.org)*

In Figure 5.1, the path of totality is represented by the thick central line, starting southeast off the Brazilian coast, curving through the Atlantic Ocean, traversing Africa and ending east of Madagascar in the Indian Ocean. The thinner lines parallel to this line respectively represent the 80%, 60%, 40%, 20% and 0% phases, respectively, of the partial eclipse. The dashed line orthogonal to the path of totality, stretching from western Africa along the Atlantic Ocean towards the South Pole, represents the peak line. The intersection between this line and the path of totality west of Angola indicates the eclipse peak at 11°15' S, 02°45' E, where the path of totality had its maximum width (204 km). For an observer at that point, the eclipse occurred at 12:03:42 UT, 105% of the solar disk was obscured and totality would last 5'01".

Since Southern Africa is situated towards the east of the eclipse peak, it experienced the eclipse in the waning phase. Another interesting fact is that the Southern Hemisphere (SH) winter solstice occurred at 07:37:42 SAST, only about 4 hours after the start of the eclipse. The appearance of the eclipse on the shortest day of the year for the SH, was in itself a unique occurrence.

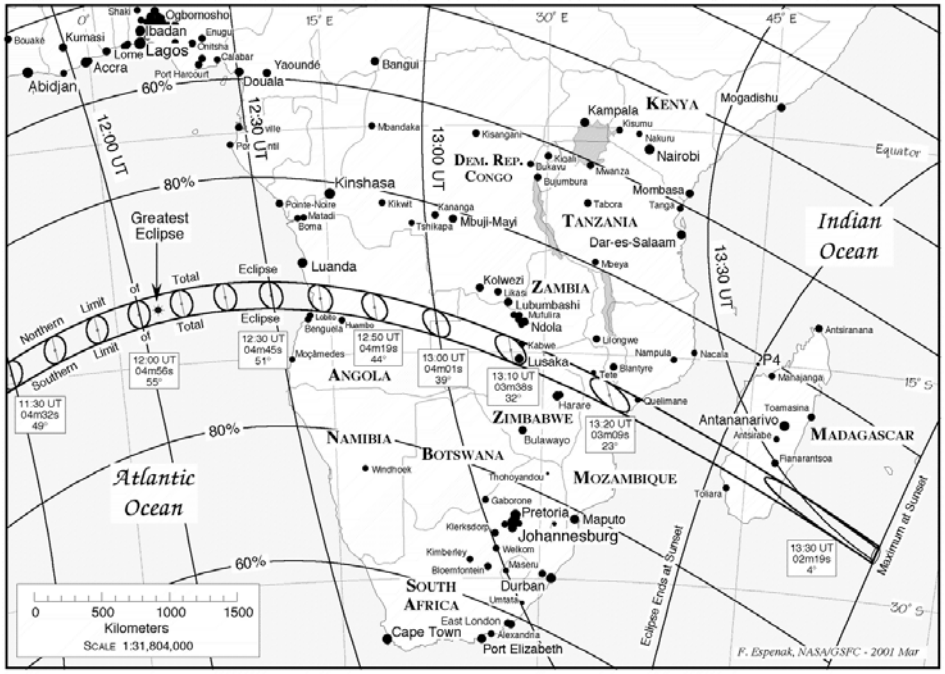

Figure 5.2 *Close up view of 2001 eclipse path through Africa, showing detail of partial phase. Map from Espenak and Anderson (1999). Times in UT*

Figure 5.2 provides a closer view of the eclipse path through Africa, showing details about the partial phases. The totality path entered Africa at the Angolan coast, passing Zambia through the central west, including northern Zimbabwe, southern Zambia and central-west Mozambique as well as the southernmost tip of Malawi. Lusaka in Zambia was the most prominent urban point in Southern Africa under the totality path.

5.3.2 Eclipse in South Africa

In South Africa, partial phase magnitudes were between 51 % at Cape Town, in the extreme Southwest, and up to 80 % at the Kruger National Park in the extreme northeast. Local circumstances for a few major centra in South Africa (Espenak and Anderson, 1999) are listed in Table 5.3.

Table 5.3 *Local circumstances for a few centra in South Africa during eclipse 2001*

Location	Latitude	Longitude	First contact	Last contact	Max eclipse	Magni-tude
Bloemfontein	29°12'S	26°07'E	13:35:21	16:10:21	16:57:45	65.3%
Cape Town	33°55'S	18°22'E	13:17:46	15:49:29	16:36:52	51.3%
Durban	29°55'S	30°56'E	13:46:12	16:15:08	15:05:31	67.7%
East London	33°00'S	27°55'E	13:39:58	16:06:26	14:57:27	58.7%
Johannesburg	26°15'S	28°00'E	13:39:35	16:17:01	15:03:46	73.5%
Kimberley	28°43'S	24°46'E	13:31:59	16:09:14	14:55:32	65.3%
Port Elizabeth	33°58'S	25°40'E	13:35:15	16:01:33	14:52:22	55.2%
Pretoria	25°45'S	28°10'E	13:40:00	16:17:53	15:04:29	74.8%

5.3.3 The weather

In general, the meteorological conditions over South Africa in mid-winter are dominated by a strongly developed high-pressure system on the surface, echoed in the upper-air over the interior. This is accompanied by a regular succession of cold fronts sweeping the Western Cape and coastal areas up to Northern Kwa-Zulu Natal, often stretching far inland and causing partly cloudy to cloudy conditions in some places. In general, these conditions prevailed over South Africa at the time of the 2001 eclipse.

The weather events leading to the eclipse day on 21 June 2001 are now described in more detail, using daily 12:00 UT synoptic maps featured in Figures 5.3 to 5.6 (SAWB, 2001).

Starting three days before the eclipse day (viz., on 18 June 2001), a cold front passes over the southern interior causing partly cloudy and cold conditions in its wake (Figure 5.3). Over the interior, fine weather dominates well ahead of the cold front. From the far west, the Atlantic High ridges eastward. There is a reasonable chance to expect an upper-air trough accompanying the cold front sweeping the country.

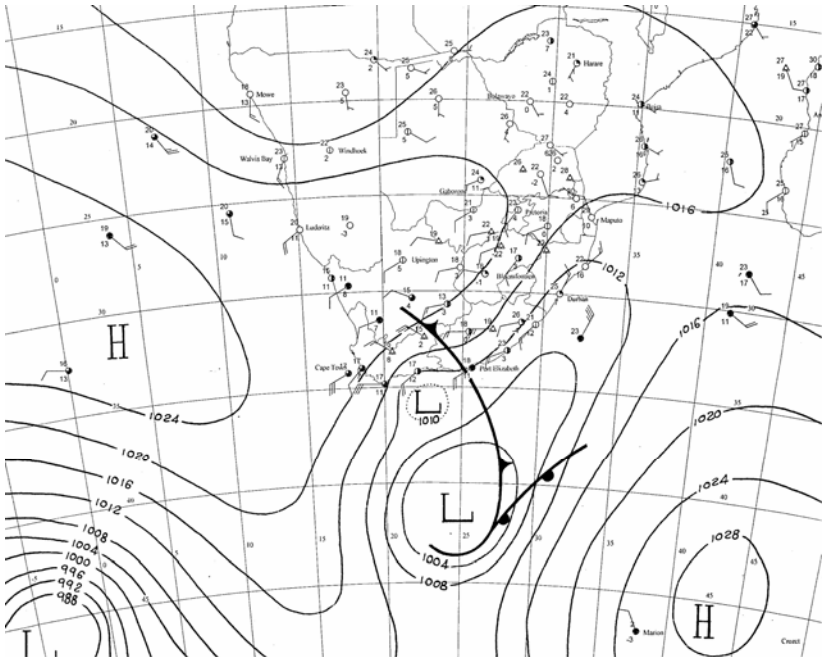

Figure 5.3 *Synoptic conditions at 12:00 UT on 18 June 2001 - three days before eclipse day (SAWB, 2001)*

The following day, 19 June 2001, the cold front had swept the eastern parts of the country, bringing partly cloudy and windy conditions in its wake. The Atlantic Ocean High ridging in behind it, causes rapid clearing from the west, with cold conditions and strong winds along the coast. (Figure 5.4.). The high-pressure system now extends over the country's interior and dominates the circulation, advecting cold air over the southern parts.

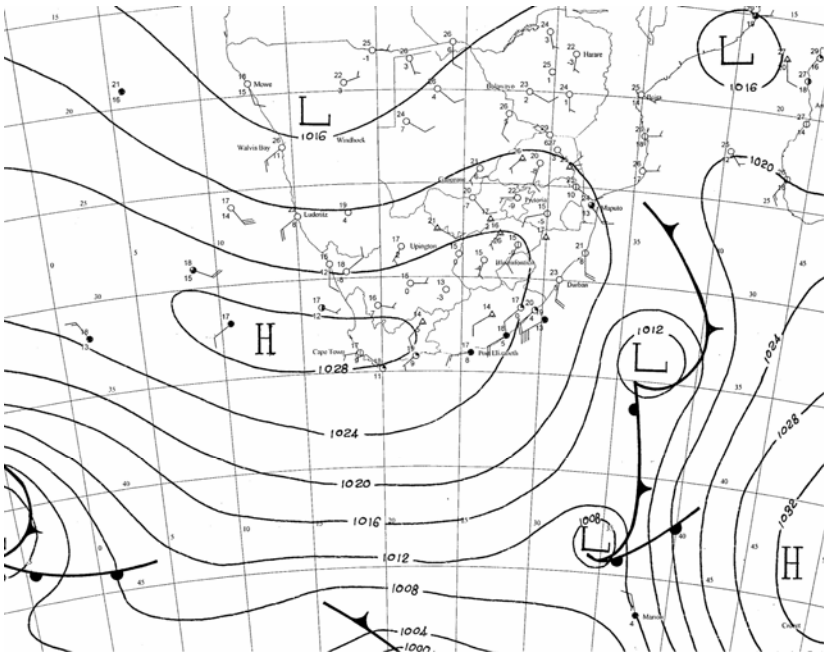

Figure 5.4 *Synoptic conditions at 12:00 UT on 19 June 2001 - two days before eclipse day (SAWB, 2001)*

The following day, 20 June 2001 (eclipse eve), the high-pressure system had established itself south-East of the continent (Figure 5.5). The advection of moist, cool air towards the eastern parts of the country lead to partly cloudy to cloudy and windy conditions along the coast of Kwa-Zulu Natal. The development of two small areas of low pressure (a twin-low pressure system) east of Durban, created a pressure gradient for strong onshore flow, aiding in the advection of moisture. Over the South African interior, conditions favoured the development of an upper-air ridge, causing subsidence and clear sky over most of the interior.

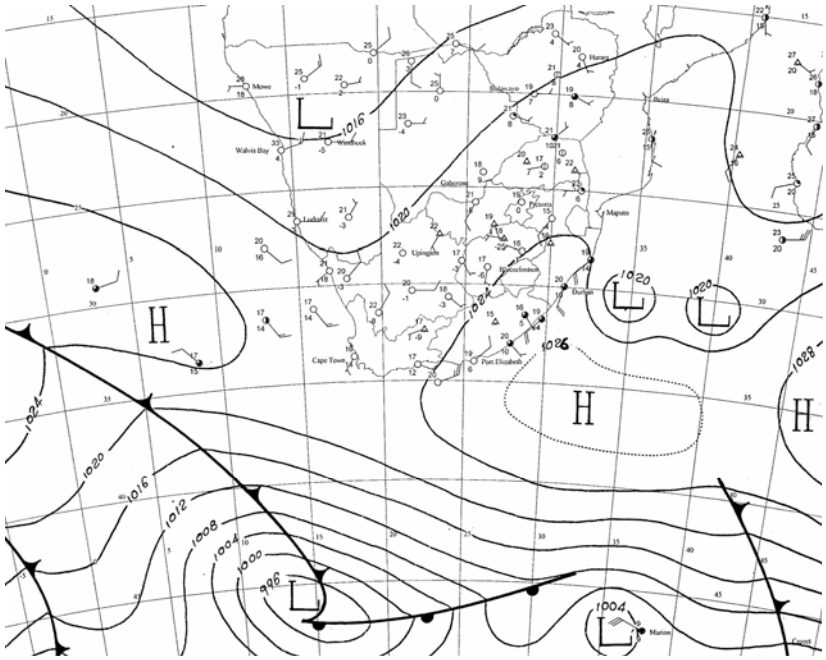

Figure 5.5 *Synoptic conditions at 12:00 UT on 20 June 2001 - one day before eclipse day (SAWB, 2001)*

On eclipse day, 21 June 2001, the circulation was dominated by a high-pressure system over the country's interior, centered where the borders of South Africa, Botswana and Zimbabwe meet (Figure 5.6). A cold front was situated to the far south and the Atlantic Ocean High, still deepening, advected warm air ahead of the front further west, pushing the front southwards and leading to only partly cloudy conditions along the southern coast.

A coastal low developed in the East London area, causing partly cloudy conditions in its wake. The twin low-pressure cells have migrated further northwards east of Maputo, whilst still maintaining a weak onshore flow, creating partly cloudy conditions along the northernmost parts of the South African eastern coastline.

It follows from Figure 5.6, that cloudless skies (good eclipse weather) were dominant over most of the country, except the southern coast and the eastern coastline. In particular, no clouds were present over the De Aar BSRN station.

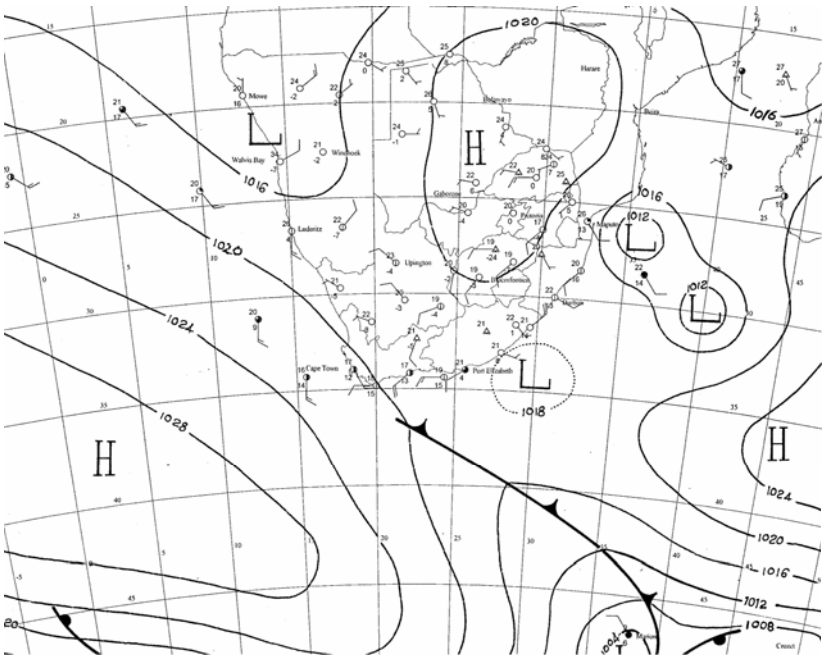

Figure 5.6 *Synoptic conditions at 12:00 UT on 21 June 2001 - eclipse day (SAWB, 2001)*

5.3.4 The BSRN measurements

The term “datapoint” refers to the standard one-minute average value as measured at BSRN stations. Consider Figure 5.7, showing a time-series of SW datapoints for eclipse day 2001.

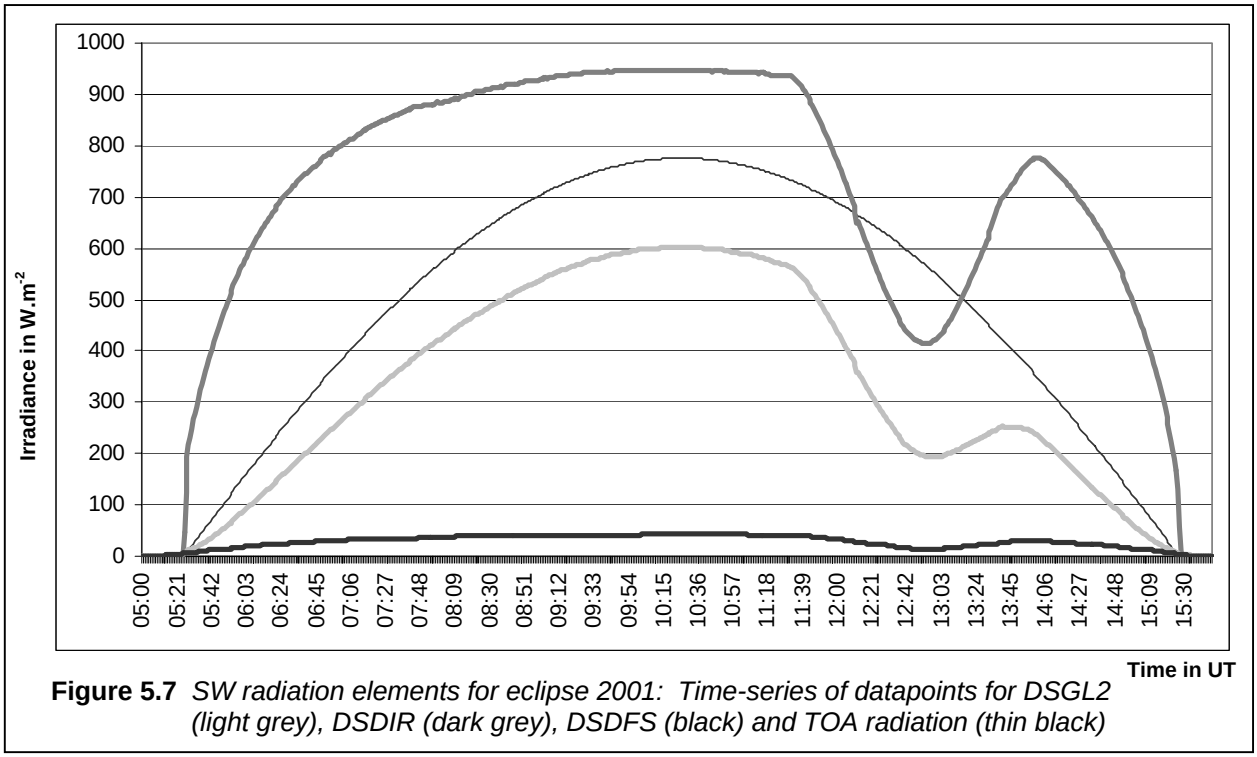

Figure 5.7 *SW radiation elements for eclipse 2001: Time-series of datapoints for DSGL2 (light grey), DSDIR (dark grey), DSDFS (black) and TOA radiation (thin black)*

Eclipse day (21 June) in 2001, was a clear sky day, resulting in smooth curves for all the SW components, hence showing the eclipse in a distinct and unique way. In Figure 5.7, DSDIR (direct), DSDFS (diffuse) and DSGL2 (global) radiation each show a smooth regular dip at the time of the partial eclipse (11:30 UT to 14:04 UT). The exception was the theoretically calculated TOA radiation.

One special remark about DSDFS: Under normal circumstances, when DSGL2 and DSDIR decrease, it is accompanied by and *increase* in DSDFS, usually due to the presence of clouds. In the presence of broken clouds or under overcast conditions, a distorted pattern is displayed, like Figure 4.19. Between datapoints, the DSDFS relation to the other two SW components usually holds, since the occulting (diffusing) objects are *inside* the atmosphere.

The smooth indentation in Figure 5.7 is uncharacteristic of clouds, and the fact that DSDFS *decreased* in synchronization with DSDIR and DSGL2 on this particular day, means that the object of occultation was *outside* the atmosphere, i.e., a celestial object such as the moon.

5.3.4.1 Radiation loss due to eclipse

From datapoints of 21 June 2001, the radiation loss as a result of the eclipse, is now estimated for all the SW components in Figure 5.7. Let R be the integrated radiation for a specific component, and R_0 the "ideal" integrated radiation if there was no eclipse. Hence the radiation loss due to the eclipse is the difference between R_0 and R.

R equals the area under each curve in Figure 5.7, and the area under a smooth curve is approximated by the sum of trapezium elements E_i :

$$R = \sum_{i=05:21}^{i=15:31} E_i \qquad (5.1)$$

Each E_i has width W = 1 minute and side heights I_i and I_{i+1}, where I = average incident radiation over the one-minute interval. Since, for a trapezium,

$$E_i = \frac{W}{2}(I_i + I_{i+1})$$

it follows from Equation 5.1 that $$R = \sum_{i=05:21}^{i=15:31} \frac{W}{2}(I_i + I_{i+1}) \quad (5.2)$$

Datapoints from the same day are used to estimate R_0, based upon the fact that the entire day was cloud-free. Under normal circumstances, the time-series for any SW radiation component, measured during a cloud-free day, is symmetric around the solar transit time. An estimation for R_0 is therefore twice the area under each curve in Figure 5.7 from sunrise (05:21 UT) to (10:26 UT), therefore twice the half-day excluding the eclipse. Hence:

$$R_0 = 2\sum_{i=05:21}^{i=10:26} E_i = 2\sum_{i=05:21}^{i=10:26} \frac{W}{2}(I_i + I_{i+1}) = \sum_{i=05:21}^{i=10:26} W(I_i + I_{i+1}) \quad (5.3)$$

Using Equations 5.2 and 5.3:

R_0(Global)	= 13653 kJ.m^{-2}	;	R(Global) = 12590 kJ.m^{-2}
R_0(Direct)	= 29429 kJ.m^{-2}	;	R(Direct) = 27186 kJ.m^{-2}
R_0(Diffuse)	= 1218 kJ.m^{-2}	;	R(Diffuse) = 1117 kJ.m^{-2}

Therefore, radiation loss due to the 2001 eclipse amounts to:

Global :	1063 kJ.m^{-2}	(7.78%).
Direct :	2243 kJ.m^{-2}	(7.62 %).
Diffuse:	101 kJ.m^{-2}	(8.34 %).

5.3.4.2 Focus on SW elements

In this Section, patterns for the following radiation datapoints for the 2001 eclipse are shown:

- BSRN one-minute standard deviations (OSD) for SW components.
- The DSGL2 : DSGL1 relationship.
- The normalized K-plots as used by NREL (1993)
- LWD radiation and individual terms of pyrgeometer Equation 3.4.

In each of Figures 5.8 to 5.10, the behaviour of a SW component, as well as the associated OSD for eclipse day, 20 June 2001, is displayed. The scale of the left Y-axis is associated

with the SW component in W.m^{-2}, while the scale of the right Y-axis is associated with the relevant OSD (dimensionless).

Figure 5.8 depicts DSDIR (direct irradiance) and associated OSD for eclipse day 2001.

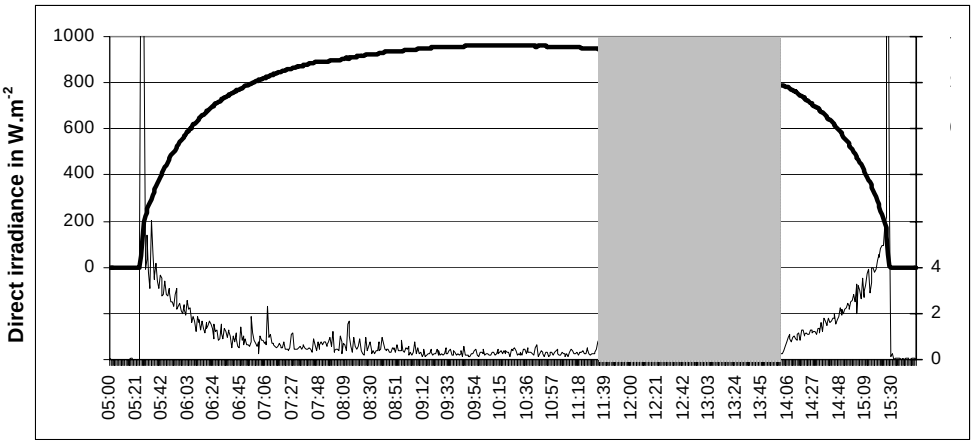

Figure 5.8 *DSDIR and the associated OSD. Eclipse time is shaded.*

Relatively low OSD values (roughly less than 1) outside the eclipse time and between one hour after sunrise and one hour before sunset, indicate just how clear the sky was during eclipse day. The value of OSD is a direct indication of the change in DSDIR from one minute to the next. For about the first hour after sunrise and the hour before sunset, OSD values are more than 1, indicating a rapid change in DSDIR from one minute to the next, which reaches a maximum when the sun is near the horizon. On the minute before sunrise, OSD is still zero, and in the first minute after sunrise, it is a high value (more than 10) since the appearance of the sun constitutes a big change in OSD. A similar argument holds for sunset. At solar noon (10:26 UT), OSD is expected to reach a minimum value.

During the day, outside the eclipse time, small variations in OSD from one minute to the next, occur on almost a continuous basis, in the form of “background noise”. The background noise becomes markedly less during the eclipse, indicating that the variation from one minute to the next, as a result of the eclipse, supercedes the background noise, which one can assume to be still present during the eclipse. An interesting zero-point in OSD is reached during the middle of the eclipse (12:52 UT). The zero point is surrounded by two local maxima.

Figure 5.9 depicts DSGL2 (global irradiance) and associated OSD. Figure 5.9 shows similarities with Figure 5.8: The same OSD background noise, but slightly larger in

magnitude, but also suppressed during the eclipse, for the same reason as DSDIR. The maximum daily DSGL2 is less than DSDIR, and the DSGL2 curve is also "flatter".

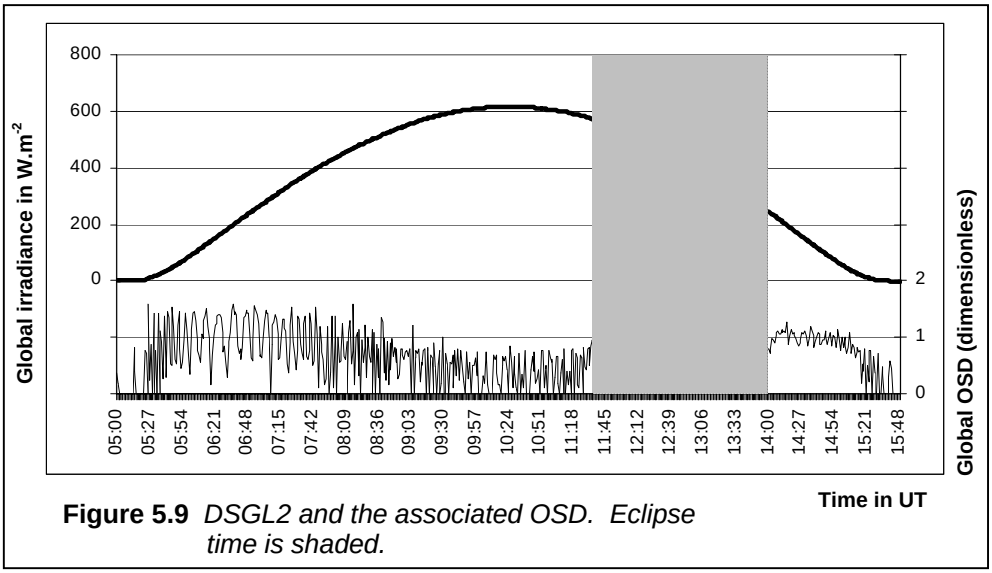

Figure 5.9 *DSGL2 and the associated OSD. Eclipse time is shaded.*

Figure 5.10 depicts DSDFS (diffuse irradiance) and associated OSD.

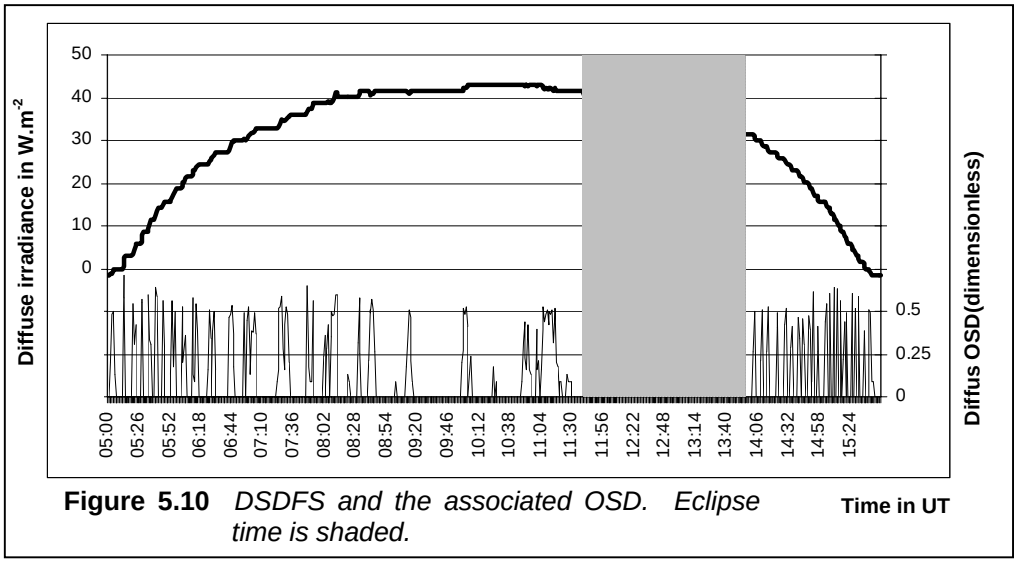

Figure 5.10 *DSDFS and the associated OSD. Eclipse time is shaded.*

In Figure 5.10, the magnitude of the numbers is less than in Figure 5.8 or Figure 5.9. Therefore, small amounts of background noise will feature as relatively larger numbers. The presence of the solar eclipse is clearly marked in the DSDFS time-series, and a small variation of OSD during the middle of the eclipse. Keep in mind that diffuse radiation is in general a more conservative parameter as far as variations due to changing atmospheric conditions are concerned. The attention is now focused on DSGL1 (global irradiance calculated using DSDIR and DSDFS) and DSGL2 (global irradiance directly measured using an unshaded pyranometer).

For any solar zenith angle Z at time instant t, DSGL1 is defined (Gilgen *et al.*, 1995) as:

$$DSGL1(t) = DSDFS(t) + DSDIR(t).\cos Z \qquad (5.4)$$

Figure 5.11 shows a time-series of the absolute difference DSGL2–DSGL1 and the ratio DSGL2/DSGL1 for eclipse day, 21 June 2001. Eclipse time is shaded.

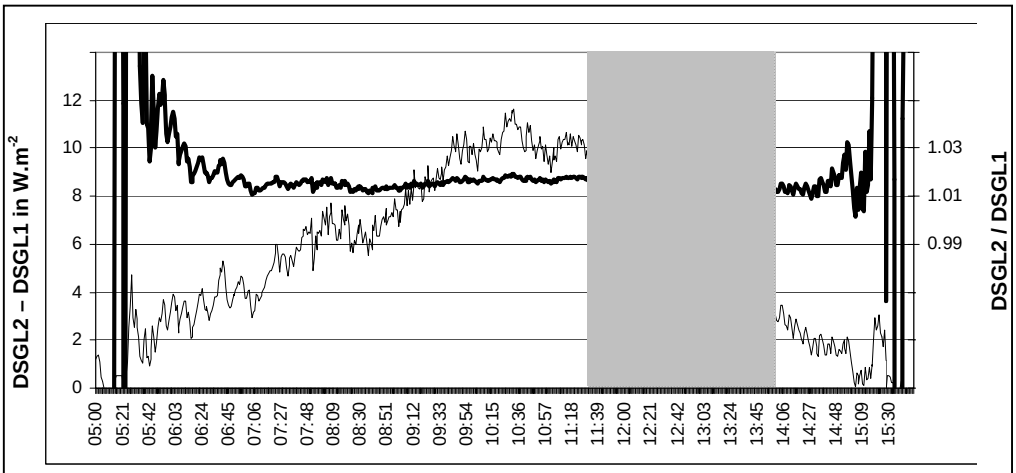

Figure 5.11 *Time-series of DSGL2–DSGL1 (thin line) and DSGL2/DSGL1 (thick line). Eclipse time is shaded.*

From Figure 5.11 it is evident that DSGL2/DSGL1 is conservative with respect to the solar eclipse, since the eclipse (shaded area) has no visible influence on its time-series. To a lesser extent this is also true for (DSGL2-DSGL1). Disruptions in these specific time-series are the result of "shocks" where the different instruments measuring DSGL2, DSDIR and DSDFS recover at different rates to a passing cloud or the sun rising/setting. Evidence of this behaviour can be seen in Figure 5.11 roughly at 05:20 UT and 15:30 UT. During the eclipse, none of these shocks are visible. An explanation is, that the transition in intensity during the eclipse from one minute to the next was smooth enough, so that the instruments under consideration could adjust accordingly.

Using TOA radiation as normalization factor, definitions for K-plots (NREL, 1993) can be defined for the SW components, per datapoint, at time instant t and solar zenith angle Z:

- K_n = DSDIR(t) * cos$Z$ / TOA(t)
- K_t = DSGL2(t) / TOA(t)
- K_d = DSDFS(t) / TOA(t)

The time-series for K_n , K_t and K_d as well as $K_t - (K_n + K_d)$, are depicted for 21 June 2001 in Figure 5.12.

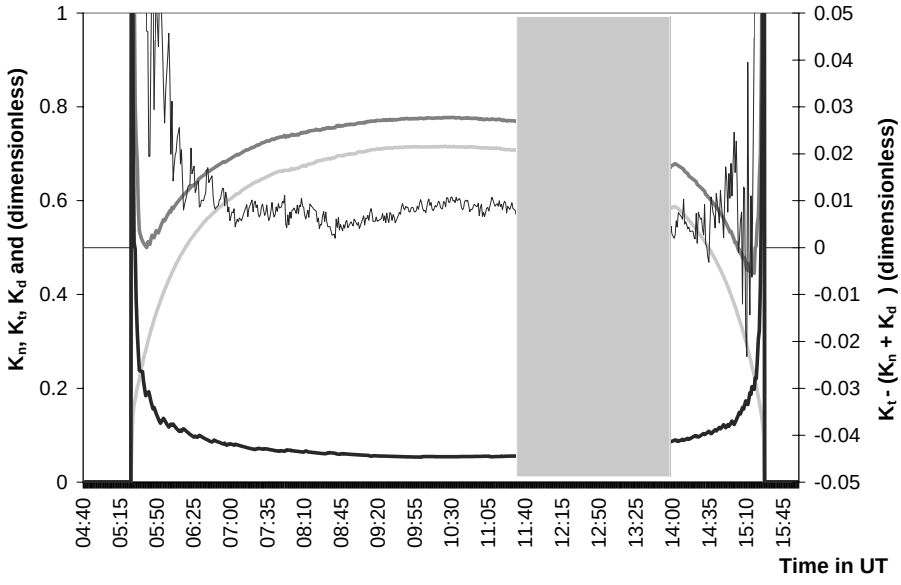

Figure 5.12 *Time-series for K_t (light grey), K_n (dark grey), K_d (thick black), and $K_t - (K_n + K_d)$. Eclipse time is shaded.*

Each of K_n , K_t and K_d shows the eclipse presence in a clear indentation, the latter less distinct, . The slight "noise" in $(K_t - (K_n + K_d))$ is insignificant, keeping in mind that the scale for $(K_t - (K_n + K_d))$ is ten times that of the other parameters in Figure 5.12.

Another NREL analysis method is a scatter diagram of K_n vs K_t, for Z < 80°, (Figure 5.13):

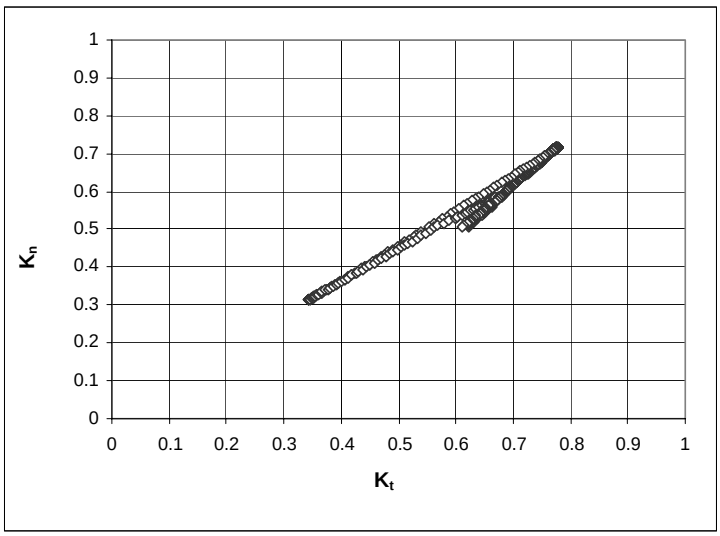

Figure 5.13 *Scatter diagram of K_n versus K_t for 21 June 2001*

No major deviations from a straight line are observed in Figure 5.13, which leads to the conclusion that K_n, and K_t are conservative for this data representation with respect to the eclipse on a clear day. The slight "hook" between K_t = 0.6 ; K_n,= 0.5 and K_t = 0.78 ; K_n,= 0.72 indicates the presence of the solar eclipse. See also Figure 5.32.

5.3.4.3 Focus on LW elements

In the pyrgeometer Equation 3.4, the significance of each of the three terms, as well as LWD, were discussed in Section 3.1.3.1. Figure 5.14 represents time-series of the three terms of Equation 3.4, as well as LWD.

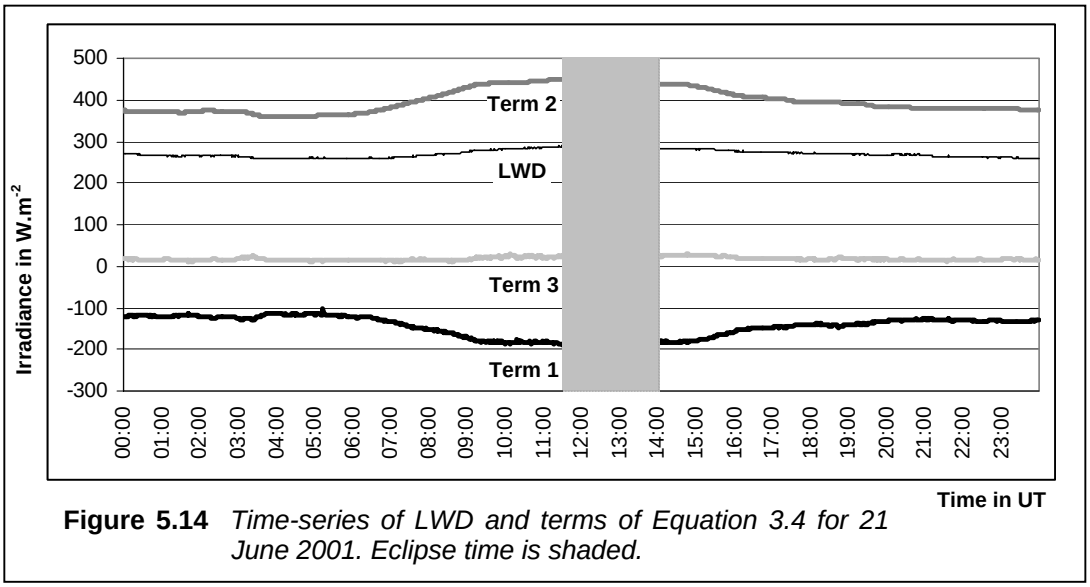

Figure 5.14 *Time-series of LWD and terms of Equation 3.4 for 21 June 2001. Eclipse time is shaded.*

Figure 5.14 resembles Figure 3.5 (a clear sky winter day). Term 2 is mirrored by Term 1 to a large extent and Term 3 is relatively small. This means that there is a small diurnal variation in LWD, in line with a clear sky winter day. All four time-series during the eclipse (shaded area in Figure 5.14) are not noticeably different from the areas outside the eclipse, therefore the eclipse of 21 June 2001 had no major effect on LWD or any of its terms. In Figure 5.15, only the LWD data for eclipse day was plotted, using a different scale. Eclipse time is shaded.

Note in Figure 5.15, that the LWD only increases about 1 hour after sunrise. The same delay is observed in the maximum LWD only reached about 1 hour after the maximum solar input had been reached (solar noon). The same effect is not so explicit after sunset. It should be kept in mind, that no clouds were present on that day, therefore only the effect of

the atmosphere is portrayed. The diurnal maximum LWD is 298 W.m^{-2} and the minimum is 251 W.m^{-2}. The eclipse (shaded area) however, does not seem to make a noticeable impact on LWD.

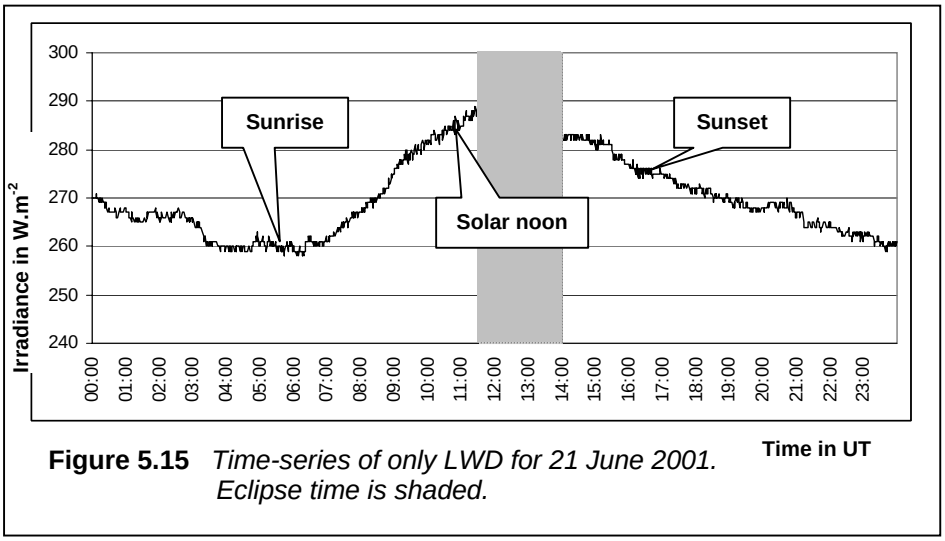

Figure 5.15 *Time-series of only LWD for 21 June 2001. Eclipse time is shaded.*

For a closer zoom on the behaviour of LWD during the eclipse, consider Figure 5.16.

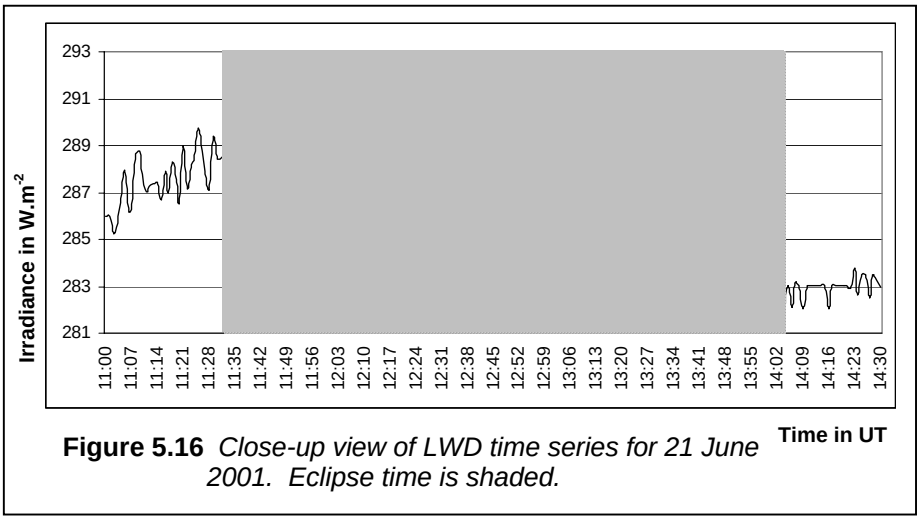

Figure 5.16 *Close-up view of LWD time series for 21 June 2001. Eclipse time is shaded.*

Keeping the delay of about 1 hour in mind, as observed in Figure 5.15, no noticeable changes in LWD as a result of the eclipse, are observed in Figure 5.16.

5.3.4.4 Non-radiation measurements

The 5-minute meteorological data for the eclipse day was extracted from the co-located AWS. Figure 5.17 depicts a time-series of the surface (Stevenson Screen) temperature and relative humidity, with eclipse time shaded. Keep in mind that relative humidity is dependent upon temperature, explaining the apparent mirror-images. If one inspects the eclipse period,

a steady drop in temperature of about 3°C, followed by a small rise of 1°C, is observed. This trend is inverted in the time-series of the relative humidity.

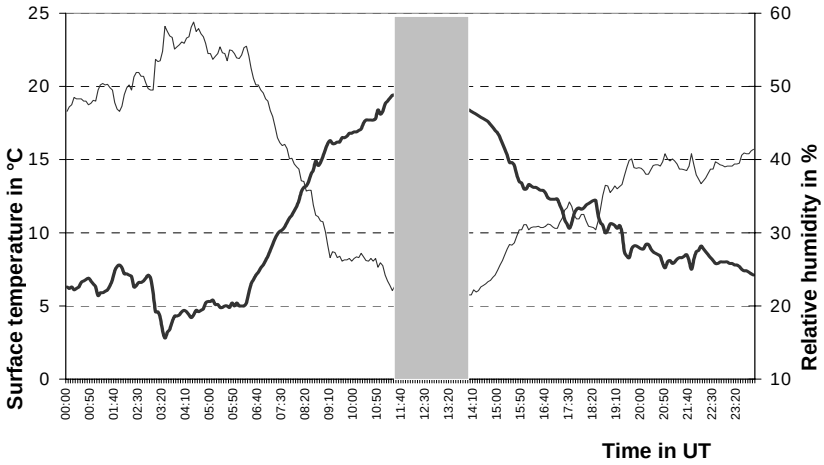

Figure 5.17 *Time-series of surface temperature (thick line) and relative humidity (thin line) for eclipse 2001. Eclipse time is shaded.*

In Figure 5.18, time-series of the wind speed and wind direction are presented, with eclipse time being shaded.

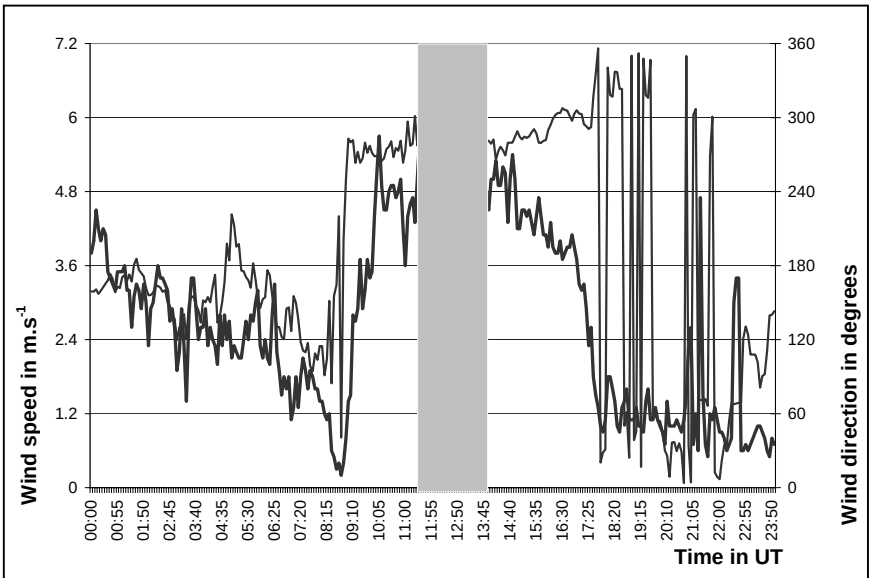

Figure 5.18 *Time-series of wind speed (think line) and wind direction (thin line) for elipse 2001. Eclipse time is shaded.*

The wind speed increased strongly in the mid-morning (at around 09:00 UT) and reached a maximum at about 12:00 UT. By this time the eclipse had already started. A sharp decrease in wind speed is observed for almost the rest of the eclipse, recovering after the end of the eclipse, and returning to calm at about 18:00 UT. During the eclipse, the wind direction remained roughly constant, viz., 270° (West).

5.4 ECLIPSE OF 4 DECEMBER 2002

5.4.1 General description

The path of totality for this total solar eclipse is illustrated in a global context in Figure 5.19 and in more detail in Figure 5.20, using an even closer up view in Figure 5.21.

In Figure 5.19, the path of totality is represented by the thick central line starting off the Angolan coast, crossing Southern Africa, curving upwards as it crosses the Southern Indian Ocean, entering the Australian Bight and ending in the Outback. The thinner lines parallel to this line respectively represent the 80%, 60%, 40%, 20% and 0% phases, respectively, of the partial eclipse. The dashed line orthogonal to the path of totality, stretching from a point in the central Indian Ocean directly south of India, towards Antarctica, represents the peak line. The intersection between this line and the path of totality west of Angola, is the eclipse peak at 39°27' S, 59°33' E, where the path of totality had its maximum width (90 km). For an observer at that point, the eclipse occurred at 07:31:11 UT, 102.5% of the solar disk was obscured, and totality would last 2'08".

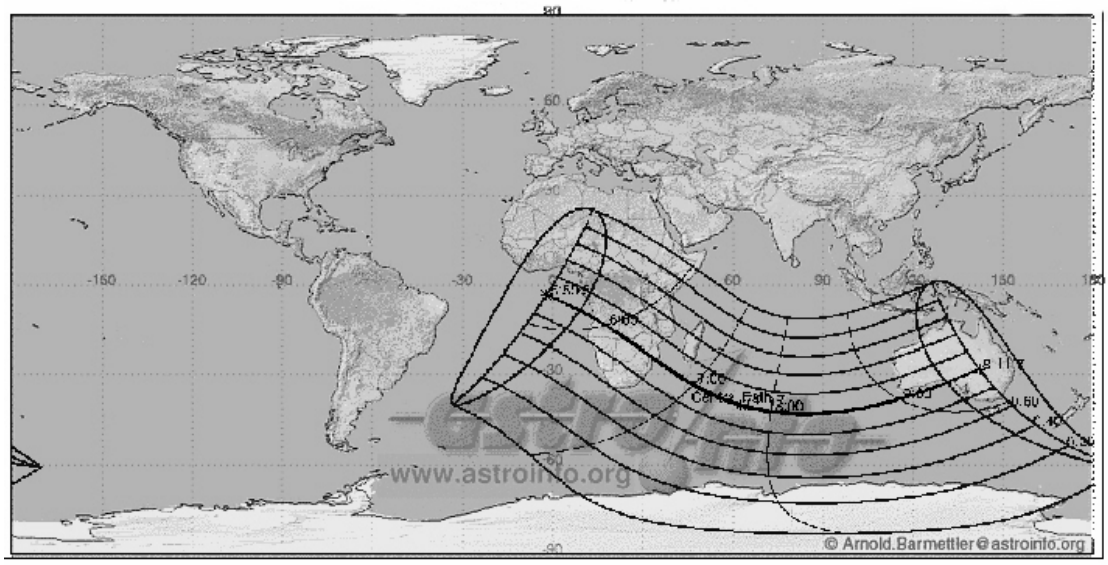

Figure 5.19 *Global orthographic projection of solar eclipse, 4 December 2002. Map by Arnold Barmettler at Astro-Info (www.astro-info.org)*

Note that totality path width, central duration and solar disk obscuration are significantly smaller than during the 2001 eclipse. Since South Africa is located to the west of the eclipse peak this time, the eclipse 2002 was observed in the waxing phase. The 2002 path of totality also intersected a 40 km narrow strip on the Angolan coast (Figure 5.20), where the

2001 eclipse crossed into Africa. This means, that totality was experienced here twice in less than a year and a half.

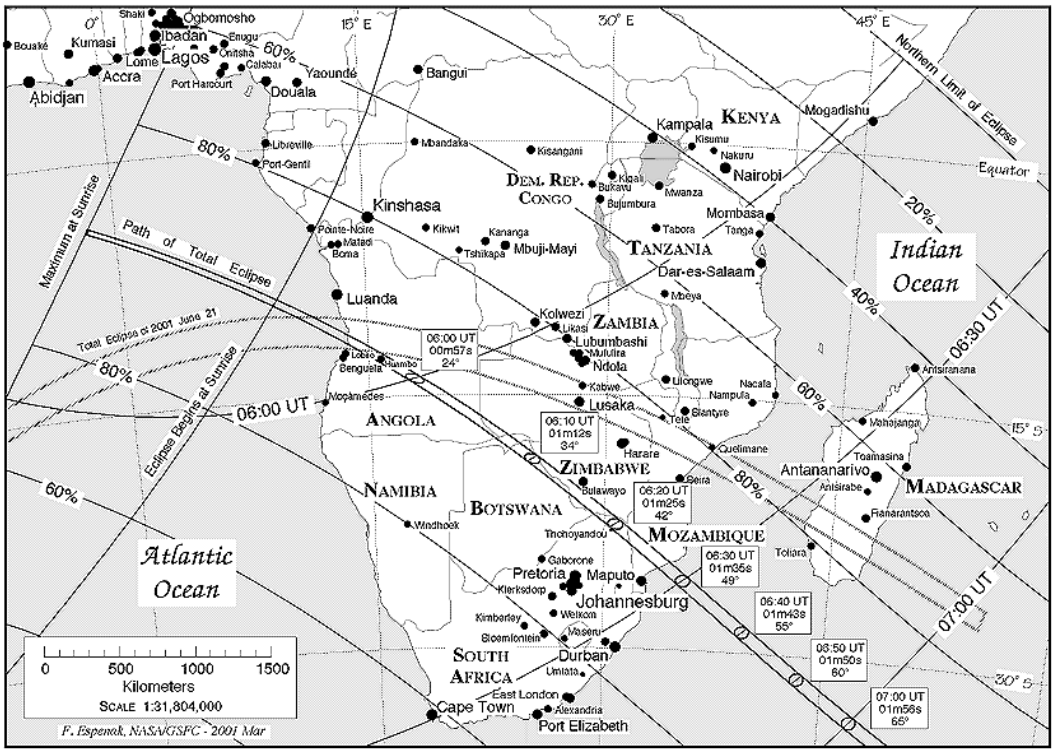

Figure 5.20 *Close-up view of the 2002 eclipse path through Africa, showing details of the partial phase. For reference, the totality path for 2001 is also shown. Map after Espenak and Anderson (2001). Times in UT.*

In Southern Africa (Figure 5.20), the path of totality crosses Southern Angola, the Caprivi Strip of Namibia, and runs almost along the Zimbabwe-Botswana border. It clips the northernmost part of the Limpopo Province of South Africa, before crossing southern Mozambique. Messina, South Africa, was the most populated point under the totality path.

5.4.2 Eclipse in South Africa

As mentioned before, this is the first time since 1 October 1940, that the path of totality of an eclipse covered South African soil. Phase magnitudes ranged between 60 % at Cape Town in the extreme south-west, and up to more than 100 % at Messina.

The close-up view in Figure 5.21 shows the path of totality, as well as the partial 80% and 60% phase lines. All times in UT.

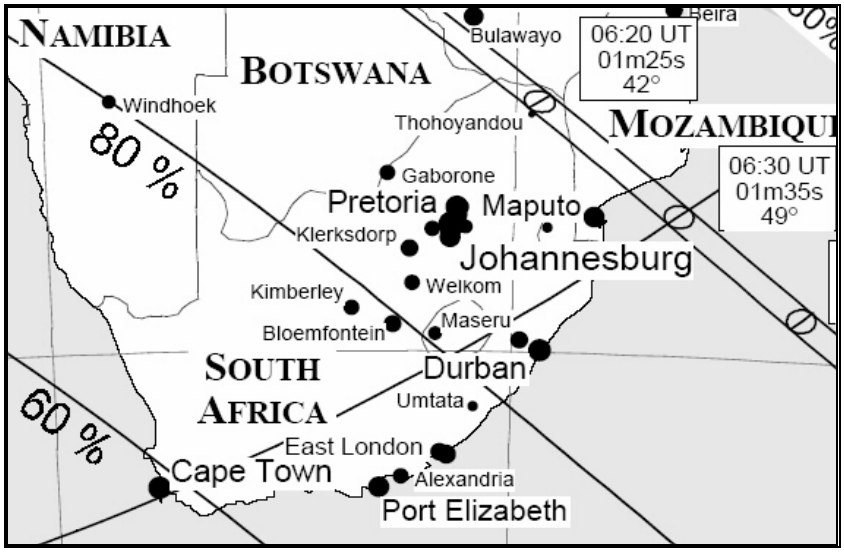

Figure 5.21 *Close-up view of totality path and partial phases for South Africa. Map after Espenak and Anderson (2001) and cropped.*

Table 5.4 shows local circumstances for a few major centra during the 2002 eclipse (Espenak and Anderson, 2001).

Table 5.4 *Local circumstances for major South African centra during the 2002 eclipse.*

Location	Latitude	Longitude	First contact	Last contact	Max eclipse	Magni-tude
Bloemfontein	29°12'S	026°07'E	07:22:30	09:39:10	08:26:53	79.3%
Cape Town	33°55'S	018°22'E	07:32:11	09:32:33	08:29:28	58.7%
Durban	29°55'S	030°56'E	07:24:42	09:48:26	08:32:18	85.1%
East London	33°00'S	027°55'E	07:29:59	09:47:03	08:34:46	74.1%
Johannesburg	26°15'S	028°00'E	07:17:35	09:38:10	08:23:33	88.5%
Kimberley	28°43'S	024°46'E	07:21:32	09:36:20	08:25:03	78.3%
Port Elizabeth	33°58'S	025°40'E	07:31:43	09:44:17	08:34:31	68.8%
Pretoria	25°45'S	028°10'E	07:16:46	09:37:41	08:22:51	89.9%

5.4.3 The weather

Since the eclipse occurred in mid-summer, the typical summer synoptic weather pattern for South Africa can be expected, which comprises surface and upper-air troughs over the interior joining the Inter-tropical Convergence Zone (ITCZ). In such a situation, tropical moist air is circulated over the interior, causing thundershowers associated with the uplift by virtue

of upper-air troughs and heat convection. Around the coast, high-pressure systems advect cool maritime air, adding orographic precipitation on the wind-side of high-lying areas. The presence of quasi-stationary high-pressure systems, one to the west (Atlantic Ocean) and another to the east (Indian Ocean) causes frontal systems to pass well south (more than 40° South) so that cold fronts do not frequently sweep the country in summer time.

The weather leading to eclipse day is described in terms of a series of 12:00 UT surface synoptic maps (SAWS, 2002).

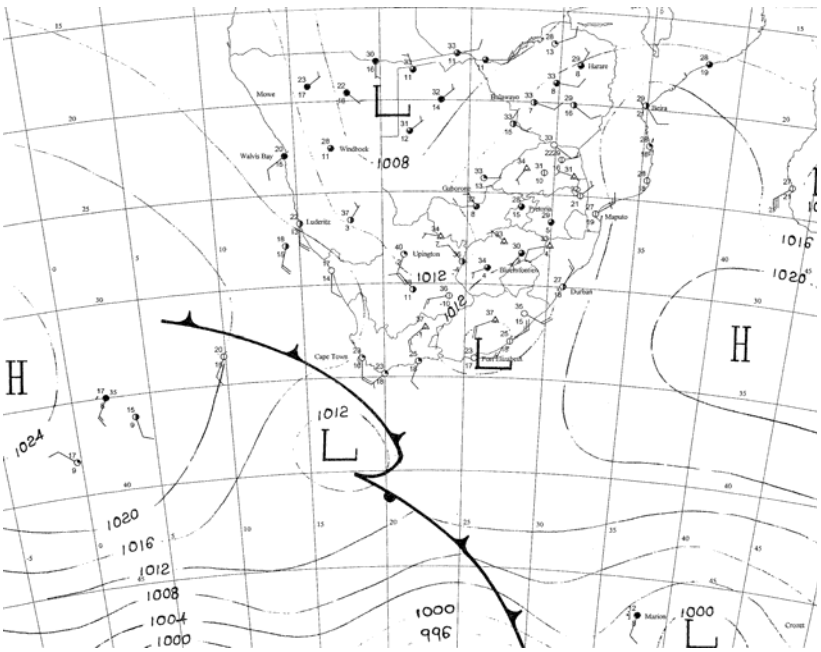

Figure 5.22 *Synoptic conditions at 12:00 UT on 1 December 2002 - three days before eclipse day (SAWS, 2002)*

On 1 December 2002 (Figure 5.22), three days prior to eclipse day, a surface trough is present over the western interior, feeding moist tropical air southwards, resulting in the development of isolated thundershowers over the provinces of North-West, Northern Free State, Gauteng and Mpumalanga. A cold front approaches the south-western Cape. Very hot conditions prevailed in the northern parts of the North Cape (Upington measuring 40°C).

Two days before eclipse day, 2 December 2002, (Figure 5.23), the interior surface trough was well-developed. The influx of moist, tropical air to the east of the trough-axis, brought partly cloudy to cloudy conditions with scattered thundershowers over the Northern and Eastern Cape, as well as isolated thundershowers over the North-West and in places over the Free State, Gauteng, Kwa-Zulu Natal and the Western Cape in lieu of what can be a closed separated cell of low pressure over the Karoo. Over the central interior, the conditions are ideal for the presence of an upper-air trough. The cold front passed to the far

south in the presence of the strong quasi-stationary high-pressure systems respectively in the Atlantic Ocean and the Indian Ocean, respectively.

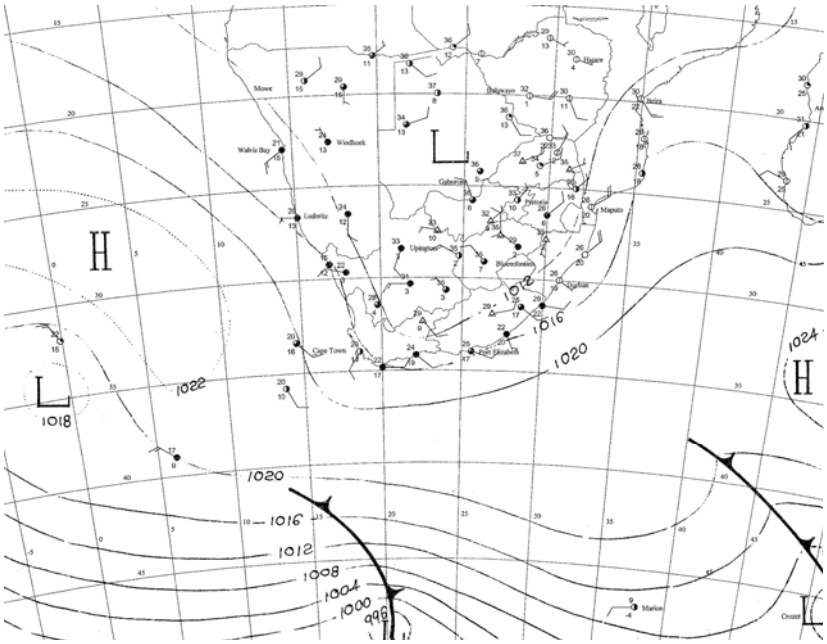

Figure 5.23 *Synoptic conditions at 12:00 UT on 2 December 2002 - two days before eclipse day (SAWS, 2002)*

On the following day, 3 December 2002, eclipse eve (Figure 5.24), the interior surface trough was still present and deepening, with an upper-air trough to the west of the surface trough.

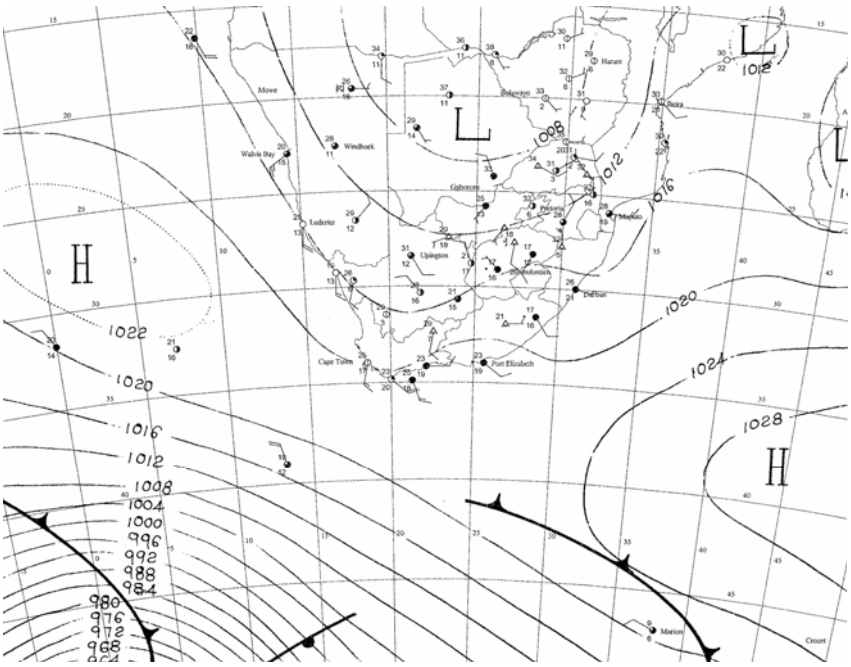

Figure 5.24 *Synoptic conditions at 12:00 UT on 3 December 2002 – one day before eclipse day (SAWS, 2002)*

The advected tropical air continued to bring widespread scattered thundershowers to the east of the trough-axis (parts of the Free State, North West, Eastern and Northern Cape and Kwa-Zulu Natal), including isolated thundershowers over Mpumalanga (SAWS, 2002).

On eclipse day, 4 December 2002, the meteorological scene was dominated by the interior surface trough, still deepening (Figure 5.25). Along the perimeter of the Indian Ocean High, a well- developed circulation was established, advecting moist air towards the eastern half of the country, aided by an influx of maritime air from the Mozambiquean channel. This caused overcast to partly cloudy conditions extending as far south as the central Free State and Lesotho. This was also accompanied by light rain in places, and rainfall totals of 1 to 3 mm were reported in those areas (SAWS, 2002).

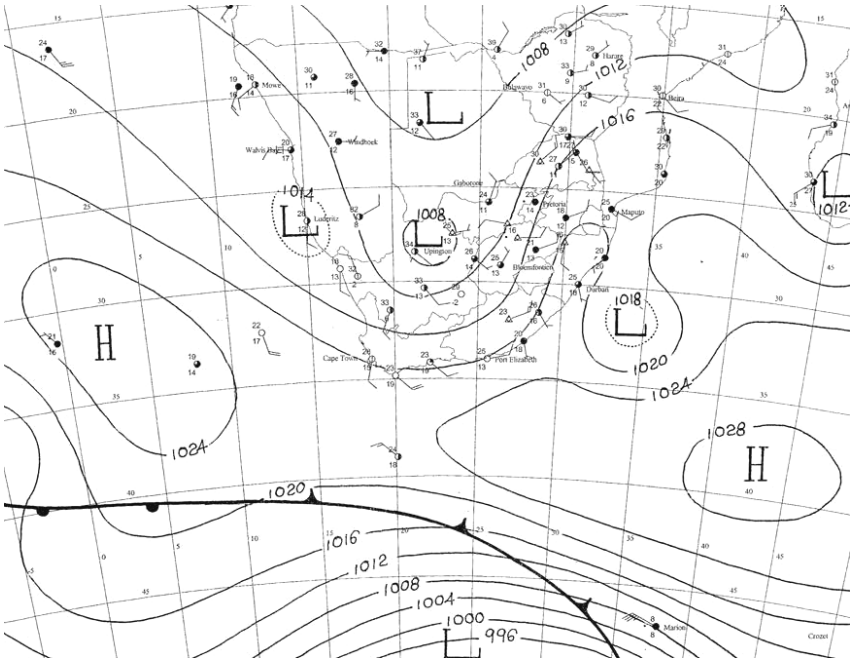

Figure 5.25 *Synoptic conditions at 12:00 UT on 04 December 2002 – eclipse day (SAWS, 2002)*

However, a well- defined low pressure system south-east of Durban, caused the axis of the surface and upper-air trough over the interior of the country to bend south-eastwards. This shifted the overcast to partly cloudy conditions eastwards, allowing the sky southwest of Bloemfontein to clear. De Aar BSRN station was in this region and hence experienced perfectly clear skies for the entire day, just like during the 2001 eclipse.

5.4.4 The BSRN measurements

Similar to the 2001 eclipse, a pristine set of SW measurements could again be performed at De Aar, by virtue of a cloud-free day. Figure 5.26 features the SW components together with TOA radiation, for eclipse day, 4 December 2002.

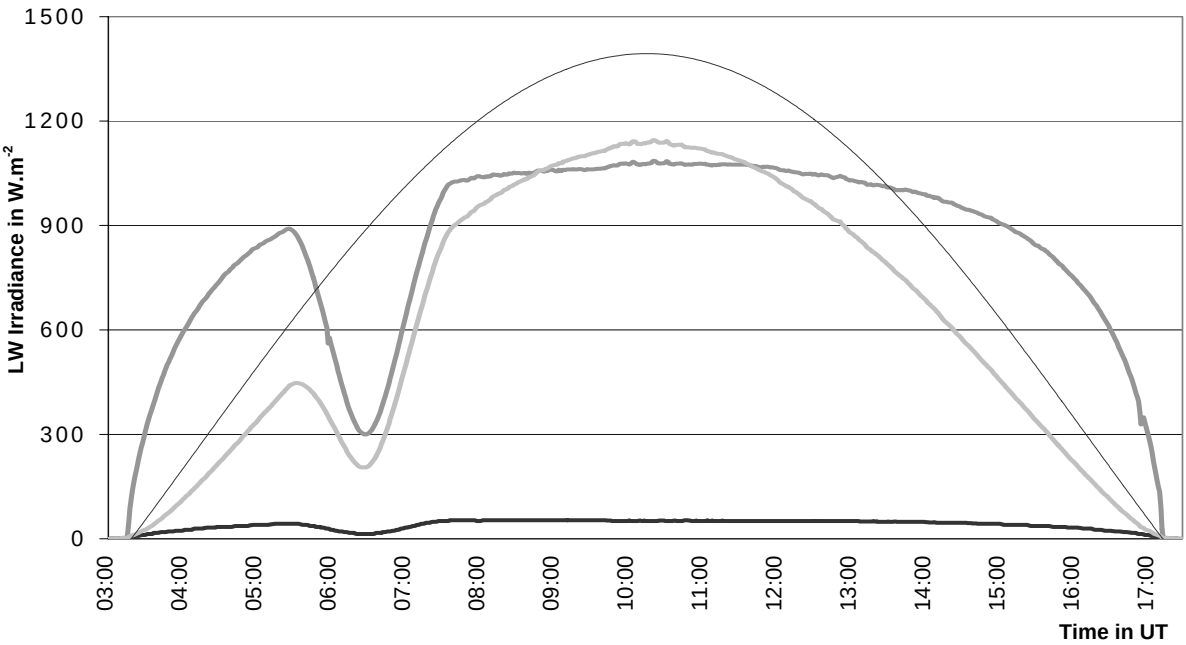

Figure 5.26 *SW radiation elements for eclipse 2002: Time-series of datapoints for DSGL2 (light grey), DSDIR (dark grey), DSDFS (black) and TOA radiation (thin black line)*

From Figure 5.26 it is clear, that the effect of the eclipse, and only the eclipse, appears in the time-series of DSDIR and DSGL2. The DSDFS shows the clear effect of an extraterrestrial object (moon) occulting the sun since an object in the atmosphere would have increased DSDFS and decreased the DSDIR.

5.4.4.1 Radiation loss due to eclipse

The amount of solar radiation loss on 4 December 2002 is calculated using the basic forms of Equations 5.2 and 5.3, adapted for sunrise (03:14 UT), solar transit (10:14 UT) and sunset (17:15 UT).

$$R = \sum_{i=03:14}^{i=17:15} E_i \qquad (5.5)$$

$$R_0 = \sum_{i=10:14}^{i=17:14} W(I_i + I_{i+1}) \qquad (5.6)$$

Using Equations 5.5 and 5.6 with datapoints for 4 December 2002:

R_0(Global) = 32537 kJ.m^{-2} ; R(Global) = 30513 kJ.m^{-2}

R_0(Direct) = 43292 kJ.m^{-2} ; R(Direct) = 40391 kJ.m^{-2}

R_0(Diffuse) = 2024 kJ.m^{-2} ; R(Diffuse) = 2121 kJ.m^{-2}

Therefore, radiation loss due to the 2002 eclipse amounts to:

Global : 2024 kJ.m^{-2} (6.22%)
Direct : 2901 kJ.m^{-2} (6.70%)
Diffuse : 97 kJ.m^{-2} (4.56%)

The radiation losses of the 2001 and 2002 eclipses are now compared in Table 5.5. Although solar disk obscuration was more in 2002 (73.1% in 2002 versus 60.7% in 2001), the day was also longer (14 hours and 1 minute in 2002 versus 10 hours and 10 minutes in 2001). Therefore, although the actual radiation loss in 2002 is more in absolute terms in 2002, it is smaller in relative terms as a result of a longer day. Global and direct radiation loss percentages are comparable for both eclipses, unlike the diffuse, which is considerably less in absolute terms.

Table 5.5 *Comparison of radiation losses for the two eclipses*

Eclipse	2001		2002	
	kJ.m^{-2}	%	kJ.m^{-2}	%
Global	1063	7.78	2024	6.22
Direct	2243	7.62	2901	6.70
Diffuse	101	8.34	97	4.56

5.4.4.2 Focus on SW elements

Datapoints of individual SW elements are now analyzed together with the corresponding OSD for eclipse day, 4 December 2002.

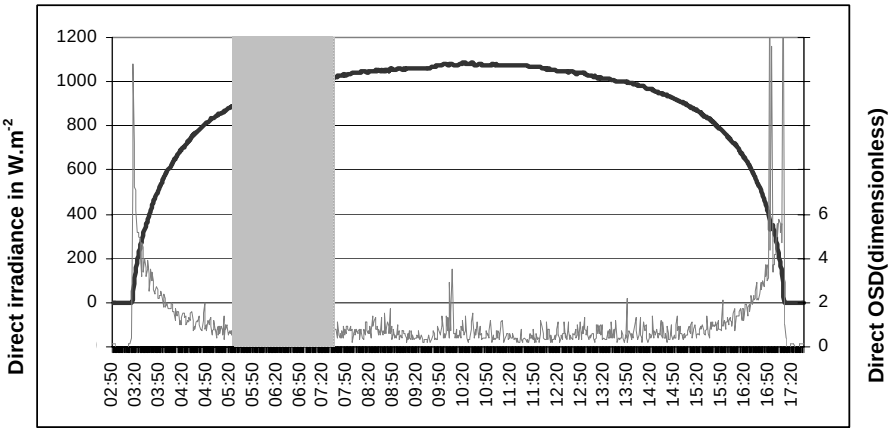

Figure 5.27 *DSDIR and the associated OSD. Eclipse time is shaded.*

The corresponding analysis of Figure 5.27 is shown in Figure 5.8 for the 2001 eclipse. The same level of background noise in OSD is experienced, except for a slight disturbance at about 10:10 UT. Put in context of the OSD values during the eclipse, it is relatively small and one can assume, that the same degree of sky clearness existed as during the 2001 eclipse.

The OSD values during the eclipse resemble the 2001 eclipse (Figure 5.8) with a zero point in the middle of the eclipse at 06:27 UT, surrounded by two local maxima, denoting a sharp change in DSDIR superceding the background noise which one can assume to be present. The same OSD anomalies for DSDIR during sunrise and sunset are also present during the 2002 eclipse. Figure 5.28 depicts DSGL2 for the 2002 eclipse together with the associated OSD.

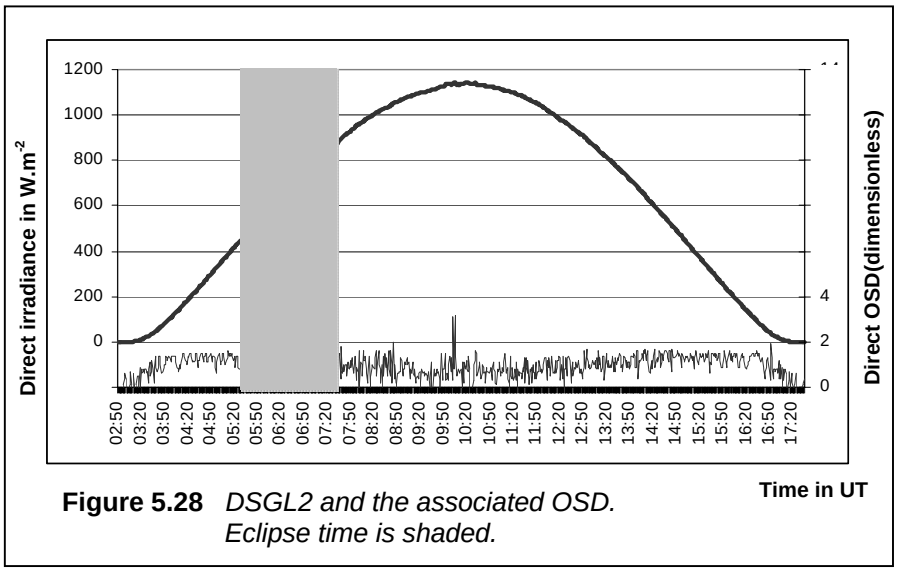

Figure 5.28 *DSGL2 and the associated OSD. Eclipse time is shaded.*

Figure 5.28 resembles Figure 5.10 (the corresponding graph of eclipse 2001). A distinct disturbance in OSD occurs at about 10:10 UT, but otherwise the level of background noise is comparable to that of the 2001 eclipse. During the eclipse, a zero-level OSD is experienced in the middle of the eclipse (06:28 UT), surrounded by two local maxima, the latter being larger in magnitude than the former, since the eclipse occurs as the sun is rising, and the change from one minute to the next is more significant when the sun is further from the horizon.

Figure 5.29 depicts DSDFS and the associated OSD. Eclipse time is shaded. The corresponding graph for eclipse 2001 is Figure 5.10, which also resembles Figure 5.29 to a large extent. Although the background noise in OSD is larger for the 2002 eclipse than the 2001 eclipse, the same distinct lower OSD values are present in the middle of the eclipse, surrounded by larger numbers for OSD.

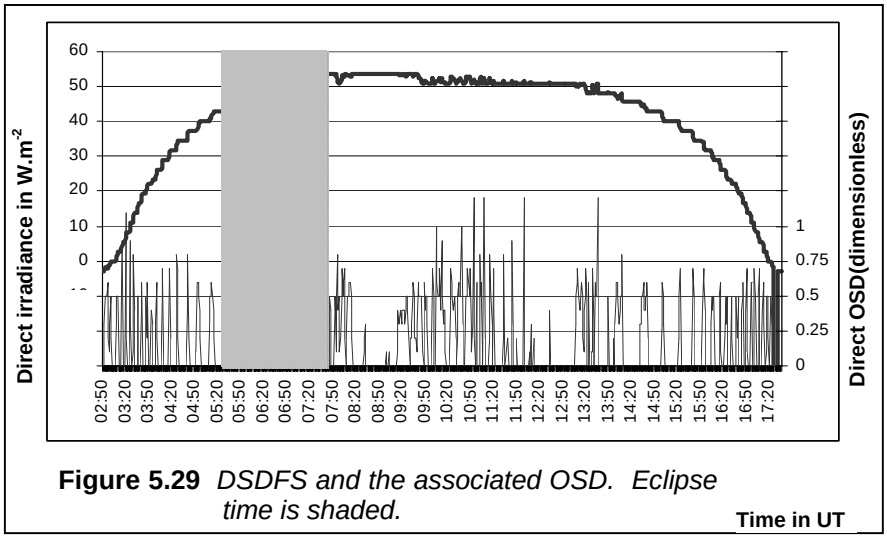

Figure 5.29 *DSDFS and the associated OSD. Eclipse time is shaded.*

In summary, the SW components and associated OSD values show similar features between the 2001 and 2002 eclipses. The background noise values of OSD are similar, which leads to the conclusion that the sky was equally clear on both days.

Next, the focus is placed on the relationship between DSGL1 and DSGL2. Figure 5.30 is a time-series of the ratio DSGL2 / DSGL1 as well as the absolute difference DSGL2 - DSGL1.

The graph corresponding with Figure 5.30 for the eclipse 2001 is Figure 5.11. The comparison shows that the relationship between DSGL2 and DSGL1 is very conservative with respect to the solar eclipse. In Figure 5.30, a clear disruption of DSGL2/DSGL1 can be

observed during eclipse 2002, which is not present outside the eclipse. An indentation in (DSGL2-DSGL1) is also present during the eclipse.

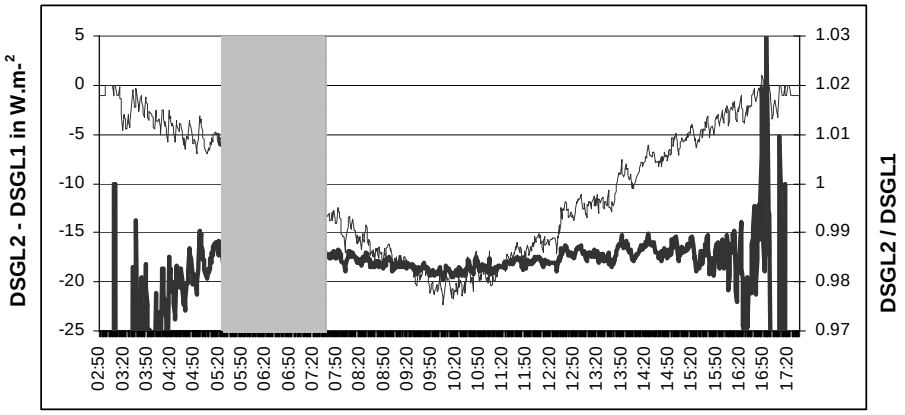

Figure 5.30 *Time-series of DSGL1 - DSGL2 (thin line) and DSGL2/DSGL1 (thick line). Eclipse time is shaded.*

K-plots are presented in Figures 5.31 and 5.32, similar to Figures 5.12 and 5.13 for the 2001 eclipse.

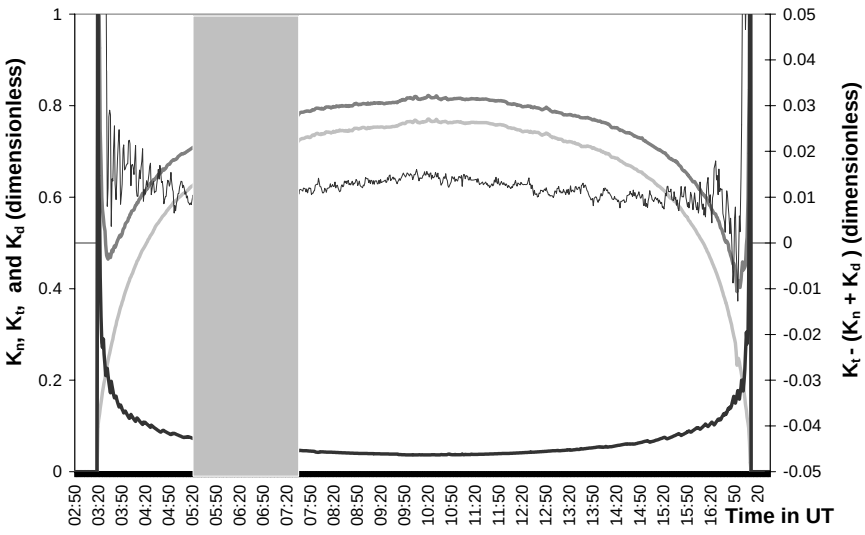

Figure 5.31 *Time-series for K_t (light grey), K_n (dark grey), K_d (thick black), and K_t – (K_n + K_d) (thin black). Eclipse time is shaded.*

In Figure 5.31, each time-series marks the eclipse with a clear indentation. Unlike the 2001 eclipse, K_t – (K_n + K_d) now shows a clear indentation, indicating that this parameter is less conservative for the 2002 eclipse than the 2001 eclipse.

The K_n versus K_t scatter diagram (Figure 5.32) shows an indication between K_t = 0.58 ; K_n = 0.45 and K_t = 0.83 ; K_n = 0.78 that a disturbance took place. This feature is also present in Figure 5.13 (eclipse 2001) but not as prominent. Keep in mind that Figure 5.32 contains more datapoints than Figure 5.13 (2001 eclipse) since the 2002 eclipse occurred on a summer (longer) day.

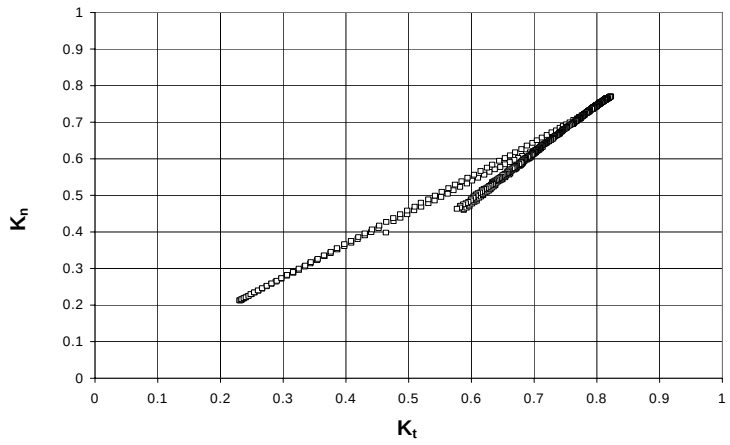

Figure 5.32 *Scatter diagram of K_n versus K_t for 4 December 2002.*

5.4.4.3 Focus on LW elements

In Section 5.3.4.3, time-series of the three terms of Equation 3.4, as well as LWD, were discussed. In this Section, a similar discussion for the 2002 eclipse is conducted. Keep in mind that eclipse day 2002 was a clear summer day. Therefore, it is expected to resemble Figure 3.7 and the associated description.

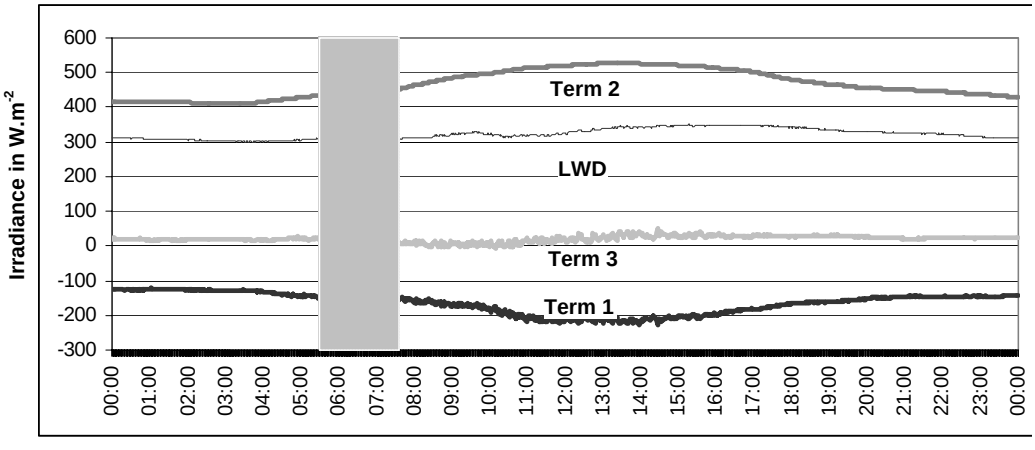

Figure 5.33 *Time-series of LWD and terms of Equation 3.4 for 4 December 2002. Eclipse time is shaded.*

Figure 5.33 shows time-series of LWD, as well as the three terms of Equation 3.4 (the pyrgeometer equation). Term 2 is mirrored to a large extent by Term 1 and Term 3 is relatively small. This leads to LWD having a small diurnal variation. Like in Figure 5.14 (the 2001 eclipse), all time-series in the shaded area (during eclipse) are not noticeably different from those outside the eclipse, therefore eclipse 2002 also had no noticeable effect on LWD.

In Figure 5.34, only the LWD data for eclipse 2002 was plotted, using a different scale. Eclipse time is shaded. Figure 5.34 does not show the same smooth diurnal pattern that Figure 5.15 exhibited. Roughly 1 hour after sunrise, LWD increases, just like in Figure 5.15. The lack of an effect of sunset on LWD in Figure 5.34 is the same as in Figure 5.15. However, no effect is seen after solar noon. The diurnal maximum LWD is 351 $W.m^{-2}$ and the minimum is 300 $W.m^{-2}$.

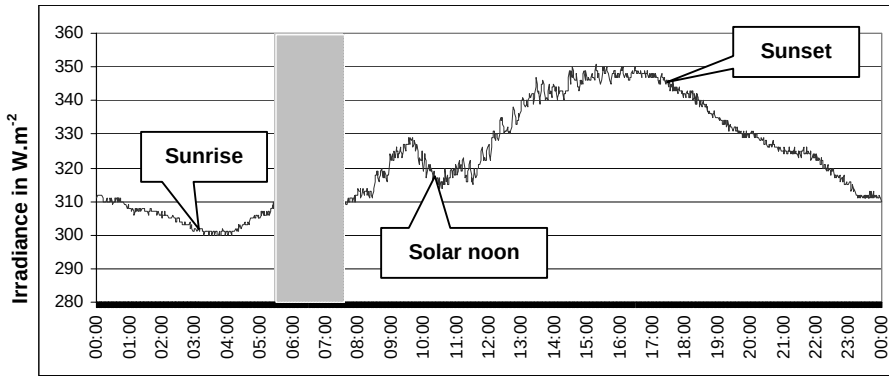

Figure 5.34 *Time-series of only LWD, for 4 December 2002. Eclipse time is shaded.*

The eclipse (shaded area) makes a small impact on LWD, which is explored in Figure 5.35.

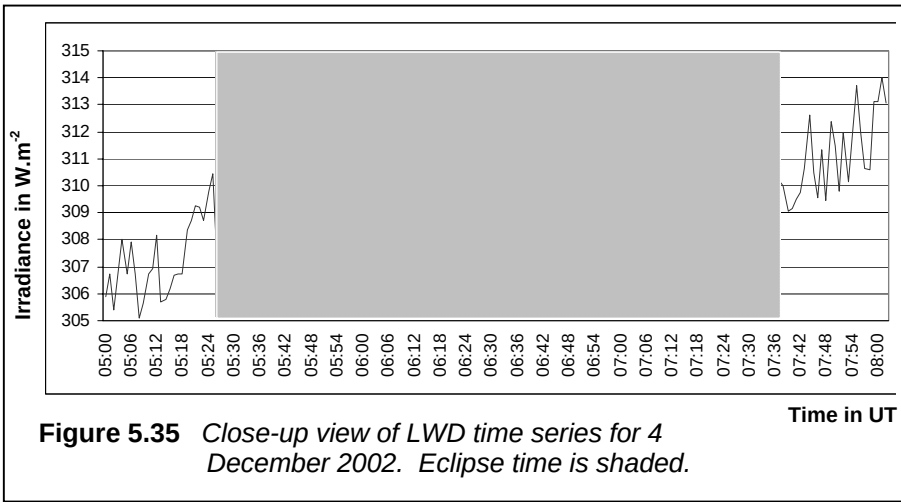

Figure 5.35 *Close-up view of LWD time series for 4 December 2002. Eclipse time is shaded.*

In Figure 5.35, a clear change in LWD can be observed during the eclipse, which could be attributed to the eclipse. At about 06:07 UT, 40 minutes after first contact (start of eclipse), LWD starts decreasing until roughly 07:12 UT, 45 minutes after maximum eclipse. It should be remembered, that these times represent an early morning, therefore LWD is expected to be in a rising trend. This explicit pattern in LWD during the eclipse, is not displayed in the corresponding time-series of eclipse 2002 (Figure 5.16).

5.4.4.4 Non-radiation measurements

Time-series of 5-minute surface (Stevenson Screen) temperature and relative humidity from the co-located AWS are shown in Figure 5.36, indicating definite features of the eclipse.

The steady temperature rise of about 2°C per hour since sunrise (03:15 UT), is halted by the eclipse, and even turned around (start of eclipse: 17.9°C; minimum in middle of eclipse: 17.5°C). This steady rise continues again after the eclipse effect starts to wane. A similar, mirrored feature, is expressed in the time-series of relative humidity, since it is inversely proportional to temperature within a given air mass.

Figure 5.36 *Time-series of surface temperature (thick line) and relative humidity (thin line) for eclipse 2002. Eclipse time is shaded.*

Figure 5.37 displays is a time-series of the AWS wind speed and direction. No significant change in wind speed or direction during or as a result of the eclipse.

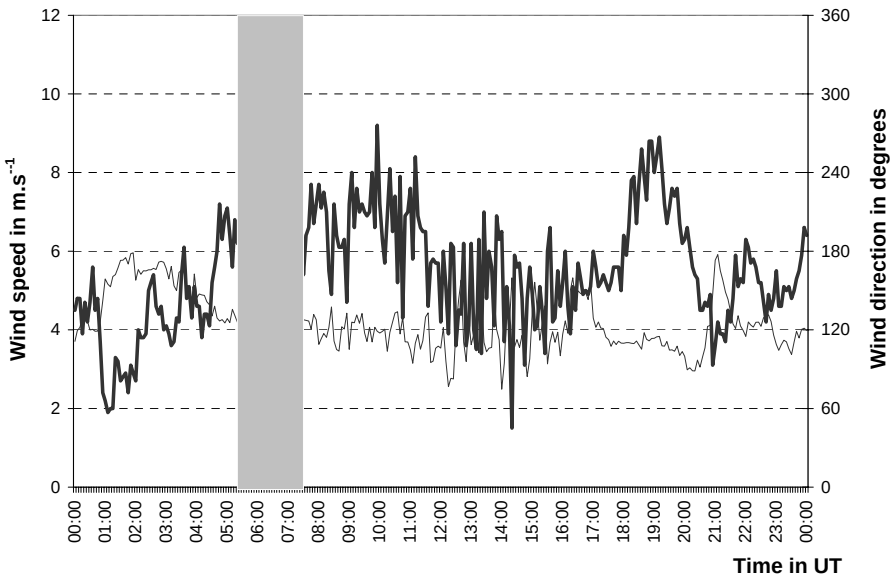

Figure 5.37 *Time-series of wind speed (thick line) and wind direction (thin line) for eclipse 2002. Time of eclipse shaded.*

5.5 CONCLUSION

The BSRN site was well placed to take maximum advantage of the clear sky conditions on both the 2001 and 2002 eclipse days, making pristine radiation measurements. This enabled the performance of analysis, as well as comparisons between the two eclipses, which were both experienced as partial eclipses at the De Aar BSRN station. There were interesting similarities, as well as differences observed for the two eclipses:

- The 2001 eclipse occurred in winter (in fact on the same day as the SH winter solstice), while the 2002 eclipse occurred in the summer (less than 3 weeks before the SH summer solstice).

- The 2001 eclipse occurred late in the afternoon, while the 2002 eclipse occurred early in the morning.

- Solar disk obscuration was comparable for both events (61% in 2001 and 73% for 2002).

- Solar elevation was comparable for both events (26° in 2001 and 40° in 2002).

- The absolute loss of radiation due to the eclipse was smaller for the 2001 eclipse than for the 2002 eclipse, but larger in relative terms.

- Background noise on OSD was comparable for both eclipses, confirming that the sky was equally clear on both days.

- Some of the expected signatures of radiation and meteorological time-series are displayed more explicitly for one eclipse than another.

CHAPTER 6

CONCLUSION AND RECOMMENDATIONS

The De Aar BSRN system became operational on 29 July 1999. Since that day, through the sustained operational activities of the system, a continuous learning process towards establishment a perfect operational system was initiated, some of which precipitated in this dissertation. Although the system can now be regarded as fully operational, it is certainly not perfect, and the recommendations verbalised in this final chapter should be seen as fruits of the development process and honest pointers for a better way forward. It is the wish of the author that they be considered for implementation as capacity (resources and time) permits.

6.1 MAIN ACHIEVEMENTS

The South African BSRN station at De Aar, number 40 in the global network, was established in 1999 using WMO-donated instrumentation and the minimum funding from local sources. A combination of local expertise, as well as generous help from abroad in the form of ideas, encouragement and fragments of program code, aided in the process.

The station had several setbacks. The most severe setbacks were caused by lightning strikes that disabled the on-site computer on three occasions, i.e., February 2000, September 2001 and December 2002. Additionally, numerous power failures occurred, the majority of which could be filled in by the Uninterrupted Power Supply (UPS) without disruption of the tracker and ventilators. There were, however, a number of power failures that exhausted the UPS and left the system stranded for several hours, resulting in the rejection of all data for that period, except global (DSGL2) radiation.

Notwithstanding these setbacks, a relatively small number of data points overall were lost, as illustrated in Figure 6.1. This can be attributed mainly to timely reporting of system failures by site personnel, but also to a good design of data storage capacity in the logger as discussed in Section 3.1.6. This design allows roughly one week's data to be accumulated in the logger before being overwritten by fresher data. The time window of one week allows for timely execution of plans to repair the system and, since station establishment, resulted

in at least one occasion when not a single datapoint was lost, despite a computer failure of almost a full week.

Apart from lightning strikes and power failures, the other reasons for data loss are all "natural", viz., due to maintenance. This includes daily and monthly radiometer maintenance and the six-monthly pyrheliometer calibration and global/diffuse exchange. Datapoints lost in this way, are the trade-off for good data for the rest of the time and is, in fact, a small price to pay.

The number of missing datapoints for the three-year evaluation period of Section 4.3 (June 2000 to May 2003) is shown in Figure 6.1 as a time-series graph of monthly percentage values.

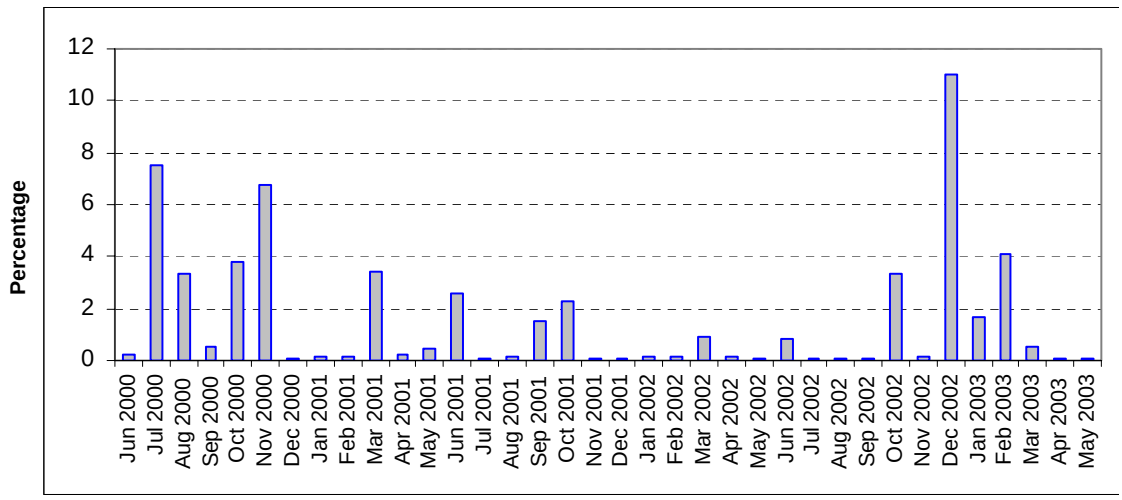

Figure 6.1 *Monthly percentage of missing data: June 2000 to May 2003*

December 2002 is the month having the most missing datapoints (11.0%), followed by July 2000 and November 2000. All other months have 4% missing data or less. The high percentage of missing data in December 2002 results is due to the severe lightning strike and subsequent loss of LW data, as discussed in Section 4.3.1.4. All months have at least 23 missing datapoints (about 0.05% per month) due to daily cleaning of the radiometers resulting in the loss of at least one, but no more than three, minutes of data per cleaning session. The total number of missing datapoints for the 36 months between June 2000 and May 2003 is 31873, which translates to 2.02 % of all possible datapoints.

Currently, a full basic set of BSRN data is measured. Regular maintenance is carried out,

data management systems that were put in place, are fully functional, and datasets are cast in specific formats using in-house developed suitable Fortran programs. The monthly datasets are regularly submitted to the WRMC in Zürich, all of which were accepted and inserted in the international BSRN database at the time of writing this document.

The De Aar BSRN station gained international recognition in the BSRN network and to the author's knowledge, three international researchers were using the De Aar data.

6.2 THE WAY FORWARD

Regular reflection on any activity also includes meditation on achievements, the way forward and a contextualization between the two. The following questions need to be answered with regards to the De Aar BSRN station:

- Is the current system justifying its existence – viz., was the capital investment put to good use ?

- What are future scenarios in terms of its strategic positioning within SAWS, regionally, as well as internationally ?

6.2.1 Justifying its existence

The scientific plan of Chapter 2 and the system design of Chapter 3 are aimed towards enabling the South African BSRN station to fulfil its obligation towards the international BSRN community, and also towards the SAWS as a regional GAW observation site. The strategic international geographic positioning of the South African BSRN station as discussed in Section 1.2.1, the regular submission of data to the WRMC database and acceptance of the datasets, plus the expressed international research interest in the data, already justifies its existence.

6.2.2 Present and future role in SAWS

The BSRN project and associated activities are fully integrated in the GAW group within the SAWS. De Aar is regarded as a regional GAW station, along with only a handful of its kind in South Africa. The existence of the BSRN project has attracted additional international

attention to South Africa's GAW activities and in particular the only Southern African Global GAW station situated at Cape Point doing internationally renowned atmospheric trace-gas monitoring and research.

Continued operation of the De Aar BSRN station shall lead to fulfilling its long-term obligation towards the WMO, the international BSRN community, and also towards the SAWS justifying sustained capital investment.

6.2.3 NEPAD potential

The New Plan for African Development (NEPAD) initiated in 1998 by the South African Government has, as one of its goals, the initiation of sustained development of partnerships and sharing of expertise between African countries. The BSRN site currently has a radiometric system directly traceable to the WRR, and arguably the best of its kind in the SADC region.

The high-quality instrumentation at De Aar has the potential to be used for other applications besides radiation monitoring, like calibrating operational radiometers of other radiation-monitoring institutions, not only in South Africa, but also elsewhere in Africa. This could be performed in years between International Pyrheliometric (IPC) events which are held only every five years. The SAWS has, apart from the BSRN equipment, also a PMO-6 radiometer which is still the standard radiometric reference instrument, which participated in the last IPC event the SAWS attended. If such calibration services can be initiated and sustained, it has the potential to generate funds and foster more international recognition for the SAWS.

As a regional GAW Radiation Station, De Aar BSRN has potential to be the focal point for radiation in the SADC region. It can also be a cornerstone for further BSRN activities in Africa or the SADC region, should plans develop to establish a second Southern African BSRN station.

6.2.4 International potential

Naturally, the benefits of a national asset are more significant towards the hosting country, but the exploration of international potential for that national asset should never be

disregarded. One possibility for the South African BSRN station is its "twinning" with a similar site in another country, in a similar way that global GAW sites have "twinning" partners. This practice of "twinning partners" leads to the in-depth sharing of expertise and resources and creates unique partnership opportunities, that would not have been possible otherwise. The BSRN station produces data in this region so abundant in solar energy, that it can offer unique study opportunities to scientists and students alike, possibly from neighbouring countries or internationally.

Another international potential is the possibility of South Africa hosting a future BSRN workshop and conference (typically 80 delegates, held usually every two years). Such a workshop would attract a wealth of international attention and expertise towards the SAWS, and unlocks tourism potential for the hosting province and our country. Such an event would most likely be held in or around Cape Town, since the facilites at De Aar itself, would not be adequate to host a conference of this magnitude. The traditional site excursion during such an event can be the SAWS global GAW station at Cape Point, which is not a BSRN station, but is very likely to draw more international attention to the SAWS GAW activities.

6.3 RECOMMENDATIONS

One corollary flowing from sustained interaction with academic and practical material during the establishment of a dissertation, is the spontaneous identification of specific areas where improvements are needed. They are recommended here, grouped into three categories:

6.3.1 BSRN in general

1. The instatement of BSRN site audits either exclusive to BSRN or in partnership with related institutions, as discussed in Section 2.1.3.2, have the potential to add significant value to measurements. The added advantage of such audits would be, that other developing sites could be given correct guidance in measurement techniques, in order to take necessary and correct steps in recording useful data from day 1 of site establishment.

2. The WRMC database procedures, as discussed in Section 4.3 and highlighted in Section 4.3.2.4, can be refined, both theoretically and empirically, to be more site-specific and in such a way, render an honest and unbiased evaluation of data

recorded at a specific site. In a global network, this kind of refinement could be a step towards improvement of data evaluation.

6.3.2 Site improvement

The studies have identified the following shortcomings in the current operational system:

1. The exact times of tracker failures must be noted and reported as frequently and as accurately as possible. A non-operative tracker is difficult and sometimes impossible to identify in the recorded data alone, as discussed in Section 3.1.4.2. If no report of a stationary tracker is received, it can happen that data recorded when the tracker was stationary, is regarded as "good". Over and above regular inspection, one recommendation is an alarm device attracting attention to a standing tracker and/or a device logging tracker performance on a continuous basis.

2. The upgrading of the present passive tracker to an active tracker using a quadrant sensor, as discussed in Section 3.1.4.1, should be seriously considered. The majority of global/diffuse/direct mismatches, as analyzed in Section 4.3.3.4, can be attributed to the passive tracker drifting off track. The added advantage of a quadrant sensor is that its output, if correctly evaluated, can also be utilized to provide additional radiation data in the applicable spectral band, since the quadrant sensors have specific spectral characteristics.

3. More frequent inspection of the pyrheliometer sunspots should be undertaken, in order to identify and possibly quantify tracker drifts or consistent misalignments, should be undertaken until the tracker is upgraded to an active tracker. A practical solution suggested here, is sunspot inspections carried out on three different times of the day (middle of the morning, around solar noon and middle of the afternoon). The comparable solar zenith angle during the morning and afternoon inspections can best reveal tracker deviations as a result of time-offsets or misalignment towards solar declination. If there are days where clouds interfere with inspections, it should be carried out once it is observed that the sun casts a discernible shadow, regardless of the time of day.

4. Frequent checking of the pyranometer levels should be undertaken, since slight

skewness can lead to erroneous readings, as pointed out in Sections 4.2.3.2 and 4.3.2.1. Presently, the levels are checked on a monthly basis, but more frequent checking (weekly) and reporting, in order to timeously identify the causes of error, is recommended.

5. Further refinement and integration of current quality assurance procedures to resemble Section 4.2 is recommended. This can be executed on recorded data prior to WRMC submission, as an addition to the current Fortran programs. This can also include the development of site-customized quality assurance boundaries applicable specifically to South African conditions.

6. Thermal offsets of the thermopile instruments, as discussed in Section 3.1.2.3, must be addressed in a scientifically accountable way. At the moment all pyranometers are ventilated with devices designed by the manufacturers, in an attempt to make the thermal offset negligible. However, ventilator fans can stop without warning and the exact downtimes are often unknown to data collectors. A new strategy, comprising responsibly reporting fan failures and how to properly compensate for these errors, should be investigated. Possibly adopting and adapting the Australian model, as discussed in Section 3.1.2.3, is a consideration.

7. Tracker failures have a specific impact on LW radiation, as discussed in Section 3.1.4.2, specifically since the dome compensation term (term 3) of the LWD equation (Equation 3.4) becomes too large and therefore invalid when the dome is not shaded. Instead of simply rejecting LW data affected by tracker failures, a means of developing a more applicable dome constant can be investigated. If successful, the missing percentage of 1.3% for LWD data, as mentioned in Section 4.3.1.4, can be halved. However, a thorough assessment of the usefulness of this data must be performed before proceeding.

8. The measurement of upwelling LW and SW quantities from raised structures such as 10 - 30 m towers, should be seriously considered. If upwelling quantities are measured simultaneously with the basic downwelling quantities, an additional check and balance for the all involved quantities exists in both the LW and SW case as encountered in Sections 4.3.1.5, 4.3.2.2, 4.3.2.5, 4.3.2.6 and 4.3.3.2. Upwelling LW minus downwelling LW radiation can control pyrgeometer thermopile irradiance (Term 1 of Equation 3.4). In the case of upwelling

(reflected) SW, the ratio between reflected and downwelling SW irradiance equals surface albedo, which can add in the usefulness of the De Aar data, as ground-truthing of remote measurements, as well as a control of albedo measurements obtained by other means.

6.3.3 System upgrading

Since instrumentation is very expensive, especially in the South African context of a variable currency, the capital purchase of instruments is a long-term budget item. However, this should not be a reason for not considering upgrading. The following items are placed here on a wish list as possible upgrades, in order of priority in the opinion of the author:

1. The most important recommendation is upgrading the current passive solar tracker to an active tracker. Terminology: a passive tracker follows the sun "blindly", i.e., depends upon calculations of solar position and the operation of stepper motors to point an instrument or array of instruments continuously at the sun. If the tracker time is not regularly updated, the tracker drifts off, pointing is erroneous and stays that way until external rectifications can be done. An active tracker combines the infrastructure of passive tracking with an array of sensors providing "feedback" to the tracker stepper motors to point the tracker continuously at the sun. A significant percentage of erroneous or semi-erroneous measurements was a result of the tracker being passive.

2. Another important recommendation is to consider the introduction of some form of sun photometry. Data resulting from this type of measurement, provide insight into spectral characteristics of transmitted radiation and can largely aid in satellite applications and the validation of radiative transfer models. Furthermore, a form of spectral measurement yields valulable insight in the gaseous composition of the atmosphere and aerosol optical depth (AOD), especially as a function of time, season, land usage, and other activities, such as biomass burning. The AOD at a clean-air site such as De Aar, can also provide valuable insight referring to background air quality in a South African context and aid in the growing understanding of diffuse radiation, as discussed in Section 2.1.3.3. This is one area of expertise where global GAW activities and BSRN activities have areas of overlapping and potential for co-operation. The current BSRN solar tracker at De Aar can accommodate at least one more 35 mm tubular instrument, such as a multifilter

rotating radiometer, having typically a four-wavelength filter.

3. The measurement of screen temperature and humidity in one-minute increments (the same time-resolution as irradiance quantities) using a separate, dedicated temperature-humidity probe instead of relying on the five-minute dataset from the AWS, will be a good step forward. This would not only provide better resolution surface data leading to a better understanding of LWD, but can also be a backup measurement for the AWS and a second control measurement which can fill data gaps in case of AWS breakdowns. In other words, this has the potential to enhance SAWS-AWS measurements, which in itself is a good motivation towards the procurement of such an item. The logging capacity to execute this measurement is already present at De Aar, so this is possibly the most feasible, executable and worthwhile option, if a useful site upgrade is considered in the near future.

4. The following list of parameters were selected from the list of possible extended measurement parameters (Table 2.5). Instatement of the measurement of one or more of these quantities in the future taking available resources, as well as usefulness of the data into account, can be considered as a long-term project:

- Surface narrowband UV radiation to complement the existing measurements of erythemal UVB as part of the SAWS sunburn awareness programme. The current 7-site SAWS sunburn monitoring network frequently has De Aar as the site with the highest daily maximum UV radiation intensity.
- Photosynthetically active radiation (PAR), using newly developed Kipp & Zonen radiometers.
- Precipitable water vapour (PWV) - possibly also indirectly by means of newly developed GPS methods – there is an established GPS reference station on site.
- Spectral downwelling parameters and/or spectral albedo using a sunphotometer by possible interaction with the NASA-GSFC-AERONET network.
- Surface ozone (De Aar is a non-industrial site with low background values; thus, possible ozone transport, resulting from biomass burning could be well identified).
- Total (column) ozone by a ground-based instrument, such as the Dobson or Brewer spectrophotometer. A Dobson instrument shall enhance the existing SAWS measurements at Irene (Gauteng) and Springbok (Namaqualand).
- Ozonesoundings (vertical profile of ozone distribution). Conventional rawinsonde upper-air facilities already exist at De Aar.

REFERENCES

Albrecht, B. and Cox, S.K. 1977. *Procedures for improving pyrgeometer performance.* Journal of Applied Meteorology. **16:** 188 - 197.

Archer, C.B. 1989. (Report on) *COSPAR/WCRP workshop on surface radiation budget for climate and global change.* South African Weather Bureau circular letter W8/1/1, Pretoria.

Archer, C.B. 1997. *Visit to De Aar: proposed station for the Baseline Surface Radiation Network.* Internal SAWS research report RES/27. South African Weather Bureau, Pretoria.

Asmus, K.W. and Grant, C. 1999. *Surface Based Radiometer Data Acquisition System.* Int. Journal of Remote Sensing. **20:** 3125 – 3129.

Augustine, J.A., De Luisi, J.J. and Long, C.N. 2000. *SURFRAD: A national Surface Radiation Budget Network for Atmospheric Research.* Bulletin of the American Meteorological Society. **81 (10):** 2341 - 2358.

Batlles, F.J., Olmo, F.J. and Alados-Arboledas, L. 1995. *On shadowband correction methods for diffuse irradiance measurements*. Solar energy. **54(2):** 105 -114.

Brutasert, W. 1975. *On a derivable formula for long-wave radiation from clear skies.* Water Resources Research. **11:** 742 - 744.

Bunskoek, D.A., Van Lammeren, A.C.A.P. and Feijt, A.J. 1998. *Temperature corrections on radiation measurements using MODTRAN3.* Technical Report TR-204, KNMI, De Bilt, The Netherlands.

Campbell. 2001. *User's guide to CM6B and CM11 pyranometer sensors.* Campbell Scientific Corporation, Logan, Utah, USA.

Cannas, M., Gelardi, F.M., Pullara, F., Barbara, M., Collura, A. and Varisco, S. 2001. *Absorption band at 7.6 eV induced by c-irradiation in silica glasses*. Journal of non-crystalline solids, **280:** 188 – 192.

Cannas, M. 2002. *Luminescence properties of point defects in silica*. GNSR2001 State of Art and Future Development in Raman Spectroscopy and Related Techniques, edited by S. Santangelo and G. Messina. IOS press, Amsterdam. Cond-mat/0203284.

Cook, R.R. 1999. *Assessment of Uncertainties of Measurement for calibrating and testing laboratories*. National Association of testing laboratories Australia. ISBN 0-909307-46-6.

De Luisi, J.J., 1989. *Report to the COSPAR/WCRP workshop on surface radiation budget for climate and global change: GBSRN.* Report to NOAA, 325 Broadway, Boulder Colorado 80303 USA.

DiPasquale, R.C., Whitlock, C.H. 1993. *First WCRP long-term satellite estimates of solar flux for the globe and selected regions.* Proceedings of the 25th International Symposium on Remote sensing and Global Environment Change, Grz, Austria. 4 to 8 April 1993, NASA, USA.

Dominguez, B.A.C. 2001. *Characterization of Pyranometer Thermal off-set and Correction of historical data.* M.Sc. thesis, Department of Mechanical Engineering, Virginia Polytechnic Institute and State University. Blacksburg 24061, VA, USA.

Dutton, E.G. 1996. *Baseline Surface Radiation Network, Newsletter January 1996.* Circular letter to BSRN-involved and -interested parties. US Dept of Commerce, National Oceanic and Atmospheric Administration, Boulder, CO, 80303.

Dutton, E.G., Michalsky, J.J., Stoffel, T., Forgan, B.W., Hickey, J., Nelson, D.A., Alberta, T.L. and Reda, I. 2001. *Measurement of Broadband Diffuse Solar Irradiance using current Commercial Instrumentation with a correction for thermal offset errors*. Journal of Atmospheric and Oceanic Technology. **18:** 297 - 313.

Dutton, E.G. 2002. *Report on GEWEX Baseline Surface Radiation Network (BSRN) Activities, 19 December 2002.* Global Energy and Water Cycle Experiment, Boulder, CO, USA.

Enz, J.W., Klink, J.C. and Baker, D.G. 1975. *Solar radiation effects on Pyrgeometer performance*. Journal of Applied Meteorology. **15:** 1297 - 1302.

Eplab. 1997. *Instrument manual for model HF radiometer*. (Ring-bound and included with instrument). Eppley Laboratory, Newport 02840, RI, USA.

Espenak, F. and Anderson, J. 1999. *Total solar eclipse of 2001 June 21.* NASA technical paper, NASA/TP-1999-209484. NASA/GSFC, Greenbelt 20771, MD, USA.

Espenak, F. and Anderson, J. 2001. *Total solar eclipse of 2002 December 4.* NASA technical paper, NASA/TP-2001-209990. NASA/GSFC, Greenbelt 20771, MD, USA.

Esterhuyse, D.J. 2000. *Launching the South African BSRN station at De Aar.* SAWB internal research report RES/59, South African Weather Bureau, Pretoria.

Fairall, C.W., Persson, P.O.G., Bradley, E.F., Payne, R.E. and Anderson, S.P. 1998. *A new look at Calibration and Use of Eppley Precision Infrared Radiometers: Part 1: Theory and Application.* Journal of Atmospheric and Oceanic Technology. **15:** 1229 - 1242.

Forgan, B.W. 1995. *Pyranometer calibration: in search of the "c".* Presentation at IPC Workshop, 25 September to 13 October 1995. Davos, Switzerland.

Forgan, B.W. 1996. *A new method for Calibrating Reference and Field Pyranometers.* Journal of Atmospheric and Oceanic Technology. **13:** 638 - 645

Forgan, B.W. 2001. *BSRN station status: Alice Springs (Australia).* Presentation at Sixth BSRN Science and Review Workshop, 1 - 5 May 2000, Melbourne, Australia.

Foukal, P.V. 1985. *Advances in absolute radiometry – proceedings of an International meeting held June 24 - 25, 1985.* Atmospheric and Environmental Research, Incorporated. Cambridge, MA, USA.

Fröhlich, C. 1989. *Solar irradiance variability.* Proceedings at symposium "Our Changing Atmosphere", June 1989. Davos, Switzerland.

Gilgen, H., Whitlock, C., Koch, F., Müller, G., Ohmura, A., Steiger, D. and Wheeler, R. 1991. *Technical Plan for BSRN (Baseline Surface Radiation Network) Data Management, Version 1.0.* WMO/TD-No. 443. WCRP/WMO, Geneva, Switzerland.

Gilgen, H., Whitlock, C., Koch, F., Müller, G., Ohmura, A., Steiger, D. and Wheeler, R. 1993. *Technical Plan for BSRN (Baseline Surface Radiation Network) Data Management, Version 1.1.* (WRMC technical report nr 1). WMO/TD-No. 443, WCRP/WMO, Geneva, Switzerland.

Gilgen, H., Whitlock C., Koch F., Müller G., Ohmura A., Steiger D. and Wheeler R. 1995. *Technical Plan for BSRN (Baseline Surface Radiation Network) Data Management, Version 1.1 – final update* (WRMC technical report nr 1). WMO/TD-No. 443, WCRP/WMO, Geneva, Switzerland.

Gilgen, H., Wild, M. and Ohmura, A. 1997. *Global Energy Balance Archive (GEBA) – Report 3: The GEBA version 1995 Database.* ETHZ, Zürcher Geographische Schriften. **74:** 105. ETHZ, Winterthurstrasse 190, CH-8057 Zürich, Switzerland.

Gilgen, H., Wild, M. and Ohmura, A. 1998. *Means and trends of shortwave irradiance at the surface estimated from Global Energy Balance Archive data.* Journal of Climatology. **11(8):** 2042 - 2061.

Gilgen, H. and Ohmura, A. 1999. *The Global Energy Balance Archive (GEBA).* Bulletin of the American Meteorological Society. **80 (5):** 831 - 850.

Haeffelin, M.P., Kato, S., Smith, A.M., Rutledge, C.K., Charlock, T.P. and Mahan, J.R. 2001. *Determination of the thermal offset of the Eppley precision spectral pyranometer*. Journal of Applied Optics. **40:** 472 - 484.

Hegner, H., Müller, G, Nespor, V., Ohmura, A., Steigrad, R. and Gilgen, H. 1998. *Technical Plan for BSRN Data Management, 1998 update.* (WRMC technical report nr 2) WMO/TD-No. 882, WCRP/WMO, Geneva, Switzerland.

Heimo A., Vernez, A. and Wasserfallen, P. 1993. *Baseline Surface Radiation Network (BSRN). Concept and Implementation of a BSRN Station.* WMO/TD-No. 579, WCRP/WMO, Geneva, Switzerland.

Hickey, J.R. and Nelson, D.W. 1993. *Automated cavity pyrheliometer systems: Operational experience, test results and modification.* Technical paper presented at 1993 American Energy Society Conference, Washington, D.C.

Hirose, Y, 1998; *Calibrations of pyrgeometers in Japan.* Presentation at 5th BSRN scientific and review workshop, Budapest, 1998.

Hofer, P., Buchmann, B. and Herzog, A. 1998. *Standard operating procedure for Performance Auditing Ozone Analyzers at Global and Regional WMO-GAW sites.* EMPA-WCC report 98/6, EMPA, Dübendorf, Switzerland, September 1998.

IPCC. 2001. *Baker institute report on Global Warming: Science and Policy Conference.* Nr. 15, January 2001.

Iqbal, M. 1983. *An introduction to Solar Radiation.* Academic Press, New York.

IUCC. 1993. *An introduction to the climate system: information leaflet.* Information Unit on Climate Change (IUCC). UNEP, P.O. Box 356, CH-1219 Chütelaine, Switzerland.

Iziomon, M.G., Mayer, H. and Matzarakis, A. 2003. *Downward atmospheric longwave irradiance under clear and cloudy skies: Measurement and parameterization.* Journal of Atmospheric and Solar-Terrestrial Physics. **65:** 1107 – 1116.

Ji, Q. and Tsay, S.C. 2000. *On the Dome effect of Eppley Pyrgeometers and Pyranometers.* Geophysical Research Letters. **27:** 971 – 974.

Jiménes, J.I., Alados-Arboledas, L., Castro-Diez, Y. and Ballester, G. 1987. *On the estimation of long-wave radiation flux from clear skies*. Theoretical and Applied Climatology. **38:** 37 - 42.

Kasten, F. and Young, A.T. 1989. *Revised optical air mass tables and approximation formula.* Applied Optics **28** (22): 4735 - 4738.

Kipp & Zonen. 1992. *Instruction manual for CM3 pyranometer.* Kipp & Zonen BV, Röntgenweg 1, Delft 2624 BD, The Netherlands, 0338-300 (9506).

Kipp & Zonen, 1994, *Instruction manual for CV1 ventilation system.* Kipp & Zonen BV,

Röntgenweg 1, Delft 2624 BD, The Netherlands, 0305-204 (9503).

Kipp & Zonen. 1995. *Instruction manual for CM11/14 pyranometer.* Kipp & Zonen BV, Röntgenweg 1, Delft 2624 BD, The Netherlands, 0305-201 (9205).

Kipp & Zonen. 1997a. *Instruction manual for CH1 pyrheliometer.* Kipp & Zonen BV, Röntgenweg 1, Delft 2624 BD, The Netherlands, 0334-300 (9212).

Kipp & Zonen. 1997b. *Instruction manual for CM21/31 pyranometer.* Kipp & Zonen BV, Röntgenweg 1, Delft 2624 BD, The Netherlands, 0305-205 (9407).

Kondratyev, K. Ya, 1972. *Radiation processes in the atmosphere.* WMO publication no. 309. WMO, Geneva.

Koshiek, W. 1996. *On the KNMI calibration of net radiometers.* Technical report 189. KNMI, Royal Dutch Meteorological Institute, De Bilt 3730AE, The Netherlands.

Kuik, F. 1997. *Global Radiation Measurements in the Operational KNMI Meteorological Network.* Technical report 197, KNMI, Royal Dutch Meteorological Institute, De Bilt 3730AE, The Netherlands.

Long, C.N. and Ackerman, T.P. 1994. *Surface measurements of solar irradiance: a study of the spatial correlation between simultaneous measurements at separated sites.* Journal of Applied Meteorology. May 1995. **14:** 1039 - 1046.

Long, C.N. 1996. *Report on Broadband Solar Radiometer Inconsistencies at the Atmospheric Radiation Measurement (ARM) Southern Great Plains (SGP) Central Facility During the ARM Enhanced Shortwave Experiment (ARESE).* ARM-TR 003, Pacific Northwest National Laboratory, Richland, Washington, USA.

Long, C. N., and Ackerman, T.P. 2000. *Identification of clear skies from pyranometer measurements and calculation of downwelling shortwave cloud effects,* Journal of Geophysical Research. **105:** (D12), 15609-15626.

Major, G. 1994. *Circumsolar correction for pyrheliometers and diffusometers.* WMO-TD 635, World Meteorological Organization, Geneva, Switzerland.

Major, G. 1995. *The role of geometry amongst the standard pyrheliometers.* Idojaras (Quarterly Journal of the Hungarian Meteorological Service). **99(2):** 77 - 84.

Marion, W. 1993. *Summary Information and Data sets for NREL's Solar Radiation Research Laboratory, 1981 - 1991.* National Renewable Energy Laboratory, 1617 Cole Boulevard, Golden 80401, CO, USA.

Mc Arthur, L.B.J. 1995. *Quality control and quality assurance.* Presentation at IPC workshop, 25 September - 13 October 1995, Davos, Switzerland.

Mc Arthur, L.B.J. 1998. *BSRN operation manual (version 1.0)* WMO-TD no 879, WCRP/WMO.

Meteorological Office. 1982. *Observer's Handbook, Fourth Edition.* Her Majesty's Stationery Office, London, UK.

Morel, P. 1990. *Plan for the Global Baseline Surface Radiation Network (GBSRN).* Letter number 38.653/G/GBSRN from WCRP to the Council of Scientific Industrial Research (CSIR) of South Africa, 12 June 1990, Geneva, Switzerland.

NREL. 1992. *User's manual for the National Solar Radiation Data Base 1961-1990.* NREL, 1617 Cole Boulevard, Golden, Colorado 80401-3393, USA.

NREL. 1993. *User's manual for SERI-QC software – assessing the quality of solar radiation data.* NREL, 1617 Cole Boulevard, Golden, Colorado 80401-3393, USA.

Ohmura, A, Dutton, E.G., Forgan, B., Fröhlich, C,. Gligen, H., Hegner, H., Heimo, A., König-Langlo, G., Mc Arthur, B., Müller, G., Philippona, R., Pinker, R., Whitlock, C.H., Dehne, K. and Wild, M. 1998. *Baseline Surface Radiation Network (BSRN/WRMC), a new precision radiometry for climate research.* Bulletin of the American Meteorological Society. **79:** 2115 - 2136.

Oliviéri, J. 1992. *Accuracy of the Radiometric measurements.* Presentation at WMO Technical Conference on Instruments and Methods of Observation, (TECO 1992), Vienna (Austria). IOM report 49, WMO/TD 462.

Oliviéri, J. 2003. (BSRN colleague). *Personal communication*, May 2003.

Persson, T 2000. *Measurements of solar radiation in Sweden.* Swedish Meteorological and Hydrological Institute, Stockholm, Sweden.

Phillipona, R., Fröhlich, K. and Betz, C. 1995. *Characterization of pyrgeometers and the accuracy of atmospheric long-wave radiation measurements.* Applied Optics. **34:** 1598 - 1605.

Philipona, R.,Fröhlich, C., Dehne, K.,DeLuisi, J., Augustine, J., Dutton, E., Nelson, D., Forgan, B., Novotny, P., Hickey, J., Love, S.P., Bender, S., McArthur, B., Ohmura, A., Seymour, J.H., Foot, J.S., Shiobara, M., Valero, F.P.J., and Strawa, A.W. 1998. *The Baseline Surface Radiation Network pyrgeometer round-robin calibration experiment.* Journal Atmospheric and Oceanic Technology. **15**, 687 - 696.

Philipona, R., Dutton, E.G., Stoffel,T., Michalsky,J., Reda,I., Stifter,A., Wendling,P., Wood,N., Clough, Mlawer, E.J., Anderson, G., Revercomb, H.E. and Shippert, T.R. 2001. *Atmospheric longwave irradiance uncertainty: Pyrgeometers compared to an absolute sky-scanning radiometer, the atmospheric emitted radiance interferometer, and radiative transfer model calculations.* Journal of Geophysic Research. **106:** 28129 - 28141.

Philipona, R. 2002. *Substantial underestimation of Solar global and Diffuse radiation caused by Pyranometer Thermal Offsets.* Presentation delivered at the 11th AMS conference on atmospheric radiation, 3 to 7 June 2002, Ogden, UT, USA.

Pinker, R., Fouin, J, and Li, Z. 1995. *A review of satellite methods to derive surface shortwave radiative fluxes.* Remote Senses. Environment **51:** 108 - 124.

Pirazzini, R., Nardino, M., Orsini, A., Calzolari, F., Georgiadis, T. and Levizzani, V. 1998. *Parameterization of the downward longwave radiation from clear and cloudy skies at Ny Alesund (Svalbard).* Conference Presentation to International Radiation Symposium (IRS), from 24 to 29 July 2000, St. Petersburg, Russia. Obtained in Portable Document File (PDF) format: http://www.isao.bo.cnr.it/~surrball/immagini/irs.pdf.

Reda, I. 1996. *Calibration of a solar absolute cavity radiometer with traceability to the World Radiometric Reference*. NREL-TP-463-20619. National Renewable Energy Laboratory, Golden, Colorado, USA.

Richardson, S. 2000. *Southern Great Plains Site Scientist Research Program Annual Progress Report and Planning Update For September 1, 1999 – August 31, 2000.* University of Oklahoma, Norman, Oklahoma.

Schiffer, Robert A. 1990. *Global Baseline Surface Radiation Network: (GBSRN): A plan for the World Climate Research Programme.* Communication paper on 1 November 1990 from Director: WCRP to NASA, Washington D.C.

Schreder, J.G., Blumthaler, M. and Huber, M. 1998. *Design of an input optic for solar UV-measurements.* Contribution for The Internet Photochemistry and Photobiology Protection against the hazards of UV radiation, Institute of Medical Physics, Univ of Innsbruck, Austria.

Seckmeyer, G., Bais, A., Bernhard, G., Blumthaler, M., Booth, C.R., Disterhoft, P., Eriksen, P., McKenzie, R.L., Miyauchi, M. and Roy, C. with contributions from K. Dehne, U. Feister, B. Mayer, P. Taalas, E. Weatherhead, and A. Webb. 2001. *Instruments to measure solar ultraviolet radiation. Part 1: Spectral instruments.* WMO-GAW Publication No. 125, WMO TD No. 1066, Geneve, Switzerland.

Smith, Amie M. 1999. *Prediction and measurement of thermal exchanges within pyranometers.* M.Sc. thesis. Department of Mechanical Engineering, Virginia Polytechnic Institute and State University, Blacksburg 24061, VA, USA.

South African Weather Bureau (SAWB). 1959. *Report of the Third meeting of WMO Regional association I, working group on Radiation, Leopoldville, Congo, 24 March - 3 April 1958.* Document 7.6. Pretoria.

South African Weather Bureau (SAWB). 1986. *The Climate of South Africa: climate statistics.* Department of Transport, Pretoria.

South African Weather Bureau (SAWB). 2001. *Daily Weather Bulletin June 2001.* Department of Environmental Affairs and Tourism, Pretoria.

South African Weather Service (SAWS). 2002. *Daily Weather Bulletin December 2002*, Pretoria.

Swinbank, W.C. 1963. *Long-wave radiation from clear skies.* Quarterly Journal of the Royal Meteorological Society. **89:** 339 - 348.

Van Cittert-Eymers. 1979. *Biografisch Woordenboek van Nederland.* Den Haag 1979.

Van den Berg, H. 1998. (Town clerk of the De Aar (*Enthamjheni*) municipality). *Personal communication,* February 1998.

Van den Bos, K. and Hoeksema, E. 1997. *An introduction to Atmospheric Radiation Measurement*. Kipp & Zonen / Sci-Tek Instruments technical paper 970529, Delft, The Netherlands.

Van den Bos, K. and Hoogendijk, C.H. 1998. *Characterization of pyrgeometers.* Proceedings at fifth BSRN scientific workshop, Budapest, Hungary, May 1998.

Van der Molen, M.K. and Kohsiek, W. 1995. *Nauwkeuriger Nettostraling meten (The more accurate measurement of Net radiation).* Technical Report, TR-177, KNMI, De Bilt, The Netherlands.

Van Lammeren, A.C.A.P. and Hulshof, A. 1994. *Standaard Stralingsmetingen met een Zonnevolger (Standard Radiation measurements with a Solar Tracker)*, Technical Report TR-164, KNMI, De Bilt, The Netherlands.

Wallace, J.M. and Hobbs, P.V. 1977. *Atmospheric science: An introductory survey.* Academic Press, San Diego, CA, USA.

WCRP-54. 1991. *Radiation and Climate. Workshop on Implementation of the Baseline Surface Radiation Network. (Washington, DC, U.S.A., 3 - 5 December 1990).* WCRP-54, report no. 406, World Meteorological Organization, Geneva.

WCRP-64. 1991. *Radiation and Climate. Second Workshop on the Implementation of the Baseline Surface Radiation Network. (Davos, Switzerland, 6 - 9 August 1991).* World Meteorological Organization, Geneva.

WCRP. 1995. *Baseline Surface Radiation Network (BSRN). Scientific Workshop and Review Meeting. (Zurich, Switzerland, 12 - 16 September 1994)*. World Meteorological Organization, Geneva.

WCRP. 1997. *Baseline Surface Radiation Network (BSRN). Scientific Workshop and Review Meeting. (Boulder, Colorado, USA, 12 - 16 August 1996).* Informal Report No. 3/1997, World Meteorological Organization, Geneva.

WCRP. 1998. *Baseline Surface Radiation Network (BSRN). Report of the fifth BSRN science and review workshop. (Budapest, Hungary, 18 - 22 May 1998).* Informal Report No. 10/1998, World Meteorological Organization, Geneva.

WCRP. 2001. *Baseline Surface Radiation Network (BSRN). Report of the sixth BSRN science and review workshop (Melbourne, Australia, 1 - 5 May 2000).* Informal Report No. 17/2001, World Meteorological Organization, Geneva.

WCRP. 2002. *Baseline Surface Radiation Network (BSRN). Report of the seventh BSRN science and review workshop (Regina, Canada, 28 - 31 May 2002).* Informal Report No. 18/2002, World Meteorological Organization, Geneva.

Whitlock, C.H. 1990. *Informal GBSRN Memorandum.* Circular letter to all Washington GBSRN workshop participants, 28 December 1990, NASA Langley Research Centre, Hampton, VA, USA.

Whitlock, C.H., Charlock, T.P., Staylor, W.F., Pinker, R.T., Laszlo, I., DiPasquale, R.C. and Ritchley, N.A. 1993. *WCRP surface radiation budget shortwave data product description – version 1.1.* NASA technical memorandum 107747, March 1993, Langley Research Centre, Hampton 23681, VA , USA.

Whitlock, C.H., Charlock, T.P., Staylor, W.F., Pinker, R.T., Laszlo, I, Ohmura, A., Gilgen, H., Konzelmann, T., Di Pasquale R.T., Moats, C.D., Le Croy, S.R. Ritchey, N.A. 1995. *First Global WCRP Shortwave Surface Radiation Budget Dataset*. Bulletin of the American Meteorological Society. **76:** 905 - 922.

Willson, R.C. and Mordvinov, A.V. 2003. *Secular total solar irradiance trend during solar cycles 21-23.* Geophysical Research Letters **30(5):** 1199. doi:10.1029/2002GL016038.

WMO. 1983. *Guide to Meteorological Instruments and Methods of Observation (Fifth Edition).* WMO No. 8. Secretariat of the World Meteorological Organization, Geneva, Switzerland.

WMO. 2003. *Report of the CAS working group on environmental pollution and Atmospheric Chemistry, Geneva, Switzerland, 18-19 March 2003.* WMO-TD no 1181, WMO report no 151. Secretariat of the World Meteorological Organization, Geneva, Switzerland.

WRC. 2001. *International Pyrheliometer Comparison IPC IX, 25.09.2000 – 13.10.2000 Davos Switzerland : Results and Symposium.* Working report no 197, Meteo-Swiss, Davos and Zurich, Switzerland.

APPENDICES

APPENDIX A: *PHOTOPAGES*

APPENDIX B: *STATION-TO-ARCHIVE FILE FORMAT*

APPENDIX C: *SPECIFIC DATA FOR A TYPICAL YEAR AT DE AAR*

APPENDIX D: *THE KÖPPEN CLIMATE ZONE CLASSIFICATION*

APPENDIX E: *CONNECTION AND OPERATION OF A PYRGEOMETER*

APPENDIX A

PHOTOPAGES

All the photos on these two photo pages are the original work of the author himself and bears the caption © Danie Esterhuyse. In order to allow more picture area, the captions are presented in two frames on this page, with the actual photos in corresponding boxes on the next two pages.

PICTURE CAPTIONS FOR PHOTOPAGE 1

31 December 1997: The author is seen unpacking the first consignment of WMO-sponsored instrumentation at the Forum Building, Pretoria.	20 November 1998: Decisions on site layout was made during a visit. The position of tracker and main instrument box are indicated here.
26 October 1996: Entrance to De Aar from a northern direction, leading to the main street.	13 February 1998: The neat and functional interior of Weather Office De Aar.
28 July 1999: First installation, connecting power plug and serial connection for the solar tracker.	28 July 1999: First installation, digging a trench for burying cable conduits.
25 July 2000: Panoramic view of De Aar, looking northwards from the Weather Office hillock.	

PICTURE CAPTIONS FOR PHOTOPAGE 2

25 July 2000: Instrument camp setup in early morning light complete with perimeter fence. A GPS station features towards the extreme right.	30 July 1999: Complete setup: Pyrheliometers, diffusometer and pyrgeometer on tracker, global pyranometer on separate fixed table to the right.
8 March 2001: Global pyranometer at sunrise. Morning dew can be seen on the mounting plate.	26 July 1999: Lockable instrument box mounted on tracker pole containing all terminals for power (right side) and communication (left side). Main power distribution sockets with transformer for DC power is featured, connected to two dataloggers complete with battery backup and line drivers.
26 September 2001: A cloudless day: six-monthly calibrations are in full swing with Eppley cavity radiometer operated parallel with complete instrumentation on tracker and computer on desk.	
20 November 1998: Panoramic view of open area to the east of the instrument camp hillock where a 30-metre tower for the measurement of upwelling quantities, can be constructed.	


WELKOM
Pofadder

University of Pretoria etd – Esterhuyse, D J (2004)

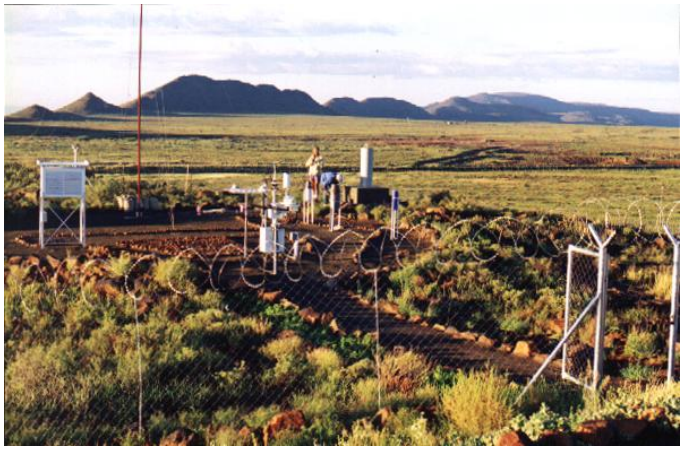

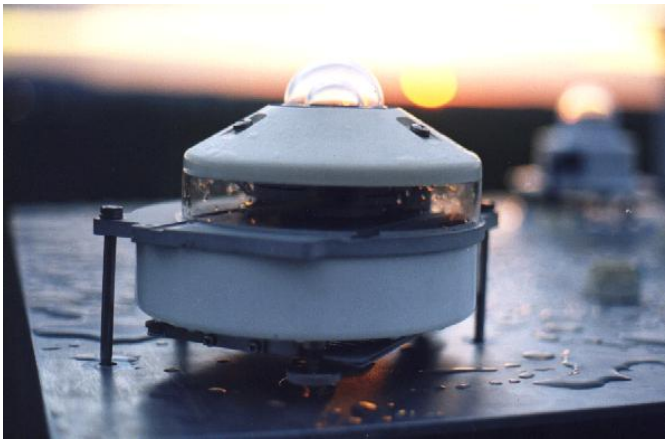

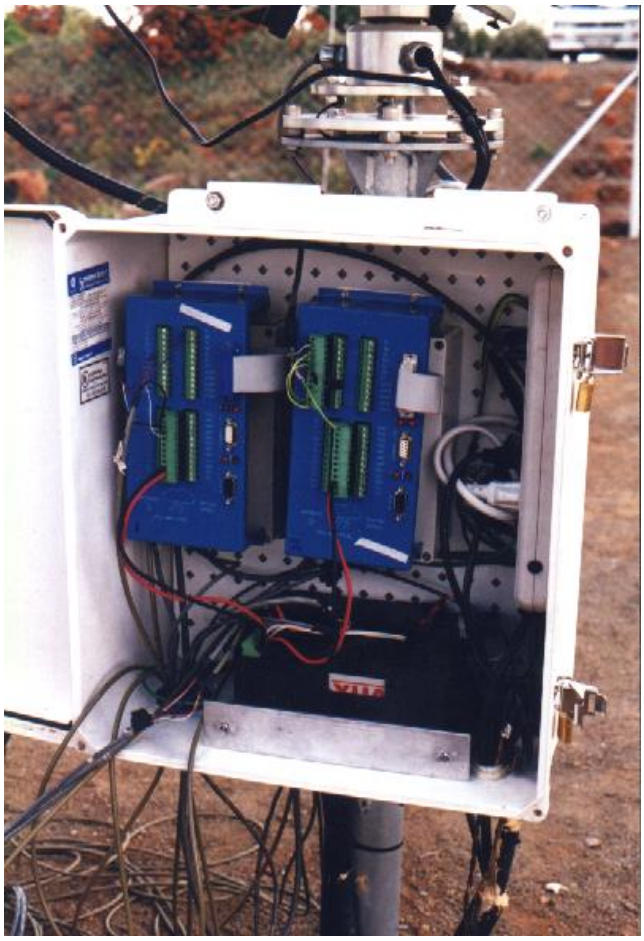

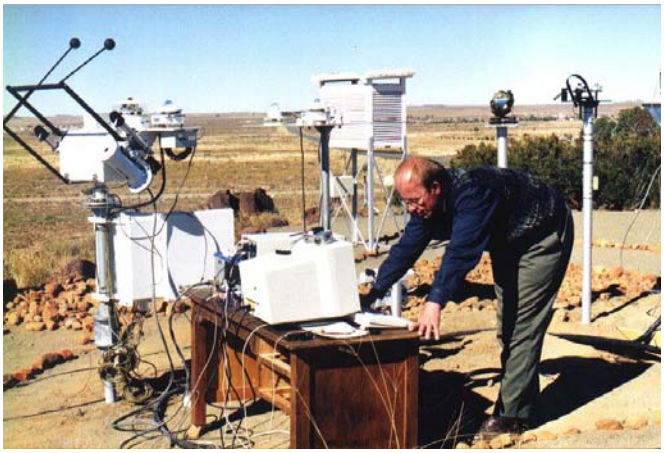

APPENDIX B

STATION-TO-ARCHIVE FILE FORMAT

This annexure reflects the station-to-archive file format in two ways: In Section B.1, the official description of the format required for data files prior to submission is presented, and in Section B.2, a real De Aar file that complied to the conditions and have been accepted in the database.

B.1 FORMAT DESCRIPTION

This is the official description of the BSRN station-to-archive file format as described by WMO (1995). The data file is identified in logical record 0001, by the station identification number, year and month. The dates of change in logical records 0002, 0004, 0005, 0006, 0007, 0008 and 0009 are given by day, hour and minute (dhm) with values ranging from 1...31, 0...23 and 0...59 respectively. The dates of measurement in logical records 0100, 0200, ... are recorded in days and minutes (dm) with values ranging from 1...31 and 0...1439 respectively. This format also applies to quantities measured in hourly intervals.

logical record	line no.	description of field/ format of line	Range of values	Missing code	Format of V1
0001	1	station identification number	Table 4.1		I2
id. of	1	month of measurements	1 - 12		I2
file	1	year of measurement	1992		I4
	1	version of data		- 99	I2
	1	(X,I2,X,I2,X,I4,X,I2)			
	2	id.no.of 1st, 2nd, ... quantity	Table 4.13		I9
		measured (8(X,I9)); missing	Table 4.13		I9
		values -1 to fill up line, as many lines as needed			
0002	1	date when scientist changed (dhm)	0 - 59	-1	3(X,I2)
scien-	2	name of station scientist			A38
tist	2	telephone no. of station scientist			A20
	2	FAX no. of station scientist			A20
	2	(A38,X,A20,X,A20)			
	3	TCP/IP no.		XXX	A15
	3	e-mail address		XXX	A50
	3	(A15,X,A50)			
	4	address of station scientist			A80
	5	date when deputy changed (dhm)	0 - 59	-1	3(X,I2)

	6	name of station deputy			A38
	6	telephone no. of station deputy			A20
	6	FAX no. of station deputy			A20
	6	(A38,X,A20,X,A20)			
	7	TCP/IP no. of deputy		XXX	A15
	7	e-mail address of deputy		XXX	A50
	7	(A15,X,A50)			
	8	address of deputy			A80
0003	1	messages not to be inserted in the BSRN database, as many lines as needed		XXX	A80
0004	1	date when stat. descr. ch. (dhm)	0 - 59	-1	3(X,I2)
station	2	surface type	Table 4.14		I2
descrip-	2	topography type	Table 4.14		I2
tion,	2	(X,I2,X,I2)			
horizon	3	address (A80)			
	4	telephone no. of station		XXX	A20
	4	FAX no. of station		XXX	A20
	4	(A20,X,A20)			
	5	TCP/IP no. of station		XXX	A15
	5	e-mail address of station		XXX	A50
	5	(A15,X,A50)			
	6	latitude [degrees, 0 is South pole, positive is northw.]	0 - 179		F7.3
	6	longitude [degrees, 0 is 180 W, positive is eastwards]	0 - 359		F7.3
	6	altitude [m above sea level]			I4
	6	identification of ``SYNOP'' station		XXXXX	A5
	6	(2(X,F7.3),X,I4,X,A5)			
	7	date when horizon changed (dhm)	0 - 59	-1	3(X,I2)
	8	azimuth [degrees from north clockw.]	0 - 359	-1	I3
		elevation [degrees]	0 - 89	-1	I2
		(11(X,I3,X,I2)); as many lines with 11 pairs to give horizon, last line filled up with -1			
0005	1	date when change occurred (dhm)	0 - 59	-1	3(X,I2)
radio-	1	is radiosonde operating?	Y, N		A1
sonde	1	(3(X,I2),X,A1)			
eqip-	2	manufacturer			A30
ment	2	location			A25
	2	distance from radiation site [km]			I3
	2	time of 1st launch [h UTC]	0 - 23		I2
	2	time of 2nd launch [h UTC]			I2
	2	time of 3rd launch [h UTC]		-1	I2
	2	time of 4th lanch [h UTC]		-1	I2
	2	identification of radiosonde			A5
	2	(A30,X,A25,X,I3,4(X,I2),X,A5)			
	3	remarks about radiosonde		XXX	A80
0006	1	date when change occurred (dhm)	0 - 59	-1	3(X,I2)
ozone m.	1	are ozone measurements operated?	Y, N		A1
equip-	1	(3(X,I2),X,A1)			
ment	2	manufacturer			A30
	2	location			A25
	2	distance from radiation site [km]			I3
	2	identification number of ozone instrument			A5
	2	(A30,X,A25,X,I3,X,I5)			
	3	remarks about ozone measurement		XXX	A80
0007	1	date when change occurred (dhm)	0 - 59	-1	3(X,I2)

station	2	method est. cloud amount (digital proc.)		XXX	A80
history	3	method est. cloud base h. (with instr.)		XXX	A80
	4	method est. cloud liquid water cont.		XXX	A80
	5	method est. cloud aerosol vertical distr.		XXX	A80
	6	method est. water vapor press. v.d. (A80)		XXX	A80
	7	6 flags indicating if the SYNOP and/or the corresponding quantities of the expanded programme, are measured	Y,N		A1
	7	(A1,X,A1,X,A1,X,A1,X,A1,X,A1)			
0008	1	date when change occurred (dhm)	0 - 59	-1	3(X,I2)
radia-	1	is instrument measuring	Y,N		A1
tion	1	(3(X,I2),X,A1)			
instru-	2	manufacturer			A30
ments	2	model			A15
	2	serial number			A18
	2	date of purchase [MM/DD/YY]		XXX	A8
	2	identification number assigned by the WRMC			I5
	2	(A30,X,A15,X,A18,X,A8,X,I5)			
	3	remarks about the radiation instrument		XXX	A80
	4	pyrgeometer body compensation code		-1	I2
	4	pyrgeometer dome compensation code		-1	I2
	4	wavelength of band 1 of spectral i. [micron]		-1.000	F7.3
	4	bandwidth of band 1 of spectral i. [micron]		-1.000	F7.3
	4	wavelength of band 2		-1.000	F7.3
	4	bandwidth of band 2		-1.000	F7.3
	4	wavelength of band 3		-1.000	F7.3
	4	bandwidth of band 3		-1.000	F7.3
	4	max. zenith angle [degree]	0 - 90	-1	I2
	4	min. zenith angle [degree]	0 - 90	-1	I2
		of direct (spectral) instrument			
	4	(2(X,I2),6(X,F7.3),2(X,I2))			
	5	location of calibration			A30
	5	person who calibrated			A40
	5	(A30,X,A40)			
	6	start of calibration period (band 1 of spectr. instr.)			A8
	6	end of ... (both [MM/DD/YY])			A8
	6	number of comparisons (band 1 of spectr.instr.)		-1	I2
	6	mean calibration coefficient (band 1 of spectr. instr.)			F12.4
	6	standard error of cal. coeff.		-1.0000	F12.4
		(band 1 of spectral instrument)			
	6	(A8,X,A8,X,I2,2(X,F12.4))			
	7	start of calibration period band 2 of		XXX	A8
		spectral instrument			
	7	end of ... (both [MM/DD/YY])		XXX	A8
	7	number of comparisons band 2 of spectr. instr.		-1	I2
	7	mean calibration coefficient band 2 of		-1.0000	F12.4
		spectral instrument			
	7	standard error of cal. coeff. band 2 of		-1.0000	F12.4
		spectral instrument			
	7	(A8,X,A8,X,I2,2(X,F12.4))			
	8	start of calibration period band 3 of		XXX	A8
		spectral instrument			
	8	end of ... (both [MM/DD/YY])		XXX	A8
	8	number of comparisons band 3 of spectr. instr.		-1	I2
	8	mean calibration coefficient band 3 of		-1.0000	F12.4
		spectral instrument			
	8	standard error of cal. coeff. band 3 of		-1.0000	F12.4
		spectral instrument			
	8	(A8,X,A8,X,I2,2(X,F12.4))			
	9	remarks on calibration,		XXX	A80

e.g. units of calibration coefficients

	10	remarks on calibration (continued)		XXX	A80
	11	date when change occurred	0 - 59	-1	3(X,I2)
	11	...			

Every radiation instr. at the station is described by 10 lines in the format given above (radiation subrecord)

0009	1	date when change occurred (dhm.)	0 - 59	-1	3(X,I2)
assign-	1	id. no. of radiation quantity	Table 4.14		I9
ment of		measured			
radia-	1	id. no. of instrument which measured quantity			I5
tion	1	no. of band (for spectral instruments)		-1	I2
quanti-	1	(3(X,I2),X,I9,X,I5,X,I2)			
ties to	2	date when change occurred (dhm.)	0 - 59	-1	I2
instru-	2	...			
ments		as many lines to list all quantities together with the instruments; e.g.,			

...

```
  1  0  0       101 21013  1
  1  0  0       102 21013  2
  1  0  0       103 21013  3
  1  0  0         3 21005 -1
  1  0  0         4 21006 -1
 15  0  0         3 21007 -1
```

...

The above lines mean that

(i) the shortwave spectral fluxes at bands 1, 2 and 3 are measured with instrument 21013, bands 1,2,3

(ii) the direct radiation is measured with instrument 21005 from the 1st day of the month until the 14th day of the month, with instrument 21007 since the 15th day of the month, and

(iii) the diffuse radiation is measured with instrument 21006.

Legal quantity id. nos. are listed in relation *measvar*, legal instrument id. nos. are assigned to the instruments at theBSRN stations by the WRMC. If an instrument measures more than one quantity, lines with the same instrument id. no. and the same date, but with different quantity id. nos. are repeated. However it is not allowed to repeat lines with the same date and the same quantity id. no. As a consequence, the following two lines are illegal, as

(i) quantity id. no. 1 is not in relation *measvar*, but in relation *calcvar*, and

(ii) there is more than 1 line with the same time and quantity id. no.

```
 < 1  0  0         1 21005  -1   not allowed >
 < 1  0  0         1 21006  -1   not allowed >
```

Thus calculated quantities are calculated at the WRMC, (Sect. 4.1).

0100	1	date [day]	1 - 31		I2
basic	1	time [minute]	0 - 1439		I4
meas.	1	global 2 (mean, std. dev., min., max.: columns 12 - 31)		-999 or	I4 or
	1	direct (mean, std. dev., min., max.: columns 35 - 54)		-99.9	F5.1

```
          2     diffuse (mean, std. dev., min., max.:
                columns 12-31)
          2     downward longwave radiation (mean, std. dev.,
                min., max.: columns 35 - 54)
          2     air temperature at downw. longw. instr. height  -99.9    F5.1
          2     relative humidity at ...                        -99.9    F5.1
          2     pressure at ...                                 -999     I4
                (X,I2,X,I4,2(3X,I4,X,F5.1,X,I4,X,I4),/
                8X,2(3X,I4,X,F5.1,X,I4,X,I4),4X,F5.1,X,F5.1,X,I4)
          3     date [day]                          1 - 31               I2
          3     ...
                2 lines for each time measured

0200      1     date [day]                          1 - 31               I2
expanded  1     time [minute]                       0 - 1439              I4
meas.     1     downw. shortw. spectr. at wavel. 1                -999 or  I4 or
          1     (mean, std. dev., min., max.: columns 12-31)      -99.9    F5.1
          1     ... at wavel. 2 (mean, std. dev., min., max.: col. 35 - 54)
          1     ... at wavel. 3 (mean, std. dev., min., max.: col. 58 - 77)
                (X,I2,X,I4,3(3X,I4,X,F5.1,X,I4,X,I4))
          2     ...
                1 line for each time measured

0300      1     date [day]                          1 - 31               I2
other     1     time [minute]                       0 - 1439             I4
meas.     1     upward shortwave reflected                        -999 or  I4 or
in                (mean, std. dev., min., max.: columns 12-31)    -99.9    F5.1
minutes   1     upward longwave
interv.           (mean, std. dev., min., max.: columns 35-54)
          1     net radiation (net radiometer)
                (mean, std. dev., min., max.: columns 58-77)
          1     (X,I2,X,I4,3(3X,I4,X,F5.1,X,I4,X,I4)
          2     ...
                1 line for each time measured

0400      1     date [day]                          1 - 31               I2
special   1     time [minute]                        0 - 1439             I4
spectral  1     downw. shortw. spectr. at wavel. 4                -999 or  I4 or
meas.     1     (mean, std. dev., min., max.: columns 12-31)      -99.9    F5.1
          1     ... at wavel. 5 (mean, std. dev., min., max.: col. 35 - 54)
          1     ... at wavel. 6 (mean, std. dev., min., max.: col. 58 - 77)
          2     ... at wavel. 7 (mean, std. dev., min., max.: col. 12 - 31)
          2     ... at wavel. 8 (mean, std. dev., min., max.: col. 35 - 54)
          2     ... at wavel. 9 (mean, std. dev., min., max.: col. 58 - 77)
          3     ... at wavel. 10 (mean, std. dev., min., max.: col. 12 - 31)
          3     ... at wavel. 11 (mean, std. dev., min., max.: col. 35 - 54)
          3     ... at wavel. 12 (mean, std. dev., min., max.: col. 58 - 77)
                (X,I2,X,I4,3(3X,I4,X,F5.1,X,I4,X,I4)/
                2(8X,3(3X,I4,X,F5.1,X,I4,X,I4)/))
          4     ...
                3 lines for each time measured

0500      1     date [day]                          1 - 31               I2
UV        1     time [minute]                       0 - 1439             I4
meas.     1     uv-a global (mean, std. dev., min., max.:      -99.9     F5.1
                columns 10 - 32)
          1     uv-b direct (mean, std. dev., min., max.:
                columns 34 - 56)
          2     uv-b global (mean, std. dev., min., max.:
                columns 10 - 32)
          2     uv-b diffuse (mean, std. dev., min., max.:
```

		columns 34 - 56)			
	2	uv-b upward reflected (mean, std. dev., min., max.:			
		columns 58 - 80)			
		(X,I2,X,I4,4(X,F5.1),4(X,F5.1)/			
		8X,4(X,F5.1),4(X,F5.1),4(X,F5.1)			
	4	date [day]	1 - 31		I2
	4	...			
		2 lines for each time measured			
1000	1	YYGG9 IIiii Nddff 1SnTTT 2SnTdTdTd 3P0P0P0 4PPPP			A80
surface		7wwW1W1 8NhClCmCh 333 8NsChshsh 8NsChshsh 8NsChshsh			
SYNOP		as many lines as needed in format (A80)			
1100	1	date [day]	1 - 31		I2
radio-	1	time [minute]	0 - 1439		I4
sonde	1	observation number			I4
meas. in	1	pressure at level		-999	I4
launch	1	height at level			I5
interv.	1	temperature		-99.9	F5.1
	1	dew point		-999.9	F6.1
	1	wind direction, azimuth	0 - 359	-99	I3
	1	wind speed		-99	I3
	1	ozone concentration		-9.9	F4.1
	1	(X,I2,X,I4,3X,I4,X,I4,X,I5,X,F5.1,X,F6.1,X,I3,X,I3,X,F4.1)			
	2	date [day]	1 - 31		I2
	2	...			
		1 line for each level measured			
1200	1	date [day]	1 - 31		I2
ozone	1	time [minute]	0 - 1439		I4
meas.	1	total ozone amount		-999	I4
in hours	1	(X,I2,X,I4,3X,I4)			
interv.	2	date [day]	1 - 31		I2
	2	...			
		1 line for each time measured			
1300	1	date [day]	1 - 31		I2
expanded	1	time [minute]	0 - 1439		I4
meas.	1	total cloud amount with instrument		-9	I2
in hours	1	cloud base height with instrument in m			
interv.		(no clouds 99999)		-9999	I5
1st part	1	cloud liquid water in mm		-99.9	F5.1
	1	spectral aerosol optical depth at wavelength 1		-9.999	F6.3
	1	spectral aerosol optical depth at wavelength 2		-9.999	F6.3
	1	spectral aerosol optical depth at wavelength 3		-9.999	F6.3
	1	(X,I2,X,I4,3X,I2,X,I5,X,F5.1,2X,3(X,F6.3))			
	2	date [day]	1 - 31		I2
	2	...			
		1 line for each time measured			
1400		expanded measurements second part in hours intervals			
		(water vapour vertical profile by lidar):			
		to be defined later			
1500	1	date [day]	1 - 31		I2
other	1	time [minute]	0 - 1439		I4
measurem.	1	thermal spectral at wavelength 1		-9	I4
in hours	1	thermal spectral at wavelength 2		-9	I4
intervals	1	thermal spectral at wavelength 3		-9	I4
	1	hemispheric solar spectral at wavelength 1		-9	I4
	1	hemispheric solar spectral at wavelength 2		-9	I4

```
         1     hemispheric solar spectral at wavelength 3      -9       I4
         1     (X,I2,X,I4,2(3X,I4,X,I4,X,I4)
         2     ...
               1 line for each time measured
```

These are two examples for logical records defined for the measurements at the height of 10 and 30 m on the tower of the Payerne (Swiss) station. Such logical records and the corresponding relations in the BSRN database are defined according to the configuration of the instruments at the BSRN stations that perform measurements at heights other than the standard height, i.e., for BSRN stations with a tower. The formats of both records are approximately the same as the format for logical record 100, thus the software for writing the records to the station-to-archive file at Payerne and for reading and inserting the data in the BSRN database at the WRMC is more standardized.

```
3010     1     date [day]                              1 - 31            I2
other    1     time [minute]                           0 - 1439          I4
meas.    1     global 2                                          -999 or  I4 or
at                (mean, std. dev., min., max.: columns 12 - 31)
10 m     1     shortwave upward                                  -99.9    F5.1
                  (mean, std. dev., min., max.: columns 35 - 54)
         2     downward longwave radiation
                  (mean, std. dev., min., max.: columns 12 - 31)
         2     upward longwave radiation
                  (mean, std. dev., min., max.: columns 35 - 54)
         2     air temperature                                   -99.9    F5.1
         2     relative humidity                                 -99.9    F5.1
               (X,I2,X,I4,2(3X,I4,X,F5.1,X,I4,X,I4),/
               8X,2(3X,I4,X,F5.1,X,I4,X,I4),4X,F5.1,X,F5.1)
         3     date [day]                              1 - 31            I2
         3     ...
               2 lines for each time measured

3030     1     date [day]                              1 - 31            I2
other    1     time [minute]                           0 - 1439          I4
meas.    1     global 2                                          -999 or  I4 or
at                (mean, std. dev., min., max.: columns 12 - 31)
30 m     1     shortwave upward                                  -99.9    F5.1
                  (mean, std. dev., min., max.: columns 35 - 54)
         2     downward longwave radiation
                  (mean, std. dev., min., max.: columns 12 - 31)
         2     upward longwave radiation
                  (mean, std. dev., min., max.: columns 35 - 54)
         2     air temperature                                   -99.9    F5.1
         2     relative humidity                                 -99.9    F5.1
               (X,I2,X,I4,2(3X,I4,X,F5.1,X,I4,X,I4),/
               8X,2(3X,I4,X,F5.1,X,I4,X,I4),4X,F5.1,X,F5.1)
         3     date [day]                              1 - 31            I2
         3     ...
               2 lines for each time measured
```

B.2 A REAL DE AAR DATAFILE

Date: June 2003. Large homogeneous sections omitted. Read in two-column newspaper-style.

```
*C0001
 40  6 2003  1
       2       3       4       5      21      22      23      -1
      -1      -1      -1      -1      -1      -1      -1      -1
*C0002
  1  0  0
Mr. Danie Esterhuyse                +2712 3676053       +2712 3676175
 10.226.  1.187 danie@weathersa.co.za
SAWB,  Private Bag X097,  Pretoria,  0001,  Rep. of South Africa
  1  0  0
Mr. Danie Ferreira                  +2753 6311053       +2753 6310628
192.168.145.36  fadyoc@weathersa.co.za
Resp. officer,  De Aar Weath Off,  P.O. Box 270,  De Aar,  7000,  Rep.
of S.A.
*C0003
Take note new IP- address and phone number.
*C0004
  1  0  0
 21  2
De Aar Weather Office  P.O. Box 270  De Aar  7000  Rep. of South
Africa
+2753 6311054       +2753 6310628
192.168.145.37  fady@weathersa.co.za
  59.335 203.993 1287 68536
  1  0  0
0 14   3 14   4 12  14  8  15  2  16  4  18  4  19  1  20  2  21  2  22  1 23
2  24  2  25  1  26  2  27  2  28  1  29  1  30  0  36  0  38  1  40  1 42  1
47  0  48  2  50  1  59  0  61  1  81  1  82  0  87  1  90  1  92  0  93  1  97
1  98  0 100  0 120  0 140  0 141  7 152  7 153  0 160  0 169 0 173  1
174  1 176  0 180  0 182  1 183  0 185  2 187  1 189  3 191  2 192  3
193  2 197  2 199  1 200  1 201  2 202  1 203  0 204  1 205  2 206  1
207  1  208  2 210  1 219  0 224  0 240  0 260  0 280  0 300  0 318  0
319  1 320  1  321  0 322  1 324  0 325  1 326  2 330  2 333  1 337  0
339  1 340  2 341  1  343  1 346  2 347  3 349  2 352  2 353 14 354 14
355 17 356 18 357 18 358 17  359 14  -1 -1  -1 -1  -1 -1  -1 -1  -1 -1  -1
-1  -1 -1  -1 -1  -1 -1  -1 -1
*C0005
  1  0  0 Y
Vaisala DigiCora            De Aar                  0 10 -1 -1 -1 RS80
Station use old VLF radiosondes - find upper-air winds by optic
theodolite
*C0007
  1  0  0
XXX
XXX
XXX
XXX
XXX
Y N N N N N
*C0008
  1  0  0 N
Kipp & Zonen                CH1         970156          12/31/97 40001
Mounted on Sci-Tek 2AP Gear solar tracker
 -1 -1  -1.000  -1.000  -1.000  -1.000  -1.000  -1.000 -1 -1
De Aar                      D. J. Esterhuyse
01/27/03 01/27/03 37      12.6200       0.0410
XXX      XXX      -1      -1.0000       -1.0000
XXX      XXX      -1      -1.0000       -1.0000
Calibration coeff units are in microvolt / Watt / square metre.
Instrument directly compared with AHF cavity nr. 31109
  1  0  0 Y
Kipp & Zonen                CH1         970157          12/31/97 40002
Mounted on Sci-Tek 2AP Gear solar tracker
 -1 -1  -1.000  -1.000  -1.000  -1.000  -1.000  -1.000 -1 -1
De Aar                      D. J. Esterhuyse
01/27/03 01/27/03 37      13.4400       0.0440
XXX      XXX      -1      -1.0000       -1.0000
XXX      XXX      -1      -1.0000       -1.0000
Calibration coeff units are in microvolt / Watt / square metre.
directly compared with AHF cavity nr. 31109
  1  0  0 Y
Kipp & Zonen                CM21        970442          12/31/97 40003
Instrument gets ventilated artificially
 -1 -1  -1.000  -1.000  -1.000  -1.000  -1.000  -1.000 -1 -1
De Aar                      D. J. Esterhuyse
01/27/03 01/27/03 21      19.2700       0.1100
XXX      XXX      -1      -1.0000       -1.0000
XXX      XXX      -1      -1.0000       -1.0000
Calibration coeff units are in microvolt / Watt / square metre.
Alternate sun / shade comparisons with CH1 pyrheliometer.
  1  0  0 Y
Kipp & Zonen                CM21        970443          12/31/97 40004
Instrument gets ventilated artificially
 -1 -1  -1.000  -1.000  -1.000  -1.000  -1.000  -1.000 -1 -1
De Aar                      D. J. Esterhuyse
01/27/03 01/27/03 21      22.4900       0.0270
XXX      XXX      -1      -1.0000       -1.0000
XXX      XXX      -1      -1.0000       -1.0000
Calibration coeff units are in microvolt / Watt / square metre.
Alternate sun / shade comparisons with CH1 pyrheliometer.
  1  0  0 Y
Eppley                      PIR         32200F3         02/28/98 40005
Instrument gets ventilated artificially.
  2  7  -1.000  -1.000  -1.000  -1.000  -1.000  -1.000 -1 -1
Eppley Laboratories         Factory constants
01/08/98 01/08/98 -1      4.2700       -1.0000
XXX      XXX      -1      -1.0000       -1.0000
XXX      XXX      -1      -1.0000       -1.0000
Calibration coeff units are in microvolt / Watt / square metre.
using factory calibrations.
  1  0  0 N
Eppley                      PIR         32201F3         02/28/98 40006
Instrument gets ventilated artificially.
  2  7  -1.000  -1.000  -1.000  -1.000  -1.000  -1.000 -1 -1
Eppley Laboratories         Factory constants
01/08/98 01/08/98 -1      4.1700       -1.0000
XXX      XXX      -1      -1.0000       -1.0000
XXX      XXX      -1      -1.0000       -1.0000
Calibration coeff units are in microvolt / Watt / square metre.
using factory calibrations.
  1  0  0 N
Eppley                      PIR         32202F3         02/28/98 40007
Instrument gets ventilated artificially.
  2  7  -1.000  -1.000  -1.000  -1.000  -1.000  -1.000 -1 -1
Eppley Laboratories         Factory constants
01/08/98 01/08/98 -1      3.8800       -1.0000
XXX      XXX      -1      -1.0000       -1.0000
XXX      XXX      -1      -1.0000       -1.0000
Calibration coeff units are in microvolt / Watt / square metre.
using factory calibrations.
*C0009
  1  0  0        2 40004 -1
  1  0  0        3 40002 -1
  1  0  0        4 40003 -1
  1  0  0        5 40005 -1
*C0100
  1   0     0   0.0    0    0     0   0.0    0    0
            0   0.0    0    0   271   0.5  270  272     9.1  36.1  878
  1   1     0   0.0    0    0     0   0.0    0    0
            0   0.0    0    0   270   0.5  269  271   -99.9 -99.9 -999
  1   2     0   0.0    0    0     0   0.0    0    0
            0   0.0    0    0   270   0.8  269  272   -99.9 -99.9 -999
  1   3     0   0.0    0    0     0   0.0    0    0
            0   0.0    0    0   270   0.4  269  271   -99.9 -99.9 -999
  1   4     0   0.0    0    0     0   0.0    0    0
            0   0.0    0    0   270   0.7  270  271   -99.9 -99.9 -999
  1   5     0   0.0    0    0     0   0.0    0    0
            0   0.0    0    0   271   0.6  270  271     9.1  36.2  878
  1   6     0   0.0    0    0     0   0.0    0    0
            0   0.0    0    0   271   0.5  270  272   -99.9 -99.9 -999
  1   7     0   0.0    0    0     0   0.0    0    0
            0   0.0    0    0   270   0.6  269  271   -99.9 -99.9 -999
  1   8     0   0.0    0    0     0   0.0    0    0
            0   0.0    0    0   270   0.7  269  271   -99.9 -99.9 -999
  1   9     0   0.0    0    0     0   0.0    0    0
            0   0.0    0    0   270   0.6  269  271   -99.9 -99.9 -999
  1  10     0   0.0    0    0     0   0.0    0    0
            0   0.0    0    0   270   0.7  269  271     9.0  36.5  878
  1  11     0   0.0    0    0     0   0.1    0    0
            0   0.0    0    0   270   0.8  268  271   -99.9 -99.9 -999
  1  12     0   0.0    0    0     0   0.0    0    0
            0   0.0    0    0   270   0.8  269  271   -99.9 -99.9 -999
  1  13     0   0.0    0    0     0   0.0    0    0
            0   0.0    0    0   270   0.5  269  271   -99.9 -99.9 -999
```

(continuing . . .)

```
 1 295    0  0.0   0   0    0  0.0   0   0
        0  0.1   0   0   312  0.8 310 313    7.2 44.5 878
 1 296    0  0.1   0   0    0  0.1   0   0
        0  0.0   0   0   311  0.5 310 313   -99.9 -99.9 -999
 1 297    0  0.0   0   0    0  0.0   0   0
        0  0.1   0   0   311  0.9 309 312   -99.9 -99.9 -999
 1 298    0  0.0   0   0    0  0.0   0   0
        0  0.0   0   0   310  1.0 308 311   -99.9 -99.9 -999
 1 299    0  0.1   0   0    0  0.0   0   0
        0  0.1   0   0   308  0.8 306 309   -99.9 -99.9 -999
 1 300    0  0.1   0   0    0  0.0   0   0
        0  0.1   0   0   306  0.7 305 308    7.3 44.2 878
 1 301    0  0.2   0   1    0  0.0   0   0
        0  0.2   0   0   304  0.6 303 306   -99.9 -99.9 -999
 1 302    1  0.3   1   1    0  0.0   0   0
        1  0.3   0   1   302  0.4 302 303   -99.9 -99.9 -999
 1 303    2  0.2   1   2    0  0.0   0   0
        2  0.2   1   2   300  1.1 298 302   -99.9 -99.9 -999
 1 304    2  0.1   2   2    0  0.0   0   0
        2  0.1   2   2   298  1.0 296 299   -99.9 -99.9 -999
 1 305    2  0.1   2   2    0  0.0   0   0
        2  0.1   2   2   295  1.0 294 297    7.3 44.4 878
 1 306    3  0.1   2   3    0  0.0   0   0
        2  0.0   2   2   293  1.1 291 295   -99.9 -99.9 -999
 1 307    3  0.0   3   3    0  0.0   0   0
        2  0.0   2   2   291  0.9 289 292   -99.9 -99.9 -999
 1 308    3  0.0   3   3    0  0.0   0   0
        3  0.1   2   3   288  0.7 286 289   -99.9 -99.9 -999
 1 309    3  0.1   3   3    0  0.0   0   0
        3  0.1   2   3   286  1.1 285 288   -99.9 -99.9 -999
 1 310    3  0.0   3   3    0  0.1   0   0
        3  0.0   3   3   284  0.4 283 285    7.3 44.2 878
 1 311    3  0.0   3   3    0  0.1   0   0
        3  0.0   3   3   283  0.7 282 285   -99.9 -99.9 -999
 1 312    3  0.1   3   3    0  0.0   0   0
        3  0.0   3   3   282  0.7 281 283   -99.9 -99.9 -999
 1 313    3  0.0   3   3    1  0.1   0   1
        3  0.1   3   3   282  0.6 280 282   -99.9 -99.9 -999
 1 314    3  0.1   3   4    1  0.1   1   1
        3  0.1   3   3   280  0.6 278 280   -99.9 -99.9 -999
 1 315    4  0.1   4   4    1  0.0   1   1
        4  0.1   3   4   278  0.7 277 280    7.3 44.2 878
 1 316    4  0.2   4   5    1  0.2   1   2
        4  0.1   4   4   278  0.7 277 279   -99.9 -99.9 -999
 1 317    5  0.4   5   6   24 16.7   2  55
        5  0.1   4   5   277  0.7 276 279   -99.9 -99.9 -999
 1 318    7  0.5   6   8   91 20.0  56 122
        5  0.1   5   5   277  0.7 276 279   -99.9 -99.9 -999
 1 319    8  0.3   8   9   134  4.2 124 140
        5  0.1   5   6   277  0.6 276 278   -99.9 -99.9 -999

( continuing . . . )

 18 360   78  0.8  77  79   442  2.5 438 446
       27  0.1  26  27   265  0.8 263 266    6.1 49.2 881
 18 361   81  0.8  80  82   449  2.4 445 454
       27  0.1  27  27   265  0.5 264 266   -99.9 -99.9 -999
 18 362   84  0.8  82  85   457  1.9 453 461
       27  0.1  27  27   265  0.7 264 267   -99.9 -99.9 -999
 18 363   86  0.8  85  88   464  2.1 461 468
       28  0.1  27  28   265  0.8 264 266   -99.9 -99.9 -999
 18 364   89  0.9  88  90   472  2.3 468 475
       28  0.1  28  28   264  0.7 263 266   -99.9 -99.9 -999
 18 365   92  0.8  91  93   479  1.9 475 482
       29  0.2  28  29   265  0.7 264 266    6.3 48.6 881
 18 366   95  0.8  93  96   485  1.7 482 487
       29  0.1  29  29   265  0.6 264 266   -99.9 -99.9 -999
 18 367   97  0.8  96  99   490  1.9 487 494
       30  0.1  29  30   265  0.8 264 266   -99.9 -99.9 -999
 18 368  100  0.8  99 101   497  1.6 494 499
       30  0.1  30  30   265  0.9 264 267   -99.9 -99.9 -999
 18 369  103  0.9 101 104   503  1.9 500 506
       30  0.1  30  31   265  0.6 265 267   -99.9 -99.9 -999
 18 370  106  0.9 104 107   509  2.1 506 512
       31  0.1  31  31   265  0.8 264 267    6.4 48.1 881


30 1426    0  0.0   0   0    0  0.0   0   0
        0  0.0   0   0   252  0.6 251 253   -99.9 -99.9 -999
 30 1427    0  0.0   0   0    0  0.0   0   0
        0  0.0   0   0   252  0.6 251 253   -99.9 -99.9 -999
 30 1428    0  0.0   0   0    0  0.1   0   0
        0  0.0   0   0   252  0.3 251 253   -99.9 -99.9 -999
 30 1429    0  0.0   0   0    0  0.1   0   0
        0  0.0   0   0   253  0.3 252 253   -99.9 -99.9 -999
 30 1430    0  0.0   0   0    0  0.1   0   0
        0  0.0   0   0   252  0.6 252 254    6.3 31.6 879
 30 1431    0  0.0   0   0    0  0.1   0   0
        0  0.0   0   0   253  0.5 252 253   -99.9 -99.9 -999
 30 1432    0  0.0   0   0    0  0.0   0   0
        0  0.0   0   0   252  0.7 251 253   -99.9 -99.9 -999
 30 1433    0  0.0   0   0    0  0.0   0   0
        0  0.0   0   0   252  0.6 251 253   -99.9 -99.9 -999
 30 1434    0  0.0   0   0    0  0.0   0   0
        0  0.0   0   0   252  0.6 251 253   -99.9 -99.9 -999
 30 1435    0  0.0   0   0    0  0.0   0   0
        0  0.0   0   0   252  0.6 251 253    6.3 31.5 879
 30 1436    0  0.0   0   0    0  0.0   0   0
        0  0.0   0   0   252  0.6 251 253   -99.9 -99.9 -999
 30 1437    0  0.0   0   0    0  0.0   0   0
        0  0.0   0   0   252  0.5 252 253   -99.9 -99.9 -999
 30 1438    0  0.0   0   0    0  0.0   0   0
        0  0.0   0   0   252  0.6 251 253   -99.9 -99.9 -999
 30 1439    0  0.0   0   0    0  0.0   0   0
        0  0.0   0   0   252  0.6 251 253   -99.9 -99.9 -999
*U1000
01009 68538 /1506 10091 21052 38796 48584 7//// 8////   333 8//// 8//// 8////
01019 68538 /1508 10072 21048 38791 48578 7//// 8////   333 8//// 8//// 8////
01029 68538 /1510 10066 21045 38789 48576 7//// 8////   333 8//// 8//// 8////
01039 68538 21510 10076 21045 38789 48576 7//// 80001   333 8//// 8//// 8////
01049 68538 21508 10070 21041 38791 48577 7//// 80001   333 8//// 8//// 8////

( continuing . . . )

30189 68538 00504 10092 21088 38812 48595 70500 8////   333 8//// 8//// 8////
30199 68538 /0406 10093 21087 38811 48593 7//// 8////   333 8//// 8//// 8////
30209 68538 /0404 10087 21092 38812 48594 7//// 8////   333 8//// 8//// 8////
30219 68538 /0000 10085 21094 38813 48595 7//// 8////   333 8//// 8//// 8////
30229 68538 /0404 10089 21091 38811 48593 7//// 8////   333 8//// 8//// 8////
30239 68538 /0404 10076 21093 38804 48585 7//// 8////   333 8//// 8//// 8////
*C1100
  1 720    1 877 1287 22.2  -2.5 340   6 -9.9
  1 720    2 873 1331 19.2  -3.6 -99 -99 -9.9
  1 720    3 867 1386 18.8  -3.9 -99 -99 -9.9
  1 720    4 861 1444 18.2  -3.8 -99 -99 -9.9
  1 720    5 855 1507 17.5  -3.8 -99 -99 -9.9
  1 720    6 849 1569 16.9  -3.2 -99 -99 -9.9
  1 721    7 843 1627 16.3  -2.7 313  14 -9.9
  1 721    8 838 1683 15.8  -3.1 -99 -99 -9.9
  1 721    9 832 1737 15.3  -3.1 -99 -99 -9.9
  1 721   10 827 1793 14.8  -3.0 -99 -99 -9.9
  1 721   11 821 1852 14.2  -2.7 -99 -99 -9.9
  1 721   12 815 1918 13.6  -2.8 -99 -99 -9.9
  1 722   13 808 1988 13.1  -3.2 309  12 -9.9
  1 722   14 802 2051 12.5  -2.9 -99 -99 -9.9
  1 722   15 796 2117 12.0  -3.4 -99 -99 -9.9
  1 722   16 789 2184 11.5  -4.6 -99 -99 -9.9
  1 722   17 783 2249 11.0  -5.5 -99 -99 -9.9
  1 722   18 777 2316 10.6  -7.1 -99 -99 -9.9

( continuing . . . )

 30  765  271  80 17808 -65.6  -87.1 -99 -99 -9.9
 30  765  272  80 17864 -65.4  -86.9 -99 -99 -9.9
 30  765  273  79 17919 -65.3  -86.9 -99 -99 -9.9
 30  765  274  78 17973 -65.3  -86.9 -99 -99 -9.9
 30  765  275  78 18027 -64.4  -86.2 -99 -99 -9.9
 30  766  276  77 18077 -63.8  -85.7 -99 -99 -9.9
 30  766  277  76 18127 -63.3  -85.3 -99 -99 -9.9
 30  766  278  76 18185 -63.1  -85.1 -99 -99 -9.9
 30  766  279  75 18244 -62.9  -85.0 -99 -99 -9.9
 30  766  280  74 18299 -62.8  -84.9 -99 -99 -9.9
 30  766  281  73 18357 -62.8  -84.9 -99 -99 -9.9
 30  766  282  73 18415 -62.6  -84.7 -99 -99 -9.9
 30  767  283  72 18476 -62.4  -84.6 -99 -99 -9.9
 30  767  284  71 18537 -62.5  -84.7 -99 -99 -9.9
 30  767  285  71 18597 -62.7  -84.8 -99 -99 -9.9
 30  767  286  70 18658 -62.9  -85.0 -99 -99 -9.9
 30  767  287  69 18718 -63.1  -86.9 -99 -99 -9.9
 30  767  288  69 18781 -63.2  -86.9 -99 -99 -9.9
 30  768  289  68 18845 -63.2  -86.9 -99 -99 -9.9
```

APPENDIX C

SPECIFIC DATA FOR A TYPICAL YEAR AT DE AAR

Date	Sun-rise	Sun-set	Solar noon	Day-length	TOA kJ.m^{-2}	Date	Sun-rise	Sun-set	Solar noon	Day-length	TOA kJ.m^{-2}
01 Jan	05:24	19:30	12:27	14:05	43938	05 Jul	07:21	17:35	12:28	10:13	18423
06 Jan	05:28	19:30	12:29	14:02	43754	10 Jul	07:21	17:37	12:29	10:16	18747
11 Jan	05:32	19:31	12:31	13:58	43490	15 Jul	07:19	17:40	12:29	10:20	19172
16 Jan	05:36	19:30	12:33	13:53	43144	20 Jul	07:17	17:42	12:30	10:24	19693
21 Jan	05:41	19:29	12:35	13:47	42719	25 Jul	07:15	17:45	12:30	10:30	20305
26 Jan	05:45	19:27	12:36	13:41	42213	30 Jul	07:12	17:48	12:30	10:36	21002
31 Jan	05:50	19:24	12:37	13:34	41629	04 Aug	07:08	17:51	12:30	10:43	21778
05 Feb	05:54	19:21	12:38	13:26	40969	09 Aug	07:04	17:54	12:29	10:50	22626
10 Feb	05:59	19:17	12:38	13:18	40235	14 Aug	06:59	17:57	12:28	10:58	23537
15 Feb	06:03	19:12	12:38	13:09	39431	19 Aug	06:54	18:00	12:27	11:06	24504
20 Feb	06:07	19:08	12:37	13:00	38560	24 Aug	06:49	18:03	12:26	11:14	25519
25 Feb	06:11	19:02	12:37	12:51	37629	29 Aug	06:43	18:06	12:25	11:22	26572
02 Mar	06:15	18:57	12:36	12:42	36644	03 Sep	06:37	18:09	12:23	11:31	27655
07 Mar	06:18	18:51	12:35	12:33	35610	08 Sep	06:31	18:12	12:21	11:40	28759
12 Mar	06:22	18:45	12:33	12:23	34536	13 Sep	06:25	18:14	12:20	11:49	29876
17 Mar	06:25	18:39	12:32	12:14	33429	18 Sep	06:18	18:17	12:18	11:58	30997
22 Mar	06:28	18:33	12:31	12:04	32299	23 Sep	06:12	18:20	12:16	12:07	32113
27 Mar	06:31	18:27	12:29	11:55	31153	28 Sep	06:06	18:23	12:14	12:17	33216
01 Apr	06:34	18:21	12:28	11:46	30002	03 Oct	06:00	18:26	12:13	12:26	34298
06 Apr	06:37	18:15	12:26	11:37	28854	08 Oct	05:53	18:29	12:11	12:35	35351
11 Apr	06:41	18:09	12:25	11:28	27720	13 Oct	05:48	18:32	12:10	12:44	36368
16 Apr	06:44	18:03	12:23	11:19	26609	18 Oct	05:42	18:36	12:09	12:53	37342
21 Apr	06:47	17:58	12:22	11:10	25530	23 Oct	05:37	18:39	12:08	13:02	38267
26 Apr	06:50	17:53	12:21	11:02	24493	28 Oct	05:32	18:43	12:07	13:11	39137
01 May	06:53	17:48	12:21	10:54	23507	02 Nov	05:27	18:47	12:07	13:19	39946
06 May	06:57	17:44	12:20	10:47	22581	07 Nov	05:23	18:51	12:07	13:27	40691
11 May	07:00	17:40	12:20	10:40	21723	12 Nov	05:20	18:55	12:08	13:35	41367
16 May	07:03	17:37	12:20	10:33	20940	17 Nov	05:17	19:00	12:08	13:42	41972
21 May	07:06	17:34	12:20	10:27	20241	22 Nov	05:15	19:04	12:10	13:48	42503
26 May	07:09	17:32	12:21	10:22	19631	27 Nov	05:14	19:08	12:11	13:54	42958
31 May	07:12	17:30	12:21	10:18	19116	02 Dec	05:13	19:12	12:13	13:59	43336
05 Jun	07:15	17:29	12:22	10:14	18701	07 Dec	05:13	19:16	12:15	14:02	43637
10 Jun	07:17	17:29	12:23	10:12	18388	12 Dec	05:14	19:20	12:17	14:05	43858
15 Jun	07:19	17:29	12:24	10:10	18180	17 Dec	05:16	19:23	12:20	14:07	44000
20 Jun	07:20	17:30	12:25	10:09	18080	22 Dec	05:18	19:26	12:22	14:07	44062
25 Jun	07:21	17:31	12:26	10:09	18087	27 Dec	05:21	19:28	12:24	14:07	44044
30 Jun	07:22	17:33	12:27	10:10	18202	31 Dec	05:24	19:30	12:27	14:05	43945

APPENDIX D

THE KÖPPEN CLIMATE ZONE CLASSIFICATION

The Köppen climate zone criteria is widely recognized as a tool for classifying regions of the world in climate zones, and was also used as a criterium to denote BSRN geographical climate zone representivity. The classification system was developed in 1928 by the German geographer-meteorologist Wladimir Köppen (1884–1931) based upon and described by dominant types of vegetation found in the respective regions. Although the classifications are mainly driven by climate characteristics, vegetation type also features prominently as depicted in Table D.1.

Five main classes denoted by the capital letters A to E, were originally developed with a sixth, H, added later. Other letters added after the capitals denote sub-divisions per class:

Subtypes for Temperature

- **a** Warmest month above or equal to 22 °C (for C or D climates)
- **b** Warmest month below 22 °C (for C or D climates)
- **c** Less than four months over 10 °C (for C or D climates)
- **d** Same as 'c' but coldest month below -37 °C (for D climates)
- **h** Hot and dry: all months above 0 °C (for B climates)
- **k** Cool and dry: at least one month below 0 C (for B climates)

Subtypes for Precipitation

- **s** Dry season in summer: when 70% or more of annual precipitation falls in winter (for C climates)
- **w** Dry season in winter: when 70% or more of annual precipitation falls in summer (for A, C, or D climates)
- **f** Constantly moist: rainfall consistent throughout the year (for A, C, or D climates)
- **m** Monsoon rain: short dry season, precipitation in driest month < 60 mm and total annual precipitation > 1250 mm, when both 'w' and 'm' subtypes are met, 'm' subtype takes precedence, don't use both subtypes (for A climates)

---

[1] *http://www.squ1.com/climate/koppen.html*

Table D.1 *Descriptive properties of the Köppen climate zone classification*

<table>
<tr><th>A: Tropical</th><th>B: Dry</th><th>C: Temperate</th><th>D: Cold</th><th>E: Polar</th></tr>
<tr><td>Average coolest month ≥ 18°C.</td><td>Annual precipitation < 860 mm.</td><td>Coldest month > 0°C and < 18°C. Warmest month > 10°C.</td><td>Coldest month < 0°C. Warmest month > 10°C.</td><td>Tundra: Warmest month < 10°C, Polar: all months < 0°C.</td></tr>
<tr><td>Af (Tropical rainforests). Perpetual precipitation. Monthly temp vary < 3°C. Typical max/min 22°C and 32°C.</td><td rowspan="3">BW (Arid) A true desert climate. It covers 12 % of the Earth's land surface.</td><td rowspan="2">Cfa (Humid subtropical) Hot muggy summers with mainly thunderstorms. Mild winters with precipitation via mid-latitude cyclones. Vegetation deciduous and non-deciduous trees (mangrove, magnolia, cypress, mossy oak trees).</td><td>Dfa and Dfb (Humid Continental) – perpetually wet with cool summers, all trees defoliate but needle-leaf.</td><td rowspan="3">ET (Tundra) – no trees, rolling grasslands covered with snow throughout most of the year; at least 1 month of above freezing temperatures. Wide occurrence of permafrost. Vegetation dominated by mosses, lichens, dwarf trees and scattered woody shrubs.</td></tr>
<tr><td>Ds (Dry summers)</td></tr>
<tr><td>Am (Tropical monsoon) Dry season with almost no rain, hot season with more rain than Af.</td><td>Csa (Mediterranean) Rain primarily during winter via mid-latitude cyclone, with extreme summer aridity. Vegetation oak woodlands, grasslands and chaparral.</td><td>Dfc (Subartic) - associated with the boreal or taiga forests of single stands of trees such as the firs or spruce tree.</td></tr>
<tr><td>Aw (Tropical wet and dry-Savannah) Extended dry winter and only summer rainfall, usually < 1000 mm.</td><td>BS (Steppe) Dry semiarid grassland climate that covers 14% of the Earth's land surface.</td><td>Cfb (Marine west coast) Humid climate with short dry summer. Heavy precipitation occurs during the mild winters because of continuous presence of mid-latitude cyclone. Vegetation mixed evergreen forests coniferous [cone-bearing] and deciduous [leaves fall-off] trees.</td><td>Dw (Dry winters)</td><td>EF (Polar ice) Ice caps that have a surface that is permanently covered with snow and ice since temperatures never exceed freezing.</td></tr>
</table>

H *(Highlands)* A climate zone in itself due to the unique climate properties that places of exceptional high altitude, exhibit.

The following map (Figure D.1) reflects how these regions are geographically represented :-

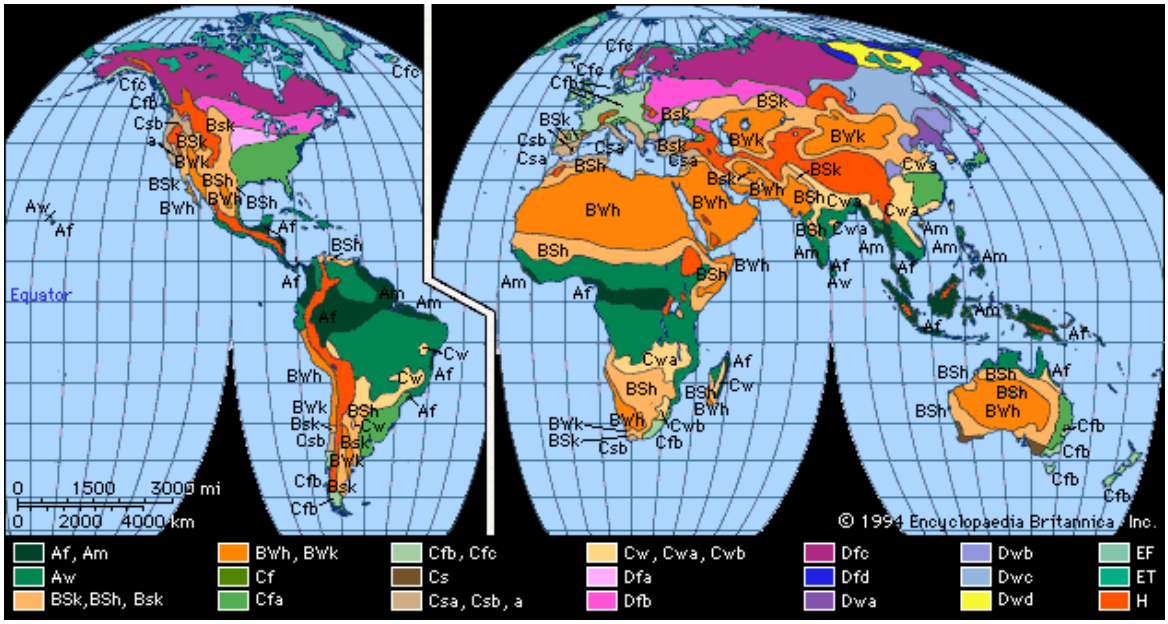

Figure D.1 *Geographical representation of Köppen climate zones*

The

- Group of stations thereafter up to 1996: **C:** Carpentras (Cs), Billings (Cfa), Tateno (Cfa), **D:** Regina (Dfb)

- Group of stations thereafter up to1998: **A:** Ilorin (Aw), **B:** Sede Boqer (BW), Alice Springs (BW), De Aar (BS), **C:** Florianopolis (Cwa), Lindenberg (Cfb), **D:** Toravere (Dfc), **E:** Syowa (EF)

- Most recent stations: **A:** SGP1 (Am), Manus (Aw), Nauru (Am), **B:** Taman-rasset (BW), Boulder SURFRAD (BS), Desert Rock (BW), **C:** Lauder (Cfa), Penn State (Cfa), Goodwin Creek (Cfb), **D:** Fort Peck (Dfb), Bondville (Dfb)

In total, the main groups were represented as follows:- A = 6, B = 7, C = 8, D = 4, E = 5. This is a fair distribution through the climate zones. Geographic as well as climatic representivity was therefore maintained in the BSRN network.

APPENDIX E

CONNECTION AND OPERATION OF A PYRGEOMETER

The setup and data reduction procedures of a pyrgeometer is more complex than that of a pyrheliometer or pyranometer. The author have amassed the following information in co-operation with several institutions and wishes to present it here as one concise unit. At the De Aar site, an Eppley PIR pyrgeometer was connected to a Campbell- Scientific CR10X–logger using dedicated PC208W software. The explanations in this appendix are therefore focused on those particular hardware and software types.

In this section, a circuit diagram of the PIR–to–logger connections and some explanations are offered. This is followed by expressions converting the measured quantities to data, and a complete Edlog programme (the user-programmable input for the datalogger) is presented.

E.1 CIRCUIT DIAGRAM

On the Eppley pyrgeometer, the input plug on the side have holes numbered A to H, which corresponds to pins on the matching plug numbered A to H. Pins A, B and C are used in connection to the thermopile (pin B, the battery compensation circuit connection, that was rejected by the BSRN community). D and E are the case (body) thermistor connections, F and G are the dome thermistor connections, and H is the earth (ground) connection.

On the logger, a Campbell Scientific CR10X, there are input terminals known as 1L, 1H, 2L, 2H, 3L and 3H. This represents differential signal input terminals, for channels 1, 2 and 3 respectively. The letters “L” and “H” represents lower and higher input channel connections. The “agnd” notation refers to an analogue ground connection (not the same as a power ground or Earth connection, and the terminals E1 and E2 are voltage-specific pulse excitation channels used in connection with the dome and body thermistors.

The pyrgeometer pins and logger terminals are connected in the way depicted in Figure E.1.

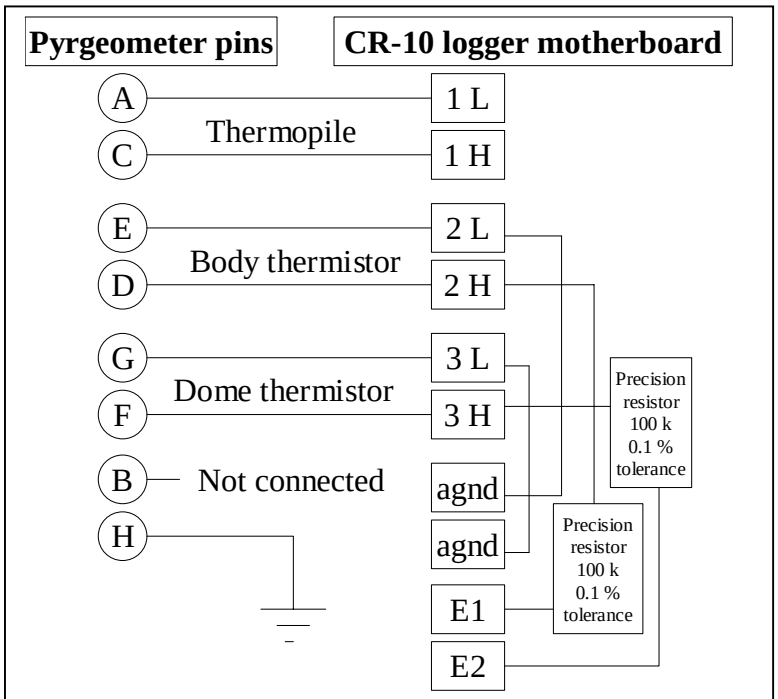

Figure E.1 *Circuit diagram for pyrgeometer-logger connections.*

Note: The precision resistors quoted here, are *not* ring-type resistors – it is very important that the resistors are of 0.1 % tolerance type and have negligible temperature dependence since their outputs are balanced against temperature-dependent devices (thermistors) used to measure the case and dome temperatures accurately.

E.2 EQUATIONS

The logger excites the differential channels 2H and 3H through the precision resistors R_v using excitation channels E1 and E2 with a precise voltage E_v for a specific period (typically 0.01s), at a preset frequency (100Hz). The voltage drops experienced at the ”agnd” terminals through the temperature–dependent thermistors are recorded at 2L and 3L as millivoltages V_b and V_d, dependent only on the case and dome temperatures.

Using Ohm's law and the definitions used in the previous paragraph for these circuits:

$$R_b = \frac{R_v V_b}{E_v - V_b} \quad \text{for the body thermistor, and}$$

$$R_d = \frac{R_v V_d}{E_v - V_d} \quad \text{for the dome thermistor} \qquad \text{(E.1)}$$

The resistance of the thermistors are used to convert to temperature using the Steinhart-Hart equation which is a least-squares fit for the YSI-44031 thermistors' table of dependence of temperature T to resistance R (Eplab, 1995).

$$T_b = \frac{1}{a + b \ln R_b + c \ln R_b^{\,3}} \quad \text{for the body thermistor, and}$$

$$T_d = \frac{1}{a + b \ln R_d + c \ln R_d^{\,3}} \quad \text{for the dome thermistor} \qquad \text{(E.2)}$$

where the regression constants a, b and c have the following values:-

a = *1.0295 E -03*

b = *2.39 E -04*

c = *1.568 E -07*

Finally, temperature is converted to irradiance using the operational Albrecht and Cox (1977) expression, also featured in Section 3.1.3:

$$E_{LW} = \frac{p}{C_1} + \sigma T_b^{\,4} + 3.5\sigma (T_b^{\,4} - T_d^{\,4}) \qquad \text{(E.3)}$$

E.3 EDLOG PROGRAMME

In the case of SW radiation, the very quantities direct, diffuse and global radiation, needed in the database, is directly sampled and measured. Therefore, the logger can be programmed to produce BSRN one-minute statistics (average, standard deviation, minimum and maximum). Since the individual 1Hz samples are not essential to produce the BSRN one-

minute statistics, they are not stored and a minimal amount of logger space is consumed by SW radiation.

However, it is totally different with LW radiation, the irradiance values are *not* sampled as a quantity *per se.* Instead, only the directly measurable native quantities *pile, body* and *dome* can be sampled every second. Presenting one-minute statistics of *those* quantities, will not enable the scientist to calculate any LW irradiance quantities or statistics. Bear in mind that the said quantities will have to be treated using equations E.1, E.2 and E.3. The non-linearity of the last two equations implies that it does not make sense to use one-minute statistics of the native values to obtain one-minute statistics of the irradiance values.

There are two extreme options to address this problem.

(A) One extreme option is to store all the one-second samples of *pile, case* and *dome*, calculate the LW irradiance quantities in 1Hz resolution, and then produce accurate one-minute statistics. This option is unfeasible for De Aar, since there is simply not enough space on one logger, and data is in fact generated at a rate comparable to the speed of downloading it. If, therefore, a power failure or lightning strike temporarily breaks the connection between the logger and PC (such as on three previous occasions), data is lost almost immediately. This option was exercised on a trial basis in October 2001, but it soon proved unfeasible.

(B) The other extreme option is not to store any *pile, case* and *dome* samples. The logger is then programmed to calculate all LW irradiance and one-minute statistics internally. This uses the logger as a “black box” and it is unconditionally trusted to produce correct results. If, for any reason, LW irradiances look suspicious and re-calculation is required, it would not be possible if individual *pile, case* and *dome* samples are not available.

There solution is a compromise between (A) and (B). Samples must be stored, but how much ? It was found that a sampling period of 6 seconds produces 10 samples of *pile, case* and *dome* per minute, which still produces valid LWD values. The author developed a programme that performs LW irradiance calculations and one-minute statistics, and store 6-second samples. Since one program cycle takes about three to four seconds to repeat itself (i.e. do the complex calculations and record samples of the native quantities), one-second samples cannot be recorded in practice.

The complete Edlog programme code (original file SKY_PIR.CSI) is now presented here.

Take note: Three columns in newspaper-style per page.

```
;{CR10X}

; BSRN Datalogger program to sample LW constituents (pile,case,dome) and perform internal calculations of LWD in order to report a true avg, std, min and max per minute. The samples are done every second and reported every 6 sec in order to redo calculations if internal calc of LWD fails.
;
;  D.J. Esterhuyse, 16 October 2002.

; Program 1 samples Pile/Case/Dome

; Program 2 calculates LW irradiance avg, std, min, max.



*Table 1 Program
  01: 1          Execution Interval (seconds)

1: Ex-Del-Diff (P8)
 1: 1       Reps
 2: 15      2500 mV Fast Range
 3: 2       DIFF Channel
 4: 1       Excite all reps w/Exchan 1
 5: 10      Delay (units 0.01 sec)
 6: 2000    mV Excitation
 7: 1       Loc [ Case    ]
 8: 1.0     Mult
 9: 0.0     Offset

2: Ex-Del-Diff (P8)
 1: 1       Reps
 2: 15      2500 mV Fast Range
 3: 3       DIFF Channel
 4: 2       Excite all reps w/Exchan 2
 5: 10      Delay (units 0.01 sec)
 6: 2000    mV Excitation
 7: 2       Loc [ Dome    ]
 8: 1.0     Mult
 9: 0.0     Offset

3: Volt (Diff) (P2)
 1: 1       Reps
 2: 2       7.5 mV Slow Range
 3: 1       DIFF Channel
 4: 3       Loc [ Pile    ]
 5: 1.0     Mult
 6: 0.0     Offset

4: Batt Voltage (P10)
 1: 4       Loc [ BatV    ]

5: Internal Temperature (P17)
 1: 5       Loc [ IntT    ]

6: If time is (P92)
 1: 0       -- Minutes (Seconds --) into a
 2: 6       Interval (same units as above)
 3: 10      Set Output Flag High (Flag 0)

7: Real Time (P77)
 1: 1121    (Same as 1221)
Y,D,Hr/Mn,Sec

8: Resolution (P78)
 1: 01      High Resolution

9: Average (P71)
 1: 1       Reps
 2: 3       Loc [ Pile    ]

10: Average (P71)
 1: 1       Reps
 2: 1       Loc [ Case    ]

11: Average (P71)
 1: 1       Reps
 2: 2       Loc [ Dome    ]

12: Serial Out (P96)
 1:                 71 SM192/SM716/CSM1

; Program 1 samples Pile / Case / Dome

; Program 2 calculates LW irradiance avg, std, min, max.



*Table 2 Program
  02: 4          Execution Interval (seconds)

; CALCULATION PHASE of LW irradiance avg, min, max and std.

; Stefan-Bolzmann constant Sigma defined:
1: Z=F (P30)
 1: 5.67    F
 2: -8      Exponent of 10
```

```
 3: 25       Z Loc [ Sigma     ]

; TERM 1 = Pile irradiance - 1/0.00427 = 234.192
2:  Z=X*F (P37)
 1: 3        X Loc [ Pile      ]
 2: 234.192  F
 3: 7        Z Loc [ TERM_1    ]

; For calculations: different signs of hundred thousand:
; Minus hundred thousand:-
3:  Z=F (P30)
 1: -1       F
 2: 5        Exponent of 10
 3: 23       Z Loc [ Min_Hu_th ]

; Plus hundred thousand:-
4:  Z=F (P30)
 1: 1        F
 2: 5        Exponent of 10
 3: 9        Z Loc [ Hund_thou ]

; Resistances of case and dome:-

5:  Z=X*Y (P36)
 1: 1        X Loc [ Case      ]
 2: 23       Y Loc [ Min_Hu_th ]
 3: 8        Z Loc [ R_c_upper ]

6:  Z=X+F (P34)
 1: 1        X Loc [ Case      ]
 2: -2000    F
 3: 13       Z Loc [ R_c_lower ]

7:  Z=X/Y (P38)
 1: 8        X Loc [ R_c_upper ]
 2: 13       Y Loc [ R_c_lower ]
 3: 10       Z Loc [ R_case    ]

8:  Z=X*Y (P36)
 1: 2        X Loc [ Dome      ]
 2: 23       Y Loc [ Min_Hu_th ]
 3: 14       Z Loc [ R_d_upper ]

9:  Z=X+F (P34)
 1: 2        X Loc [ Dome      ]
 2: -2000    F
 3: 15       Z Loc [ R_d_lower ]

10:  Z=X/Y (P38)
 1: 14       X Loc [ R_d_upper ]
 2: 15       Y Loc [ R_d_lower ]
 3: 16       Z Loc [ R_dome    ]

; TEMPERATURES of case and dome

11:  Z=LN(X) (P40)
 1: 10       X Loc [ R_case    ]
 2: 24       Z Loc [ ln_R_case ]

; Polynomial pre-scaled with 10^5 to enable coefficient entry.
12:  Polynomial (P55)
 1: 1        Reps
 2: 24       X Loc [ ln_R_case ]
 3: 22       F(X) Loc [ Poly_T_cx ]
 4: 102.95   C0
 5: 23.91    C1
 6: 0.0      C2
 7: 0.01568  C3
 8: 0.0      C4
 9: 0.0      C5

; and apply de-pre-scaling to polynomial:-

13:  Z=X/Y (P38)
 1: 22       X Loc [ Poly_T_cx ]
 2: 9        Y Loc [ Hund_thou ]
 3: 20       Z Loc [ Poly_T_c  ]

14:  Z=1/X (P42)
 1: 20       X Loc [ Poly_T_c  ]
 2: 18       Z Loc [ T_case    ]

15:  Z=LN(X) (P40)
 1: 16       X Loc [ R_dome    ]
 2: 26       Z Loc [ ln_R_dome ]

; Polynomial pre-scaled with 10^5 to enable coefficient entry.
16:  Polynomial (P55)
 1: 1        Reps
 2: 26       X Loc [ ln_R_dome ]
 3: 27       F(X) Loc [ Poly_T_dx ]
 4: 102.95   C0
 5: 23.91    C1
 6: 0.0      C2
 7: 0.01568  C3
 8: 0.0      C4
 9: 0.0      C5

; and apply de-pre-scaling to polynomial:-

17:  Z=X/Y (P38)
 1: 27       X Loc [ Poly_T_dx ]
 2: 9        Y Loc [ Hund_thou ]
 3: 21       Z Loc [ Poly_T_d  ]

18:  Z=1/X (P42)
 1: 21       X Loc [ Poly_T_d  ]
 2: 19       Z Loc [ T_dome    ]


; TERM_2 calculation

19:  Z=F (P30)
 1: 4        F
 2: 0        Exponent of 10
 3: 28       Z Loc [ Four      ]

20:  Z=X^Y (P47)
 1: 18       X Loc [ T_case    ]
 2: 28       Y Loc [ Four      ]
 3: 29       Z Loc [ T_c_four  ]
```

```
21: Z=X*Y (P36)
 1: 25      X Loc [ Sigma    ]
 2: 29      Y Loc [ T_c_four ]
 3: 30      Z Loc [ TERM_2   ]


; TERM_3 calculation

22: Z=X^Y (P47)
 1: 19      X Loc [ T_dome
]
 2: 28      Y Loc [ Four     ]
 3: 31      Z Loc [ T_d_four ]

23: Z=X-Y (P35)
 1: 29      X Loc [ T_c_four ]
 2: 31      Y Loc [ T_d_four ]
 3: 32      Z Loc [ Bracket  ]

24: Z=X*F (P37)
 1: 25      X Loc [ Sigma    ]
 2: 3.5     F
 3: 33      Z Loc [ Bracket_2 ]

25: Z=X*Y (P36)
 1: 32      X Loc [ Bracket  ]
 2: 33      Y Loc [ Bracket_2 ]
 3: 34      Z Loc [ TERM_3   ]


; LW Irradiance calculation

26: Z=X+Y (P33)
 1: 30      X Loc [ TERM_2   ]
 2: 34      Y Loc [ TERM_3   ]
 3: 35      Z Loc [ tempterms
]

27: Z=X+Y (P33)
 1: 35      X Loc [ tempterms
]
 2: 7       Y Loc [ TERM_1   ]
 3: 36      Z Loc [ LW_IRR   ]

; OUTPUT PHASE of LW
irradiance avg, min, max
and std.

28: If time is (P92)
 1: 0       Minutes (Seconds
--) into a
 2: 1       Interval (same
units as above)
 3: 10      Set Output Flag
High (Flag 0)

29: Real Time (P77)
 1: 1120    (Same as 1220)
Y,D,Hr/Mn

30: Resolution (P78)
 1: 01      High Resolution

31: Average (P71)
 1: 1       Reps
 2: 36      Loc [ LW_IRR   ]

32: Standard Deviation
(P82)
 1: 1       Reps
 2: 36      Sample Loc [
LW_IRR   ]

33: Minimize (P74)
 1: 1       Reps
 2: 00      Time Option
 3: 36      Loc [ LW_IRR   ]

34: Maximize (P73)
 1: 1       Reps
 2: 00      Time Option
 3: 36      Loc [ LW_IRR   ]

35: Sample (P70)
 1: 1       Reps
 2: 7       Loc [ TERM_1   ]

36: Sample (P70)
 1: 1       Reps
 2: 30      Loc [ TERM_2   ]

37: Sample (P70)
 1: 1       Reps
 2: 34      Loc [ TERM_3   ]

*Table 3 Subroutines

End Program

-Input Locations-
1 Case     1 3 1
2 Dome     1 3 1
3 Pile     1 2 1
4 BatV     1 0 1
5 IntT     1 0 1
6 Pile_cal 1 0 0
7 TERM_1   1 2 1
8 R_c_upper 1 1 1
9 Hund_thou 1 2 1
10 R_case  1 1 1
11 R_lower 1 0 0
12 R_upper 1 0 0
13 R_c_lower 1 1 1
14 R_d_upper 1 1 1
15 R_d_lower 1 1 1
16 R_dome  1 1 1
17 R_d_uppe 1 0 0
18 T_case  1 1 1
19 T_dome  1 1 1
20 Poly_T_c 1 1 1
21 Poly_T_d 1 1 1
22 Poly_T_cx 1 1 1
23 Min_Hu_th 1 2 1
24 ln_R_case 1 1 1
25 Sigma   1 2 1
26 ln_R_dome 1 1 1
27 Poly_T_dx 1 1 1
28 Four    1 2 1
333 _________ 1 0 0
29 T_c_four 1 2 1
30 TERM_2  1 2 1
31 T_d_four 1 1 1
32 Bracket 1 1 1
33 Bracket_2 1 1 1
34 TERM_3  1 2 1
35 tempterms 1 1 1
36 LW_IRR  1 4 1
-Program Security-
0000
0000
0000
-Mode 4-
-Final Storage Area 2-
0
-CR10X ID-
0
-CR10X Power Up-
3
```